Univerzita Karlova v Praze

Přírodovědecká fakulta

Charles University in Prague

Faculty of Science

Academy of Sciences of the Czech Republic

Institute of Physiology, v.v.i

Význam metabolismu tukové tkáně pro celotělovou energetickou rovnováhu

Importance of adipose tissue metabolism for whole-body energy balance

Disertační práce / Ph.D. thesis

RNDr. Petr Zouhar

Školitel / Supervisor: RNDr. Pavel Flachs Ph.D.

Praha 2015

Prohlášení:

Prohlašuji, že jsem závěrečnou práci zpracoval/a samostatně a že jsem uvedl/a všechny použité informační zdroje a literaturu. Tato práce ani její podstatná část nebyla předložena k získání jiného nebo stejného akademického titulu.

Statement of authorship

I certify that the thesis represents valid work elaborated under the supervision of RNDr. Pavel Flachs, Ph.D., and that neither this manuscript nor one with substantially similar content under my authorship has been submitted in support of an application for any other academical degree. My participation in the published papers is specified in the text, and summarized in the list of Publications on the page 122.

19. 3. 2015 in Prague

RNDr. Petr Zouhar

Statement of co-authors

I certify that Petr Zouhar substantially contributed to the formation of the papers used as a basis of this thesis, and that his participation specified in the text of the thesis is correct.

19. 3. 2015 in Prague

RNDr. Pavel Flachs, Ph.D.

Acknowledgement

I would like to express my sincere thanks to my supervisor RNDr. Pavel Flachs, Ph.D., and to MUDr. Jan Kopecký, DrSc., the head of the department, for their scientific and financial support during my Ph.D. studies. I also want to acknowledge all the co-authors of publications summarized in this thesis. I thank all my colleagues for creating a stimulating and friendly working environment, and my family and friends for being close to me all the time.

Abstract

Adipose tissue plays a crucial role in nutrient and energy homeostasis. At the time of worldwide pandemy of obesity and consequent metabolic syndrome, a great effort is made to find new treatments with potential to preserve insulin sensitivity, or even counteract development of obesity and type 2 diabetes. There are three principal possibilities how the adipose tissue biology can contribute to this goal: 1) induction of UCP1-dependent energy dissipation in brown adipose tissue; 2) conversion of white adipose depots to brown-like tissue (i.e. "browning"); and 3) stimulation of UCP1-independent thermogenesis in white adipose tissue.

This thesis is based on two published works and one article under preparation. Generaly, it is focused on three different approaches targeting the above mentioned processes in adipose tissue of laboratory mouse: 1) diet supplementation with bile acids; 2) combination treatment of ω-3 polyunsaturated fatty acids and calorie restriction; and 3) cold exposure.

In the experiments with administration of bile (specifically chenodeoxycholic) acid to mice, we confirm specific induction of UCP1 in both brown and subcutaneous white adipose tissue, as well as reversion of obesity in the response to the treatment. Nevertheless, most of the acute beneficial effects are mediated by transiently decreased food intake, while elevated thermogenesis in brown fat may play role rather in long term.

Combination of calorie restriction and feeding by ω-3 polyunsaturated fatty acids proves to counteract deleterious effects of high fat feeding due to UCP1-independent stimulation of lipid catabolism in epididymal white adipose tissue without consequent recruitment of brown adipose tissue. The excessive energy is probably consumed by consequently stimulated synthesis of triglycerides and/or fatty acids.

The phenomenon of inducible futile cycling was confirmed also in epididymal adipose tissue of mice exposed to cold for 7 days. The rate of triglyceride synthesis was especially high in animals of AJ strain (in comparison to B6 strain), which are known for their resistance to dietary obesity. Flexible futile cycling thus may contribute to protection of AJ metabolism in conditions of high-fat feeding.

Despite the fact that both white adipose tissue browning and UCP1-independent induction of futile cycling probably fail to influence whole body energy expenditure, but they can exert beneficial effects in buffering plasma and tissue fatty acids levels, and thus preventing impairment of glucose tolerance.

Abstract (in Czech)

Tuková tkáň hraje klíčovou roli v udržování homeostázi živin a energie. V současnosti nabývá Rozšíření obezity a s ní souvisejících metabolických poruch nabývá v současnosti rozměrů pandemie, a nemalé úsilí je proto věnováno vývoji nových léčebných postupů, které by tento stav mohly zvrátit. Při plnění tohoto cíle se přitom zvažuje i možná modulace aktivity tukové tkáně, a to trojím možným způsobem: 1) indukcí spalování energie v hnědé tukové tkáni závislého na odpřahovacím proteinu UCP1; 2) „hnědnutím“, tj. konverzí bílé tukové tkáně na „hnědou“; a 3) stimulací termogeneze v bílé tukové tkáni bez zapojení UCP1.

Tato práce je založena na dvou publikovaných studiích a jednom článku v přípravě. Na modelu laboratorní myši zkoumá možné ovlivňování všech třech výše zmíněných procesů a to pomocí: 1) suplementace diety žlučovými kyselinami; 2) kombinovaného působení ω-3 vícenenasycených mastných kyselin a kalorické restrikce; a 3) chladové expozice.

V pokusech s podáváním žlučových kyselin (konkrétně kyseliny chenodeoxycholové) jsme potvrdili indukci proteinu UCP1 jak v hnědé, tak v podkožní bílé tukové tkáni, což bylo spojeno s reverzí obezity. Většina příznivých účinků byla nicméně způsobena přechodným poklesem spotřeby potravy, zatímco aktivace termogeneze v hnědém tuku patrně může hrát významnější roli pouze při dlouhodobějším působení.

V druhé sérii pokusů bylo prokázáno, že kombinace mírné kalorické restrikce a příjmu ω-3 vícenenasycených mastných kyselin pomáhá předcházet rozvoji obezity vyvolané nadměrným příjmem tuků. Děje se tak prostřednictvím stimulace katabolismu lipidů v epididymální bílé tukové tkáni. Mitochondrie jsou přitom plně spřažené, takže uvolněná energie musí být zužitkována jiným způsobem – pravděpodobně je použita k syntéze triglyceridů a mastných kyselin, jejíž obrat je také navýšen.

Existence indukovatelného jalového metabolického cyklování triglyceridů a volných mastných kyselin v epididymální tukové tkáni byla potvrzena také na modelu myší vystavených po 7 dní chladu. Syntéza triglyceridů byla výrazněji zvýšena u myší kmene AJ (ve srovnání s kmenem B6), což může souviset s rezistencí AJ myší k dietou indukované obezitě. Flexibilnější cyklování lipidů u AJ zvířat tak může přispívat k ochraně metabolismu před nepříznivým působením zvýšeného příjmu tuků.

Ačkoli „hnědnutí“ bílé tukové tkáně, ani výše popsané jalové cykly patrně nemohou významněji ovlivnit energetický výdej na celotělové úrovni, stále mohou příznivě působit na homeostázu lipidů v plazmě a tkáních a předcházet tak glukózové intoleranci.

Contents

List of abbreviations

15d-PGJ2	15-deoxy-prostaglandin J2
AA	arachidonic acid
ACAD	acyl-CoA dehydrogenase
ACC	acetyl-CoA carboxylase
ACS	acyl-CoA synthase
AGPAT	acylglycerolphosphate acyltransferase phosphatidate phosphatase
AJ	A/JOlaHsd (murine strain)
ALA	α-linolenic acid
AMPK	AMP-activated kinase
ANP	atrial natriuretic peptide
ATF-2	activating transcription factor 2
ATGL	adipose triglyceride lipase
AUC	area under curve
B6	C57BL/6J (murine strain)
BAT	brown adipose tissue
BDNF	brain derived neurotrophic factor
BNP	brain natriuretic peptide
BSA	bovine serum albumin
CDCA	chenodeoxycholic acid
ChREBP	carbohydrate responsive element-binding protein
CoA	coenzyme A
cHF	composite high-fat diet
cHF+F	composite high-fat diet supplemented with ω-3 concentrate from fish oil
CL	ATP-citrate lyase
CLS	crown-like structure
CR	calorie restriction
CoA	coenzyme A
CPT1	carnitine palmitoyl transferase 1
DGAT	diacylglycerol acyltransferase
DHA	docosahexaenoic acid
EPA	eicosapentaenoic acid

eWAT	epididymal white adipose tissue
FA	fatty acid(s)
FAS	fatty acid synthase
FXR	farnesoid X receptor
G3P	glycerol-3-phosphate
GK	glycerol kinase
GLUT4	glucose transporter 4
GPAT	glycerol-3-phosphate acyl transferase
HMW	high molecular weight (adiponectin)
HSL	hormone sensitive lipase
IL	interleukin
IR	insulin resistance
LA	linoleic acid
LCAD	long chain ACAD
LPL	lipoprotein lipase
MCAD	medium chain ACAD
MCP1	monocyte chemotactic protein 1
MGL	monoglyceride lipase
NEFA	non-esterified fatty acids
NMR	nuclear magnetic resonance
NST	non-shivering thermogenesis
OGTT	oral glucose tolerance test
PDH	pyruvate dehydrogenase
PDK4	pyruvate dehydrogenase lipoamide kinase isozyme 4
PEPCK	phosphoenolpyruvate carboxykinase
PGC1	PPARγ coactivator 1
PKA	protein kinase A
PKB	protein kinase B, Akt
PKG	protein kinase G
PPAR	peroxisome proliferator-activated receptor
PPRE	peroxisome proliferator-responsive element
PUFA	polyunsaturated fatty acids
qPCR	quantitative polymerase chain reaction
RQ	respiratory quotient

RXR	retinoid X receptor
scWAT	subcutaneous white adipose tissue
SCAD	short chain ACAD
SREBP	sterol regulatory element-binding protein
STD	standard chow diet
T3	triiodothyronine
TAG	triacylglycerol(s)
TZD	thiazolidinediones
UCP1	uncoupling protein 1
VLCAD	very long chain ACAD
WAT	white adipose tissue

1. Introduction

Adipose tissue plays critical role in whole-body energy metabolism, since it serves as the main storage place for metabolic energy. In the case that its capacity is exceeded, plasma lipids are ectopically stored in other tissues including liver and muscle, which impairs sensitivity of those organs to insulin. Thus, central obesity, dislipidaemia, and insulin resistance are linked together and recognized as a part of so-called metabolic syndrome (more specifically defined in (Alberti and Zimmet 1998)). This cluster of disorders is a risk factor for development of cardiovascular disease and type 2 diabetes.

In Western society, sedentary lifestyle with minimal energy expenditure and increased calorie intake result in a shift in energy balance towards increased storage. Therefore, treatment of obesity and its comorbidities becomes major medical challenge. One of the most promising approaches involves potentiation of energy expenditure directly in adipose tissue. If successful, this process could counteract fat accumulation, and also normalize glycaemia and lipidaemia by consumption of excess glucose and lipids. One direction, which traditionally attracts big attention, is a stimulation of non-shivering thermogenesis (**NST**) in brown adipose tissue (**BAT**). On the other hand, our laboratory is also engaged in projects demonstrating the importance of classical white adipose tissue (**WAT**). Both approaches to increase the energy dissipation and to normalize plasmatic levels of nutrients are discussed in following chapters.

1.1 Typology, function, and origin of adipose tissue

In mammals, two types of adipose tissue are distinguished according to their morphology and function: WAT with unilocular adipocytes and BAT with multilocular adipocytes.

Adipocytes of classical WAT are characterized by relatively small amount of mitochondria and one big lipid droplet in the cell. Their main purpose is serving as repository for storage lipids and their metabolic turnover is relatively small. In addition, WAT functions also as a potent endocrine organ influencing other tissues. The WAT is interspersed in several depots, which may be simplistically classified as visceral (located in trunk cavity), or subcutaneous (**scWAT**, under the skin). Detailed terminology of individual depots is not unified and generally accepted. According to (Walden, et al. 2012), rodent WAT depots include anterior subcutaneous WAT (in the scapular region), inguinal WAT (whose dorsolumbar part is used in our studies as typical scWAT), perigonadal WAT (in males called epididymal, **eWAT**), retroperitoneal WAT (along the dorsal wall of abdominal cavity), and mesenteric WAT (lining the surface of the intestine). These individual WAT depots vary

with respect to the endocrine function, responsiveness to hormones (e. g. glucocorticoids), and potential for "browning" (see below). Moreover, epidemiological studies reveal strong correlation between accumulation of visceral (but not subcutaneous fat) and metabolic disease (i. e. hypertension, atherosclerosis, insulin resistance, dyslipidemia, hepatic steatosis, type 2 diabetes); (Baik, et al. 2000; Carey, et al. 1997; Meisinger, et al. 2006; Misra, et al. 1997; Pischon, et al. 2008; Qiao and Nyamdorj 2010; Snijder, et al. 2003; Wang, et al. 2005; Zhang, et al. 2008). This correlation can be partially attributed to the fact that blood from visceral WAT (but not from scWAT) is drained directly to the liver causing damage. Other differences among depots, which may be also important, involve various origin of adipocytes (see below in this chapter), or different amount and type of other cells, especially infiltrating leukocytes (see chapter 1.5).

In contrast to WAT, BAT is highly metabolically active, which corresponds to its role of the center of NST. It contains significant number of mitochondria (causing the brownish color of whole depot) and numerous small lipid droplets (loculi). This arrangement allows fast and efficient lipolysis and lipid combustion in mitochondria supplying substrates for thermogenesis. The thermogenesis is enabled by presence of specific proton transporter in inner mitochondrial membrane – uncoupling protein 1 (**UCP1**, thermogenin; for details see chapter 1.3.3).

NST in BAT (together with shivering of skeletal muscles) prevents decrease in body temperature in case of cold stress (see chapter 1.2.1). Chronically cold environment leads to the recruitment of BAT (i. e. biogenesis of mitochondria, induction of UCP1, and angiogenesis in the tissue), whereas acute cold exposure immediately activates BAT thermogenic capacity triggering mobilization of its energy stores, uptake of glucose and fatty acids from blood, and heat production. On the other hand, BAT atrophies in thermoneutral temperatures.

Full activation of BAT requires previous recruitment of its thermogenic capacity. Therefore, first phase of cold exposure (until attainment of sufficient BAT recruitment) is usually overcome using muscle shivering. On the contrary, BAT is essential for certain mammal species during arousal from hibernation and for newborns during postnatal cold shock.

In rodents, occurrence of BAT depots is referred especially in interscapular region, along the cervical spine (Walden, et al. 2012), and further around aorta and kidneys (Fitzgibbons, et al. 2011). In humans, BAT was long thought to be present only in newborns. However, recent positron emission tomography scans displaying ^{18}F-deoxyglucose uptake revealed surprising

presence of functional BAT in adult humans exposed to cold condition (Nedergaard, et al. 2007; Saito, et al. 2009; van Marken Lichtenbelt, et al. 2009; Virtanen, et al. 2009; Zingaretti, et al. 2009).

Ontogenetic origin of adipocytes is still controversial. Several research groups are tracing the origins of mature adipocytes back to their adult precursor and embryonic ancestor. It was suggested, that brown adipocyte arises from lineage common with skeletal muscle cells and characterized by expression of myogenic factor 5 (Myf-5), whereas white adipocyte precursors are Myf-5-negative (Seale, et al. 2008; Timmons, et al. 2007). Despite the fact that this hypothesis seemed to be consistent with apparent physiological divergence of WAT and BAT, it must have been later reformulated when newer studies revealed surprisingly complex ontogenesis of WAT. White adipocytes differentiate from at least three distinct cell lines (reviewed in (Rosenwald and Wolfrum 2014)) while majority of cells from anterior subcutaneous WAT is also Myf-5-positive (Sanchez-Gurmaches, et al. 2012). The differences in abundance of these cell lineages in individual WAT depots could explain above mentioned various features of depots. Nevertheless, the distinct origin does not necessarily mean distinct properties (Bronner-Fraser 1994).

Further studies are needed to clarify the role of distinct ontogenetic origin in differences between WAT and BAT and between individual WAT depots. In this respect, it is interesting that multilocular UCP1-positive adipocytes can appear even in certain rodent WAT depots after adrenergic stimulation (Cannon and Nedergaard 2012; Cinti 2009; Cinti 2011; Cinti 2012; Frontini and Cinti 2010; Ishibashi and Seale 2010; Petrovic, et al. 2010; Schulz, et al. 2011; Young, et al. 1984). These adipocytes are called "brite" (brown-in-white), "beige", or "inducible brown", and the process of their recruitment is known as "browning" of WAT. As already mentioned, propensity to browning differ in individual depots: Inguinal and retroperitoneal depots were reported to be most prone to browning, whereas eWAT is relatively resistant to inducing stimuli (Cinti 2011; Cinti 2012). In non-stimulated state, brite adipocytes are not morphologically distinguishable from classical white adipocytes. It is not clear yet what happens after stimulation, i. e. if the brite cells differentiate from some progenitor or if they rather originate from transdifferentiation (conversion) of classical white adipocytes. The strong argument in favor of the latter possibility arises from the lineage tracing of brite cells in inguinal depot during the cold induction and following return to normal conditions (Rosenwald, et al. 2013). This study indicated that brite adipocytes are not only converted from already differentiated adipocytes with classical white morphology, but they also can return back to the original state (Rosenwald, et al. 2013). Contradictory results

of other studies suggest that brite adipocytes from scWAT arise from some undifferentiated progenitors (Wang, et al. 2013). In any case, the mechanism of browning is probably depot-dependent (Cinti 2009; Lee, et al. 2012).

For completeness, we should mention also the "pink" adipose tissue of lactating mammals. In pregnant mice, certain depots of scWAT turn into a specialized milk producing (mammary) gland (reviewed in (Giordano, et al. 2014)). This other type of adipose tissue shows additional dimension of WAT plasticity.

The capability of BAT to dissipate energy attracts attention of researchers developing strategies to combat obesity and its comorbidities. Until recently, the hope for hypothetical use of mitochondrial uncoupling in human medicine was restricted by the opinion that functional BAT is lacking in adult humans. Therefore, both the new phenomenon of WAT browning and the proof of BAT presence in adults have revived the effort to employ adipose tissue metabolism in modulation of whole body energy balance. The relevance of adipose tissue in this respect is discussed in following chapter. However, besides its direct contribution to metabolic turnover, adipose tissue (even the classical WAT) represents crucial site of lipid and glucose uptake buffering their plasma levels, which can also significantly influence metabolic health.

1.2 Metabolic rate and adipose tissue activity

In general, energy balance consists of energy intake in form of food on the one hand, and energy expenditure on the other hand. Roughly 10% of ingested food cannot be exploited and is excreted in form of feces, urine, and sweat (Blaxter 1989). The resting 90% is the metabolisable energy, which covers all energetic requirements of the body, including external work, tissue production and repair, and in endotherms also heat production. The thermogenesis represents by far the most striking contribution of adipose tissue (especially BAT) to whole-body energy expenditure. While metabolic rate of classical WAT is mostly neglected, BAT (and browning WAT) metabolism is extensively studied in conditions of both cold exposure and special recruiting diets, as discussed below.

1.2.1 "Thermoregulatory" thermogenesis in brown adipose tissue

Most animals are ectotherms, i.e. their body temperature follows the values of ambient temperature and their metabolic rate is exponentially related to ambient temperature. By contrast, mammals and birds, as typical endotherms, invest significant proportion of energy

in maintenance of stable body temperature (approximately 37 °C in mammals) in broad range of ambient temperature. As a result, their metabolic rate is approximetaly 5-8 times higher than that of the same-size ectotherms (Rolfe and Brown 1997).

The obligatory processes of normal metabolism (ensuring the vital functions) produce as a by-product some amount of heat. In certain range of ambient temperature called thermoneutral zone, this basal heat production is sufficient to retain the stable body temperature, i.e. the resting metabolic rate in the thermoneutral zone is the lowest. Protection of body core temperature out of the thermoneutral zone requires some additional energy for thermogenesis, or cooling.

Thermoneutral zone can be significantly extended to lower temperature by better insulation of body surface (e.g. by thick hair and subcutaneous fat). For instance, the magnitude of thermoneutral zone in some arctic animals can be as much as 70 °C (Cannon and Nedergaard 2011). Thus, the first reaction to cold exposure usually involves improvement of insulation (such as posture minimizing body surface, piloerection and vasoconstriction of skin vessels). Moreover, body temperature can be raised also by muscle activity such as voluntary excercise, non-excersise activity (fidgeting), and especially shivering. The latter represents the major mechanism of protection against acute cold. Nevertheless, the endurance of shivering thermogenesis is limited; thus, it must be substituted by more comfortable way of energy dissipation if the cold exposure is prolonged. Therefore, BAT oxidative capacity is recruited and NST gradually replaces the muscle activity. The full induction of BAT can take weeks (Cannon and Nedergaard 2004). As described in details in chapter 1.4.3, both recruitment and activation of BAT is regulated by sympathetic innervation. Because of adaptive BAT recruitment, mice acclimated to mild cold exhibits higher capacity to NST in comparison to animals maintained in thermoneutral temperature. The above described scenario (with BAT as the major if not only place of NST) can be applied to rodents, especially mouse. The situation in humans remains controversial (see below).

It is important to note that the thermoneutral zone of mouse is around 30 °C. While breeding in standard temperature of 20 °C, the animals have constantly activated BAT, which is reflected by 60% higher food intake in comparison to the situation in thermoneutrality (Cannon and Nedergaard 2009). The food consumption futher increases when temperature is lowered. In 5 °C, animals eat 4-5 times as much as in thermoneutrality (Cannon and Nedergaard 2009). Virtually all this additional energy is consumed by BAT. It was calculated

that maximal heat-producing capacity of BAT is approximately 300 $W.kg^{-1}$, i.e. two orders of magnitude of the metabolic rate of other tissues (Cannon and Nedergaard 2004).

Mice are routinely used as a model organism mimicking the situation in humans, in spite of numerous interspecies differences. Especially transfer of findings in the field of metabolic rate and thermogenesis faces considerable limitations. First of all, according to Kleiber's law, metabolism increases in proportion to the body weight to the power 0.75 (Kleiber 1947). It means that humans has several times lower metabolic rate per gram than mice. This corresponds with smaller ratio of (heat producing) body volume to (heat loosing) body surface. Futhermore, the human thermoneutral zone is also shifted to lower temperature. As a result, thermogenesis does not play as a crucial role in man under standard conditions as it does in mouse. Nevertheless, non-shivering adaptive thermogenesis exists in human as well, as documented by gradually decreasing shivering and steadily elevated oxygen consumption during daily repeated cold exposure of men (Davis 1961). Later studies reported NST varying between 0 and 30% of basal metabolic rate (Celi, et al. 2010; Claessens-van Ooijen, et al. 2006; van Ooijen, et al. 2001; Warwick and Busby 1990; Wijers, et al. 2010). The greater values are usually observed in short-term experiments where the conditions can be more strictly controlled (van Marken Lichtenbelt and Schrauwen 2011). Comparison of the same volunteers in winter and summer period reveals higher inducibility of NST during cold season (van Ooijen, et al. 2004). This collectively demonstrates that also humans exhibit inducible and adaptive NST which is great enough to influence significantly the whole-body energy expenditure.

The privileged role of BAT (with small contribution of browned WAT) in rodent NST is generally accepted (based on studies such as (Golozoubova, et al. 2006)). If some other tissues are also involved in NST (as is suggested for muscle e.g. in (Kus, et al. 2008)), their contribution is just minor. The situation in human is different. Before the confirmation of its occurrence in adult humans (Nedergaard, et al. 2007; Saito, et al. 2009; van Marken Lichtenbelt, et al. 2009; Virtanen, et al. 2009; Zingaretti, et al. 2009), BAT was thought to be absent in adults for a long time; thus, alternative places of NST was searched. Skeletal muscle was the most promising candidate. Even in recent studies, it was shown that cold-induced NST is related to mitochondrial uncoupling in muscle (Wijers, et al. 2008) and that both BAT and muscle are involved in NST (Wijers, et al. 2011). As muscle lacks UCP1 protein and other members of UCP group (such as UCP3) probably cannot facilitate real uncoupling (Gong, et al. 2000), mechanism of muscle NST remains mysterious. Therefore, some researchers advocate BAT as probably the only tissue capable of substantial NST in

both mice and humans (Cannon and Nedergaard 2004), while others call for futher studies of UCP3 and other candidate genes in muscle (van Marken Lichtenbelt and Schrauwen 2011).

Is the amount of BAT in human body sufficient at all to be able to explain all the observed NST? Some calculations was made, based on the assumption that maximal BAT metabolic rate in mice and human is the same (300 $W.kg^{-1}$, see above). If this is true, only 40-50 g of maximally stimulated BAT account for 20% of daily energy expenditure (Rothwell and Stock 1979). However, BAT is unlikely to be stimulated to such extent for prolonged period of time. Moreover, as the basal metabolic rate in humans is several times lower in comparison to mouse, also the BAT metabolism is probably slowlier in humans. After consideration of allometric relations, it was approximated that coverage of 20% of daily metabolic rate requires rather 200-350 g BAT (van Marken Lichtenbelt and Schrauwen 2011). Similar data were obtained also by another approach: Dynamic PET scanning revealed that 100 g of BAT take up 12.2 μmol glucose uptake in BAT (Virtanen, et al. 2009). If glucose represents 10% of BAT energetic substrate (Ma and Foster 1986), the heat production of activated BAT will be 55 $W.kg^{-1}$ - result quite close to the former estimation. Taken together, activated human BAT is theoretically able to substantially influence whole-body metabolic rate. Possible involvement of other tissues remains controversial.

1.2.2 "Metaboregulatory" thermogenesis and brown adipose tissue in prevention of obesity

Interestingly, recruitment of BAT and decrease in metabolic efficiency are reported not only in response to cold exposure, but also as a result of feeding by certain diets, specifically so-called cafeteria (Rothwell and Stock 1979), high-fat (Mercer and Trayhurn 1987), and high-carbohydrate diets (Bukowiecki, et al. 1983). In comparison to standard chow diet with balanced composition, these diets are usually more tasty, palatable, and consequently preferred by experimental animals. Nonetheless, all these diets contain lower proportion of essential nutrients, namely proteins, per calorie amount. Thus, excessive energy must be consumed to obtain the necessary amount of protein. BAT uncoupling can thus serve as an adaptation to "protein-diluting" diet intake, providing way to combustion of surplus lipids and saccharides (Rothwell and Stock 1979).

Activation of above described metaboregulatory thermogenesis is probably triggered rather by accumulation of stored lipids in white fat depots than directly by intake of low-protein diet. Accordingly, animals fattened by cafeteria diet and later reexposed to chow diet

decrease their food intake, but preserve both obese phenotype and increased activity of BAT (Llado, et al. 1991; Rodriguez, et al. 2001). Most likely mediator of obesity signal is hormone leptin. It is produced in elevated amount from hypertrophic white adipocytes and its central action results in reduced food intake and increased metabolic rate. Leptin treatment was indeed shown to enhance the sympathetic nervous activity (Collins, et al. 1996; Sivitz, et al. 1997) and UCP1 expression in BAT (Commins, et al. 2000; Rouru, et al. 1999; Wang, et al. 1997). Thus, BAT may serve as "adipostat" combusting excessive lipids when WAT grows. Importantly, metaboregulatory thermogenesis can be observed only in thermoneutral temperature (for mice around 30 ºC) (Feldmann, et al. 2009). In lower ambient temperature, the effect is covered up by more prominent cold induction of BAT.

As demonstrated above, BAT has the potential to be a determinant in metabolic efficiency. Uncoupling between substrate combustion and ATP production leads inevitably to lower fraction of consumed energy converted in bodily fat. Based on this general conclusion and observation of atrophied BAT in genetically obese animals (Himms-Hagen and Desautels 1978; Trayhurn, et al. 1976; Trayhurn, et al. 1977), critical role of NST in lean phenotype preservation was suggested (Himms-Hagen 1979; Thurlby, et al. 1978). In accordance with this hypothesis, UCP1-ablated mice reared at thermoneutral temperature (but not in standard housing temperature (Enerback, et al. 1997)) become obese (Feldmann, et al. 2009). On the other hand, the physiological relevance of diet-induced thermogenesis in prevention of obesity is still questioned by some authors (Fromme and Klingenspor 2011; Kozak 2010).

Regardless of the acivating stimulus (i.e. diet, cold, or other), induced BAT is obviously able to dissipate substantial amount of energy, which may have a consequence in body weight gain restriction. If this implication is correct, we should be able to detect negative correlation between thermogenetic response and BMI. This was demonstrated even in humans: e.g. the overnight metabolic response upon mild cold exposure was significantly increased in lean, while reduced in obese diabetic women (Lean, et al. 1988). Similar result was demonstrated upon 1-h cold exposure and 1-h rewarming in lean vs. ovese subjects (Claessens-van Ooijen, et al. 2006). However, such indirect evidence cannot be overinterpreted. It is clear that excessive fat pads function as insulative tissue and thus reduce the necessity of active thermogenesis (Wijers, et al. 2010). Hence, it is difficult to distinguish the cause and the consequence in this case. This can be said also about reduced NST observed in elderly people, who usually exhibit higher adiposity as well (van Marken Lichtenbelt and Schrauwen 2011).

1.2.3 Importance of metabolic rate in white adipose tissue

In general, activated BAT is characteristic by extremely high metabolic rate, whereas WAT metabolism turnover is far below the average of other tissues. It also means, that majority of whole body energy expenditure is localized to lean body mass while adipose tissue contributes by relatively small portion. Therefore, values of energy expenditure in two subjects differing dramatically in adiposity but not in lean body mass are closer to each other than would be expected just with regard to their body weight (Butler and Kozak 2010; Cannon and Nedergaard 2011). Nevertheless, regarding the large size of fat depots, the metabolism of WAT is not completely insignificant. It was calculated that WAT represents 5% of resting metabolic rate in lean human subjects and doubles in obesity (reviewed in (Bottcher and Furst 1997)).

Great attention is paid to proccess of WAT browning. Browning program can largely increase metabolic rate of WAT. In spite of very low total number of brite cells in activated WAT depots (usually just few procents - practicly negligible amount in comparison to highly active classic brown adipocytes in interscapular region), the extreme size of WAT depots strengthen their contribution to energy expenditure. In adult mice reared in 20 °C, the oxidative capacity of WAT is equivalent to 30-50% of that in BAT (Kopecky, et al. 1996). It was observed that abundance of brite cells in animal WAT depots correlates negatively with propensity to obesity while being under genetic control (Guerra, et al. 1998). In contrast to well characterized role of brown (and brite) cells in rodents, it is not clear what the physiological significance of multilocular adipocytes in humans is. We know for sure neither the nature of BAT recently identified in adult humans. Does it represents classical BAT corresponding to interscapular BAT of rodents or is it rather white fat depot with extensive browning proccess? Mice and rats differ significantly from humans regarding their response to cold stimulus.

1.3 Overview of adipose tissue metabolism

BAT and WAT share numerous basic metabolic pathways and differ in others. The complete summary is provided by classical textbooks (Murray, et al. 2005; Voet and Voetova 1994). However, because many of the enzymes are studied in experimental part of this work (particularly on the level of gene expression) and because turnover of main metabolic pathways and its relevance for whole body energy metabolism represent the main

topic of this thesis, it is necessary to present at least brief overview of key enzymes and specifics of adipose tissue. The role of the below mentioned enzymes is summarized in Figure 1-1. The regulation of described metabolic processes is summarized below in chapter 1.4.

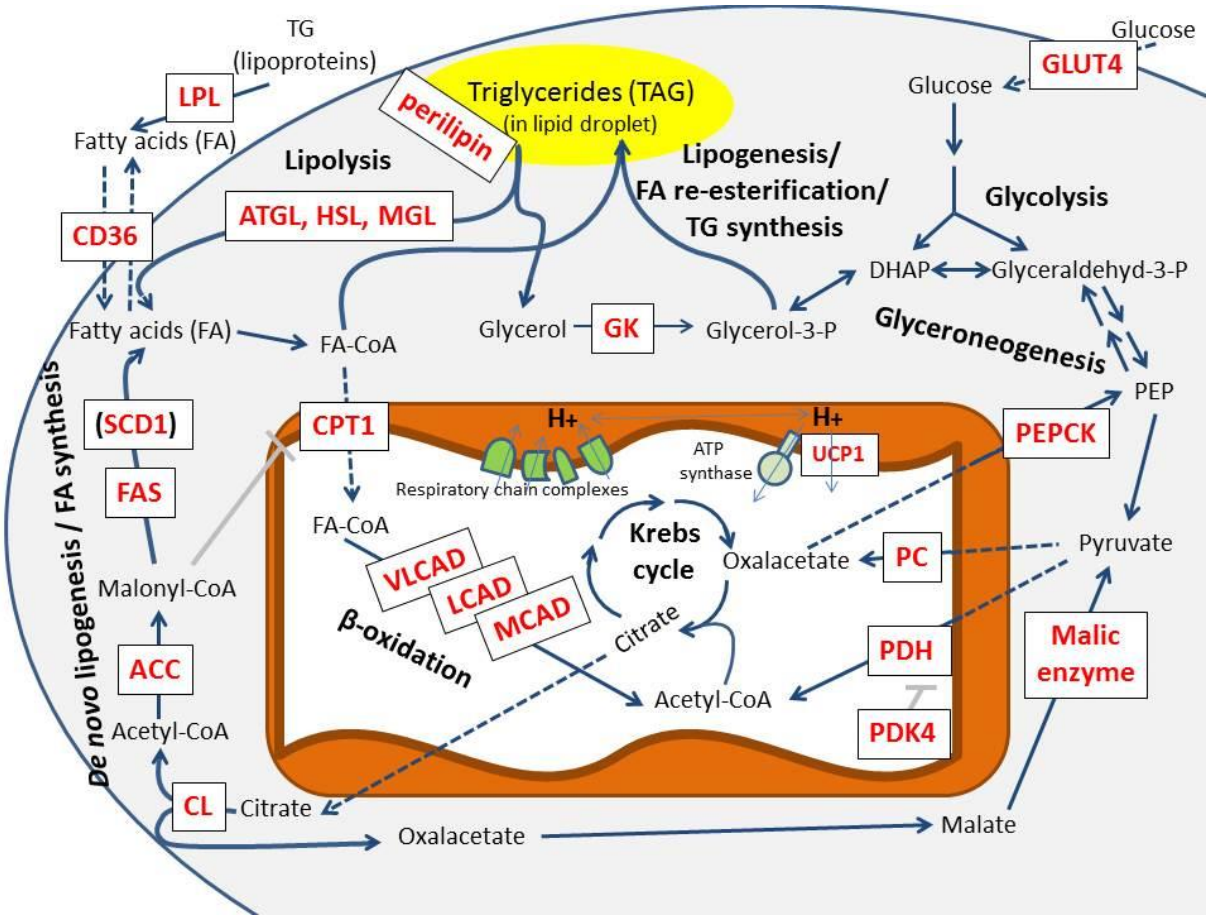

Fig. 1-1 Overview of adipocyte metabolism

1.3.1 Lipogenesis

As both BAT and WAT are characterized by their ability to store triacylglyceroles (**TAG**) in lipid droplets, **TAG synthesis** (lipogenesis, esterification of fatty acids – **FA**) represents a crucial metabolic pathway in adipocyte. Prior to the esterification, FA must be converted to the form of acyl-CoA by acyl-CoA synthetase (**ACS**), which costs ATP. The other precursor is glycerol-3-phosphate (**G3P**). TAG are subsequently created by series of reactions involving gradual esterification of acyl-CoAs to G3P and dephosphorylation of glycerol. These reactions are catalyzed by following enzymes: glycerol-3-phosphate acyl transferase (**GPAT**), acylglycerolphosphate acyltransferase (**AGPAT**), phosphatidate phosphatase and finally diacylglycerol acyltransferase (**DGAT**). DGAT1 isoform is thought

to process FA received from extracellular space (including re-esterification of the FA secreted after lipolysis), whereas DGAT2 is involved rather in esterification of endogenous de novo synthesized FA (Yen, et al. 2008).

Most FA used for lipogenesis come from TAG in blood-borne lipoproteins. They are liberated by secreted lipoprotein lipase (**LPL**) and imported to adipocyte via FA transport proteins such as FAT/CD36 (Ibrahimi and Abumrad 2002) or FATP1 (Hajri and Abumrad 2002; Kalant and Cianflone 2004). This uptake significantly influences plasmatic lipid levels, lipidemia. Especially, activated BAT is known to clear the plasma lipids very efficiently (Cannon and Nedergaard 2004).

Nevertheless, endogenous **FA synthesis** (or *de novo* lipogenesis) in adipocyte also represents significant source of FA, particularly in rodents. Even in humans, where the lipogenic activity is localized predominantly to liver, WAT may account up to 40% of whole-body lipogenesis, when subjects are fed by lipogenic diet (Chascione, et al. 1987). The precursor of FA synthesis, acetyl-CoA, is generated by catabolic processes in mitochondria and has to be transported to cytoplasm where the whole FA synthesis takes place. To overcome the inner mitochondrial membrane, acetyl-CoA is joined with oxaloacetate creating citrate, which subsequently passes the membrane via tricarboxylic carrier and is cleaved back to acetyl-CoA and oxaloacetate by ATP-citrate lyase (**CL**). Acetyl-CoA is then converted to malonyl-CoA by acetyl-CoA carboxylase (**ACC**). Malonyl-CoA is then processed by multimeric complex of fatty acid synthase (**FAS**) which incorporates it in growing chain of new fatty acid. The activity of FAS requires reductans in form of $NADPH^{+}$, which is provided mostly by pentose phosphate pathway and by oxidation of malate by malic enzyme (malate originate from the oxaloacetate created by CL (see above in this paragraph and Figure 1-1). In theory, the synthesis of a molecule of palmitate from acetyl-CoA requires 49 ATP (Baldwin 1970). On the whole, the *de novo* FA synthesis in adipose tissue represents substantial energy-consuming pathway interconnected both with lipogenesis on the one hand, and catabolism in mitochondria on the other hand.

Primary product of FA synthesis is 16-carbon saturated FA palmitate. This compound can be further elongated or dehydrogenated. Among enzymes catalyzing conversion of saturated FA to monounsaturated FA (such as oleate or palmitoleate), Δ-9 desaturase - stearoyl-CoA desaturase (**SCD1**) is the most principal. Expression of this enzyme is regulated by demand for its products. Therefore, diet high in unsaturated fatty acids decreases SCD1 transcription levels. Mammals are lacking higher desaturases, namely Δ-12 and Δ-15

desaturases which makes them unable to synthesize ω-6 and ω-3 fatty acids (see chapter 1.6.2).

Besides fatty acyl-CoA, G3P has to be produced to allow TAG synthesis. In many organs including BAT (Festuccia, et al. 2003), G3P is created directly from glycerol by glycerol kinase (**GK**). On the contrary, GK is absent in WAT under normal conditions (even though it can be stimulated by some drugs such as thiazolidinediones (**TZD**) (Guan, et al. 2002). Hence, in WAT, G3P must originate from hydroxyacetone phosphate, which can come either from glycolysis or from glyceroneogenesis, while the **glyceroneogenesis** was shown to represent the dominant source of G3P (Nye, et al. 2008). This pathway starts with pyruvate which can come from glucose oxidation. When G3P is needed, pyruvate undergoes conversion to oxaloacetate by pyruvate carboxylase, instead of decarboxylation by pyruvate dehydrogenase (**PDH**) and entering mitochondrial Krebs cycle ((Patel and Hanson 1970); see chapter 1.2.3 and Figure 1-1). Further processing of oxaloacetate to phosphoenolpyruvate is ensured by phosphoenolpyruvate carboxykinase (**PEPCK**), the rate limiting enzyme of whole glyceroneogenic pathway.

In conclusion, the process of lipogenesis requires complex system of anabolic reactions providing activated substrates, acyl-CoA and G3P. The energy cost of these processes is not negligible in spite of its relatively small magnitude in comparison to demands of uncoupled respiration.

1.3.2 Lipid catabolism

Lipid mobilization during **lipolysis** represents the complementary pathway to TAG synthesis described in previous chapter. Lipolysis in WAT provides free non-esterified FA (**NEFA**) as an energy source for other tissues during fasting and other physiological states, whereas lipolysis in BAT supplies the predominant substrate for NST. In both cases, TAG in lipid droplets are hydrolyzed by adipose triglyceride lipase (**ATGL**, catalyzing hydrolysis of TAG to diacylglycerols), hormone-sensitive lipase (**HSL**, catalyzing both TAG to diacylglycerols and diacylglycerols to monoacylglycerols conversion), and monoglyceride lipase (**MGL**). Lipid droplet is normally coated by protective layer of proteins (for example perilipin), which must at first dissociate from the lipid surface making it available for lipolytic enzymes. In cytosol, FA are usually not found in free form but rather bound to fatty acid binding proteins (FABP). WAT express the adipocyte form of FABP, whereas BAT contains both adipocyte and heart form of FABP (Haemmerle, et al. 2006).

Both lipolysis and lipogenesis work always simultaneously and only the ratio between these two processes determines the net amount of liberated FA. In a basal state, re-esterification converts 30-90% of lipolyzed fatty acids back to TAG, whereas the ratio can decrease to 10-20% upon lipolytic stimulus (Bezaire, et al. 2009; Wang, et al. 2003). Interestingly, some works indicate, that all lipolysis-derived FA are at first secreted from the adipocyte and part of them is just after that taken back by FAT/CD36 and re-esterified (Zhou, et al. 2012). Every turn of lipolysis/re-esterification cycle requires 8 ATP per TAG molecule (Baldwin 1970).

The fate of glycerol and FA from lipolyzed TAG differs markedly regarding the type of adipose tissue. In BAT, glycerol can be directly recycled by GK (and used for another turn of lipogenesis or oxidized by glycolysis), whereas vast majority of FA is burned in mitochondria by process of **β-oxidation**. In contrast, most of the glycerol and FA released from lipid droplets in classical WAT are secreted to plasma and used as a substrate for hepatic gluconeogenesis, or source of energy for other tissues. Thus, β-oxidation is usually negligible in WAT, but it can be upregulated under certain conditions. E.g., its turnover is doubled during fasting (Wang, et al. 2003) and can be even more induced by other specific stimuli (as documented in chapter 4.2.2). It was suggested that the ATP obtained by oxidation of FA can be used to cover energy costs of lipogenesis (Cho, et al. 2009).

In any case, FA must be activated by ACS prior to the oxidation. Resultant fatty acyl-CoA can be transported to mitochondria using carnitine palmitoyltransferase 1 (**CPT1**). Both BAT and WAT contain the muscle isoform of CPT1 (Esser, et al. 1996), which is highly sensitive to inhibition by malonyl-CoA. It means that CPT1 activity (and consequently whole pathway of β-oxidation) will be stopped if FA are synthesized in cytoplasm. Once transported to mitochondria, FA-CoA can undergo the repeating set of four reactions which shortens FA by 2 carbons in each cycle creating acetyl-CoA (see Figure 1-1) and reduced electron carriers $NADH^+$ and $FADH_2$. First of these four reactions is catalyzed by enzymes from group of acyl-CoA dehydrogenases (**ACAD**). According to preferred substrate, we distinguish very long chain ACAD (alias **VLCAD**), long chain ACAD (**LCAD**), medium chain ACAD (**MCAD**), and short chain ACAD (**SCAD**) operating optimally on 16-, 14-, 10- and 4-carbon fatty acyl substrates, respectively (Ikeda, et al. 1985; Izai, et al. 1992).

1.3.3 Respiratory chain and mitochondrial uncoupling

Acetyl-CoA generated by β-oxidation (or pyruvate decarboxylation) is further oxidized in Krebs cycle while producing another set of reduced electron carriers. Most $NADH^+$ and $FADH_2$ created by catabolic reactions transmit their electrons to complexes of respiratory chain in inner mitochondrial membrane. The energy of electron flow is used for extrusion of protons from mitochondrial matrix to intermembrane space. The resultant electrochemical gradient forces protons back to matrix. In most tissues, this potential propels generating ATP by membrane enzymatic complex called ATP synthase. BAT is unique due to its relatively small content of ATP synthase (Andersson, et al. 1997; Houstek, et al. 1995) and high content of proton transporter UCP1. Therefore, the proton motive force in BAT mitochondria is not coupled with ATP production, but instead, protons pass the UCP1 while energy is dissipated in form of heat (Nicholls, et al. 1978).

As was indicated in previous chapters, predominant substrate for thermogenesis in BAT is pool of FA. FA are not only used as a source of reduced electron carriers for respiratory chain, but serves also as an activator of UCP1 (the possible mechanisms are summarized in (Cannon and Nedergaard 2004)). Actually, stimulation of thermogenesis by norepinephrine (see chapter 1.4.3) is mediated by increased lipolysis and higher intracellular concentration of FA, as is suggested by the same UCP1-dependent thermogenic response of brown adipocytes both to norepinephrine and to oleate addition (Matthias, et al. 2000).

Nevertheless, intrinsic lipid stores in brown adipocyte are not sufficient for long term thermogenesis. Therefore, BAT rapidly increases activity of LPL and fatty acid uptake immediately after cold stimulus (Carneheim, et al. 1984). In parallel, glucose uptake is induced during BAT stimulation (this uptake is regulated by norepinephrine, not insulin (Shibata, et al. 1989). Glucose anaerobic oxidation provides the necessary ATP, which cannot be produced in uncoupled mitochondria. Therefore, most of the glucose is just converted to lactate and exported back to blood (Ma and Foster 1986). However, transformation of part of glucose into pyruvate, which can be processed into oxaloacetate (by one of anaplerotic reactions), allows rapid increase in Krebs cycle capacity to combustion of β-oxidation-derived acetyl-coenzyme A. Finally, simultaneous replenishment of TAG by increased lipogenesis from intermediates of glucose metabolism may help to sustain long-term thermogenesis (reviewed in (Flachs, et al. 2013)).

During BAT activation, the blood perfusion of the tissue is increased in order to supply lipids and glucose and to futher distribute the generated heat (Foster and Frydman 1978). Futhermore, an induction of angiogenesis was reported both in BAT and browning scWAT in

response to adrenergic stimulus (Xue, et al. 2009). The uptake of FA to activated brown adipocyte is so large that BAT can very efficiently decrease plasma TAG levels. Similarly, BAT is able to regulate whole body glucose homeostasis independently on insulin (Stanford, et al. 2013), which inspires attempts to use BAT in combating diabetes-associated hyperglycaemia.

1.4 Regulation of metabolism in adipose tissue

All the above mentioned metabolic pathways must be finely tuned in response to immediate and chronic demands. Therefore, they are strictly controlled by hormones, as well as neural system and cellular autoregulatory circuits. Catabolism in BAT involves lipolysis and combustion of fuels in uncoupled mitochondria, which is activated by sympathetic innervation during cold exposure. On the other hand, WAT lipolysis is induced by catecholamines (from both neural connections and blood) during cold exposure, fasting, and exercise. Enhanced lipolysis is usually connected with increased rate of FA re-esterification. In addition, β-oxidation can be stimulated in WAT under certain conditions. In most cases, induction of lipid catabolism is accompanied by UCP1 expression in part of WAT cells, which can be explained by overlapping signaling pathways regulating both BAT and WAT. In this respect, it seems meaningful to consider all types of adipose tissue as a continuum of cells varying in degree of activation (Barneda, et al. 2013; Cinti 2005). Increased catabolic rate in WAT is often interpreted as an integral part of browning process (Bonet, et al. 2013), although it can occur in most of the cells while only a small part reaches the truly UCP1 induction.

The following description of metabolic control is subdivided in three parts corresponding to three levels of regulation: 1) regulation of gene expression by transcription activators; 2) intracellular homeostatic mechanisms sensing energy status of the cell; and 3) neurohumoral regulation and related signaling pathways. Besides regulation described in this chapter, metabolism of adipose tissue (or at least WAT) is also influenced by interaction with cells of immune system and vice versa. In this chapter, I provide a compendium about the most important players in adipocyte metabolic control, while chapter 1.5 will be dedicated to the role of inflammation and leukocytes in adipose tissue.

1.4.1 Control of metabolic gene expression

Many crucial metabolic genes are regulated on the level of gene expression. This task is carried out by whole set of transcription factors, co-activators and nuclear receptors (for the overview see Figure 1-2).

Expression of lipogenic genes is partially controlled by sterol and carbohydrate response element binding proteins (**SREBP** and **ChREBP**). Especially ChREBP is potent lipogenic stimulator in response to high saccharide content in the diet. As a result of ChREBP activation, glucose is converted to acetyl-CoA and used for production of FA. Therefore, the level of ChREBP is high in particular in BAT, where glucose-dependent FA synthesis plays more important role in comparison to WAT (Iizuka 2013).

Special importance in adipose tissue metabolism is ascribed to family of peroxisome proliferator-activated receptors (**PPAR**s). PPARs are nuclear receptors of various endogenous ligands - usually lipids, such as polyunsaturated FA (**PUFA**), oxylipins, phospholipids and endocannabinoids (reviewed in (Wahli and Michalik 2012)). Once they are activated, PPARs heterodimerize with retinoid X receptor (RXR) and bind to peroxisome proliferator responsive elements (PPRE) in the regulatory regions of certain genes while triggering their transcription.

PPARγ is essential for final phase of adipocyte differenciation (adipogenesis) because it potentiates lipogenesis and lipid droplet formation. For this purpose, PPARγ induces expression of several genes (see Figure 1-2b): 1) PC and PEPCK, which allows to use pyruvate as a precursor of glyceroneogenesis; 2) pyruvate dehydrogenase kinase 4 (**PDK4**), which inhibits PDH activity and blocks entry of pyruvate to Krebs cycle; and 3) CD36, which facilitates intake of FA. Thiazolidinediones (**TZD**), potent exogenous activators of PPARγ, are used in human medicine as insulin-sensitizers, because induction of adipogenic process enlarges storage capacity of WAT and allows for safety deposition of potentially toxic lipids.

PPARα, other important member of PPAR family, stimulates expression of CPT1 and consequently increases the rate of β-oxidation (Rakhshandehroo, et al. 2010). Interestingly, PPRE is contained also in promotor of UCP1 (see Figure 1-2b). Therefore, both PPARα and PPARγ agonists induce expression of UCP1 in BAT (Barbera, et al. 2001; Petrovic, et al. 2010). Nevertheless, PPARγ itself is repressed by thermogenic activation (Lindgren, et al. 2004), which led to assumption that rather PPARα controls UCP1 expression in mature brown adipocyte, whereas PPARγ may play a role in differentiation of these cells (Villarroya, et al. 2007). In spite of its predominantly catabolic action, PPARα was also shown to induce glyceroneogenesis in PPARγ-independent manner (Mazzucotelli, et al. 2007).

PPARs tightly cooperate with proteins from family of PPARγ coactivators 1 (**PGC-1**, namely PGC-1α and PGC-1β). These proteins represent major integrators of cellular metabolism. PGC-1α with PPARs stimulate expression of UCP1 both in BAT (Puigserver, et al. 1998) and brite cells, while PGC-1β is essential for TZD-induced mitochondrial biogenesis (Pardo, et al. 2011). Besides PPARs, PGC-1 cooperates with many others transcription factors (see Figure 1-2b), such as estrogen-related receptors and nuclear respiratory factors (NRF), which control the expression of mitochondrial genes encoded in nucleus and indirectly also in mtDNA (Scarpulla 2006). Generally, PGC-1 mRNA is often measured as marker of mitochondrial biogenesis. The PGC-1 activity is regulated in very complex manner (see Figure 1-2a and b) on the level of gene transcription, translation, posttranslational modifications (such as stimulatory phosphorylation and inhibitory acetylation), and recruitment to gene promotors by interaction with other proteins, as mentioned above.

PRDM16 (PR domain containing 16, one of zinc finger transcription factors) is another protein often present in transcription complexes with PPARs and PGC-1. It is found only in BAT and to smaller extent in some WAT depots where its content corresponds with their propensity to browning (Kajimura, et al. 2010).

As obvious from previous paragraphs, browning program involves synergistic activity of PPARs, PGC-1, PRDM16 and some others transcription activators. These factors not only assemble common transcription complexes, but also influence each others expression as was shown for example on PPARα-dependent induction of PGC-1α transcription (Hondares, et al. 2011). Therefore, stimulation of single transcription factor can resulted in induction of whole browning program (Hondares, et al. 2011; Puigserver, et al. 1998; Seale, et al. 2007; Tiraby, et al. 2003).

Generally, catabolic stimulators (PPARα, PRDM16) are more abundant in BAT, where increased rate of substrate oxidation is always connected with mitochondrial uncoupling and thermogenesis. Also induction of these proteins in WAT results in browning (or at least UCP1-independent mitochondrial biogenesis and lipid catabolism). Similarly to inductors of lipogenesis, signaling pathways increasing lipid catabolism are also often involved in stimulation of glyceroneogenesis and FA re-esterification.

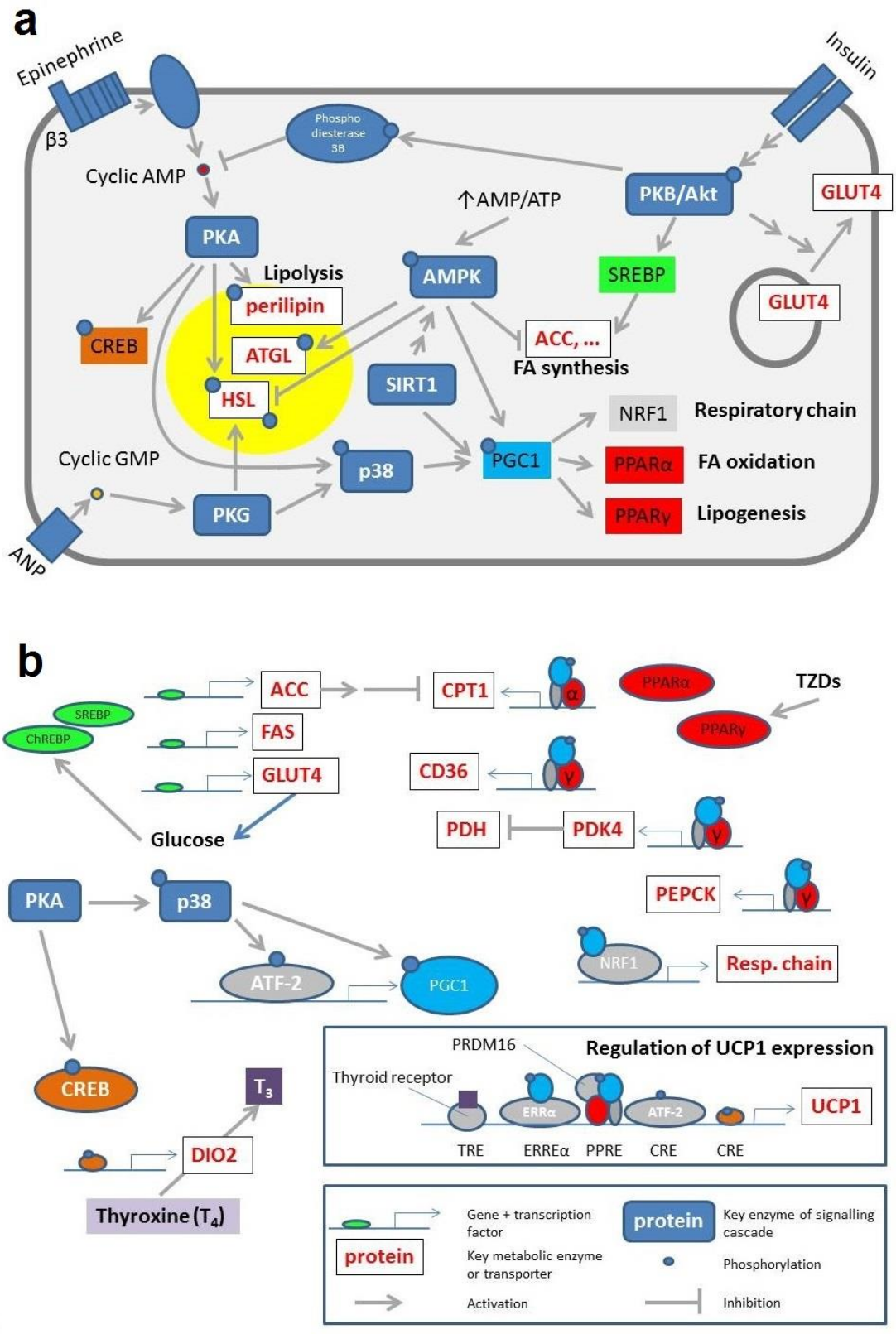

Fig. 1-2 Overview of regulation of metabolism in adipose tissue
a) Signaling cascades involved in hormonal regulation
b) Main transcriptional factors and their role in regulation of gene expression (in box below – scheme of UCP1 promoter)

1.4.2 Autoregulatory circuits sensing energy state

Most of the cells regulate their metabolism with respect to own acute energy status expressed as pool of ATP. This is essential in particular for WAT. Some enzymes of energy metabolism are inhibited or stimulated directly by binding of ATP and AMP. However, even more enzymes and transcription factors are influenced by AMP/ATP ratio indirectly via activity of AMP-activated kinase (AMPK), the master regulator of cellular energy state.

AMPK is heterotrimeric protein complex whose regulatory γ-subunit contains domains with ability to bind AMP or ATP (reviewed in (Towler and Hardie 2007)). Thus, adenosine nucleotides compete for this site with the opposite effects on AMPK activation status. The rise in AMP/ATP ratio (e.g. during exercise or fasting) leads to AMP binding which results not only in 5-fold induction of AMPK activity but also in conformational changes including exposure of Thr172 of catalytic α-subunit to phosphorylation by other kinases which can further increase the activity up to 100-fold. Phosphorylation of Thr172 is relatively reliable and widely used marker of AMPK activity.

AMPK phosphorylates numerous substrates in order to return AMP/ATP ratio to normal values. Hence, ATP consuming pathways are inhibited, and ATP producing pathways stimulated. Classically, AMPK is known to block synthesis of FA and cholesterol by inhibitory phosphorylation of ACC and 3-hydroxy-3-methyl-glutaryl-CoA reductase, respectively (Carling, et al. 1987). FA synthesis is further inhibited by blocking of SREBP-1c and ChREBP. Inactivity of ACC causes decline in concentration of malonyl-CoA, which enables CPT1 to transport FA-CoA to mitochondria and triggers β-oxidation. Also activity of LPL is elevated in response to AMPK resulting in increased uptake of FA, which can be consequently used as a substrate for β-oxidation or re-esterification. Moreover, AMPK is probably also involved in posttranslational activation of PGC-1 (Terada, et al. 2002) leading to elevated mitochondrial biogenesis and increase in oxidative capacity.

Regulation of lipolysis by AMPK is very complex. In long term, AMPK inhibits HSL (Daval, et al. 2005; Djouder, et al. 2010), but activates ATGL (Ahmadian, et al. 2011; Bezaire, et al. 2009; Gaidhu, et al. 2009). It means that under stimulation of AMPK, TAG are not fully hydrolyzed, but rather converted to diacylglycerols. Diacylglycerol accumulation can further promote FA re-esterification (Bezaire, et al. 2009). There is also indirect evidence, that AMPK stimulates PEPCK and PDK4 expression in WAT during exercise (compare (Ruderman, et al. 2003) and (Wan, et al. 2012)).

Since mitochondrial biogenesis and lipid catabolism is often accompanied by UCP1 induction in browning WAT, the potential of AMPK for stimulation of UCP1 in brite cells

was also studied; however, with conflicting results. Prolonged AMPK activation using 5-aminoimidazole-4-carboxamide ribonucleotide failed to induce UCP1 in rats (Gaidhu, et al. 2009), but let to occurrence of some UCP1-positive cells in eWAT of mice (Vila-Bedmar, et al. 2010). Considering the role of AMPK in recovery of ATP, the UCP1 induction in WAT seems to be inconsistent with the general AMPK activity. For the same reason, AMPK role in BAT is also questionable.

The function of energy sensors in BAT is much less studied. If UCP1 is ectopically expressed in WAT (such as in case of ap2-UCP1 transgenic mouse), AMPK responses to UCP1-caused decrease in AMP/ATP ratio by activation of mitochondrial biogenesis and β-oxidation (Rossmeisl, et al. 2002), and inhibition of both lipolysis (Flachs, et al. 2002) and FA synthesis (Rossmeisl, et al. 2000). This suggests the role of AMPK in promoting ATP production in uncoupled cells; however, it is not clear if this model corresponds to physiological conditions in BAT. It was shown that activity of α1 AMPK isoform is very high in BAT already in basal state and even increases with chronic cold exposure independently on norepinephrine (Mulligan, et al. 2007). Nevertheless, the exact role of AMPK in BAT as well as the mechanism of its induction remains to be elucidated.

AMPK is not the only sensor of energy status in adipocyte. Deacetylase SIRT1, which is thought to mediate effects of calorie restriction, responds to elevated NAD^+/NADH ratio. Among others, SIRT1 deacetylates PGC-1α, thus contributing to its activation (Nemoto, et al. 2005). Furthermore, SIRT1 also induces LKB1 translocation from nucleus to cytoplasm, where this enzyme phosphorylates Thr172 of AMPKα (Lan, et al. 2008). Thus, SIRT1 and AMPK cooperate on maintaining stable energy status of white adipocyte.

1.4.3 Hormonal and neuronal regulation

Metabolism of adipose tissue is influenced also by central regulation. It is one of the areas where WAT and BAT differs dramaticaly from each other. WAT must sensitively react to the cyclic alteration of postprandial and fasting state as well as to the acute stress stimuli. It has to keep the energy homeostasis in long term. Therefore, it is regulated by catecholamines, insulin, glucocorticoids, and numerous paracrine and endocrine factors derived from many cell types including immune cells. On the other hand, the most (if not the only) important regulation of BAT is provided by sympathetic nervous system in cooperation with thyroid hormones.

Adrenergic stimulation is thus crucial for BAT and very important for WAT. Since glucagon was shown to lack any effect on WAT, catecholamines are thought to be main catabolic agens in this tissue (Gravholt, et al. 2001). Generally, catecholamines stimulate mobilization of lipid stores (see Figure 1-2a), eventually followed by FA oxidation in uncoupled mitochondria, which results in induction of thermogenesis in BAT and lipolysis (or even browning) in WAT. Adipocytes contain β-adrenergic receptors, namely special isoform β3. Lack of β3 receptors severely depresses brite cells occurrence in WAT, but can be compensated by other β adrenoreceptors in BAT (Jimenez, et al. 2003).

All adipocytes are innervated by sympathetic nerves producing norepinephrine. Moreover, β3 adrenoreceptors (especially in WAT) can be influenced by epinephrine from blood as well. The signaling pathway is depicted in Figure 1-2a. Once activated, β3 receptors stimulate adenylate cyclase via G proteins which results in increase in concentration of cyclic AMP (cAMP) and subsequent activation of protein kinase A (**PKA**). PKA stimulates lipolytic activity of HSL and phosphorylates perilipin which in turn dissociates from surface of lipid droplet and loosen the blockade of lipolytic enzymes. In contrast, ChREBP is inhibited by PKA; therefore, FA synthesis is attenuated.

Moreover, PKA can also regulate gene expression by phosphorylation of cAMP response element-binding protein (CREB) and p38 mitogen-activated protein kinases (p38 MAPK) (Cao, et al. 2004). MAPKs were shown to enhance glyceroneogenesis via stimulated expression of PDK4 by PPARγ-dependent mechanism (Wan, et al. 2010). In BAT, phosphorylated CREB induces expression of II iodothyronine deiodase 2, which in turn converts thyroid hormone thyroxine to much more active triiodothyronine (**T3**). Bound to thyroid receptor, T3 contributes to regulation of gene expression. On the other hand, p38 MAPKs increase expression of PGC-1α (via activating transcription factor 2, **ATF-2**) and activate the PGC-1α by phosphorylation. All these steps are involved in stimulation of UCP1 expression in BAT and brite cells (see Figure 1-2b). UCP1 promotor contains sequences for binding of thyroid recepror, complex of PGC-1α with PPARs, activating transcription factor 2, and CREB (reviewed in (Bonet, et al. 2013)). One of the genes whose expression is induced in BAT upon adrenergic stimulation is also LPL which increases clearance of FA from blood (Mitchell, et al. 1992).

Adrenergic stimulation thus leads to increased lipolysis, FA re-esterification, mitochondrial biogenesis, and in BAT (and white depots prone to browning) also to recruitment of UCP1. Lipolysis then liberates fatty acids which acutely activate UCP1. Therefore, norepinephrine from sympathetic system is essential both for production and

activation of UCP1 in BAT (Cannon and Nedergaard 2004). On the other hand, in most white adipocytes, catabolic effect of catecholamines is not accompanied by mitochondrial uncoupling. Produced ATP can be thus consumed e.g. by TAG/FA cycle (see Discussion).

The effects of atrial and brain natriuretic peptides (**ANP** and **BNP**) are very similar to those of catecholamines (Bordicchia, et al. 2012). Their receptor NPRA (natriuretic peptide receptor A) directly produces cyclic GMP which activates protein kinase G (**PKG**). PKG subsequently phosphorylates HSL and perilipin, and triggers the thermogenic program, just as PKA. Contrarily to PKA, PKG signaling is not inhibited by insulin (see below).

The main counterpart of catecholamines in WAT is **insulin**. Insulin is secreted from pancreas in postprandial state in response to elevated glycemia. Insulin receptor is membrane tyrosine kinase, whose activation is mediated by phosphorylated insulin receptor substrates, phosphoinositide-3-kinase, and membrane phosphoinositides and results in stimulation of protein kinase B (**PKB**, also known as Akt, see Figure 1-2a). PKB activates enzyme phosphodiesterase 3B (Wijkander, et al. 1998) which interfers directly with β-adrenergic pathway by cleavage of cAMP (but not cGMP). Through several intermediate steps downstream PKB, gene expression of numerous genes is influenced (e.g. induction in lipogenic genes regulated by SREBP-1c), which collectively leads to stimulation of FA synthesis. Moreover, glucose uptake is accelerated due to translocation of glucose transporter GLUT4 to membrane. As a result, adipocyte receives higher amount of glucose, which is then converted to G3P and FA and stored as TAG in lipid droplet.

Some members of insulin signaling pathway (such as IRS1 and PKB) can be inhibited by phosphorylation or dephosphorylation of certain aminoacid residues (Lafontan 2008). Such a desensitization of insulin signaling pathway results in insulin resistance (**IR**), the early event of metabolic syndrome progression. Kinases mediating these phosphorylations (such as enzymes from NFκB and JNK pathway) are often related to chronic inflammatory state and thus represent a specific example of mutual interconnection between immune system and metabolic fluxes. This topic is discussed in following chapter.

1.5 Interplay of adipocytes and immune cells

WAT consists not only of adipocytes but contains also numerous other cell types, particularly important portion of immune cells. Especially macrophages can comprise up to 40% of total cell number in obese WAT while their number correlates with the degree of obesity (Weisberg, et al. 2003; Xu, et al. 2003). The macrophage infiltration is related to

chronic inflammatory state of hypertrophic WAT and represents strongly predictor for development of type 2 diabetes (Kloting, et al. 2010). Inflammatory signaling often interfers with insulin pathway causing insulin resistance. Chronic inflammation of WAT can impair response to insulin in other tissues. For instance, ceramide biosynthesis induced by certain cytokines is reflected by increased ceramide levels in plasma and inhibition of PKB activity in many relevant organs (Haus, et al. 2009). On the contrary, healthy WAT secretes insulin sensitizing hormone adiponectin which counteracts the deleterious effects of ceramide accumulation (Holland, et al. 2011).

Inflammatory process occurs in advanced stages of obesity. It is characterized by gradual decrease in number of anti-inflammatory leukocytes (such as eosinophils, regulatory T cells and T_{H2} cells) and increase in others (such as neutrophils, T_{H1} cells, mast cells) (reviewed in (Masoodi, et al. 2014). Regulation of the WAT inflammation involves many cytokines and lipid mediators, produced both by adipocytes and leukocytes. Interestingly, the resolution of inflammation is also an active process which includes apoptosis and efferocytosis of immune cells. The process is under control of specific lipid signaling molecules from groups of lipoxins (derived from arachidonic acid), resolvins (derived from ω-3 PUFA), maresins, and protectins (derived from docosahexaenoic acid). In general, most derivatives of arachidonic acid serve as mediators of inflammation, whereas ω-3 PUFA are often converted into pro-resolving factors. This fact provides the explanation how dietary lipid composition can influence the inflammatory status of WAT and the whole body insulin sensitivity.

The degree of inflammation is tightly connected to metabolic changes in adipose tissue. Since total number of adipocytes in adult humans is practically constant (Kissebah and Krakower 1994), increased lipid accumulation leads to their hypertrophy, connected with increased risk of cell death. In response to hypertrophy and necrosis, the profile of molecules secreted from adipocyte is changed. For instance, production of monocyte chemotactic protein 1 (MCP1) increases, which attracts macrophages from blood (Kanda, et al. 2006). Macrophages then aggregate around necrotic adipocytes while forming syncytia known as crown-like structures (**CLS**) and scavenging residual adipocyte lipids. Therefore, the necrosis in WAT probably represents the first cause of inflammatory response.

The above described pro-inflammatory type of macrophages is referred as classicaly activated cells, or **M1** macrophages. They secrete whole set of pro-inflammatory cytokines such as tumour necrosis factor α, and interleukins 1β, 6 and 12. The number of these macrophages correlates with insulin resistance (Fujisaka, et al. 2009). Apart from this type, macrophages can be also converted to anti-inflammatory, alternatively-activated **M2** cells

(reviewed in (Lumeng, et al. 2008)). This switch is triggered by interleukin 4 produced mainly by eosinophils (Wu, et al. 2011). M2 macrophages produce in turn anti-inflammatory cytokines such as interleukin 1 and 10. They promote remodeling of WAT and clearance of apoptotic cells. M2 also induce production of insulin-senzitizing hormone adiponectin in adipocytes.

Immune status of WAT is directly linked to adipocyte metabolism. Many paracrine signaling molecules involved in inflammatory response influence also rate of lipolysis in adipocytes. Especially the effects of cyclooxygenase-produced derivatives of arachidonic acid are well described: Prostaglandins E2 (PGE2) and F2α (PGF2α) inhibit adipogenesis (Mater, et al. 1998; Yan, et al. 2003) which is related to lower lipolytic rate. In contrast, 15-deoxy-prostaglandin J2 (**15-d-PGJ2**), a potent ligand of PPARγ, induces adipogenesis while interfering in production of PGE2, PGF2α, and inflammatory adipokines (Hossain, et al. 2012).

Greater number of M1 macrophages in visceral WAT (in comparison with scWAT) can be explained by higher rate of both basal and stimulated lipolysis in eWAT. Elevated lipolysis produce increased amount of NEFA which promote infiltration of M1 macrophages (Long, et al. 2013). Interestingly, the period of weight reduction is also accompanied by increased lipolysis and macrophage accumulation. However, the M2 phenotype is predominant under these conditions (Kosteli, et al. 2010). In order to normalize FA level in WAT interstitium, M2 macrophages probably secrete some unknown factor reducing lipolysis in adipocytes (Kosteli, et al. 2010). Furthermore, M2 actively absorp free FA. Part of these FA can be used for oxidative phosphorylation in mitochondria, while the resultant ATP covers the energy cost for esterification of the other part of FA. Therefore, level of oxidative phosphorylation is relatively high in M2 cells, especially in contrast to M1 macrophages relying mostly on glycolysis (O'Neill and Hardie 2013). Since M1 and M2 differ dramatically in preferred catabolic pathways and energy demands, AMPK is likely to play an important role in M1/M2 switch (O'Neill and Hardie 2013).

Moreover, leukocytes can play important role also in BAT activation and WAT browning. Namely, M2 macrophages serve as an important source of norepinephrine. Hence, M2 depletion causes severe failure in induction of BAT thermogenesis and decreases the occurrence of brite cells in WAT (Nguyen, et al. 2011; Qiu, et al. 2014).

1.6 Dietary and pharmacological activation of adipose tissue metabolism

Metabolism of adipose tissue can be influenced by many experimental treatments. This topic is of particular interest considering the general effort to development of strategies to counteract obesity and insulin resistance. Processes of adipose tissue mobilization are predominantly regulated by adrenergic signaling pathway and involve also some subordinate regulating systems, such as AMPK, or complex of PPAR transcription factors. Increased sympathetic tonus (in response to cold exposure) results in activation of thermogenesis in BAT and lipid catabolism in WAT. Eventually, the stimulation of WAT can also lead to increased mitochondrial biogenesis and FA oxidation, and even to UCP1 induction in WAT.

Most treatments influence the metabolism of both BAT and WAT in the same time. Administration of leptin influences control centres in hypothalamus and induces sympathetic activity which activates BAT on the one hand and cause WAT browning on the other hand (Kakuma, et al. 2000; Lee, et al. 2002; Wang, et al. 1999). Some neuropeptides (e.g. brain derived neurotrophic factor – **BDNF** and TLQP-21) acts also on hypothalamus but induce more potently WAT than BAT (Bartolomucci, et al. 2006; Cao, et al. 2011). Interestingly, even the living in enriched environment with complex physical and social stimulation led to WAT browning in comparison to standard housing conditions, which was ascribed to involvement of BDNF (Cao, et al. 2011).

Adrenergic system works in cooperation with thyroid hormones (as described in chapter 1.6.1 considering the possible role of bile acids in potentiation of thyroid hormone action). In parallel to norepinephrine-activated PKA, also the PKG can be involved in the regulation (see Figure 1-2a). Therefore, cardiac natriuretic peptides stimulate both BAT and WAT (Bordicchia, et al. 2012).

Besides hormonal axes, adipose tissue can be affected by direct activation of some transcription factors. Both ligands of PPARα (such as bezafibrate (Cabrero, et al. 1999; Hondares, et al. 2011)) and PPARγ (such as TZDs (Hondares, et al. 2006)) stimulates lipid catabolism in BAT and WAT and to smaller extent also browning of WAT. Similarly, some prostaglandins act as PPARγ ligands, while others rather bind to membrane receptors. It was shown that prostaglandins E2 and I2 causes occurrence of BAT-like cells in some WAT depots, but the mechanism is not yet fully understood (Madsen, et al. 2010; Vegiopoulos, et al. 2010).

Some other signaling molecules were schowed to influence adipose tissue metabolism. Irisin, hormone produced in muscle in response to exercise and acting selectively on WAT

browning, inspired hopes for fast development of new therapeutic strategy (Bostrom, et al. 2012); however, its role in humans was questioned recently (Elsen, et al. 2014). Similarly, fibroblast growth factor 21, known mainly for its metabolic effects in liver, was suggested to act as paracrine/autocrine agent, which helps to activation of BAT and browning of scWAT in response to norepinephrine stimulation (Fisher, et al. 2012). Moreover, bone morphogenetic protein 7, expressed predominantly in brain and kidney, is thought to be necessary for development of BAT (Tseng, et al. 2008), whereas its effects on WAT are not clear (compare (Tseng, et al. 2008) and (Schulz, et al. 2011)). Its effect on BAT can be observed only in subthermoneutral conditions, which suggests its dependance on adrenergic stimulation (Boon, et al. 2013).

All these compounds can be used in modulation of adipose tissue metabolism. Besides cold exposure, we have used several other approaches in our experiments: supplementation of the diets with bile acids and ω-3 PUFA, which interact with above mentioned mechanisms, or calorie restriction. The published data about these strategies are discussed in following sub-chapters, while our own results are described in detail in the experimental part of thesis (chapter 4).

1.6.1 Bile acids

Bile acids, end-products of cholesterol catabolism, are essential for lipid absorption because they emulsify fat. Primary bile acids are synthesized in liver and secreted as a part of bile into intestine, where they can be converted by gut microbiota to secondary bile acids. Moreover, all bile acids can be further conjugated to glycine or taurine in order to increase their solubility, which creates considerable variability of this set of chemicals. In humans, bile acid pool consists mainly of primary cholic and chenodeoxycholic acid (**CDCA**), and secondary deoxycholic acid (in ratio 40:40:20). In contrast, most of CDCA in mice is hydroxylated in the 6-position producing muricholic acids (reviewed in (Li and Chiang 2012)).

Bile acids are natural ligands of hepatic farnesoid X receptor (**FXR**) α. As activated FXR suppress expression of cholesterol 7 alpha-hydroxylase, the rate limiting enzyme in the bile acid synthesis, this mechanism provides important negative feedback loop in regulation of bile acid levels. However, it was shown, that FXR also down-regulates hepatic fatty acid and triglycerides synthesis and very-low-density lipoprotein production mediated by SREBP-1c (Watanabe, et al. 2004) and increase TAG clearance from plasma (Kast, et al. 2001). Moreover, FXR is also important for prevention of insulin resistance (Stayrook, et al. 2005)

and hypoglycemia during fasting (Cariou, et al. 2006), production of hepatic glycogen (Duran-Sandoval, et al. 2005) and differentiation of adipocytes (Abdelkarim, et al. 2010), Hence, new pharmaceutical strategies, including the use of natural bile acids and their semi-synthetic analogues, are being currently developed in order to regulate whole-body energy metabolism.

Added to FXR, bile acids stimulate also other receptor, G-protein-coupled receptor TGR5 (Kawamata, et al. 2003; Maruyama, et al. 2002). A set of articles from the group of Auwerx demonstrates involvement of this receptor in stimulation of energy expenditure in BAT (Watanabe, et al. 2011; Watanabe, et al. 2006; Watanabe, et al. 2012). The binding of cholic acid to TGR5 results in elevation of cAMP level and consequent activation of iodothyronine deiodinase (Watanabe, et al. 2006). Bile acids, therefore, facilitate the thyroid hormone stimulatory influence on BAT thermogenesis. It was claimed that due to this mechanism, decrease in bile acid synthesis in response to FXR activation leads to decrease in TGR5-mediated energy expenditure (Watanabe, et al. 2011). This result indicates that anti-obesogenic strategy targeting stimulation of FXR may be contraproductive considering the energy expenditure (Watanabe, et al. 2011).

In these studies, action of cholic acid was usually analyzed. It was also shown that many other bile acids, such as CDCA, influence the cell signaling and expression of certain genes in BAT in the same manner (Watanabe, et al. 2006). However, complex metabolic effects of these compounds with respect to BAT activity were never studied to the same extent as it was done with cholic acid.

Less is known about the influence of bile acids on UCP1 expression in WAT, i. e. WAT browning. The fact that action of many compounds on both BAT and WAT is overlapping suggests that bile acids may cause WAT browning as well. This assumption was indirectly tested on rats feeding with salmon protein hydrolysate rich in taurine and glycine, which are necessary for production of bile acid conjugates (Liaset, et al. 2011). In this experiment, the animals became resistant to obesity induced by high fat-feeding while their plasma levels of bile acids were elevated. This phenotype was associated with increased energy expenditure and induction of genes involved in energy metabolism and uncoupling (Ucp1, deiodinase 2 and Pgc1α) in BAT, scWAT and eWAT (Liaset, et al. 2011).

On the whole, bile acids seem to be potent stimulators of mitochondrial uncoupling in adipose tissue. However, some data are still lacking, i. e. UCP1 upregulation was not assessed at the protein level so far, most of the studies were focused just on the cholic acid

and on the influence of direct administration of bile acids in the diet on WAT browning was never tested.

1.6.2 ω-3 polyunsaturated fatty acids of marine origin

Since mammalian cells lack Δ12- and Δ15-desaturase activity which are able to create double bonds in positions ω-6 and ω-3 from the methyl end of fatty acid, PUFA represent an essential component of both human and murine diet (reviewed in (Kopecky, et al. 2007)). Linoleic acid (LA, 18:2) is the precursor of all the ω-6 PUFA, whereas α-linolenic acid (ALA, 18:3) can be converted to all other ω-3 PUFA. Because the elongations and desaturations of LA and ALA are relatively inefficient (only 4-5% of ALA is converted up to docosahexaenoic acid), dietary lipid composition significantly influences amount of individual PUFA in body.

Physiologically most important PUFA are arachidonic (**AA**, 20:4 ω-6), eicosapentaenoic (**EPA**, 20:5 ω-3), and docosahexaenoic acid (**DHA**, 22:6 ω-3). Once liberated from membrane phospholipids by phoshpolipase A_2, all these three PUFA can become substrates of enzymes like cyclooxygenase-1, cyclooxygenase-2, 12-lipoxygenase, 15-lipoxygenase, and cytochrome P450 epoxygenase, which creates bioactive molecules of eicosanoids and docosanoids. As was already described in chapter 1.5, AA-derived eicosanoids (with exception of J series prostaglandines) induce predominantly inflammation, while EPA- and DHA-based lipid mediators act usually in anti-inflammatory mannor. As both ω-3 and ω-6 PUFA compete for the same enzymes, their synthetic rates are mutually influenced and the ratio of ω-6/ω-3 is of great importance.

Both PUFA and some of their metabolites (in particular 15d-PGJ2) activates PPAR nuclear receptors which effect can explained both the observed induction of BAT thermogenesis (Oudart, et al. 1997) and induction of oxidative metabolism in WAT (Flachs, et al. 2005) in response to increased intake of EPA and DHA. The possible role of prostanoids in WAT browning was already mentioned; nevertheless, ω-3 administration is not sufficient for induction of Ucp1 expression in WAT (Flachs, et al. 2005).

All the above mentioned mechanisms contibute to hypolipidaemic, cardioprotective, and obesity-preventing effects of ω-3 PUFA in rodents and (to smaller extent) probably also in humans (reviewed in (Flachs, et al. 2014)). However, as the beneficial effects of ω-3 PUFA are rather limited in humans, research of treatments which could be able to potentiate EPA

and DHA action is needed. One of possible combination treatment is concurrent ω-3 supplementation and calorie restriction as was already tested in obese patients by our group (Kunesova, et al. 2006) and others (Su, et al. 2014).

1.6.3 Calorie restriction

Calorie restriction is so far the most efficient strategy to prolong healthy life in several species (Nisoli, et al. 2005). Severe calorie restriction is accompanied by body weight loss with elevated rate of lipolysis and all the consequences described in chapter 1.5. Limitation of available food represents substantial stressor for experimental animals. Thus, it is probably connected to increased tonus of sympathetic nervous system which augments the catabolism in adipose tissue. Furthermore, calorie restriction changes the energy status of the cell and activates AMPK and SIRT1 (reviewed in (Lam, et al. 2013)). This collectively results in induced mitochondrial biogenesis and lipid oxidation in WAT without UCP1 induction.

These assumptions are at least partially confirmed by experiments with resveratrol (Lagouge, et al. 2006; Mercader, et al. 2011; Rayalam, et al. 2008), a polyphenolic compound from red grapes, which is traditionally thought to act as mimetic of calorie restriction (Lam, et al. 2013). Resveratrol treatment triggers mitochondrial biogenesis in many organs including muscle (Lagouge, et al. 2006), liver (Baur, et al. 2006) and BAT (Lagouge, et al. 2006). In WAT, activity of ATGL is stimulated by resveratrol (Lasa, et al. 2012) and lipolysis is increased. Nevertheless, *in vivo* data supporting the role of resveratrol in browning program are lacking (Bonet, et al. 2013).

2. Aims of the thesis

The general goal of the thesis was to investigate several possible approaches to modulation of energy balance, namely by influencing metabolic fluxes in both BAT and WAT. The main focus was on specific role of stimulated mitochondrial function, UCP1-dependent energy dissipation and UCP1-independent substrate futile cycling.

Specific aims were the following:

1) to verify the expected stimulatory action of bile acid CDCA on brown adipose tissue recruitment in mouse, and to evaluate contribution of the increased energy expenditure to whole-body energy balance;

2) to investigate possible effects of CDCA on "browning" of susceptible WAT depots, and to learn whether the "brite" adipocytes can significantly increase whole-body energy expenditure;

3) to study the potential of calorie restriction and ω-3 PUFA to counteract deleterious consequences of high-fat feeding, and to characterize the mechanisms of beneficial influence of the treatment with respect to probable involvement of mitochondria in WAT;

4) to characterize the model of cold adaptation of two strains of mice (AJ and B6) differing in their propensity to obesity and associated disorders; to investigate BAT recruitment and scWAT browning in these animals;

5) to test the involvement of TAG/NEFA futile cycling in WAT in resistance to obesity using the above murine model, while stimulating metabolism of the mice by cold exposure; to compare this model with effects of combination treatment of ω-3 PUFA and calorie restriction.

3. Methods

In this section, I describe in detail only the methods, which I have used by myself (chapters 3.2, 3.3 3.6, 3.7, 3.8.1, 3.9, 3.10, 3.11, 3.12, 3.15, 3.16). The list of materials and equipment for these methods is attached as chapter 3.1. For greater clarity, providers of the materials are specified in the text of chapters 3.2 – 3.15 as well.

All other methods (chapter 3.4, 3.5, 3.8.2, 3.13, 3.14) used in the publications are described at least briefly, because they are important for following interpretation of general results. The names of the responsible colleagues are also mentioned and references are also added. These parts of text can be also distinguished by smaller font size.

3.1 List of material and equipment

General laboratory material and equipment used for several methods

Inorganic salts ($CaCl_2$, KCl, MgCl, NaCl, $NaHCO_3$, KH_2PO_4, K_2HPO_4, $Na_2HPO_4.12H_2O$, $MgSO_4.7H_2O$, $CuSO_4.5H_2O$) were acquired from Lachema (CR), Penta (CR) or Sigma (USA) at least in Reagent grade purity.

Bovine serum albumin ..... Amresco, USA
Ethanol ..... Penta, CR
Ethylenediaminetetraacetic acid (EDTA) ..... Serva, Germany
Diethylether (anesthetic) ..... Penta, CR
Glucose ..... Penta, CR
4-(2-hydroxyethyl)-1-piperazineethanesulfonic acid (HEPES) Serva, Germany
Methanol ..... Penta, CR
Pneumoxide (95% O_2, 5% CO_2) ..... Linde, CR
Sucrose ..... Penta, CR
Tris(hydroxymethyl)aminomethane) (Tris) ..... Sigma, USA

Analytical scales Pioneer ..... OHAUS, USA
Automatic pipettes ..... Gilson, France
Centrifuge Universal 320R ..... Hettich, Germany
Magnetic stirrer ..... IKA, USA
Mini centrifuge ..... Labnet, USA
MS 3D plate shaker ..... IKA, USA
pH meter InLab level ..... WTW, Germany
Scales Adam ..... Adam Equipment, UK
SigmaPlot 10 statistical software ..... SYSTAT, USA
Sonicator ..... Hielscher, Germany
Surgical instruments ..... Medin, CR
Thermal incubator ..... Biometra, Germany
Thermal incubator ..... Sanyo, Japan
Ultra-Turrax T8.01 disperser ..... IKA, Germany
Umetrics SIMCA-P+12 statistical software ..... Umetrics, Sweden
Vortex mixer ..... Scientific Industries, USA

Diets (chapter 3.2)

Standard chow diet (Ssniff EF R/M-H) ..... Ssniff, Germany

Constituents of high-fat diet (per 1 kg)
Corn oil (250 g) ..... Oleofarm, Poland
Corn starch (10 g) ..... Maizena, CR
Standard chow diet (400 g) ..... Ssniff, Germany
Sunar (340 g) ..... Hero, Switzerland

Chenodeoxycholic acid (CDCA) ..... Sigma, USA
EPA/DHA concentrate (EPAX 1050 TG) ..... EPAX, Norway

Plasma parameters (chapter 3.3)
See Table 3-a in chapter 3.3

OneTouch Ultra glucometer glucometer ..... Life Scan, USA

Primary hepatocytes isolation and cultures (chapter 3.6)
Dexamethasone ..... Sigma, USA
Insulin ..... Novo-Nordisk, Denmark
Ketamine (Narketal) ..... Vétoquilol, France
Medium-199 ..... GIBCO, USA
Penicillin-streptomycine ..... GIBCO, USA
Triiodothyronine ..... Sigma, USA
Trypan Blue dye ..... Sigma, USA
Type II collagenase ..... Sigma, USA
Ultraser G ..... GIBCO, USA
Xylazine (Xylapal) ..... Vétoquilol, France

Mitochondrial oxidative capacity assessment (chapter 3.7)
Antimycin A ..... Sigma, USA
Aprotinin (inhibitor of serine proteases) ..... Fluka, CR
Benzamidine ..... Sigma, USA
Carbonyl cyanide-4-(trifluoromethoxy)phenylhydrazone (FCCP) Sigma, USA
Cytochrom c ..... Sigma, USA
Digitonin ..... Sigma, USA
n-Dodecyl β-D-maltoside ..... Sigma, USA
Glycerol-3-phosphate ..... Sigma, USA
Leupeptin (protease inhibitor) ..... Sigma, USA
Oligomycin ..... Sigma, USA
Pepstatin (inhibitor of aspartyl proteases) ..... Sigma, USA
Phenylmethylsulfonyl fluoride (PMSF) ..... Sigma, USA
Sodium dithionite ..... Sigma, USA
Succinate ..... Sigma, USA

Oxygraph 2k ..... Oroboros Instruments, Austria
Spectrophotometer UV-Vis8453 ..... Hewlett Packard, USA
Ultracentifuge ..... Beckman Coulter, USA

Measurement of FA oxidation (chapter 3.8.1)
[1-^{14}C]-palmitate ..... Perkin Elmer, USA
Fatty acid free bovine serum albumin (BSA – FA free) ..... ICN Biomedicals, UK
Hyamine hydroxide ..... Perkin Elmer, USA
Palmitic acid ..... Sigma, USA
Scintillation solution Ultima Gold ..... Perkin Elmer, USA

Beta counter ..... Hewlett Packard, USA

Nucleic acids (RNA isolation, quantitative RT PCR, chapters 3.10 and 3.12.1**)**
Bisbenzimide Hoechst 33258 ..... Serva, Germany
Chloroform ..... Penta, CR
Dynamo Capillary SYBR Green qPCR Kit ..... Finnzymes, USA
Deoxyribonucleoside triphosphates (dNTP) ..... Invitrogen, USA
Isopropyl alcohol ..... Serva, Germany

LightCycler® 480 SYBR Green I Master mix ..... Roche, Switzerland
M-MLV reverse transcriptase ..... Invitrogen, USA
Oligo thymidine (oligoT) ..... Generi Biotech, CR
PCR primers (for sequences see Table 3-c) ..... Generi Biotech, CR
Proteinase K ..... Merck, Germany
TRIzol ..... Sigma, USA

Fluorimeter Victor ..... Perkin Elmer, USA
Lasergene software ..... DNASTAR, USA
LightCycler® 480 System ..... Roche, Switzerland
Reverse transcription equipment TGradient ..... Biometra, Germany
Spectrophotometer NanoDrop ..... NanoDrop, USA
Vacuum centrifuge Heto Hetovac VR-1 ..... Thermo Scientific, USA

Proteins (concentration measurement, Western blotting, chapters 3.11 and 3.12.2**)**

Acrylamide ..... Serva, Germany
Ammonium persulfate (APS) ..... Sigma, USA
Dithiothreitol (DTT) ..... Sigma, USA
Glycine ..... Serva, Germany
Laemmli sample buffer ..... Bio-Rad, USA
2-Mercaptoethanol ..... Serva, Germany
N,N'-Methylenebisacrylamide ..... Serva, Germany
Odyssey blocker ..... Li-cor, USA
PageRulerTM Plus Prestained Protein Ladder ..... Thermo Scientific, USA
PVDF membrane Immobilon ..... Millipore, USA
Secondary infrared-dye-conjugated anti-mouse antibody ..... Rockland, USA
Sodium azide ..... Sigma, USA
Sodium bicinchoninate (BCA) ..... Sigma, USA
Sodium dodecyl sulfate (SDS) ..... Bio-Rad, USA
Tetramethylethylenediamine (TEMED) ..... Bio-Rad, USA
Triton X-100 ..... Serva, Germany
Tween 20 ..... Serva, Germany

AIDA software ..... Raytest, Germany
Electrophoretic equipment ..... Bio-Rad, USA
Odyssey IR Imager ..... Li-cor, USA
Semi-dry blotting equipment ..... Omni-Bio, CR

Nuclear magnetic resonance (chapter 3.15)

Acetic acid ..... Sigma, USA
Acetone ..... Sigma, USA
Chloroform (with amylines as stabilizers) ..... Sigma, USA
Deuterium oxide (^2H_2O) ..... CortecNet, France
Discovery DSC-Si SPE Tubes ..... Sigma, USA
2H pyrazine (pyrazine-d_4) ..... Sigma, USA
Hexafluorobenzene ..... Sigma, USA
Hexane ..... Sigma, USA
Methyl-t-buthyl-ether (MTBE) ..... Sigma, USA
Petrolether ..... Sigma, USA
Pyrazine ..... Sigma, USA
Silica-gel plates for thin-layer chromatography ..... Sigma, USA

Bruker Avance III HD 500 MHz system ..... Bruker, Germany
NUTS software ..... ACORN NMR, USA

3.2 General description of conducted experiments

All the presented studies are based on animal experiments and, when possible, supplemented by results obtained using primary cell culture models (Publication B).

C57BL/6J mice were obtained from the Jackson laboratory (Bar Harbor, ME, USA) and bred in our animal facility for several generations (Publications A and B). The mice were weaned onto standard laboratory chow diet (**STD**; energy density 13.0 $kJ.g^{-1}$, ~35.2% $wt.wt^{-1}$ of lipids, extruded R/M-H diet, Ssniff Spezialdiäten, Soest, Germany). In cold exposure experiments (Publication C), C57BL/6JBomTac mice (**B6 mice**) were directly ordered from Taconic (Denmark) and A/JOlaHsd mice (**AJ mice**) from Harlan (UK).

With the exception of publication C, animals were maintained at 20 °C on a 12:12-hr light-dark cycle with free access to water and (unless otherwise stated) to food. Mice were single-caged during the experiments. Body weight and food intake were monitored weekly. All the experiments were conducted according to the guidelines for the use and care of laboratory animals of the Institute of Physiology AS CR, v. v. i., the directive of the European Communities Council (86/609/EEC), and the Principles of Laboratory Animal Care (NIH Publication no. 85-23, revised 1985).

Publication A

2-month-old male mice were subjected to the high-fat-diet feeding (**cHF** - composite high-fat diet; energy density 22.8 $kJ.g^{-1}$, ~35.2% $wt.wt^{-1}$ of lipids, mainly corn oil (Kuda, et al. 2009)) for another 4 months to induce obesity and its comorbidities. After that, two different reversal experiments were conducted, as depicted in Figure 3-1:

In **8-week reversion experiment**, animals were randomly divided into 3 experimental groups (n = 10-12 per group) and fed for next 8 weeks ad libitum by respective experimental diet: the cHF diet, the cHF diet supplemented with 0.5% CDCA (0.5% CDCA, $wt.wt^{-1}$), or the cHF diet supplemented with 1% CDCA (1% CDCA, $wt.wt^{-1}$). CDCA was obtained from Sigma-Aldrich (St Louis, MO, USA; 95% pure).

During the 6^{th} week of the intervention 5 animals from each group were subjected to oral glucose tolerance test (OGTT, see below). At the end of 8^{th} week, animals were dissected in random fed state (between 8:30 and 10:30 am) and samples of blood, liver, epididymal and dorsolumbar WAT were collected for further analysis. Later TAG content was evaluated in liver and gastrocnemius muscle. Levels of TAG, NEFA, cholesterol, glucose, insulin,

adiponectin, and hepatic enzymes were determined in plasma. Moreover, feces were also collected for analysis of triglyceride and cholesterol content.

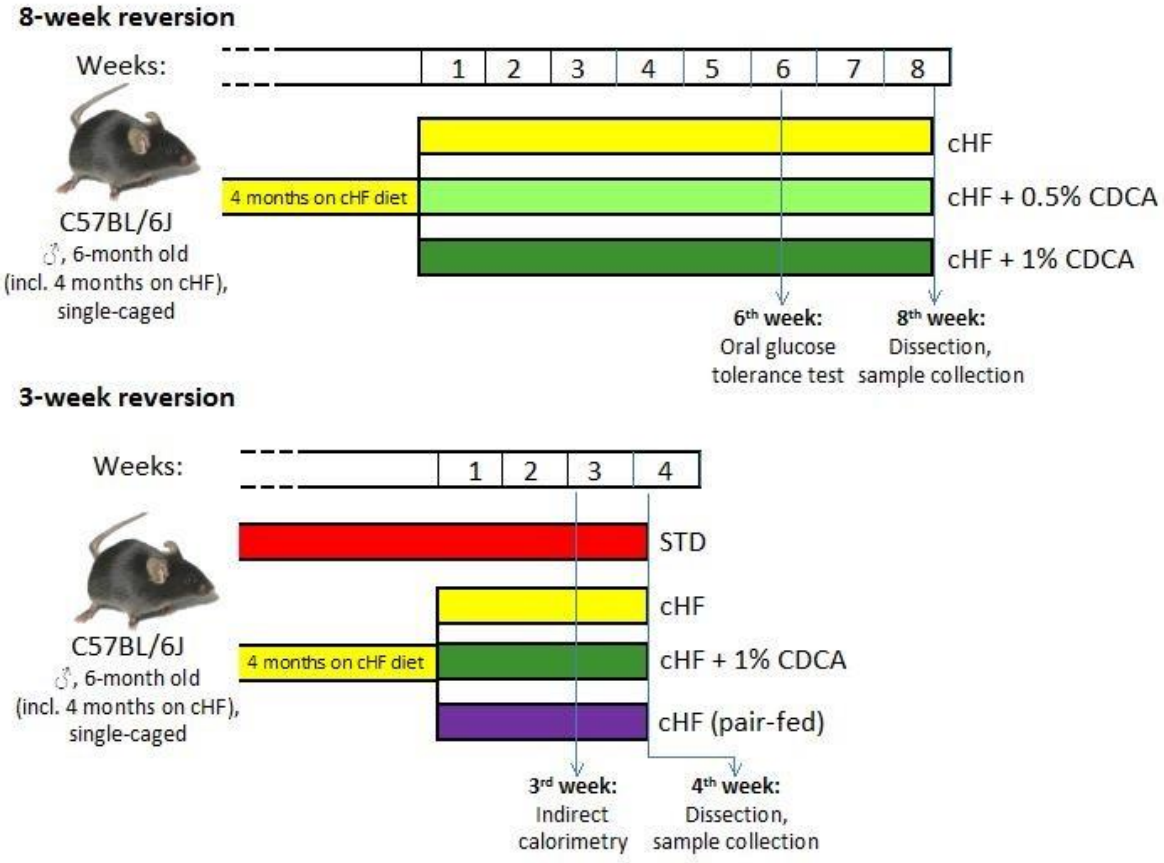

Fig. 3-1 Schema of experiments in publication A

In **<u>3-week reversion experiment</u>**, mice after 4-month cHF feeding were randomly divided into 3 groups (n = 8 per group) and assigned for 3 weeks to one of the following: (1) cHF; (2) cHF supplemented with 1% CDCA; and (3) pair-fed cHF (**PF**, i. e. food intake of this group was limited to that of animals on 1% CDCA diet. As a 4th group, animals fed STD diet since weaning were also included (n = 7). In this particular experiment, body weight and food intake were measured 4-times a week. Between 15th and 17th day of the treatment, indirect calorimetry (**INCA**) was performed. After 3 weeks, animals were dissected as in previous experiment and samples of BAT, eWAT and scWAT were collected. Later, those tissues were analyzed using immunohistochemistry, real-time quantitative PCR and immunoblotting.

Publication B

Several experiments were conducted in order to certify the results; nevertheless all of them followed the same scheme: 2-month-old male mice were habituated to cHF diet for 2 weeks and then assigned for 5 or 15 weeks to following treatments: (1) cHF, *ad libitum*; (2) cHF supplemented with long chain ω-3 PUFA concentrate (46% wt.wt^{-1} DHA, 14% wt.wt^{-1} EPA, product EPAX 1050 TG, EPAX, Ålesund, Norway) replacing 15% wt.wt^{-1} of dietary lipids (**cHF+F**), *ad libitum*; (3) **cHF+CR**, i. e. cHF with calorie restriction (**CR** - the ration of diet was reduced by 10% wt.wt^{-1} in comparison to animals fed *ad libitum* with the diet); (4) **cHF+F+CR** (i. e. cHF supplemented with ω-3 PUFA concentrate, 10% calorie restriction).

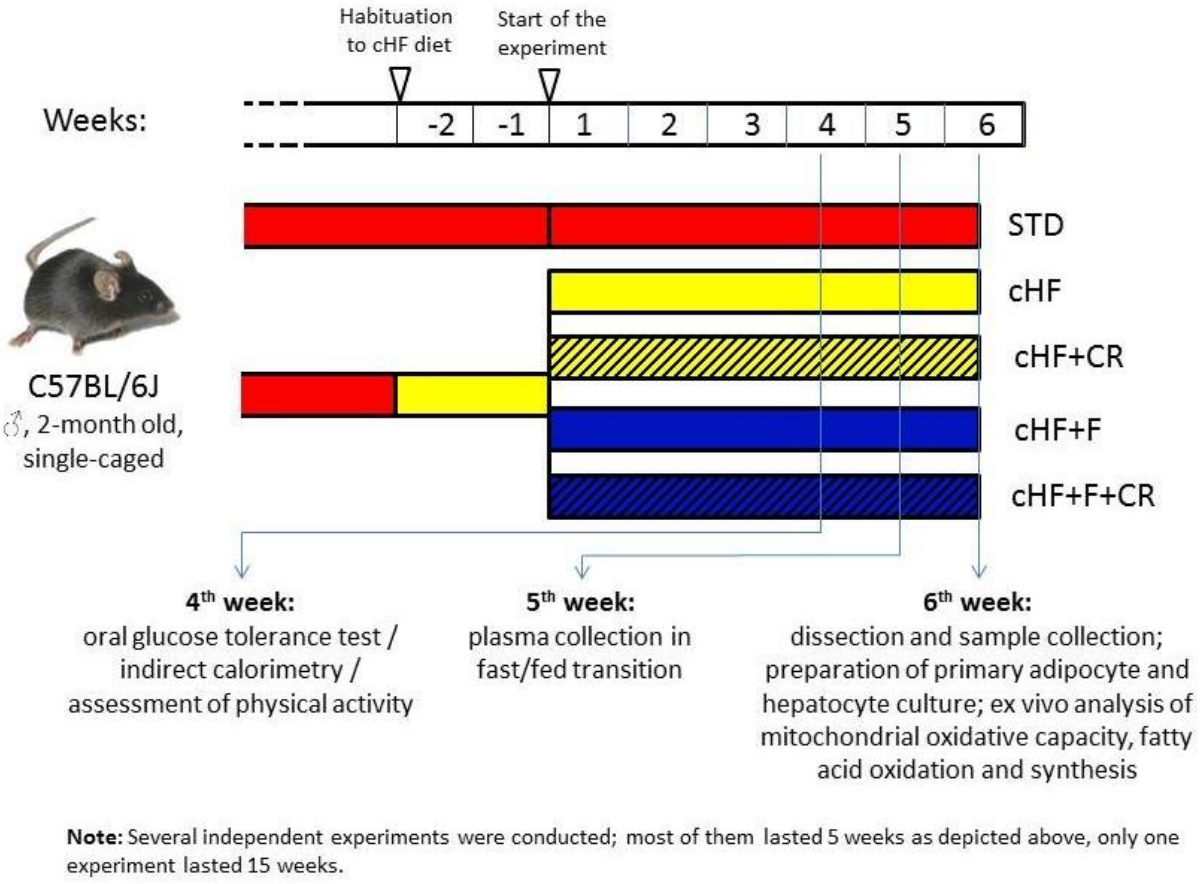

Fig. 3-2 Schema of experiments in publication B

In 4th week, several tests were performed in individual experiments, specifically oral glucose tolerance test, INCA, and monitoring of physical activity. In 5th week of treatment, plasma was collected during fast/fed transition in order to evaluate metabolic flexibility (see chapter 3.3). Animals were dissected in random fed state after 5 or 15 weeks of the treatment. Samples of plasma, liver, gastrocnemius muscle, BAT, eWAT, and scWAT were collected

for further analysis. In individual 5-week experiments some ex vivo analysis were performed immediately during dissection, namely assay for evaluation of FA oxidation in whole gastrocnemius and soleus muscles, and analysis of FA synthesis in eWAT. In freshly isolated adipocytes from eWAT, FA oxidation and mitochondrial oxidative capacity was measured. Moreover, primary hepatocyte cultures was isolated from subgroup of the animals (n = 8 per group) using liver perfusion technique. In these hepatocytes, fatty acid oxidation rate was determined.

Publication C

6-week-old male mice of B6/J and AJ strain were co-caged in groups of three and kept in thermo neutral temperature (30 °C) at least for 1 week. Thereafter, some animals were maintained as controls in thermoneutrality (9 mice of each strain), whereas others were transferred to 4 °C and left in this condition for two or six days (9 or 6 mice of each strain, respectively; see Figure 3-3). Mice were fed by STD diet during the whole experiment.

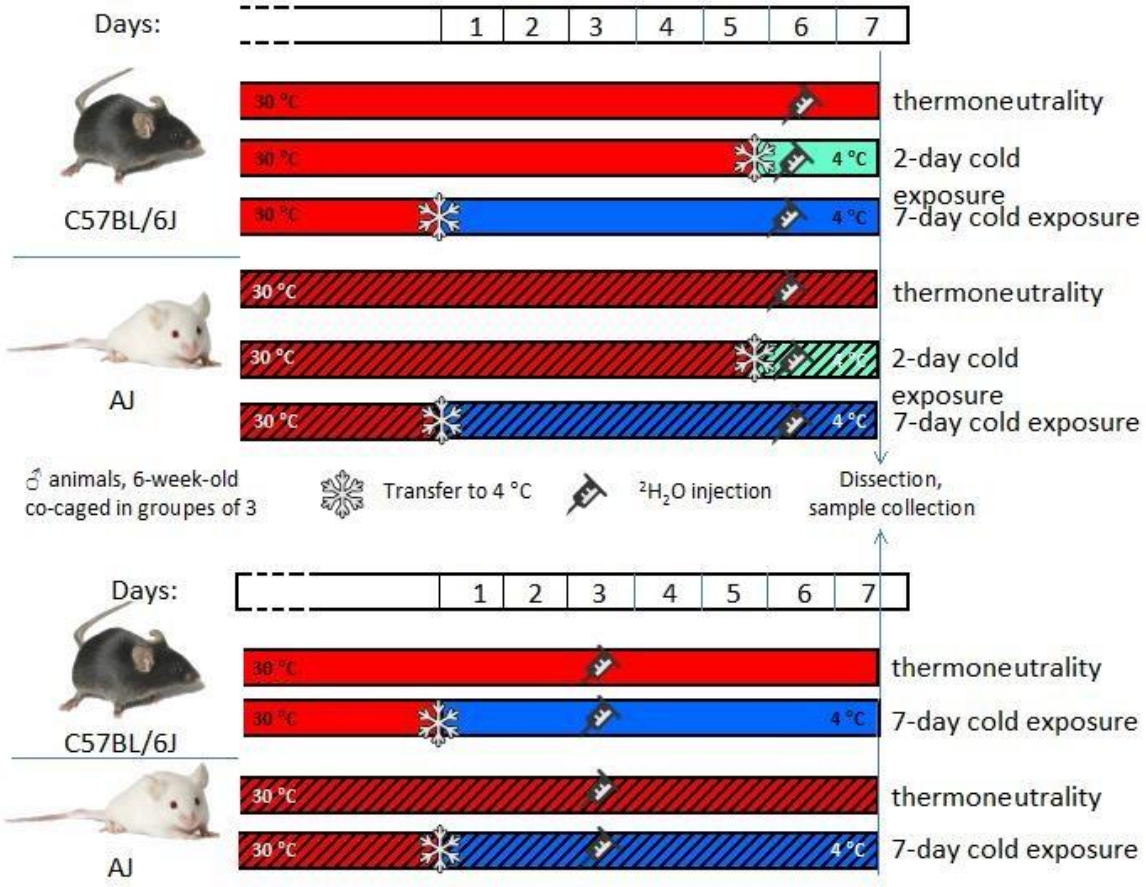

Fig. 3-3 Schema of experiments in publication C

In the evening, 40 hrs prior to dissection, mice were injected with saline in deuterium oxide (9 mg.ml^{-1} NaCl, 99.9% $^{2}H_2O$; loading dose [ml] – body weight of mouse [g] x 0.7 x 0.05) in order to reach 5% $^{2}H_2O$ enrichment of body water. Mice were then offered 5% $^{2}H_2O$ in drinking water to stabilize the ^{2}H level in body liquid. This protocol was reapeated twice, the second times, only two groups (mice from thermoneutrality and after 7 days of cold exposure) were used and $^{2}H_2O$ was injected 4 days before dissection (see Figure 3-3, the bottom part).

At the end of the experiment, mice were dissected in the morning in random fed state and blood and fat depots were collected. Plasma lipid levels and gene expression in eWAT were evaluated as well as UCP1 protein content in BAT scWAT (see chapters 3.9 and 3.10). Samples of eWAT and plasma aliquots were then sent to laboratory of our Portuguese collaborator John Jones (CNC, University of Coimbra). During my fellowship in this institution, I purified TAG from eWAT and determined ^{2}H enrichment of glycerol and FA moiety of these TAG (see chapter 3.15).

3.3 In vivo tests of glucose tolerance and metabolic flexibility; evaluation of plasma parameters

In both publications A and B, oral glucose tolerance test was performed after an overnight fasting (15-16 hrs). Glycaemia was assessed by tail bleeds at the baseline (fasted blood glucose) and then 15, 30, 60, 120, and 180 min after the oral gavage administration of D-glucose solution (1 g.kg^{-1} body weight). Results were expressed as an area under the curve for glucose (AUC). The greater is value of AUC, the lower is glucose tolerance.

For assessment of metabolic flexibility in publication B, plasma variables (specifically glucose, triglycerides, non-esterified fatty acids, and insulin) in fasted and re-fed state were analyzed in samples obtained using tail bleeding. In order to reach well-defined metabolic state for collection of blood samples, we followed the protocol described in (Galgani, et al. 2008): Animals were divided in two groups (see Figure 3-4); first day, one group was fasted for 14 hrs (between 8 am and 10 pm), whereas another group was fasted just between 8 am and 6 pm and allowed free access to food for the following 3 hours. Blood was collected between 9 pm and 10 pm from the re-fed group and between 10 pm and 11 pm from the fasted group. Groups were alternated the next day.

Plasma from tail bleeding in above described procedures (as well as samples obtained from carotid bleeding during dissection) was separated by centrifugation (900 g, 10 min, 4 °C) immediately after collection. Plasma glucose was measured using OneTouch Ultra glucometer (Life Scan, Milpitas, CA, USA).

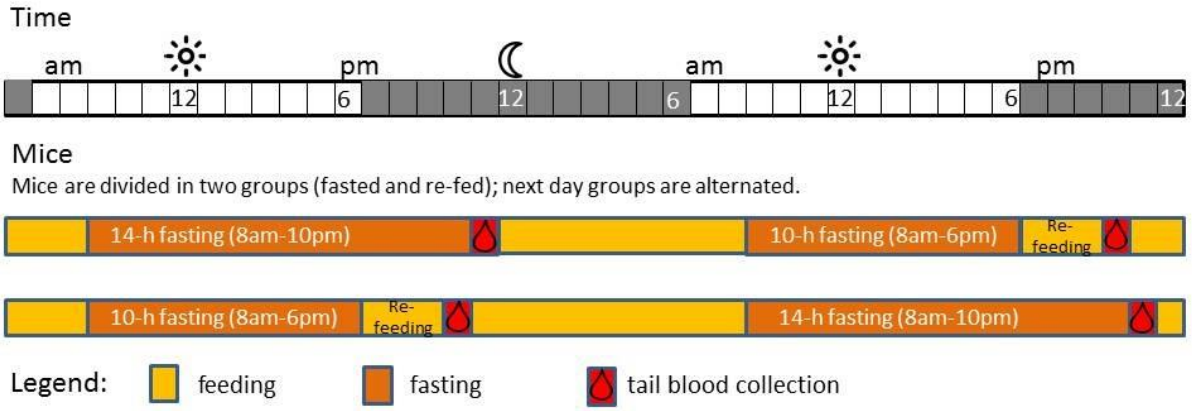

Fig. 3-4 Schema of plasma collection during fast/fed transition

Adiponectin levels were determined by Petra Janovská (in all the publications). Briefly, multimeric forms of adiponectin (10 µl of plasma diluted 1:2 with Laemmli buffer) were resolved using polyacrylamide gel electrophoresis under non-reducing conditions. After transfer onto a nitrocellulose membrane and blocking, primary rabbit anti-mouse polyclonal antibodies (BioVendor, Brno, Czech Republic) were applied, followed by secondary donkey anti-rabbit IgG infrared dye conjugated antibodies (IR Dye 800; Rockland, Gilbertsville, PA, USA). Membranes were scanned using Odyssey IR imager (Li-Cor Biosciences, Lincoln, NE, USA). Band intensities were analyzed by AIDA software (Raytest, Straubenhardt, Germany).

Other variables were analyzed using commercial kits as specified in Table 3-a.

Tab. 3-a Summary of kits used for measurement plasma variables

Variable	Kit	Supplier	Publication
Non-esterified fatty acids	NEFA C kit	Wako Chemicals (Germany)	A, B, C
Triacylglycerols	Triacylglycerol Liquid	Pliva-Lachema Diagnostica (CR)	A, B, C
Cholesterol		Pliva-Lachema Diagnostica (CR)	A, B
Insulin	Sensitive Rat Insulin RIA kit	LINCO Research (USA)	A, B
Leptin	Mouse Leptin RIA kit	LINCO Research (USA)	B
Interleukin 6	Cytoscreen mouse ELISA	Biosource Technologies (USA)	B
β-hydroxybutyrate	Autokit 3-HB	Wako Chemicals (Germany)	B
Aspartate transaminase and alanine transaminase	Enzymatic kits	Roche Diagnostics (Germany)	A

3.4 Indirect calorimetry

In publications A and B, INCA was performed either by Kristina Bardová (publication A), or by Petra Janovská (publication B). Briefly, single-caged animals were placed in a sealed measuring chamber of INCA system (Somedic, Sweden). The measurement started at 8 am (publication A) or 8 pm (publication B) and lasted for next 24 hrs. During this time, O_2 and CO_2 concentration were recorded every 2 minutes. Oxygen consumption (VO_2) and carbon dioxide production (VCO_2) were then used for calculations of energy expenditure (EE [cal] = 3.9 × VO_2 [ml] + 1.1 × VCO_2 [ml]) and respiratory quotient (**RQ** = VO_2 / VCO_2).

Respiratory quotient is an indicator of oxidized substrates. RQ for oxidation of glucose is 1, whereas RQ for oxidation of lipids is lower. Therefore, quantitative changes in RQ during feeding and fasting imply metabolic flexibility. In order to maximize this effect in publication B, RQ was measured during overnight fasting and compared with values after morning intragastric gavage of glucose (0.45 ml of 50% wt.vol^{-1} glucose).

Ideal approach to comparing subtle differences in RQ are the percent relative cumulative frequency (PRCF) curves constructed on a basis of RQ values pooled from all the animals within a given experimental group during the whole measurement period. Provided that the PRCF curves represent the normally distributed data, the values of 50th percentile of PRCF (EC_{50}) based on each individual animal correspond to RQ values. For more details about the technique see (Kus, et al. 2008).

3.5 Physical activity

In publication B, Pavel Flachs recorded animal behavior by video camera (resolution 320x240 pixels, 25 frames.s^{-1}) and analyzed offline using EthoVision XT software (Noldus Information Technology, Wageningen, Netherlands). For details see Electronic supplementary material in Publication B.

3.6 Primary hepatocyte cultures

Primary murine hepatocytes were isolated according to the modified method described for rats in (Berry and Friend 1969) and adapted by Foretz in (Foretz, et al. 1999). Perfusion solution (140 mM NaCl, 2.7 mM KCl, 0.3 mM $Na_2HPO_4.12H_2O$, 10 mM Hepes, pH 7.65) was permanently incubated in water bath at 37 °C. Each mouse was anesthetized by intraperitoneal injection of xylasine-ketamine mixture (100 μg ketamine and 20 μg xylasine per g of body weight) and its abdomen was opened. Vena cava inferior (in the section under the mouth of hepatic vein) was cannulated by winged needle connected with peristaltic pump and the warm perfusion solution was injected continously at a rate 5 ml.min^{-1}. The chest was then opened and thoracic part of vena cava inferior was clipped. Portal vein was cut which allows free perfusion of liver.

At first, liver was washed by 50 ml perfusion solution (with 0.2 mM EDTA) to remove all blood. Subsequently, 50 ml of the solution (with 6.8 mM $CaCl_2$ and 20 mg collagenase type II; Sigma, USA) was used to digest the cell connections and liberate hepatocytes. After that, liver of very soft consistency was carefully removed and transferred to 25 ml medium M199 with Earle's salts (GIBCO/BRL, USA). The living cells were calculated in Bürker chamber in solution with trypan blue (850 µl M199, 50 µl of diluted cell suspension, and 100 µl 0.4% Trypan Blue; Sigma USA). Hepatocytes were seeded on 35-mm Petri dishes at a density of 0.5×10^6 cells.dish^{-1} in medium M199 supplemented with 100 units.ml^{-1} of penicillin, 100 µg.ml^{-1} of streptomycin, 0.1% (wt/vol) BSA, 2% (vol.vol^{-1}) Ultroser G (GIBCO/BRL, USA), 100 nM dexamethasone (Sigma), 1 nM insulin (Actrapid, Novo-Nordisk, Denmark), and 100 nM triiodothyronine (Sigma, St Louis, MO, USA). After cell attachment (4 h), the medium was replaced by a medium similar to the plating medium but free of hormones, Ultroser G and albumin. Plates were incubated in humidified atmosphere of 10% CO_2 at 37 °C. The next day, palmitate oxidation rate was assessed in the cells (see chapter 3.8.1).

3.7 Evaluation of mitochondrial oxidative capacity

In publication B, mitochondrial oxidative capacity was quantified by assessment of oxygen consumption rate (3.7.2) in freshly isolated adipocytes (3.7.1); and by analysis cytochrome b content (3.7.4) and cytochrome oxidase activity (3.7.5) in membrane extract enriched with mitochondria (3.7.3).

3.7.1 Adipocyte isolation

Adipocytes from eWAT were isolated according to Rodbell (Rodbell 1964). Samples has been digested in modified Krebs-Ringer bicarbonate buffer (118.5 mM NaCl, 4.8 mM KCl, 2.7 mM $CaCl_2$, 1.2 mM KH_2PO_4, 1.1 mM $MgSO_4.7H_2O$, 25 mM $NaHCO_3$, pH 7.4) with 5 mM glucose, 4% bovine serum albumin and 3 mg.ml^{-1} collagenase type II (Sigma Aldrich, St Louis, MO, USA) shaking in 37 °C for 45 min. Liberated adipocytes were then three times washed and separated by centrifugation (1 min, 150 RPM = 400 g, 20 °C) in the absence of collagenase and BSA.

3.7.2 Respiratory chain oxidative capacity

200 μl of freshly isolated adipocytes were carefully transferred to 1.8 ml KCl medium (80 mM KCl, 10 mM tris(hydroxymethyl)aminomethane (Tris).Cl, 5 mM KH_2PO_4, 3 mM $MgCl_2$, 1 mM EDTA; pH 7.4) with 4% BSA in a chamber of high-resolution OROBOROS Oxygraph-2k (Oroboros Instruments, Austria; (Chowdhury, et al. 2000)). Plasma membranes of adipocytes were permeabilized by digitonin (Sigma, USA). The oxygen consumption rate was then measured during successive addition of several respiratory substrates (glycerol 3-phosphate, succinate), and inhibitors of respiratory chain complexes (rotenone, antimycin A). Whole protocol is described in Table 3-b. ADP, oligomycin and FCCP (carbonyl cyanide-p-trifluoromethoxyphenylhydrazone) were used to assess mitochondrial coupling. Mitochondrial integrity was tested by cytochrome c addition - the samples whose oxygen consumption increases more than by 20 % in response to cytochrome c were not taken into account. All the data were related to DNA content in the sample (see chapter 3.12.1).

Table 3-b List of respiratory substrates and inhibitors and their order of use

	Chemical	**Effect**	**Storage concentration**	**Titration volume**	**Final concentration**
1	digitonin	Permeabilizer	10 $mg.ml^{-1}$	3 μl	15 $\mu g.ml^{-1}$
2	rotenone	CI inhibitor	1 $mmol.l^{-1}$	2 μl	1 $\mu mol.l^{-1}$
3	glycerol 3-phosphate	GPDH substrate	1 $mol.l^{-1}$	20 μl	10 $mmol.l^{-1}$
4	succinate	CII substrate	1 $mol.l^{-1}$	20 μl	10 $mmol.l^{-1}$
5	cytochrome c	quality control	4 $mmol.l^{-1}$	10 μl	20 $\mu mol.l^{-1}$
6	ADP	CV substrate	0.3 $mol.l^{-1}$	10 μl	1.5 $mmol.l^{-1}$
7	oligomycin	CV inhibitor	4 $mg.ml^{-1}$	2 μl	4 $\mu g.ml^{-1}$
8	FCCP	Uncoupler	1 $mmol.l^{-1}$	0.5 μl steps	0.25 $\mu mol.l^{-1}$ steps
9	antimycin A	CIII inhibitor	5 $mmol.l^{-1}$	2 μl	5 $\mu mol.l^{-1}$

3.7.3 Membrane fraction preparation

For other analysis, membrane fractions were prepared. Frozen samples of adipose tissue (100 mg) were homogenized on ice by Ultra-Turrax T8.01 homogenizer (IKA, Germany) in STE medium (containing 50 mM Tris.Cl, 0.5 mM EDTA, and 0.25 M sucrose; pH 7.4) with protease inhibitors (1 mM phenylmethanesulphonylfluoride, 1 $\mu g.ml^{-1}$ pepstatin, 1 $\mu g.ml^{-1}$

leupeptin, 1 μg.ml^{-1} aprotinin). Then the homogenate was centrifuged twice (600 g, 10 min, 4 °C) to remove debris and finally ultracentrifuged (100 000 g, 45 min, 4 °C). Resulted pellet contains membrane fraction enriched with mitochondria. It was resuspended (using sonication) in 150 μl STE medium and divided to aliquots for protein measurement (see chapter 3.12.2), Western blotting (publications A and C, chapter 3.11) and assessment of cytochrome b content and cytochrome oxidase activity (publication B, below).

3.7.4 Cytochrome b evaluation

At first, membrane fractions were solubilized in the presence of 2% *n*-dodecyl β-D-maltoside (Sigma, St Louis, MO, USA) to liberate the cytochromes. 50 μl sample was diluted in 1800 μl medium containing 90 mM sucrose, 60 mM $MgCl_2$, 24 mM $KH_2PO_4.2H_2O$, 10 mM Tris.Cl, and 2 mM EDTA. Reduced-oxidized spectra were recorded using a Hewlett-Packard 8453 diode array spectrophotometer. In order to improve sensitivity, a pseudo-dual-wave-length arrangement was used: spectra were recorded in 2-s intervals for 3 min in 2 ml samples (0.1 mg.ml^{-1} protein in a stirred cuvette, at 25 °C). Reducing agens dithionite was added after 40 s of measurement. A typical cytochrome spectrum appeared. Cytochrome b content was then calculated using published absorbance coefficients and wavelength pairs $\Delta\varepsilon_{563\text{-}577}$ = 17.9 mM^{-1}.cm^{-1} (Bookelman, et al. 1978).

3.7.5 Cytochrome oxidase activity

Cytochrome oxidase was liberated from membranes by *n*-dodecyl-maltoside similarly as described above. 30 μl sample was then transferred to cuvette with 1 ml KP_i buffer (40 mM KP_i; pH 7.0; KH_2PO_4 : K_2HPO_4 - 38.5 : 61.5) with 1 mg.ml^{-1} BSA. Reduced cytochrome c (kindly provided by Dept. of Bioenergetics, Institute of Physiology AS CR, v. v. i.) was added to final concentration 25 μM and changes of absorbance in 550 nm were then recorded. Decrease of absorbance is proportional to amount of oxidized cytochrome c ($\Delta\varepsilon$ = 19.6 mM^{-1}.cm^{-1}).

3.8 Ex vivo analyses using radioisotopes

In publication B rate of fatty acid oxidation and synthesis in several tissues was analyzed.

3.8.1 Palmitate oxidation in muscle, adipose tissue, isolated adipocytes, and primary hepatocytes

Soleus and gastrocnemius muscle were carefully dissected and transferred into 3 ml of Krebs Ringer bicarbonate buffer (composition described in previous chapter) containing 10 mM glucose and fatty acid-free bovine serum albumin (5 mg/ml, ICN Biomedicals, High Wycombe, UK) complexed (1:3) with palmitic acid (Sigma-Aldrich) and [1-^{14}C]palmitate (0.1 μCi.ml^{-1}). After 1 h of shaking at 37 °C in a closed glass vial (15 ml total volume), the reaction was terminated by injecting 0.3 ml of 5M H_2SO_4 into the vial, and liberated CO_2 was trapped in 0.3 ml of hyamine hydroxide (Perkin Elmer, Waltham, MA, USA) contained in an Eppendorf tube inserted into the incubation vial. After 60 min of CO_2 trapping, $^{14}CO_2$ in hyamine hydroxide was quantified by liquid scintillation counting. The fatty acid oxidation rate was then normalized to the wet tissue weight.

The same procedure was performed with approximetaly 60 mg of eWAT and with cell suspension of freshly isolated adipocytes from this depot.

The technique slightly differs for the primary hepatocytes (Jelenik, et al. 2010). Cells were incubated for 45 min at 37 °C in 800 μl of a medium (M199) supplemented with 1% BSA, 50 μM cold palmitate and [1-^{14}C] palmitate (0.38 μCi.reaction^{-1}). The reactions were terminated by aspiration of the medium; cells were washed by PBS and then incubated in 800 μl of 5% perchloric acid for 15 min at room temperature. In this case, palmitate oxidation was determined by measuring production of ^{14}C-labeled acid-soluble metabolites, a measure of tricarboxylic acid cycle intermediates and acetyl esters. The acid-soluble metabolites were assessed in supernatants of the acid precipitate. Identical incubations in parallel wells without radioactivity were conducted to determine protein concentrations (chapter 3.12.2) for normalization of β-oxidation rate.

3.8.2 Fatty acid synthesis

I was not personally involved in the assessment of fatty acid synthesis rate. Nevertheless, the protocol (described in (Rossmeisl, et al. 2000)) was briefly the following: Mice were injected intraperitoneally with 50–100 ml of 0.15M NaCl containing ^3H_2O (35 mCi.g^{-1} body weight). After 60 min at 22°C, mice were killed and the rate of fatty acid synthesis in various tissues *in vivo* was measured by incorporation of ^3H_2O into saponifiable fatty acids. The activity of FA synthesis was expressed as dpm ^{3}H incorporated to FA per mg tissue and hour.

3.9 Tissue and feces lipid content

Samples of liver, gastrocnemius muscle, and feces (~50 mg) were solubilized in 0.15 ml 3M alcoholic KOH overnight according to Salmon and Flatt (Salmon and Flatt 1985). Resulted homogenates were diluted tenfold with H_2O and neutralized by 2.5N $HClO_4$. Content of triglycerides was then estimated enzymatically using Free glycerol reagent (Sigma Aldrich, St Louis, MO, USA) (Rossmeisl, et al. 2009).

3.10 Real-time quantitative PCR

Real-time qPCR were performed in both publications. I was personally involved in analysis of samples for publication B (for protocol see below). Data in publication A were measured by our Portuguese collaborators using another kits and procedures. For details of protocol in this project see attached publication A, section Methods.

In publication B, tissue samples up to 100 mg were homogenized in 1 ml TRIzol (Sigma, USA) using Ultra-Turrax T8.01 homogenizer. Consequently, 0.2 ml chloroform was added to samples, mixed vigorously and centrifuged to separate organic an aqueous phase (15 min, 14000 g, 4 °C). The upper phase was then collected and RNA was precipitated by addition of 0.5 ml isopropanol. Sample was then centrifuged again (10 min, 12000 g, 4 °C). Resulted pellet was washed by ethanol, dried in vacuum and dissolved in 10-50 μl redistilled water. RNA concentration was measured by Nanodrop instrument (Thermo Scientific, USA). Purity of isolated RNA was tested by checking the ratio between absorbance in 260 nm and 280 nm, which should be close to 2.

mRNA (1 μg) was reversely transcribed to cDNA using oligoT primers and M-MLV reverse transcriptase (Invitrogen, USA). Levels of various transcripts were evaluated using LightCycler 480 II instrument (Roche Diagnostics, Switzerland) and LightCycler 480 SYBR Green I Master kit (Roche Diagnostics, Germany). PCR conditions were following: 6 min initial denaturation at 95 °C and 45 cycles of 10 s denaturation at 95 °C, 10 s primer annealing at 55-60 °C (according to used primer), and 20 s elongation at 72 °C. Specificity of the amplified PCR products was assessed by performing a melting curve analysis at the end of whole run. To correct for intersample variation in yields of reverse transcription, levels of the transcript were normalized using geometrical mean of two reference genes - EF-1α and Cyclophilin-β.

Primers were designed using Lasergene software (DNASTAR, USA). All primer sequences used in both publications are listed in Table 3-c.

Tab. 3-c List of primer sequences

Gene	Gene ID	Forward sequence	Reverse sequence
Cd68	12514	CAC TTC GGG CCA TGT TTC TCT TG	AGG GGC TGG TAG GTT GAT TGT CGT
Cox4i1	12857	AGA AGG CGC TGA AGG AGA AGG A	CCA GCA TGC CGA GGG AGT GA
Cpt-1α	12894	GCA GCT CGC ACA TTA CAA GGA CAT	ACT ATG TGT CCT GTG GCG GGG GCT
Cpt-1β	12895	GGA TGA TGG CTA CGG GGT CTC TTA	AGG GCA GCT GGG GTA TCT CTT TTC
Cyclophilin-β	19035	ACT ACG GGC CTG GCT GGG TGA G	TGC CGG AGT CGA CAA TGA TGA
EF-1α	13627	TGA CAG CAA AAA CGA CCC ACC AAT	GGG CCA TCT TCC AGC TTC TTA CCA
Fas	14104	GGC TGC CTC CGT GGA CCT TAT C	GTC TAG CCC TCC CGT ACA CTC ACT CGT
Glut-4	20528	ACC GGC TGG GCT GAT GTG TCT	GCC GAC TCG AAG ATG CTG GTT GAA TAG
Gyk	14933	TCG TTC CAG CAT TTT CAG GGT TAT	TCA GGC ATG GAG GGT TTC ACT ACT
Lcad	11363	TGG CAT CAA CAT CGC AGA GAA ACA	ACC GAT ACA CTT GCC CGC CGT CAT
Mcad	11364	TCG CCC CGG AAT ATG ACA AAA	GCC AAG GCC ACC GCA ACT
Nrf-1	18181	GGC GGG AGG ATC TTT TAT ATG CTT TTG A	GGC CTC TGA TGC TTG CGT CGT CT
Pdk-4	27273	GGC TTG CCA ATT TCT CGT CTC TA	TTC GCC AGG TTC TTC GGT TCC
Pck1	18534	GGC AGC ATG GGG TGT TTG TAG GA	TTT GCC GAA GTT GTA GCC GAA GAA G
Pgc-1α	19017	CCC AAA GGA TGC GCT CTC GTT	TGC GGT GTC TGT AGT GGC TTG ATT
Pnpla2 (ATGL)	66853	GCC AAC GCC ACT CAC ATC TAC G	GGC AAT CAG CAG GCA GGG TCT TTA
Pparα	19013	TGC GCA GCT CGT ACA GGT CAT CAA	CCC CCA TTT CGG TAG CAG GTA GTC TTA
Prdm16	70673	AGG AAG AGG AGG AGC TGG AG	GTC GGC TCC AAA GCT AAC AG
Scd-1	20249	ACT GGG GCT GCT AAT CTC TGG GTG TA	TAA CAA ACC CAC CCA GAG ATA AAG CC
Slc25a4	11739	TCG CTG GCC TGA CTT CCT ATC CTT	TCA GAG GCA TGG GTG GCG C
Ucp-1	22227	CAC GGG GAC CTA CAA TGC TTA CAG	GGC CGT CGG TCC TTC CTT
Vlcad	11370	CAG GGG TGG AGC GTG TGC	CAT TGC CCA GCC CAG TGA GTT CC

3.11 Quantification of UCP1 protein using Western blots

For quantification of UCP1, membranous fraction was prepared as described in chapter 3.7.3 using 70 mg interscapular BAT and 100 mg scWAT. We struggle with low yield of scWAT protein. Therefore, 5 μg BAT protein, but only 2 μg scWAT protein were used for following analysis. Samples were diluted with 2x Laemli buffer (Bio-Rad, USA; with adittion of 5% mercaptoethanol) and resolved in 10% polyacrylamide gel. PageRuler^{TM} Plus Prestained Protein Ladder (Thermo Scientific, USA) was used as a size standard. Subsequently, separated proteins were blotted on PVDF membrane, which was then blocked by Odyssey blocker (diluted 1:1 in Tris-buffered saline - TBS: 10mM Tris, 150mM NaCl).

The strip of membrane containing proteins of size 25-40 kDa was cut and incubated overnight with primary murine polyclonal anti-UCP1 antibody (generated previously in our Dept. (Kopecky, et al. 1996); 1:500 in TBS and 0.05% Tween 20). Next day, 1-h incubation with secondary infrared-dye-conjugated anti-mouse antibody (Rockland, USA; 1:5000 in TBS and Tween) followed. Membrane scanning and band analysis were performed as describe for adiponectin in chapter 3.3. All band intensities were related to protein standard prepared from mitochondria isolated from BAT of cold-exposed mice and relative UCP1 content per whole BAT was calculated.

3.12 DNA and protein content evaluation

DNA or protein concentrations serve as reference for several analysis (immunoblots, oxygraph measurement, fatty acid oxidation in hepatocytes etc).

3.12.1 Fluorimetric assessment of DNA concentration

Cell suspension was mixed 1:2 vol:vol with proteinase buffer (20 mM Tris.Cl, 10 mM EDTA, 1% sodium dodecyl sulphate, 50 $\mu g.ml^{-1}$ proteinase K (Merck, Germany)) and incubated at 56 °C for 12 hrs. Subsequently, 20 µl of sample is diluted with phosphate buffer (2 M NaCl, 50 mM Na_2HPO_4, 2 mM EDTA; pH 7.4) containing DNA binding compound bisbenzimide (Hoechst 33258; Serva, Germany; 3.3 $\mu g.ml^{-1}$). After 3-16 hrs incubation in dark, fluorescence at 458 nm was measured by fluorimeter Victor (Perkin Elmer, USA). DNA standard isolated from calf thymus was used to quantification of DNA content.

3.12.2 BCA method for assessment of protein concentration

In order to determine the protein concentration, BCA method was used because it does not interfer with detergents and lipids in sample. Immediately before the measurement solution A (1% sodium bicinchoninate (Sigma, USA), 2% Na_2CO_3, 0.95% $NaHCO_3$, 0.16% sodium tartrate; pH 11.25) and solution B (4% $CuSO_4.5H_2O$) were mixed in the ratio 1:50 (vol:vol). Under basic conditions, proteins reduce Cu^{II} to Cu^{I} which reacts with bicinchonic acid creating violet product with maximal absorbance at 562 nm. Therefore, absorbance of 250 µl fresh solution mixture with 20 µl sample (diluted as needed) was assessed using Infinite 200 microplate reader (Tecan, Switzerland). Data were evaluated according to the calibration curve made of diluted BSA samples of known concentration.

3.13 Light microscopy and immunohistology analysis

Immunohistology analyses were performed by Kristina Bardová (publication A) and Zuzana Macek Jílková (publication B). Briefly, adipose tissue samples were fixed in 10% neutral buffered formalin (Sigma-Aldrich, USA) and embedded in paraffin. 5μm sections were stained with haematoxylin-eosin for morphometry or processed to detect UCP1 (publication A), or MAC-2/galectin-3 and perilipin (publication B), using specific antibodies. Digital images were captured using light microscope (AX70) and a camera (DP 70; both from Olympus, Tokyo, Japan). Morphometry was performed using a morphometric programme (Lucia IMAGE, version 4.81; Laboratory Imaging, Prague, Czech Republic). For further details and references see the methodic sections of respective papers.

3.14 HPLC MS-MS lipidomic analysis

In eWAT and liver extracts from 5-week experiment in publication B, 24 lipid molecular species were identified using HPLC MS-MS analysis. This technique was performed in our partner laboratory at the University of Debrecen, Hungary. For detail see Electronic supplementary material in Publication B.

3.15 Measurement of ^{2}H enrichment of triglycerides using nuclear magnetic resonance spectroscopy

In publication C, TAG synthesis and FA synthesis *de novo* were analyzed using nuclear magnetic resonance (NMR) spectroscopy. Body water of animals was enriched by $^{2}H_2O$ up to 5% for approximately 4 days or 40 hrs prior to dissection (see chapter 3.2). Provided that ^{2}H can be incorporated in glycerol moiety of TAG only before esterification of FA to glycerol, ^{2}H enrichment of this part of TAG reflects the rate of TAG synthesis since the $^{2}H_2O$ injection. Similarly ^{2}H enrichment of FA methyls in TAG correlates with *de novo* FA synthesis rate.

Following analyses were performed in collaboration with John Jones (CNC, University of Coimbra) during my internship in his laboratory. At first total lipids from eWAT were extracted and TAG were isolated from this fraction. ^{2}H enrichment of TAG, as well as content of $^{2}H_2O$ in body water was then analyzed, and these data were used for approximation of TAG and FA synthesis rate.

3.15.1 Triglyceride purification

Lipids from frozen pieces of eWAT (approx. 150 mg) were extracted by a Folch extraction. Briefly, tissue was macerated in 6 ml chloroform/methanol/water mixture (33:16:10, v/v) and stirred in room temparuture for 1 hour. Organic phase was then separated by centrifugation (600 g, 5 min), collected and evaporated overnight to dryness.

After that, TAG were purified by column chromatography using prepacked Discovery DSC-Si SPE Tubes (Sigma, bed weight 2 g, volume 12 ml, particle size 50 μm, pore size 70 Å). Columns were activated by 1 volume of hexane/methyl-*t*-buthyl-ether (MTBE) solution (96:4,v/v) and 3 volumes of hexane. Thereafter, lipid residues were dissolved in 700 μl hexane/MTBE mixture (200:3, v/v), and applied to the column. Columns were then washed by hexane/MTBE (200:3, v/v) and eluted fractions (approx. 20 ml each) were collected. The presence of triglycerides was checked by thin layer chromatography on silica-gel plates (Sigma, USA). Small samples of each fraction were developed in petrolether/diethylether/acetic acid (70:10:1) system and triglyceride spots were visualised by iodine vapours. (Retention factor of TAG was about 0.55.) TAG-rich fractions (usually fractions 2-6) were pooled and evaporated to dryness.

3.15.2 Nuclear magnetic resonance and spectra analysis

Isolated TAG were dissolved in 600 μl chloroform (anhydrous, containing amylines as stabilizers), and mixed with 50 μl hexafluorobenzene and 25 μl pyrazine enriched with $^{2}H_4$-pyrazine standard also dissolved in the same chloroform (approx. 25 μmol/sample and 0.25 μmol/sample of ^{1}H and ^{2}H pyrazine, respectively). Furthermore, plasma samples were prepared (10 μl plasma, 50 μl hexafluorobenzene, and 1 ml acetone standard) for the evaluation of $^{2}H_2O$ enrichment of body water according to protocol described previously in (Jones, et al. 2001).

Samples were then analyzed by ^{1}H and ^{2}H-NMR technique using a Bruker Avance III HD 500 MHz system equipped with a 5-mm ^{2}H-selective probe with ^{19}F lock and ^{1}H-decoupling coil. For ^{1}H acquisition, a spectral width of 10 kHz was used in conjunction with the acquisition pulse parameters shown in the Table 3-d. For ^{2}H acquisition, a spectral width of 921 Hz was used and broadband ^{1}H-decoupling was continuously applied. For maximizing signal-to-noise ratios of the glyceryl moiety, spectra were acquired under partial-saturation conditions (see Table 3-d). Six of the samples were also acquired under fully relaxed conditions in order to obtain a correction factor for saturation (see Table 3-d).

The spectra were analyzed using NUTS software (ACORN NMR, Fremont, CA, USA). They were adjusted by baseline correction, line broadening (LB, see Table 3-d), zero filling (ZF, see Table 3-d), exponential multiplication, and Fourier transformation. The amount of ^{1}H and ^{2}H in both glycerol and fatty-acyl moiety of TAG was then calculated from peak area with respect to the peak of the pyrazine $^{1}H/^{2}H$ standard. For representative ^{1}H and ^{2}H spectra with description of main peaks see Fig 3-5.

Tab. 3-d Specification of NMR acquisition conditions, and adjustment of final spectra.

Spectrum	**Num. of scans**	**Pulse**	**Acq. time [s]**	**Pulse delay [s]**	**Standard**	**Evaluated chemical group**	**Chem. shift [ppm]**	**Spectra adjustment**		**Minimal signal / noise**
								LB	**ZF**	
^{2}H plasma spectrum	16	3μs 30°	4	8	acetone	H_2O		1	1 x	150
^{1}H TAG spectrum	4	14.8μs 90°	3	5	pyrazine	C1+C3 glycerol	4.1-4.4 (octet)	0.5	1 x	1270
^{2}H TAG spectrum	5500	12μs 90°	0.5 (partially saturated), 1 (fully relaxed)	0.1 (partially saturated), 8 (fully relaxed)	pyrazine	C2 glycerol	5.3	3	3 x	20
						C1+C3 glycerol	4.3	3	3 x	40
						FA methyl	0.84	1	3 x	20

3.15.3 Calculations

Analysis of NMR spectra provided following variables:

(1) ^{2}H body water enrichment ($[^{2}H_2O] / ([^{2}H_2O] + [^{1}H_2O]$);

(2) $[^{1}H]$ on C1 and C3 of glycerol moiety of TAG, which was used for simple calculation of $[^{1}H]$ in whole glycerol moiety (multiplication by factor 5/4), $[^{1}H]$ on C2 of glycerol (multiplied by factor 1/4), and $[^{1}H]$ in methyl of fatty-acyl moiety (multiplied by factor 9/4)

(3) $[^{2}H]$ on C1 and C3 of glycerol moiety of TAG, $[^{2}H]$ on C2 of glycerol moiety, and $[^{2}H]$ on methyl of fatty-acyl moiety.

Based on these data, we calculated excess enrichments and fractional synthetic rates for methyl of fatty-acyl moiety, and both C1+3 and C2 of glycerol moiety, according to following formula:

$$\text{excess enrichment} = ([^{2}H] / ([^{2}H] + [^{1}H]) \times 100) - 0.015 \ [\%]$$

$$\text{fractional synthetic rate} = \text{excess enrichment} / \text{body water enrichment} \times 100 \ [\%]$$

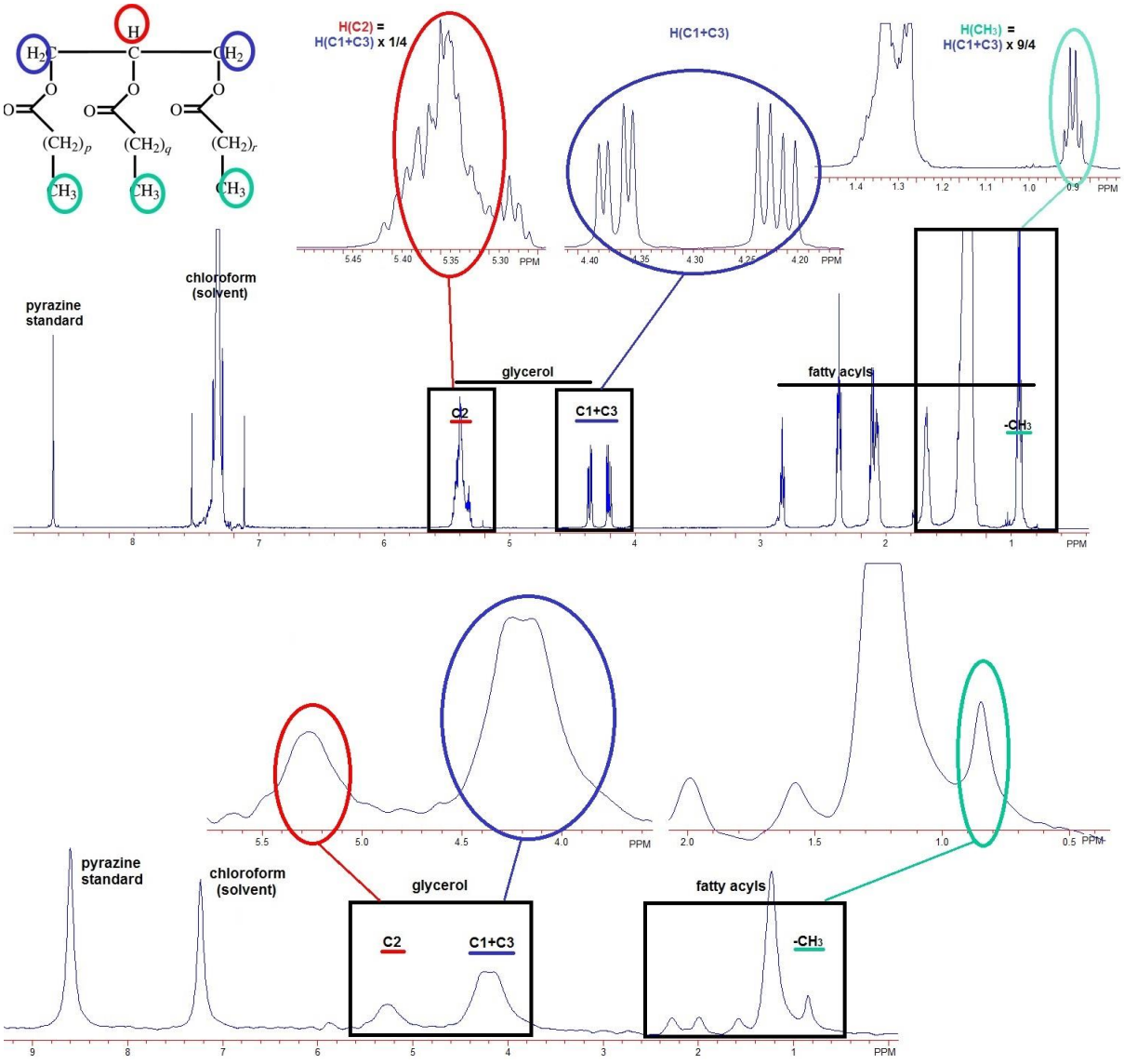

Fig. 3-5 Representative NMR spectra of TAG
1H (top) and 2H spectrum (bottom); the evaluated peaks are displayed in detail as well; red, blue and green colour represent the individual hydrogens of the TAG molecule (as characterized in the upper left corner.

3.16 Statistical analysis

All values are presented as means ± standard errors of mean. Data were analyzed by pair t-test or one-way ANOVA with Holm-Sidac posthoc tests using SigmaPlot 10 statistical software (SYSTAT Software, USA). Comparisons were judged to be significant at $p<0.05$. Repeated measures ANOVA was used to analyze the response of plasma metabolites level to fasted/refed state transition in publication B.

The PRCF curves in publication A were analyzed using nonlinear regression. Differences in energy expenditure were evaluated by ANCOVA using NCSS software. Partial least squares-discriminant analysis (PLS-DA) using Umetrics SIMCA-P+12 statistical software was used for lipidomic data evaluation.

4. Results

4.1 Publication A: Effects of chenodeoxycholic acid on energy balance and adipose tissue activation

The data reflecting the effects of bile acids (namely CDCA) on BAT recruitment and browning of scWAT was published in Paper A (see Appendix). This topic covers 1st and 2nd aims of my thesis.

4.1.1 Chenodeoxycholic acid reverses diet-induced obesity mainly by reducing food intake

First, we tested effect of two different doses of CDCA (0.5% and 1%) on animal model of diet-induced obesity - B6 mice fed cHF diet for 2 months. The most dramatic impact caused by CDCA addition to the diet was the immediate dose-dependent decrease in food consumption (Figure 4-1a). Only at the end of 2nd week of experiment, the animals became fully habituated to the new diet and their food intake reached its original level. This transient drop of food intake coincided naturally with fast reduction of body weight (Figure 4-1b). However, the body weight remained stabilized on the lower level even after the food intake was normalized again. The body weight reduction can be attributed to decrease in adiposity, as demonstrated by the significantly lower weight of both eWAT and scWAT and unchanged weight of liver (Table 4-a). Thus, the most striking effects of CDCA supplementation on adiposity and body weight occurred in the beginning of the treatment.

In addition to the decline in WAT depot size, we also observed that CDCA counteracts ectopic lipid accumulation in liver and muscle (Table 4-a), which suggests increase in insulin sensitivity of these tissues. Indeed, levels of glucose and insulin in plasma collected at the end of the experiment were significantly decreased by CDCA. Moreover, CDCA has the same effect on plasma lipids, namely TAG and NEFA. The above changes (summarized in Table 4-a) usually show tendency to dose-dependent pattern, despite the fact that the differences between both doses are not always significant. Furthermore, levels of HMW (but not total) adiponectin increases as well, which is in accordance with reduction of WAT hypertrophy. Insulin sensitizing effect of CDCA was also proved *in vivo* using OGTT (Table 4-a).

Table 4-a Parameters measured in plasma, tissues and faeces at the end of the 8-week-reversion experiment

		cHF	0.5% CDCA	1% CDCA
Plasma levels				
TAG [mmol l^{-1}]		1.56 ± 0.12	1.08 ± 0.12[a]	0.83 ± 0.10[a]
NEFA [mmol l^{-1}]		0.86 ± 0.04	0.85 ± 0.04	0.65 ± 0.04[a,b]
Cholesterol [mmol l^{-1}]		5.27 ± 0.26	3.15 ± 0.26[a]	2.70 ± 0.42[a]
Glucose [mg dl^{-1}]		257 ± 10	191 ± 13[a]	143 ± 19[a]
Insulin [ng ml^{-1}]		4.53 ± 0.43	0.71 ± 0.10[a]	0.19 ± 0.03[a]
Adiponectin	HMW [AU]	0.43 ± 0.03	0.47 ± 0.04	0.62 ± 0.07[a]
	Total [AU]	1.02 ± 0.06	0.98 ± 0.07	1.20 ± 0.10
	HMW/total	0.42 ± 0.02	0.48 ± 0.03	0.51 ± 0.03
Aspartate transaminase [uCAT l^{-1}]		3.02 ± 0.32	3.01 ± 0.39	3.26 ± 0.30
Alanine transaminase [uCAT l^{-1}]		1.12 ± 0.16	0.62 ± 0.03	0.88 ± 0.08
Oral glucose tolerance test				
Total AUC [mmol l^{-1} Glc 180 min]		3042 ± 189	2524 ± 158[a]	1654 ± 82[a,b]
Weight of tissues				
eWAT [mg]		2241 ± 105	1419 ± 147[a]	513 ± 66[a,b]
scWAT [mg]		1295 ± 60	612 ± 102[a]	191 ± 19[a,b]
Liver [mg]		2328 ± 132	1873 ± 95	2060 ± 204
Tissue TAG content				
Liver TAG [mg g^{-1} tissue]		377 ± 41	49 ± 6[a]	30 ± 1[a,b]
Muscle TAG [mg g^{-1} tissue]		113 ± 11	50 ± 7[a]	35 ± 7[a]
Faeces lipid content				
TAG [mg g^{-1}]		62.8 ± 14	47.5 ± 4.7	49.2 ± 2.9
Cholesterol [mg g^{-1}]		12.3 ± 0.8	10.4 ± 0.4[a]	10.5 ± 0.3[a]

[a] Significant differences in comparison to cHF group; [b] significant differences in comparison to 0.5% CDCA group. Data are means ± SEM (n=10-12, except for oral glucose tolerance test, where n=5; see Materials and Methods). HMW, high molecular weight

In this experiment, we also tested alternative mechanisms of bile acid action. We assessed plasmatic levels of hepatic transaminases (aspartate and alanine transaminase), which were not influenced by CDCA administration (all results are included in Table 4-a). This fact argues against the possible hepatotoxic effect of high CDCA doses. Given the physiological role of bile acids in lipid absorption, we examined the lipid content in feces. Due to considerable variability in samples, there were no significant differences in TAG content while the cholesterol levels were decreased. This finding rules out the possibility that CDCA-driven improvement of lipid absorption can explain positive effects of CDCA treatment. Nevertheless, the actual mechanism of CDCA action can be truly explored only after dissection of indirect effects caused by decreased food intake.

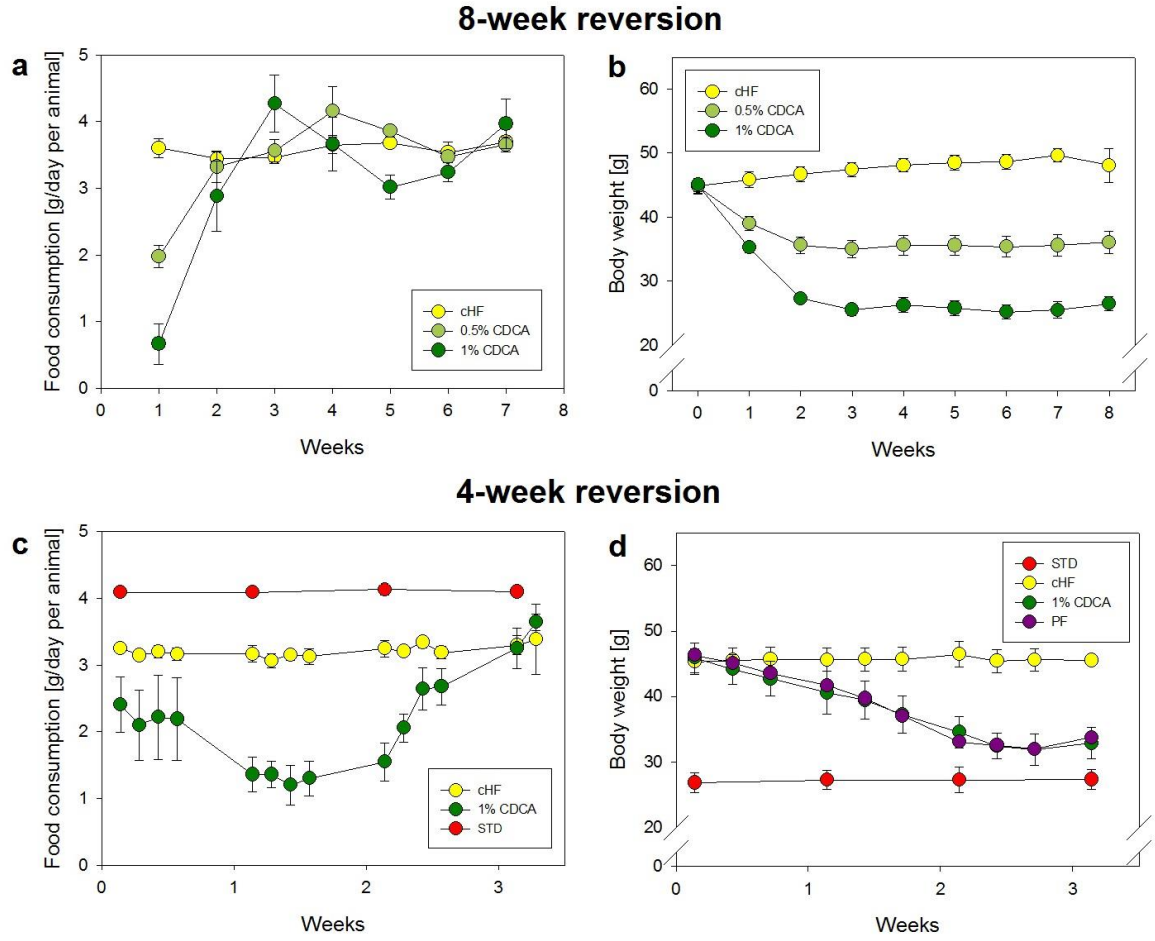

Fig. 4-1 Food intake and growth curves in experiments of publication A
a), b) Food intake (a) and development of body weight (b) during the 8-week reversion
c), d) Food intake (c) and development of body weight (d) during the 3-week reversion

4.1.2 Changes in adipose tissue are partially independent on food intake

In order to distinguish direct effect of CDCA on energy metabolism, we conducted another reversion experiment. The study included cHF and 1% CDCA groups, as well as pair-fed group and group of animals fed by STD diet since weaning. Whole experiment lasted just 3 weeks in order to cover the period of transient decline in food intake of CDCA mice. Similarly to 8-week reversion, CDCA animals reduced the food intake for first 2 weeks and lost around 30% of their original body weight, which means they drop almost to the weight of STD mice (Figure 4-1). However, the growth curve of PF animals was exactly the same, suggesting that initial decline in body weight is caused by calorie restriction.

Diet-induced obesity is characterized by increase in adiposity, as was confirmed by comparison of eWAT, scWAT and BAT weight from STD and cHF mice. Both CDCA and PF treatments partially reversed the developed obesity, with a tendency to stronger effect of CDCA. Despite that, the differences between CDCA and PF were not statistically significant.

The weight of fat depots corresponds well with the morphometrical characterization of adipose tissue. Namely, size of adipocytes both from BAT and scWAT followed the pattern described above for depot weight as can be seen on representative sections from these tissues in Figure 4-2a and Figure 4-3a. The calculated mean adipocyte size from scWAT is showed in Table 4-b. This was the only parameter which differs significantly between CDCA and PF group.

In summary, we found out that major acute effect of CDCA treatment is mediated by initial transient calorie restriction; although, minor part of the effect remains unexplained by this influence.

Table 4-b Fat depots at the end of 3-week reversion experiment

	STD	**cHF**	**1% CDCA**	**PF**
Weight of tissues				
eWAT [mg]	553 ± 94[a]	2490 ± 208	899 ± 147[a]	979 ± 154[a]
scWAT [mg]	183 ± 14[a]	1163 ± 168	417 ± 78[a]	498 ± 83[a]
Interscapular BAT [mg]	121 ± 19[a]	228 ± 20	92 ± 9[a]	125 ± 17[a]
Average adipocyte area				
scWAT [μm^2]	1040 ± 190[a]	3474 ± 240	1652 ± 193[a]	2191 ± 186[a,b]

[a] Significant differences in comparison to cHF group; [b] significant differences in comparison to STD group. Data are shown as means ± SEM (*n*=8, except for STD, where *n*=4; see Materials and Methods).

4.1.3 Chenodeoxycholic acid activates BAT and causes browning of subcutaneous white adipose tissue

Because the UCP1-mediated thermogenesis was previously identified as a mechanism of bile acid-induced energy expenditure, we quantified UCP1 mRNA and protein content in both BAT and scWAT. In BAT, we observed large induction of Ucp1 expression in CDCA (but not in PF) group when compared with cHF controls. This was in accordance with similar upregulation of Prdm16 (which is reported to be essential for Ucp1 expression and activation of UCP1-mediated thermogenesis (Seale, et al. 2011), PGC-1α (or Ppargc1a, marker of mitochondrial biogenesis), ATP/ADP translocator (Slc25a4) and subunit IV of cytochrome c

oxidase (Cox4i1) gene expression (Figure 4-2b). Furthermore, the elevation of Ucp1 gene expression was reflected in total levels of UCP1 protein in whole tissue (Figure 4-2c).

Analysis of scWAT was less conclusive. The Ucp1 transcript was detectable only in PF and CDCA group, while the level in CDCA animals was more than 3 orders of magnitude higher than in PF mice (Figure 4-3b). In spite of this dramatic increase, the total levels of Ucp1 mRNA in scWAT were still negligible in comparison to the levels in BAT (2.59e-5 A.U. in scWAT vs. 0.554 A. U. in BAT under identical conditions). Moreover, unlike in BAT, the increase in Ucp1 transcript was not accompanied by corresponding induction of Prdm16 expression (Figure 4-3c). Due to this limited amount of UCP1 in scWAT, we did not succeed in assessment of UCP1 protein using Western blots. The immunohistological analysis using UCP1-specific anti-bodies proved higher sensitivity in this case: It revealed small amount of UCP1-positive cells in sections of scWAT (but not of eWAT) from both PF and CDCA groups (Figure 4-3d). The number of these brite cells was higher in CDCA group (slightly less than 2% of all cells, Figure 4-3e).

Thus, CDCA stimulates UCP1 generation in both BAT and scWAT. However, activation of BAT is clearly more pronounced and has probably higher physiological significance.

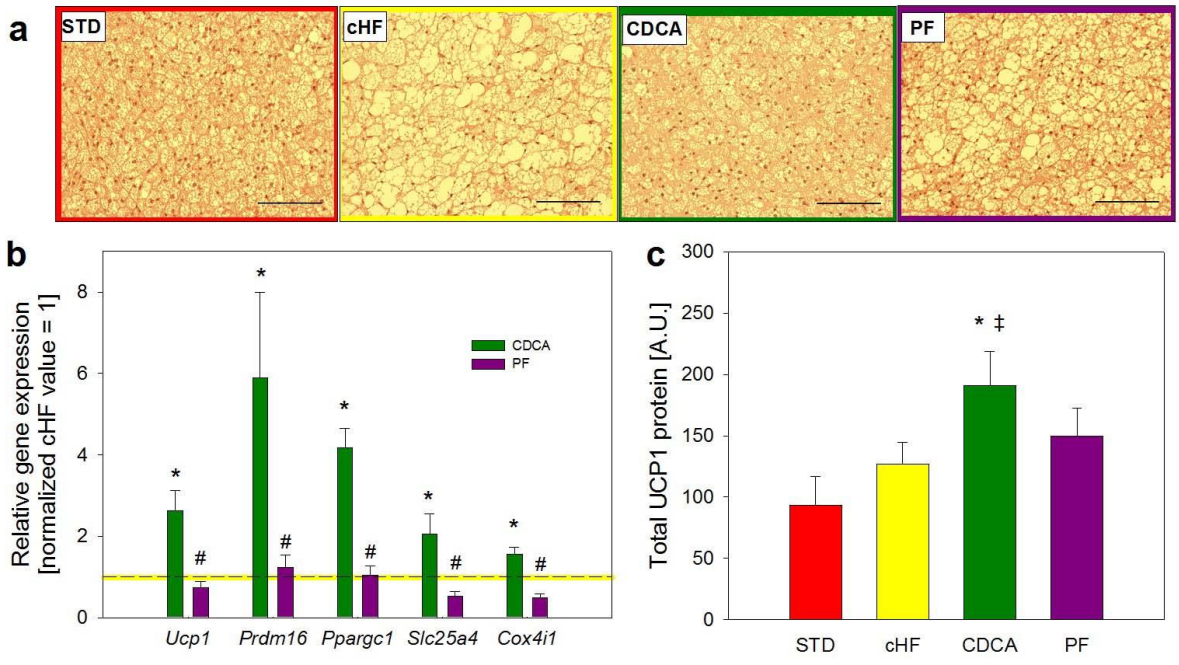

Fig. 4-2 BAT parameters in the 3-week reversion experiment
a) Representative histological images of BAT (bar = 0.1 mm);
b) Relative gene expression normalized to 18S RNA as a housekeeping gene, cHF=1 (dashed line highlighted in yellow);
c) Content of UCP1 protein in whole BAT (assessed by Western blotting);
*significant difference compared with cHF group; # significant difference compared with CDCA group; ‡ significant difference compared with STD group.

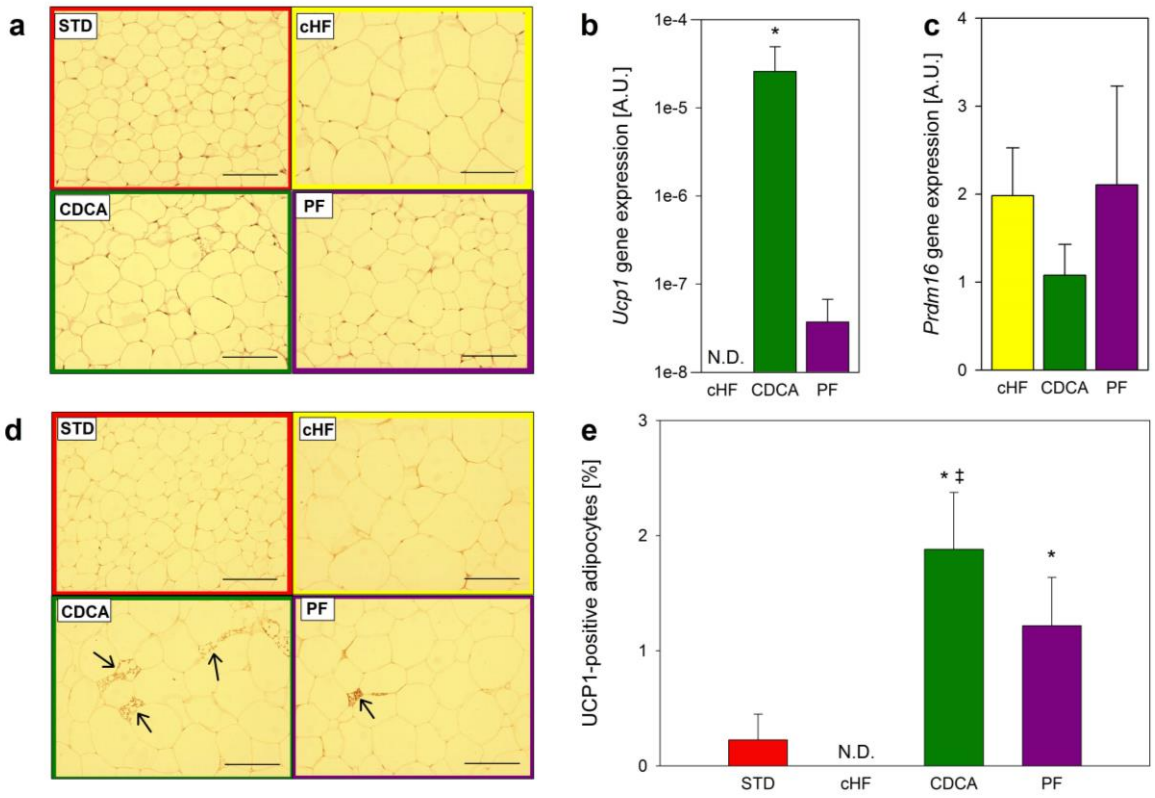

Fig. 4-3 scWAT parameters in the 3-week reversion experiment
a) Representative histological images of BAT (bar = 0.1 mm);
b), c) Relative UCP1 (b) and PRDM16 (c) gene expression normalized to 18S RNA as a housekeeping gene;
d) Representative images of UCP1 immunostaining (bar = 0.1 mm, arrows – UCP1-positive cells);
e) Percentage of UCP1-positive cells relative to total number of adipocytes;
*significant difference compared with cHF group; ‡ significant difference compared with STD group; N.D. not detected.

4.1.4 Chenodeoxycholic acid promotes lipid oxidation, but does not significantly increase energy expenditure

Using indirect calorimetry, we performed analysis of energy expenditure and substrate partitioning in control, CDCA supplemented, and pair-fed animals in order to quantify the CDCA effects on whole body metabolism. Regarding energy expenditure, both control and CDCA-treated group showed typical time course with two maximums – in the beginning and at the end of the night (Figure 4-4a) which corresponds with main feeding time. In contrast, energy expenditure of pair-fed animals was shifted because of specific conditions of food limitation. Diet was refilled every morning, which means that the pair-fed animals consumed

it at latest in the first half of night, and therefore, their energy expenditure in the later phase was decreased. Hence, only the total sum of energy expenditure during whole day can be compared among the experimental groups. Importantly, we did not observe any significant difference in this parameter expressed per animal (even when evaluated by ANCOVA reflecting body weight) (Figure 4-4d). However, when related to body weight, energy expenditure is significantly increased in both CDCA treated and pair-fed groups in comparison to control high-fat fed animals (Figure 4-4e).

Calculation of RQ can reveal changes in favored energy source during the day. Normally, RQ is close to 1 in feeding periods as a result of utilization of dietary carbohydrates, whereas it decreases during fasting reflecting the switch towards oxidation of lipid stores. This typical time course was followed only by control group of cHF-fed animals, whereas the curve for CDCA-treated and for pair-fed mice was flattened or even inversed, respectively (Figure 4-4b). In fact, the CDCA animals show lowered RQ during the dark (but not during the light) phase in comparison to controls. Nevertheless, because of the inversion of RQ time course in PF group (caused by the shift in feeding rhythmicity - similarly to the effect observed on energy expenditure), RQ data cannot be evaluated separately for dark and light phase of day, but they should rather be expressed as average value per 24 hrs, which unfortunately limits the sensitivity of our method. Accordingly, the average RQ of CDCA group tended to be the lowest among all other groups, but these differences were not statistically significant (Figure 4-4f). Only robust PRCF analysis, which takes into account all the RQ values measured in each group, exhibits apparent shift to lipid oxidation in response to both pair-feeding and CDCA administration (Figure 4-4c). Importantly, the shift was more pronounced in CDCA group which suggests some food intake-independent effect of CDCA on fuel partitioning. (Nonetheless, neither the comparison of 50^{th} percentile of the PRCF data shows any significant difference – Figure 4-4g.)

Taken together, all the effects detected using indirect calorimetry were very subtle. The significance of CDCA-driven increase in energy expenditure depends on the fact if the data are related to the body weight or not. Which of these approaches is more correct will be discussed in chapter 5.1. On the other hand, analysis of RQ suggests slightly increased lipid oxidation in CDCA mice, despite some difficulties with limited sensitivity of the method.

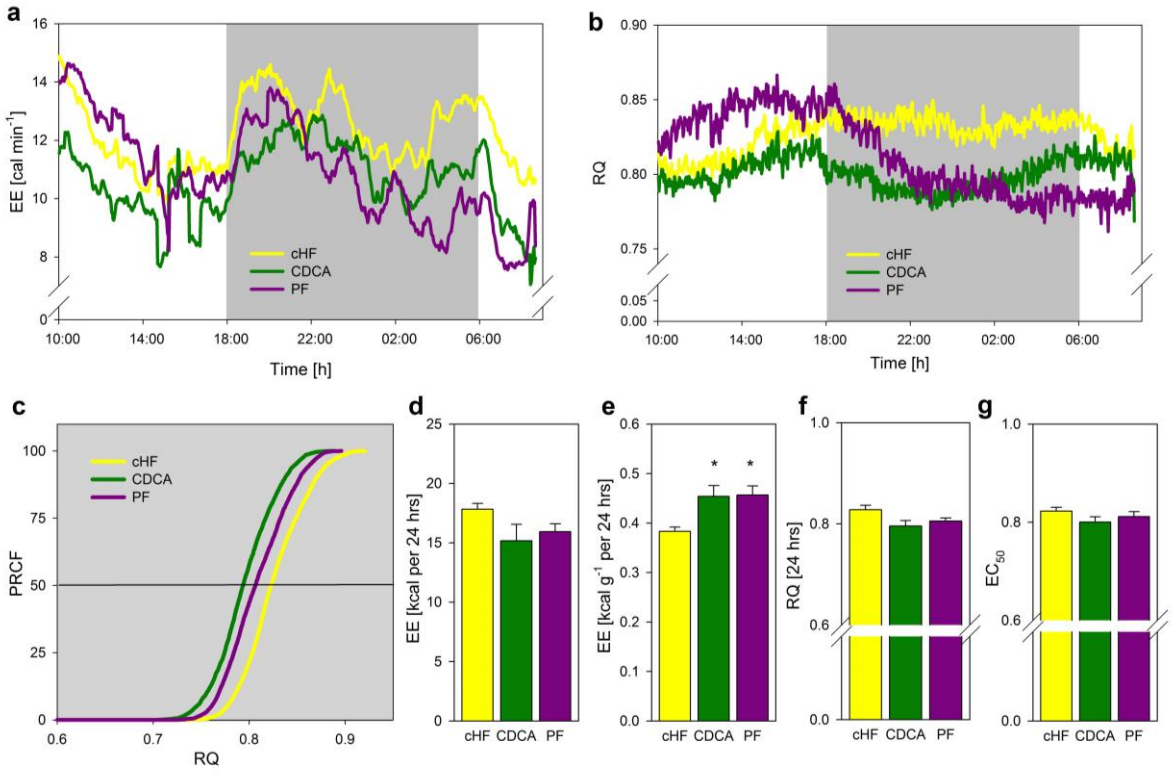

Fig. 4-4 Results of indirect calorimetry in 3-week reversion experiment

a) Time course of energy expenditure (grey area represents dark phase of the day);
b) Time course of respiratory quotient during day;
c) PRCF curves of respiratory quotients during the whole 24-h measurment (each curve data pooled from all mice in the given group);
d) Total energy expenditure per animal;
e) Total energy expenditure per g of body weight;
f) Mean respiratory quotient per 24 hrs;
g) 50th percentile of PRCF derived from curves in Fig 4-4c;

*significant difference compared with cHF group.

4.2 Publication B: Combination of ω-3 polyunsaturated acids and mild calorie restriction in prevention of diet-induced obesity

In order to characterize the effects of ω-3 PUFA in combination with mild calorie restriction, we conducted several independent prevention studies. Results of these experiments were also published in paper B. This chapter corresponds to the 3rd (and partially the 5th) aim of the thesis.

4.2.1 Combination treatment counteracts obesogenic and diabetogenic effects of high-fat feeding

cHF feeding leads to rapid induction of body weight gain, whereas both ω-3 PUFA supplementation (cHF+F) and 10% calorie restriction (cHF+CR) counteract this process. The combination of both treatments prevents the increase in body weight practically completely and cHF+F+CR animals maintain their body weight on the level of control mice fed by STD diet. The protective effect lasted even after15 weeks of treatment (Figure 4-5a). These effects cannot be explained neither by changes in food intake, which was the same in both cHF and cHF+F groups (Table 4-c), nor by induction of physical activity, which, in fact, stayed stable or was even decreased in cHF+F+CR group (Table 4-c).

The deceleration of body weight gain by ω-3 PUFA, calorie restriction, and their combination was reflected in lower adiposity. Weights of eWAT, scWAT, mesenteric WAT, and BAT tended to be decreased in cHF+F, cHF+CR, and cHF+F+CR in comparison with cHF, while this effect was the most striking in the combination group (Table 4-c). Biggest differences were observed in eWAT. Smaller WAT depot weights correspond to the decreased average adipocyte size assessed by morphometrical analysis of histological sections (Table 4-c).

Consequently, the cHF-driven ectopic lipid accumulation in liver was partially prevented by all treatments. In 5 weeks, ω-3 PUFA seem to have greater preventive impact (i. e. tissue lipids are lower in cHF+F and cHF+F+CR groups), whereas after 15 weeks, the effect of calorie restriction become more striking (i. e. ectopic lipids are lower in cHF+CR and especially in cHF+F+CR) (Figure 4-5b). We found smaller effect of cHF+F+CR also on tissue lipids in gastrocnemius muscle after 15 weeks (but not after 5 weeks) (Figure 4-5b).

Evaluation of plasma parameters in random fed state reveals improvement in lipid and glucose homeostasis. Namely, the level of plasma TAG was strongly reduced by both ω-3

PUFA and calorie restriction, but even more by combination of them (Table 4-c). This hypolipidaemic effect was negatively correlated with the effect of the treatments on β-hydroxybutyrate (marker of lipid catabolism, physiologically generated mainly during fasted state). In spite of unchanged glycaemia, the insulin levels were decreased in cHF+CR, and even more in cHF+F+CR. Regarding adipokines, we observed ω-3 PUFA-driven elevation of insulin-sensitizing hormone adiponectin, and mainly CR-driven reduction of leptin levels (again, most pronounced in cHF+F+CR group), which is in accordance with the above mentioned effects on adiposity. (Summarized in Table 4-c.)

In order to obtain data in better characterized metabolic state, lipids and glucose levels were assessed also in plasma collected from fasted and re-fed animals. Both glucose and NEFA were equivalent in all groups in re-fed state, but differ dramatically in samples from fasted animals. Physiologically, NEFA levels are elevated during fasting as a result of preferential lipid utilization, and glucose is decreased for the same reason. This typical pattern was observed in STD and cHF+F+CR animals, while the NEFA and glucose levels in cHF animals were very close to the values from re-fed state (Figure 4-5c, d). It means that cHF deteriorates metabolic flexibility, which can be prevented by combination treatment. The fact that re-feeding induces shift from lipid to glucose oxidation especially in cHF+F+CR group was proved by the measurement of increase in RQ after intragastric gavage to fasted animals (Figure 4-5e).

These data collectively point to preservation of insulin sensitivity in cHF+F, cHF+CR, and especially in cHF+F+CR group. To support this assumption, we measured plasma insulin in fasted animals and calculated HOMA index, which is considered as a standard marker of insulin sensitivity. As shown in Figure 4-5f and g, cHF increase both fasted insulin and HOMA index, which can be significantly counteracted only by combination treatment. Furthermore, we tested glucose tolerance using OGTT, which revealed increase of AUC in cHF group in comparison to STD and a return to lower values caused by cHF+F+CR (Figure 4-5h, i). Interestingly, animals subjected to calorie restriction showed increased glycaemia after overnight fasting prior to OGTT, probably as an adaptation to restricted feeding. During the OGTT, plasma samples from 30 min after glucose gavage were also collected to assess postprandial insulin levels. Similarly to other parameters, insulin was elevated by cHF and decreased by combination treatment again.

Finally, we tested insulin sensitivity also by *ex vivo* assessment of insulin-stimulated *de novo* fatty acid synthesis in eWAT. Both ω-3 PUFA and calorie restriction improved

responsiveness of eWAT to insulin, whereas combination treatment acted in synergistic manner (Figure 4-5j).

Using several independent analyses, we proved that combination of ω-3 PUFA and calorie restriction prevents synergistically the deleterious effects of diet-induced obesity on insulin sensitivity. In following analyses, we focused on possible mechanisms of this protective action.

Tab. 4-c Parameters of mice after 5 weeks of the treatment in experiment of publication B

	cHF	**cHF+F**	**cHF+CR**	**cHF+F+ CR**
Body weight gain (g)	3.7±0.5	2.9±0.6	2.1±0.3[a]	0.8±0.2[a,b,c]
Food consumption (kJ/day per animal)	74.6±0.6	73.7±1.8	67.1±0.5[a,b]	66.3±1.6[a,b]
eWAT				
Weight (mg)	624±74	566±90	408±58	262±26[a,b]
Adipocyte area (μm^2)	2395±147	1920±160	1851±300	1690±152[a]
Mesenteric fat				
Weight (mg)	298±31	277±19	268±22	205±16[a,b]
Adipocyte area (μm^2)	1217±84	1136±136	1315±153	997±108[a,c]
scWAT				
Weight (mg)	284±26	269±21	233±20	208±10[a]
Interscapular brown fat				
Weight (mg)	173±10	121±5[a]	119±4.8[a]	76±5[a,b,c]
Liver				
Weight (mg)	1148±59	1233±18	1134±26	1009±36[b]
Plasma				
TAG (mmol/l)	1.24±0.11	0.62±0.06[a]	0.65±0.06[a]	0.35±0.05[a,b,c]
β-hydroxybutyrate (mmol/l)	0.09±0.01	0.13±0.02[a]	0.20±0.01[a,b]	0.28±0.02[a,b,c]
Glucose (mg/ml)	3.09±0.08	3.07±0.02	3.13±0.09	2.80±0.01
Insulin (ng/ml)	1.75±0.20	1.27±0.21[a]	0.33±0.03[a,b]	0.20±0.05[a,b,c]
Adiponectin (μg/ml)	8.9±0.3	12.1±0.5[a]	9.3±0.2[b]	11.1±0.5[a,c]
Leptin (ng/ml)	77.2±7.6	66.2±8.3[a]	15.5±1.7[a,b]	5.3±0.7[a,b,c]

In the case of WAT, subcutaneous dorsolumbar (scWAT), epididymal (eWAT) and mesenteric depots were collected. Tissue dissection and plasma collection were performed in random-fed state (between 8 a.m. and 10 a.m.); data are means±SEM; n=10; *a, b, c* - significant differences (ANOVA) compared to cHF, cHF+F, cHF+CR, respectively.

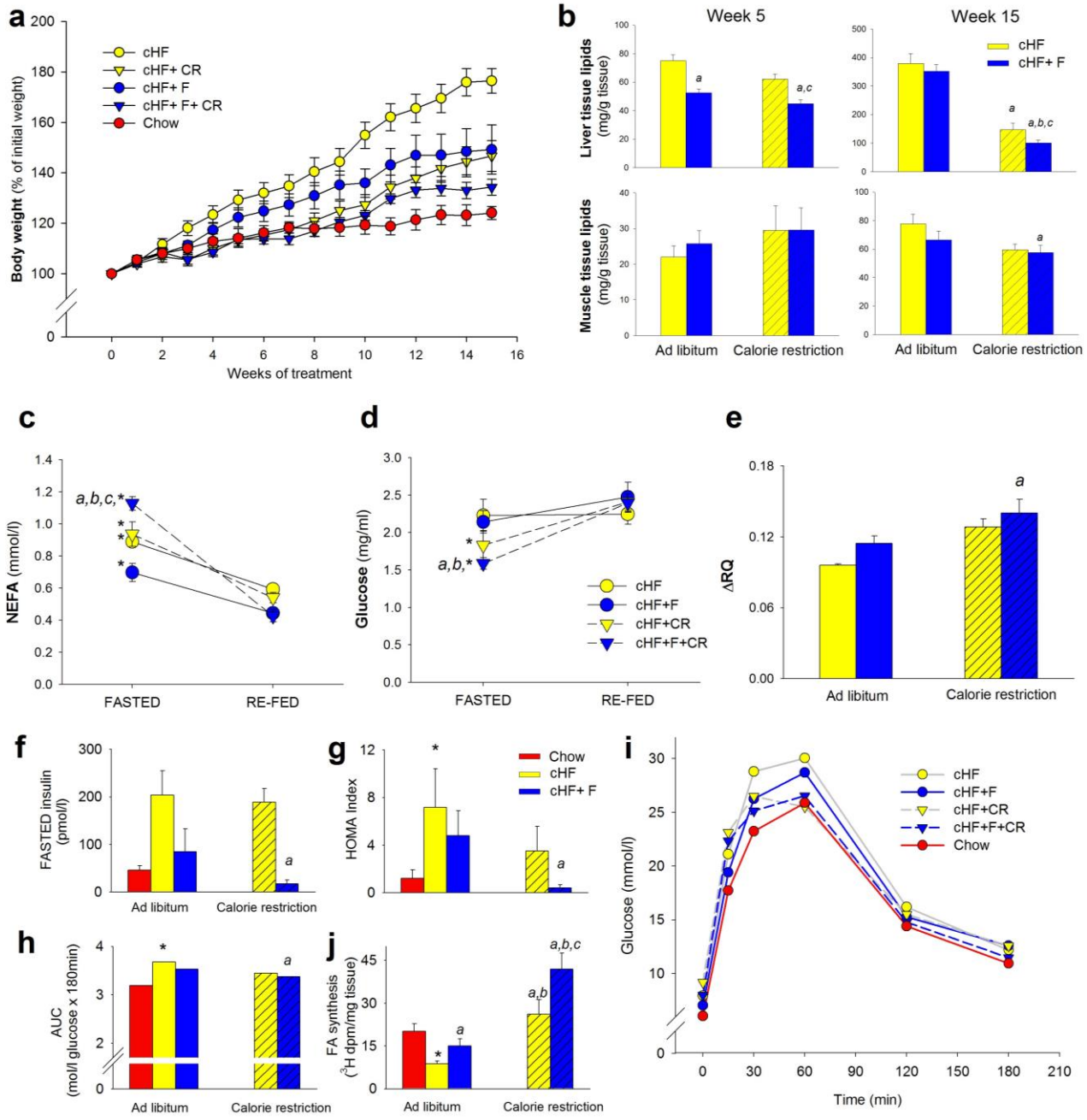

Fig. 4-5 Prevention of diet-induced obesity, hepatic steatosis, metabolic inflexibility and glucose intolerance by ω-3 PUFA and calorie restriction

a) Growth curves of mice during 15-wk experiment;

b) Ectopic lipid accumulation in liver (upper graphs) and muscle (lower graphs) after 5 weeks (on the left) or 15 weeks (on the right);

c), d) NEFA (c) and glucose (d) levels in plasma during fasted/fed transition (after 4 weeks of treatment);

e) Maximal induction of respiratory quotient by bolus of glucose after overnight fasting;

f), g) Fasted insulin level (f) and HOMA index (g) after 4 weeks of the treatment;

i), j) Results of oral glucose tolerance test: Glycemic curves (i) and integrated area under curves. (OGTT performed after 3 weeks of the treatment);

g) Ex vivo analysis of FA synthesis in eWAT in presence of insulin;

[a,b,c] significant difference compared with cHF, cHF+F, and cHF+CR, respectively (ANOVA); [d] significant difference compared to Chow group (t-test); [e] significant difference between the fasted and re-fed states (repeated measures ANOVA).

4.2.2 Combination treatment induces mitochondrial biogenesis and lipid catabolism in epididymal white adipose tissue

In order to identify the mechanism of observed effects, we performed broad gene expression analysis in all major metabolically active tissue, namely liver, muscle and several adipose tissue depots. We did not find any effect of the combination treatment in skeletal muscle and BAT, and just very small induction of genes involved in β-oxidation (Vlcad, Lcad and Mcad) in liver. (On the other hand, expression of rate-limiting enzyme of FA catabolism - Cpt1 was affected in none of the examined tissues, which is probably due to the fact that this enzyme activity is regulated mainly allosterically – see chapter 1.3.2.) In contrast, WAT expression pattern was dramatically changed. Added to increase in Vlcad and Lcad expression, markers of mitochondrial biogenesis (Pgc-1α, Pparα, and Nrf-1) and oxidative capacity (mitochondrially encoded Cyox3) were strongly induced. Interestingly, these changes were limited specifically to eWAT. In contrast, only Pparα transcript was elevated in scWAT. It is important to stress that Ucp1 expression was altered neither in eWAT, nor in BAT. Importantly, fatty acid synthase (Fas) and phosphoenolpyruvate carboxykinase (Pck1, major glyceroneogenic gene in adipose tissue) were also induced in eWAT, which was fully appreciated in later works from our department (Flachs, et al. 2013) (see chapter 5.5). As expected, ω-3 PUFA supplementation decreased expression of stearoyl-CoA desaturase 1 (Scd1) in eWAT and BAT, and tend to the same result in muscle. Scd1 is essential for production of unsaturated fatty acids, which is less important in condition of higher intake of these compounds in diet.

Increased mitochondrial oxidative capacity was then tested by 3 independent assessments. First of all, [1-^{14}C]palmitate oxidation was measured in eWAT fat pads, freshly isolated adipocytes, primary culture of hepatocytes and pieces of muscle. cHF feeding increases the FA oxidation in comparison with STD because lipids constitute the main source of energy in this type of diet. In accordance with the results of qPCR analysis, palmitate oxidation is further elevated by combination treatment in eWAT tissue samples (Fig. 4-5a), isolated adipocytes (Figure 4-5d) and cultured hepatocytes (Figure 4-5b), but not in muscle (Figure 4-5c).

In all other analyses, we focused only on eWAT of cHF and cHF+F+CR group, where we expected biggest differences. We found strong increase in both cytochrome oxidase activity (the complex IV of mitochondrial respiratory chain, Figure 4-5e) and cytochrome b content (Figure 4-5f). We also examined oxidative capacity of freshly isolated permeabilized

adipocytes. The cells from cHF+F+CR mice exerted approximately 2-fold higher rate of oxygen consumption in the presence of respiratory substrates glycerol-3-phosphate and succinate compared with the cHF mice (Figure 4-5i). The oxidation rate was limited by ATP synthase activity, as documented by the stimulatory effect of ADP addition, inhibitory effect of oligomycin, and its reversal by chemical uncoupler FCCP. The respiratory control index (state 3 / state 4 respiration, i. e. ratio of oxygen consumption before and after addition of ADP) was equal for both groups (Figure 4-5g).

Our results demonstrate that (1) mitochondrial oxidative capacity is increased cHF+F+CR (as suggested by gene expression, palmitate oxidation, cytochrome oxidase activity, cytochrome b content and mitochondrial oxygen consumption on exogenous substrates), and (2) mitochondria are fully coupled and produce ATP (as suggested by unchanged Ucp1 expression and high respiratory control ratios).

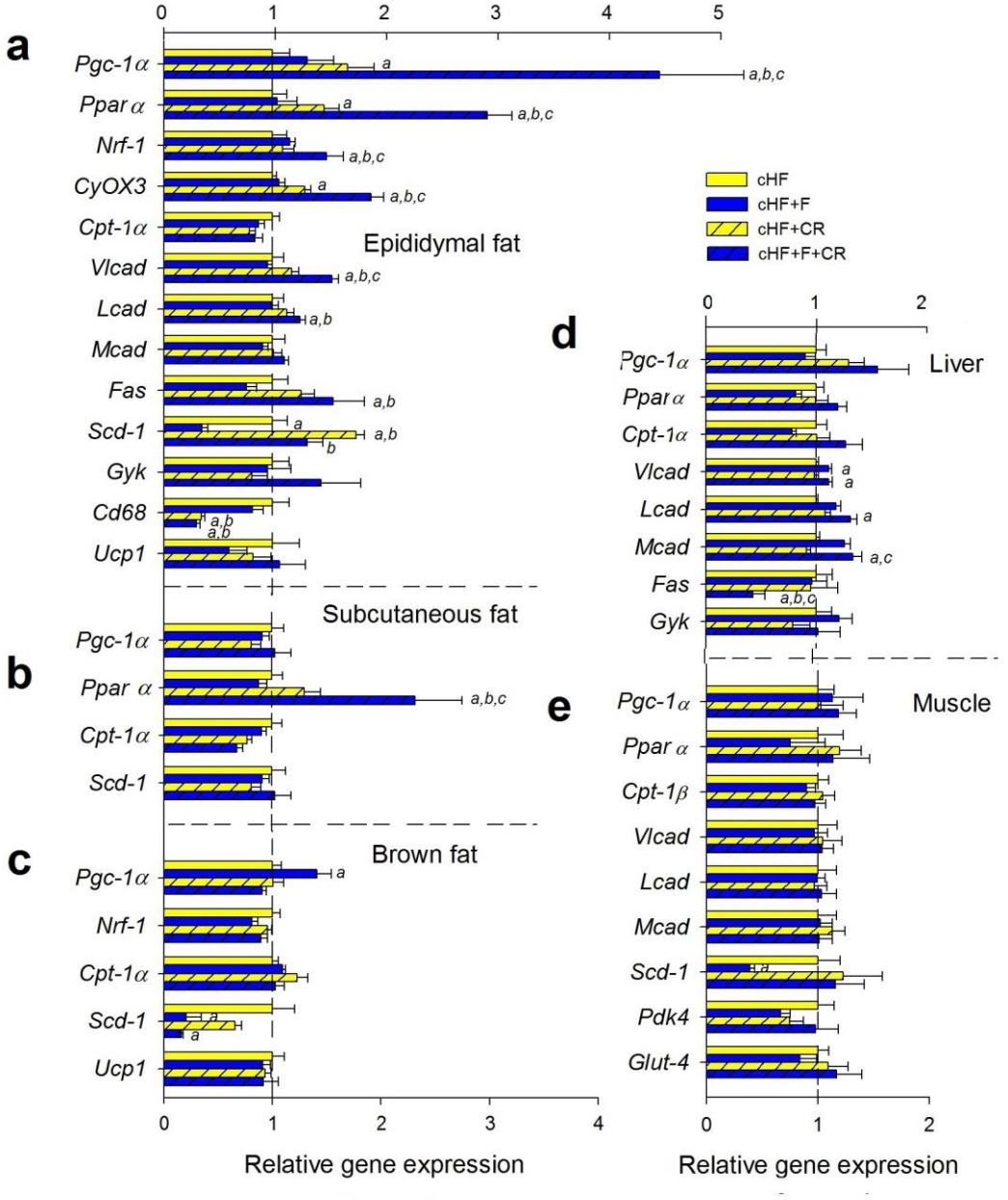

Fig. 4-6 Gene expression in response to ω-3 PUFA and calorie restriction Relative gene expression (cHF=1) in eWAT (a), scWAT (b), BAT (c), liver (d), and gastrocnemius muscle (e); gene expression was normalized to geometrical mean of housekeeping genes cyclophilin β and EF1α; ^{a,b,c} significant difference compared with cHF, cHF+F, and cHF+CR, respectively (ANOVA).

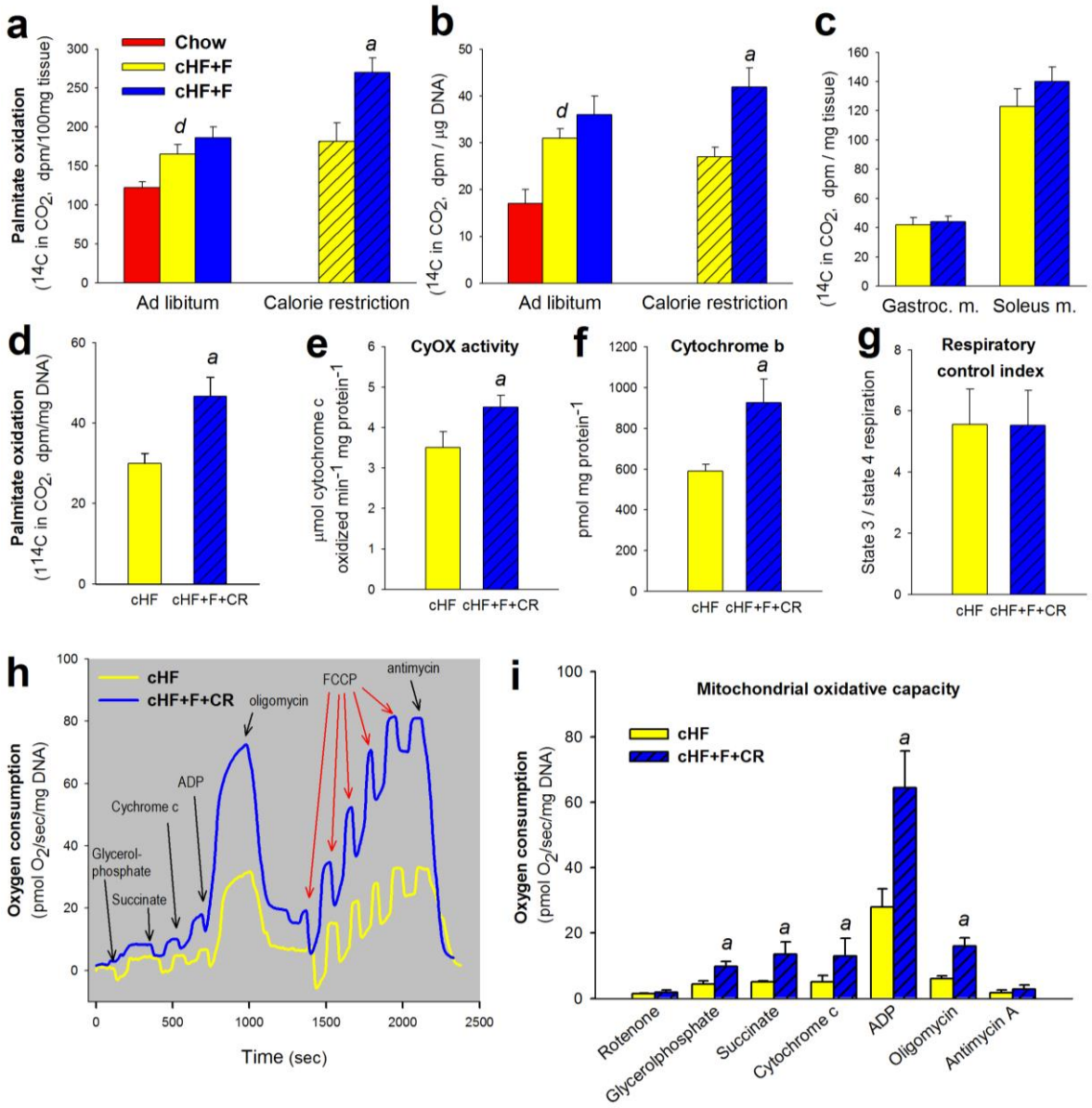

Fig. 4-7 Mitochondrial oxidative capacity in response to ω-3 PUFA and calorie restriction
a), b), c), d) Palmitate oxidation in eWAT (a), primary hepatocytes (b), soleus and gastrocnemius muscles (c), and isolated adipocytes from eWAT (d)
e) Cytochrom oxidase activity in eWAT
f) Cytochrom b content in eWAT
g), h), i) Results of high resolution respirometry: Representative curves of oxygen consumption including titration of uncoupler FCCP (h); means of oxygen consumption in conditions of given substrates and inhibitors (i); and respiratory control index (state 3 / state 4, i.e. respiration after ADP addition / respiration before ADP addition) (g);
[a] significant difference compared with cHF (ANOVA); [d] significant difference compared to Chow group (t-test).

4.2.3 Combination treatment counteracts chronic inflammation of white adipose tissue via generating anti-inflammatory lipid mediators

Obesity is characterized by chronic low-grade inflammation of adipose tissue, while ω-3 PUFA administration is reported to acts against this state. We were, therefore, interested to what extent ω-3 PUFA alleviates WAT inflammation in the context of mild calorie restriction. As was revealed by immunohistochemical analysis, eWAT is massively infiltrated by macrophages in cHF-treated animals. These immune cells aggregate around dead adipocytes creating so-called crown-like structures (Figure 4-8a). Crown-like structures abundance is reduced by calorie-restriction (independently on ω-3 PUFA). This result corresponds with expression of Cd68 (marker of macrophages) in eWAT (compare Figure 4-6a and 4-8c). Furthermore, we tested plasma levels of interleukin 6, a marker of systemic inflammation). This cytokine was significantly reduced only by the combination treatment.

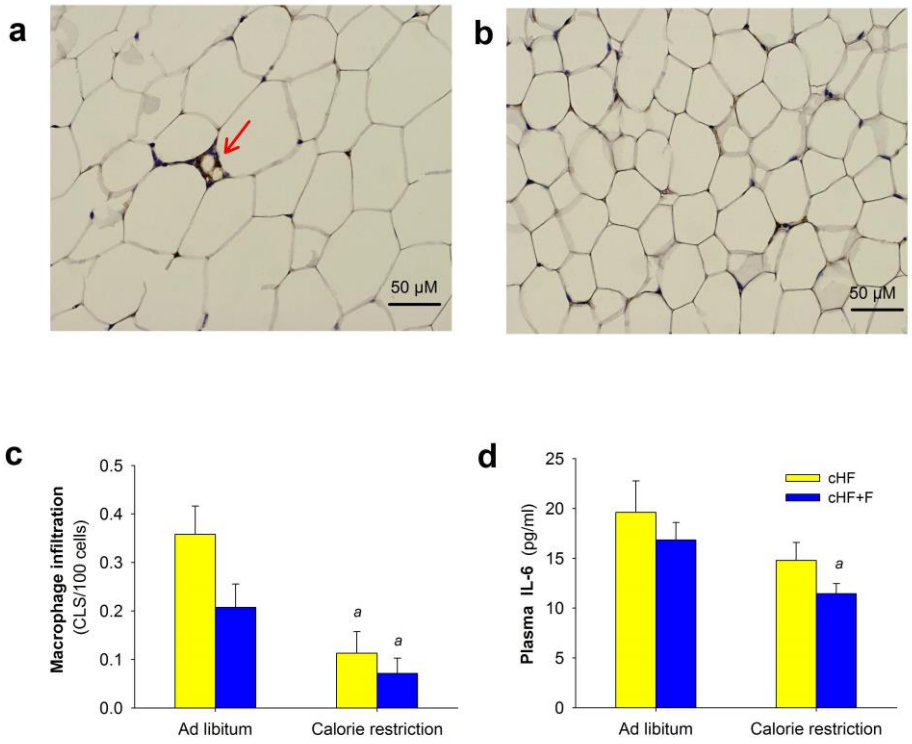

Fig. 4-8 WAT and systemic inflammation
a), b) Representative MAC-2-immunohistochemical pictures of eWAT from mice after cHF (a) and cHF+F+CR treatment (b); arrow indicates crown-like structure (CLS) – aggregate of activated macrophages;
c) Relative count of CLS;
d) Plasma levels of IL-6;
[a] significant difference compared with cHF (ANOVA).

As explained in the Introduction, PUFAs represent major source for production of lipid mediators regulating inflammatory process. On the other hand, calorie restriction can influence the liberation of these compounds from phospholipids of plasma membrane. Hence, we performed complex lipidomic analysis in eWAT and liver quantifying 24 lipid species. The data were analyzed by partial least-square-discriminant analysis, followed by contribution-score analysis in order to identify the most important lipids for each intervention group (for details see Electronic supplementary material of Publication B). Generally, all major PUFA (AA, EPA, and DHA) were significantly higher in eWAT by almost all tested treatments when compared to cHF (Figure 4-9). Data from liver were less unequivocal (Figure 4-9). Among the tested metabolites, synergistic induction by cHF+F+CR was found in protectin D1 (or possibly its isomers such as PDX), a well-described anti-inflammatory mediator derived from DHA) and 15-deoxy-$\Delta^{12,14}$-prostaglandin J_2 (15d-PGJ_2). The effect on the latter is unexpected and may have important consequences, as will be discussed below.

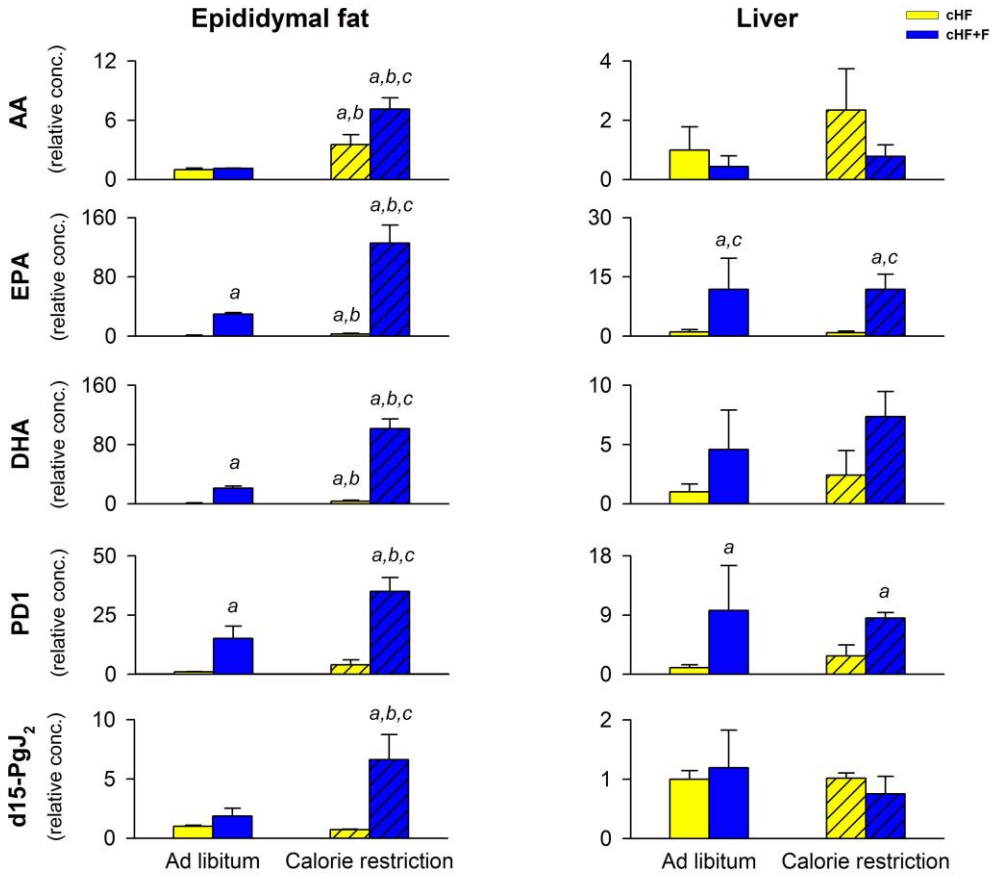

Fig. 4-9 Lipid mediators in eWAT and liver
Selected results of lipidomic HPLC MS-MS analysis;
[a] significant difference compared with cHF (ANOVA).

4.3 Publication C: Strain-dependent cold-induced changes in brown and white adipose tissue

AJ and B6 mice are often used in metabolic studies as models of obesity-resistant and obesity-prone animals, respectively. The relative resistance of AJ mice to obesity may be related to the higher sensitivity to β3 agonist treatment and greater capacity to induce UCP1 in WAT depots, especially in response to high-fat feeding (Collins, et al. 1997; Guerra, et al. 1998; Watson, et al. 2000). Therefore, we used these two murine strains to investigate the recruitment of BAT and WAT thermogenic capacity during first phase of cold adaptation, and also to adress the role of modulation of TAG/NEFA futile cycling under these conditions.

4.3.1 Cold exposure causes mobilization of lipid stores and UCP1 induction in brown and subcutaneous white adipose tissue within days

During cold exposure, the energy demands of mouse increase several times; first in order to supply substrate for muscle shivering, later to cover costs of NST. Thus, in our experiments, food intake rose almost twice during the first two days of cold exposure, and the increase continued till the end of the experiment (Figure 4-10a). Nevertheless, the energy expenditure in the very first phase of cold exposure was even higher, as documented by drop of body weight after 2 days (Figure 4-10b). The decrease in body weight in first phase of the treatment is manifested mainly in the reduction of fat mass of BAT, eWAT, and scWAT (Figure 4-10c, d, and e). Interestingly, the decrease in WAT weight was stronger in AJ mice. Lipids from WAT depots are secreted to blood in form of NEFA. However, elevated NEFA clearance causes a transient decrease in plasma NEFA levels (Figure 4-10g) in spite of obvious massive lipolysis in both eWAT and scWAT. A similar pattern can be observed in plasma TAG levels (Figure 4-10f). The transient decrease in plasma lipid levels was more pronounced in AJ mice.

If cold stress is prolonged up to 7 days, many of the above described effects are reversed. The drop in body weight is compensated by still increasing food intake; therefore mice let for 7 days in cold reach almost the body weight of their counterparts maintained in thermoneutrality (Figure 4-10b). Interestingly, individual fat depots react to these conditions in a specific manner: BAT starts to regain weight (Figure 4-10c) (probably due to lipid and glucose uptake and also substantial proteosynthesis – see below), scWAT remains stable (Figure 4-10e), while weight of eWAT continues to decline (Figure 4-10d). These effects are

observed in both strains. The absolute magnitude may differ since AJ mice are usually smaller (while having bigger WAT depots), but the pattern of changes is always analogous.

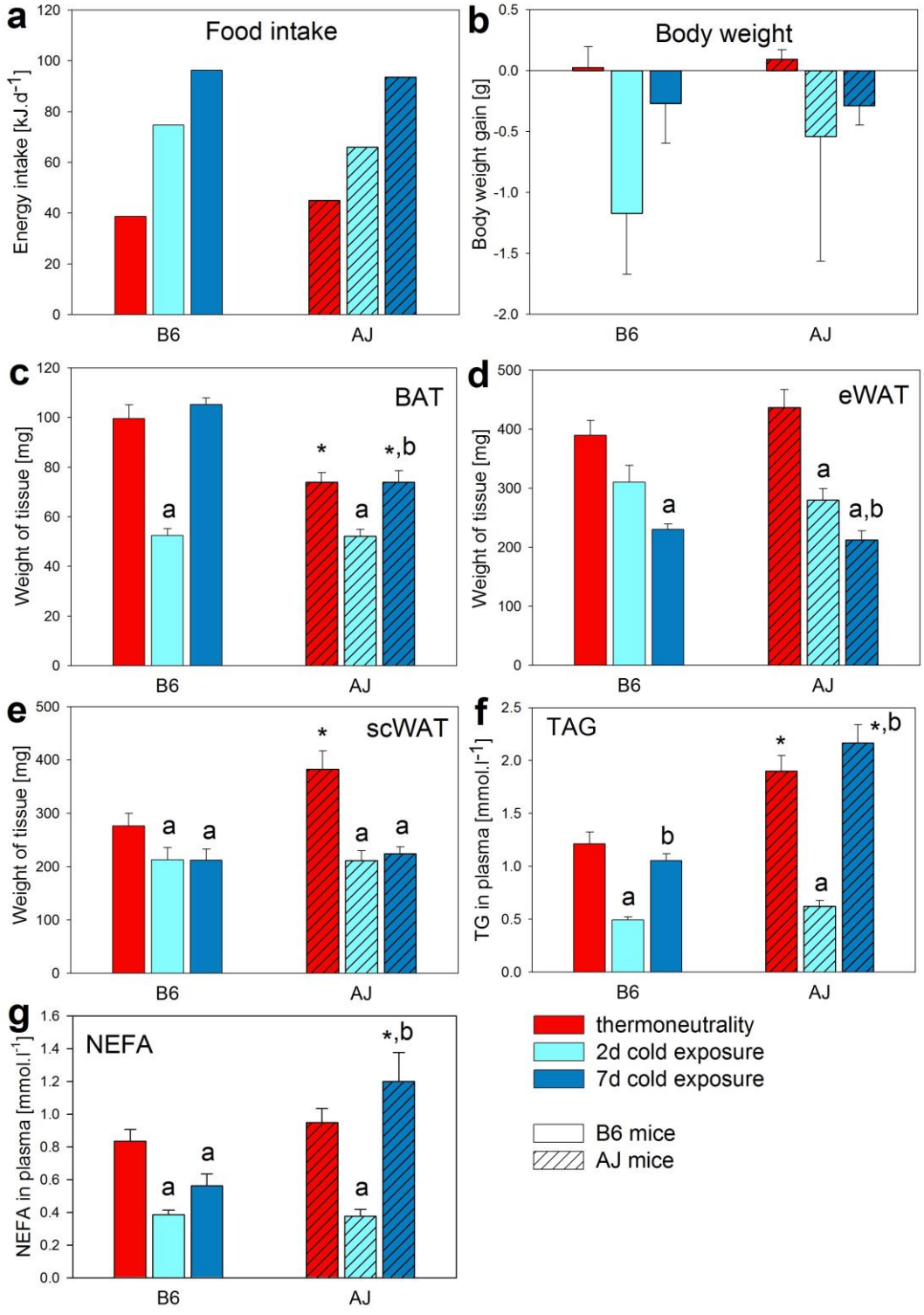

Fig. 4-10 Physiological consequences of cold exposure

a) Increase in energy intake after exposure to cold (as mice are co-caged, we do not have enough data to calculate statistics for this variable); b) Decrease in body weight;

c), d), e) Changes in adiposity as weights of main BAT (c) and WAT (d, e) depots;

f), g) Changes in plasma levels of TAG (f) and NEFA (g);

* significant difference (t-test) compared with other strain; [a] significant difference compared with thermoneutral group of the respective strain; [b] significant difference compared with group 2d-cold-exposed of the respective strain; N.D. not determined.

Importantly, also the plasma lipids are increased after 7 days in cold (Figure 4-10f). Especially in AJ mice, the NEFA are elevated (even above levels observed in thermoneutrality). As NEFA are probably derived largely from still decreasing eWAT, this result suggests higher metabolic flexibility of eWAT in AJ mice.

During prolonged cold stress, BAT gradually takes over the crucial part of thermogenesis, while inducing UCP1 protein synthesis. Thus, in the interscapular BAT, both UCP1 mRNA (Figure 4-11a) and protein levels (Figure 4-11b) are increased in response to cold. mRNA level peaks already after 2 days while UCP1 protein induction is slightly delayed. Between 2nd and 7th day in cold, UCP1 protein content related to mg of tissue does not change too much. However, its total level per tissue still significantly grows as BAT mass in the same period increases. Although the BAT depot of animals maintained in 30 °C have approximately the same weight as the organ of animals after 7 days in cold environment (Figure 4-10c), the structure and composition of the tissue differ substantially – while BAT of control animals contains great proportion of stored lipids, it becomes efficient fat-burning organ with several-fold elevated UCP1 level after several days of cold exposure. The induction of UCP1 must be accompanied by increase in lipid and glucose uptake, which are clearly smaller than demands in the first 2 days in cold.

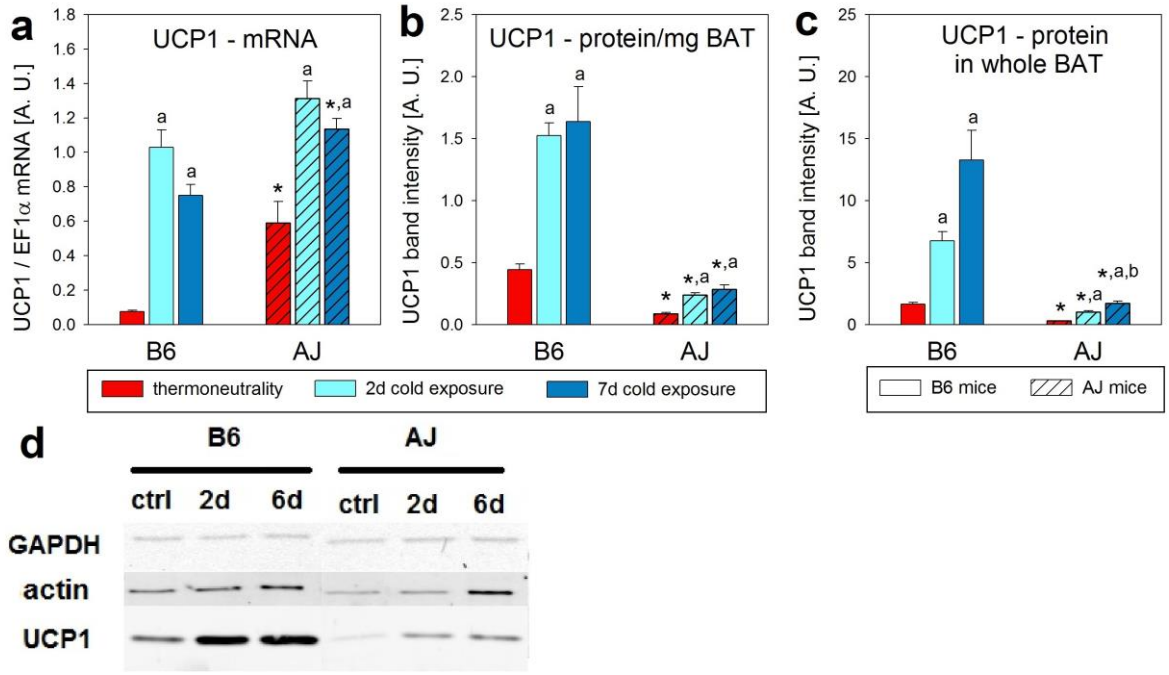

Fig. 4-11 Recruitment of UCP1 in interscapular BAT
a) Induction of UCP1 gene expression;
b), c) WB analysis of UCP1 protein content per mg protein (b) and in whole tissue (c);
d) Representative membrane scan;
*, ^{a}, ^{b} significant differences (t-test) compared with other strain, thermoneutral group of the same strain, and 2d-cold-exposed group of the same strain, respectively.

Surprisingly, we did not observe comparable UCP1 levels in both strains. Moreover, we found striking discrepancy between mRNA and protein data. While UCP1 mRNA was the same in both strains or even higher in AJ mice (Figure 4-11a), B6 animals exhibit up to 4-fold higher amount of UCP1 protein in BAT (Figure 4-11b and c), which is inconsistent with the literature. Similar results were obtained in several independent experiments using both isolated membrane fraction and crude homogenate from BAT.

Futhermore, we found a similar pattern of UCP1 expression in the scWAT, where the mRNA level also increased identically in both strains, when exposed to cold (while the level was higher in AJ mice under unstimulated conditions; Figure 4-12a). On the other hand, the protein content assessed by Western blotting was far the bigger in B6 animals (Figure 4-12b). Comparing scWAT and BAT, it is important to note that UCP1 induction in scWAT is more pronounced but the resultant total amount of UCP1 is still substantially higher in BAT.

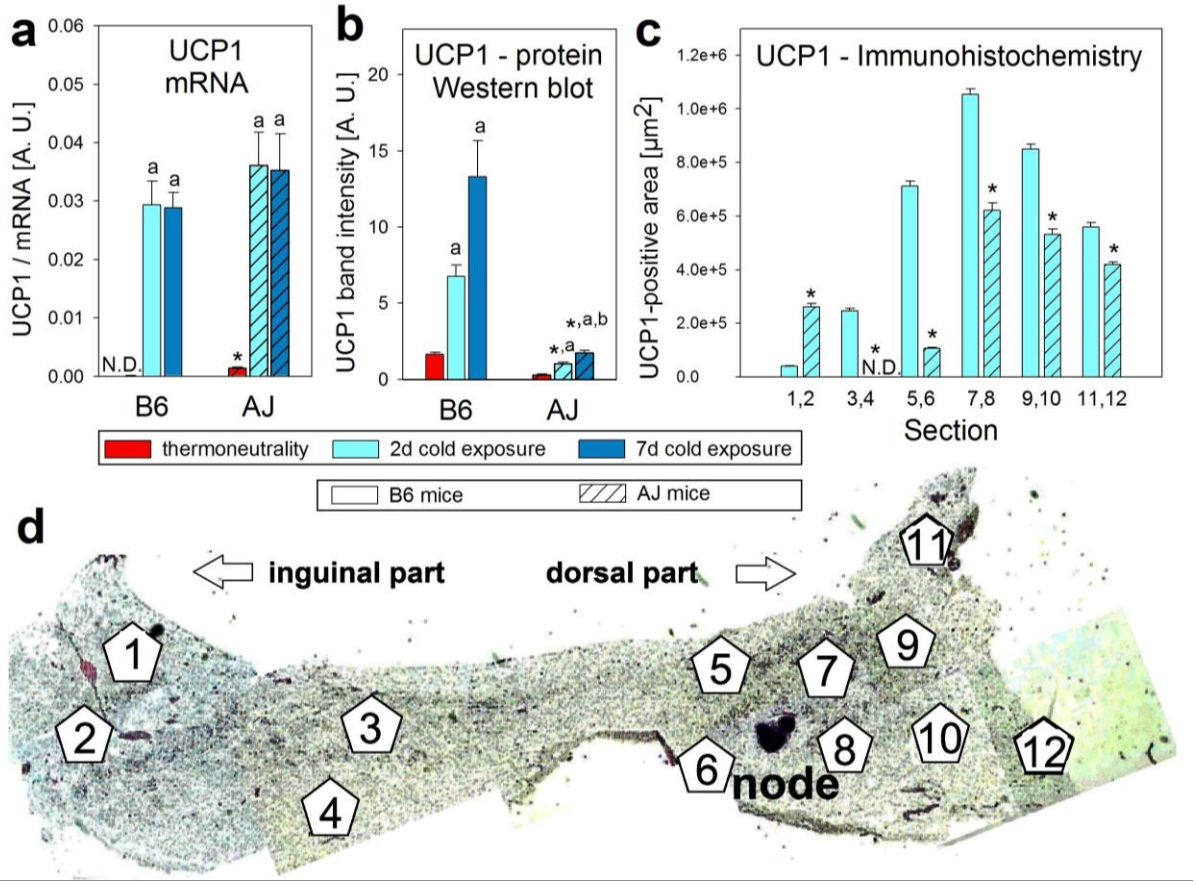

Fig. 4-12 Browning of scWAT

a) UCP1 gene expression normalized to EF1α;

b) WB analysis of UCP1 protein content in scWAT;

c), d) Immunohistochemical analysis of UCP1 content reveals significant variability along the depot; Locations of individual analyzed pictures are specified in (d);

* significant difference (t-test) compared with other strain; [a] significant difference compared with thermoneutral group of the respective strain; [b] significant difference compared with group 2d-cold-exposed of the respective strain; node – lymph node, N.D. not detected.

Then, we performed an immunohistochemical analysis of scWAT. This method does not allow accurate quantitative determination of UCP1 content, but provides better image of UCP1 location in the depot. This approach confirmed higher total UCP1-positive area in B6 animals, while revealed significant heterogenity regarding its localization (Figure 4-12c, d). The areas of UCP1-positive cells are generally concentrated around the main lymph node in the depot. The anterior dorsal part of both strains contains more UCP1 islets than the inguinal part. Importantly, if looking only on the inguinal top of the depot, AJ animals seem to exhibit higher UCP1 content, which may be confusing if UCP1 is assessed without taking the localization into account.

4.3.2 Cold exposure stimulates UCP1-independent remodeling of eWAT involving TAG/NEFA cycling

As was already shown above, eWAT undergoes gradual loss of weight during prolonged cold stress. It probably significantly contributes to elevation of NEFA level in plasma in later phases of cold exposure. The extensive lipolysis in the depot is further suggested by the induction of ATGL expression, already after 2 days in cold (Figure 4-13a).

Liberated FA are largely secreted to blood – the capacity to oxidize them *in situ* is very limited. Although there is striking induction of UCP1 mRNA in cold-exposed AJ mice (Figure 4-13b), none of the experimental groups reached UCP1 protein levels detectable by Western blotting.

However, as was described in chapter 1.3.2, lipolysis is always accompanied by certain rate of FA re-esterification, which cannot be neglected. Our next objective was, therefore, the investigation of this phenomenon. Gene expression of PEPCK, marker of glyceroneogenesis, was elevated in AJ animals, but did not change in response to cold exposure (Figure 4-13a).

As the gene expression data often do not correspond with the protein content and/or enzymatic activity, we looked for technique for functional assessment of FA re-esterification rate. Finally, in collaboration with our Portuguese partners, we developed method for tracing newly synthesized TAG by stable isotope ^{2}H. As was already described (chapters 3.2 and 3.15) mice were injected with $^{2}H_2O$ (40 hrs or 4 days before dissection) and then drank 5% $^{2}H_2O$ till the end of the experiment. We tried to reach stable 5% ^{2}H enrichment of body water, but this goal was not entirely achieved (Figure 4-13c), because calculations of $^{2}H_2O$ dose were biased by different adiposity of experimental animals, while the growth curves and

probably also the water intake varied among the groups. Notwithstanding these limitations, we succeeded in obtaining highly significant results demonstrating elevated TAG synthesis upon prolonged cold exposure (Figure 4-13e and f). Interestingly, the re-esterification is almost unaffected after 2 days in cold. Furthermore, this method provided us also data showing the kinetics of FA synthesis de novo upon cold stress. It seems that FA synthesis is repressed at the beginning of cold stress, while it rises in later phase (Figure 4-13d).

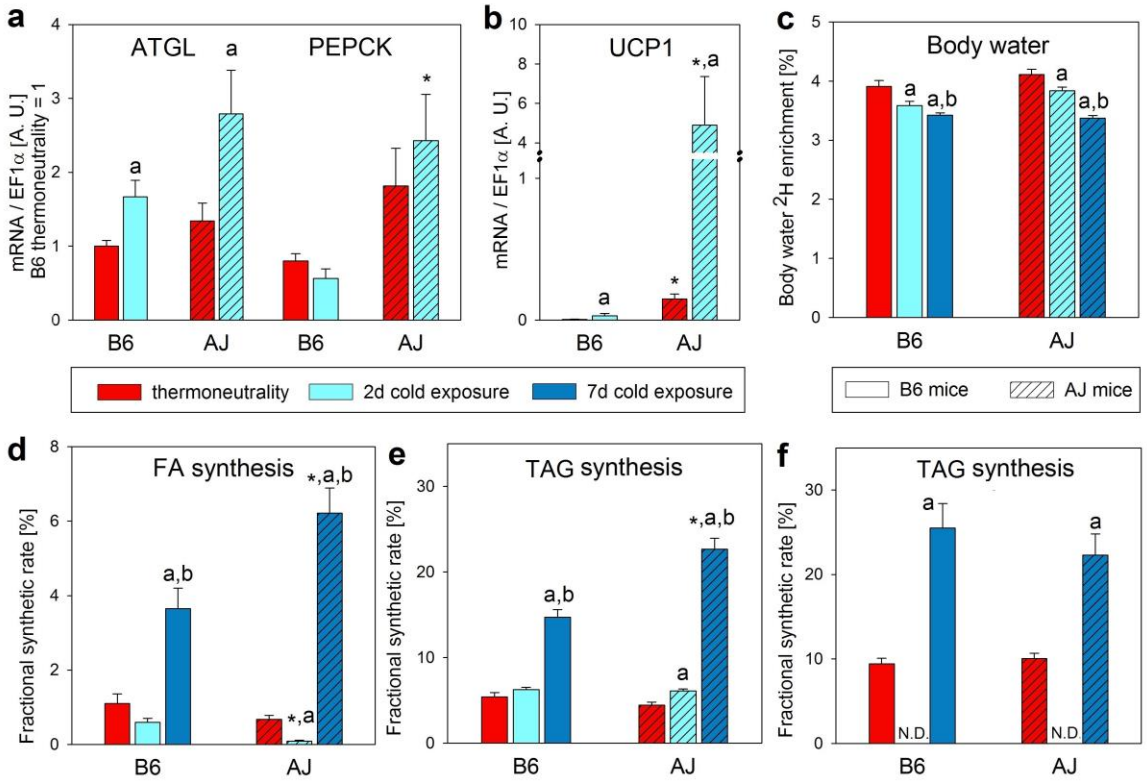

Fig. 4-13 Induction of TAG/NEFA cycling in eWAT

a) RT qPCR data normalized to housekeeping gene EF1α showing relative levels of gene expression (B6 in thermoneutrality = 1);
b) Gene expression of UCP1 normalized to EF1α;
c) ^{2}H enrichment of body water 40 hrs after $^{2}H_2O$ injection;
d) Rate of FA synthesis calculated from ^{2}H enrichment of FA methyl in eWAT TAG 40 hrs after $^{2}H_2O$ injection;
e) Rate of TAG synthesis calculated from ^{2}H enrichment of glycerol moiety in eWAT TAG 40 hrs after $^{2}H_2O$ injection;
f) Rate of TAG synthesis calculated from ^{2}H enrichment of glycerol moiety in eWAT TAG 4 days after $^{2}H_2O$ injection;

* significant difference (t-test) compared with other strain; [a] significant difference compared with thermoneutral group of the respective strain; [b] significant difference compared with group 2d-cold-exposed of the respective strain; N.D. not determined.

Importantly, induction of both TAG and FA synthesis is significantly higher in AJ mice in comparison with B6. However, this difference disappears if the $^{2}H_2O$ is injected 4 days (instead of 40 hrs) before dissection. This suggests that key effects may occur shortly before the end of investigated 7-day period.

Altogether, our data shows clearly the existence of substantial TAG/NEFA cycling in eWAT. Moreover, AJ mice exhibit higher inducibility of this cycling in comparison to B6 mice. Possible consequences of this finding will be discussed in chapter 5.5.

5. Discussion

In this chapter, I comment the results described above considering the aims of the thesis. Therefore, discussion is divided into 4 parts reflecting the individual aims. The most important findings are concluded at the end of each chapter and highlighted in bold.

5.1 Effects of chenodeoxycholic acid on brown adipose tissue recruitment and whole body energy balance

The potential of certain bile acids to activate the brown fat thermogenesis via TGR5 and counteract diet-induced obesity was extensively studied especially by the group of Auwerx (Watanabe, et al. 2011; Watanabe, et al. 2006; Watanabe, et al. 2012). Our results from the 8-week reversion of obesity show that CDCA reverses the body weight gain and improves glucose tolerance. This is in accordance with data reported for cholic acid. Stable levels of hepatic transaminases in plasma of all experimental groups suggest that CDCA does not act deleteriously in liver. Similarly to the literature, the lipid absorption remains unchanged during CDCA administration (compare Table 4-a and Supplementary Figure S-1a in the Appendix).

Most of the beneficial effects of CDCA in our first experiment can be attributed to transient reduction in food intake during habituation to diet supplemented by bitter bile acid. Interestingly, such decline in food consumption was not reported in any of the previous publications, where food intake remained unchanged after administration of bile acids (Watanabe, et al. 2012; Watanabe, et al. 2006; Watanabe, et al. 2011). However, in published studies, food intake was adjusted to body weight (Figure S-1). As the body weight-adjusted food intake was reported to be the same among the experimental groups, while the body weight differed dramatically, actual calorie intake (per animal) must have been decreased in bile acid-treated group, which was not approprietally discussed. The interpretation of data from previous studies is futher complicated by the fact that only the average food intake is shown in the figures instead of food intake curves, which could mask possible changes of food intake during the experiment. In general, our results show that bile acids can temporarily reduce food consumption, which fact was not appreciated in previous works.

The direct metabolic action of CDCA can be separated from the effects mediated by calorie restriction using two principal strategies. First, mice can be habituated to bitter diet prior to the experiment in order to prevent the later reduction in food intake; and second, CDCA-treated animals can be compared with mice fed by the respective amount of control diet (i.e. pair feeding). We chose the latter approach, which allows us to estimate the degree

of possible inaccuracy in experiments where food intake was not measured properly. The results of this experiment indicate that the initial decline in body weight (and also the improvement of insulin sensitivity) can be fully explained just by reduction of food intake. Nonetheless, we observed some small food-intake independent reduction of adiposity expressed as significantly decreased adipocyte size in scWAT.

As a mechanism of beneficial action of bile acids, the stimulation of BAT thermogenesis was suggested. In accordance with the literature, in our experiments, CDCA stimulated expression of UCP1 and other genes involved in mitochondrial biogenesis and function. Futhermore, also the UCP1 protein levels were selectively increased by CDCA, which has not been published yet. This is a particularly important finding because only the UCP1 protein (and not mRNA) is essential for NST while both parameters do not necessarily correlate (Nedergaard and Cannon 2013).

However, as it was revealed by indirect calorimetry, the activation of BAT was not sufficient for influencing the whole-body energy expenditure, although the opposite observation was already published using other bile acids (Watanabe, et al. 2006). Similarly to the situation regarding food intake (see above), inappropriate data adjustment may lead to overestimation of the values for lean animals which creates false positivity as documented on Figure 4-4d and e (p. 74). The difference in weight of cHF and CDCA animals is caused by loss of adipose mass during CDCA treatment. In general, adipose tissue exhibits widely lower energy expenditure per gram in comparison to other tissues. Therefore the best approach to express the energy expenditure is adjustment to lean body mass. Unfortunately, we did not assess this parameter in our experiment. Therefore, we prefer to express this variable just as energy expenditure per animal. Importantly, none adjustment shows significant results between CDCA and PF group, which means that all the effects on energy expenditure (if there are any) must be attributed to lowered body weight which was caused by calorie restriction and not by the direct action of CDCA.

On the contrary, we found food-intake independent changes in the RQ. RQ was lowered in CDCA group, which suggests increased lipid oxidation in these animals. This observation together with small decrease in adiposity demonstrates that the activation of BAT by CDCA has certain influence on whole body phenotype. Nevertheless, all the effects on energy expenditure are probably much smaller than it was originally suggested in the literature. Interestingly, the body weight of CDCA-treated mice in 8-week reversion remained stably lowered even after the normalisation of food intake. Such prevention of recurrent body weight gain may be a result of very small increase in energy expenditure in BAT (which is

under the resolution of indirect calorimetry). Nevertheless, 4-week reversion, which involved also the pair-fed group, was not sufficiently long to allow for testing this hypothesis. Therefore, the other longer experiment comparing CDCA and pair-fed group is needed to determine the action of chronic CDCA administration.

In conclusion, we could not prove any direct effect of CDCA-driven BAT activation on body weight decrease while most of the observed changes in body weight were clearly mediated by transient calorie restriction during the phase of habituation to bitter diet. On the other hand, CDCA significantly elevates UCP1 protein content in BAT independently on the consumption of food, which could be important for maintaining the lean phenotype after normalization of food intake.

5.2 Effects of CDCA on browning of subcutaneous white adipose tissue

In accordance with our expectation, we found significant food-intake independent Ucp1 gene induction by CDCA also in scWAT. However, this upregulation was not accompanied by similar changes in other genes involved in browning and mitochondrial energy metabolism (such as Prdm16). Despite the striking increase in Ucp1 mRNA, amount of UCP1 protein was still very low, albeit also significantly increased by CDCA. In fact, we failed to assess UCP1 protein using Western blots. Immunohistochemistry proved to be more sensitive, but the amount of UCP1-positive cells did not reach 2 % of the adipocytes. Because the effect of CDCA treatment on BAT was much higher, contribution of WAT to whole body energy expenditure is probably minimal and does not contribute to whole-body energy expenditure and preserving of lean phenotype.

With respect to the following study of mild calorie restriction and its influence on WAT metabolism, it is necessary to stress the effects of pair-feeding. Due to striking transient drop of food intake in CDCA group during the first phase of experiment, pair-feeding in first 2 weeks represents transiently up to 60% calorie restriction. After 4-week experiment (and less than 2 weeks after normalisation of food consumption), both the Ucp1 mRNA and UCP1 protein were markedly elevated also in pair-fed animals (number of UCP1-positive adipocytes in pair-fed group corresponded to more than half of the amount in CDCA animals). This finding suggests that massive calorie restriction could induce the mitochondrial uncoupling in WAT.

In short, UCP1 content in scWAT is elevated both by calorie restriction itself, and even more by CDCA treatment. Nevertheless, the total amount of UCP1 in WAT is probably not sufficient to influence the obese phenotype.

5.3 Combination of calorie restriction and ω-3 PUFA and its influence on metabolism of white adipose tissue and on whole body insulin sensitivity

The results presented in chapter 4.2, clearly demonstrate synergistic induction of lipid catabolism in eWAT as a result of mild calorie restriction and ω-3 PUFA. Increased β-oxidation consumes the excessive lipids and could help to prevent diet induced obesity and associated insulin resistance. Previous article from our laboratory demonstrated similar modulation of WAT metabolism in response to ω-3 PUFA administration alone (Kopecky, et al. 2009). The current work reveals the potentiation of these effects by calorie restriction and suggests future strategy employing the combination treatment in combating metabolic syndrome. Specifically, mitochondrial oxidative capacity and turnover of FA oxidation are increased in response to combination treatment. Concurrently, some anabolic processes (e.g. FA synthesis) are induced as well, while UCP1 remains at low level. The importance of this simultaneous activation of catabolic and anabolic processes will be futher discussed below.

The results gathered in this article together with the previously published data reveal also a possible mechanism of observed induction of lipid catabolism. As our laboratory already demonstrated, ω-3 PUFA activate AMPK in WAT (Kopecky, et al. 2009) and this enzyme is also involved in the action of ω-3 PUFA on hepatic lipid and glucose metabolism (Jelenik, et al. 2010). AMPK closely interacts with deacetylase SIRT1, which mediates the effects of calorie restriction. These two regulators activate together the transcription co-activator Pgc-1α (Ppargc1a), marker of mitochondrial biogenesis. Hence, ω-3 PUFA and calorie restriction can affect mitochondrial metabolism in additive manner. As was mentioned in the introduction, ω-3 PUFA and their metabolites serve also as ligands of nuclear receptors from PPAR family. The complex of PPARα and PGC-1α triggers transcription of enzymes involved in β-oxidation, whereas PPARγ and PGC-1α are responsible for adipocyte differentiation, lipogenesis, and eventually browning (Wilson-Fritch, et al. 2004). Therefore, the described treatment can simultaneously stimulate lipid oxidation and synthesis which provide extensive futile cycle, while the effects of the treatment are not sufficient to induce WAT browning in this case.

Moreover, the treatment resulted in anti-inflammatory changes especially in eWAT, which can be also linked to preservation of insulin sensitivity (Virtue and Vidal-Puig 2008). In contrast to generally inflammatory effects of AA derivatives, numerous metabolites of ω-3 PUFA acts in the opposite te way and contributes to resolution of inflammation. Similarly, also the SIRT1 was shown to act anti-inflammatory in WAT (Yoshizaki, et al. 2009) which may explain for the synergism of calorie restriction and treatment with ω-3 PUFA.

In accordance with literature (Gonzalez-Periz, et al. 2009; Gonzalez-Periz, et al. 2006; White, et al. 2010), administration of ω-3 PUFA lead to lower formation of various AA-derived eicosanoids and concurrent rise of anti-inflammatory molecules. Particularly the protectin PD1 and prostaglandin 15d-PGJ_2 were induced in the synergistic manner. Induction of 15d-PGJ_2 represents surprising finding because this mediator stems from AA which means that its levels should be rather decreased by ω-3 PUFA. Thus, the observation can be interpreted as a suggestion that ω-3 PUFA (in combination with calorie restriction) favorize conversion of AA rather to the 15d-PGJ_2 than to more inflammatory prostanoids. This effect can be caused by EPA- and DHA-derived peroxyl radicals (Davis, et al. 2006). Interestingly, 15d-PGJ_2 is the most potent endogenous ligand of PPARγ (Forman, et al. 1995; Kliewer, et al. 1995). Thus, the activation of PPARγ by 15d-PGJ_2 may be the crucial step in regulation of lipid metabolism. This notion is supported by finding that stimulation of PPARγ by thiazolidinediones increases expression of Pgc-1α, mitochondrial mass, palmitate oxidation, and UCP1 content in WAT of genetically obese ob/ob mice (Wilson-Fritch, et al. 2004). With exception of the latest, we observed similar phenotype using our experimental setup.

If ω-3 or ω-6-derived lipid mediators plays indeed a crucial role in modulation of eWAT oxidative capacity, their effect must depend on the lipid composition of control cHF diet, e.g. the proportion of saturated, monounsaturated, and polyunsaturated FA. This assumption opens new research area for future investigation of catabolism induction in murine eWAT under various dietary conditions. During my remaining time in Dept. of Adipose Tissue Biology, I plan to get involved in such experiments.

It is important to stress that the observed stimulation of lipid catabolism was not accompanied by Ucp1 gene induction and occurred specifically in eWAT, which is among all the depots one of the least prone to browning. Hence, a question arises what happens to all the ATP created during β-oxidation in fully coupled mitochondria in WAT adipocytes. In our opinion, the answer is to be found in the simultaneous stimulation of anabolic processes, such as FA synthesis, which is demonstrated both by the Fas gene expression and by biochemical

measurement of FA synthetic rate. Under normal conditions, malonyl-CoA, an intermediate of FA synthesis, blocks CPT1 and inhibits FA translocation to mitochondria and consequent β-oxidation. In our experiment, this inhibition is probably overruled by massive mitochondrial biogenesis which provides expanded capacity for FA oxidation despite the action of malonyl-CoA.

Additionally, after the submission of Publication B, we measured also expression of Pepck (Pck1), which was induced synergistically by combination treatment as well (see Supplementary Figure S-2 in the Appendix; (Flachs, et al. 2013)). PEPCK activity is important for creation of G3P, an essential precursor of newly synthesized (or re-esterified) TAG. Increased availability of glycerol-3-phosphate may accelerate re-esterification of FA previously liberated by lipolysis, which suggest that futile cycling of TAG and NEFA represents another ATP consuming process.

The UCP1-independent energy dissipation in eWAT may be induced not only by the specific combination treatment of ω-3 PUFA and calorie restriction, but also by other conditions. In order to test the general importance of the futile metabolic cycling in prevention of obesity and associated disorders, we wanted to prove the existence of this phenomenon in other model situation. We chose the model of cold exposure, which is characterized by increased lipolysis in WAT. The general consequences of cold adaptation, especially the induction of UCP1, are described in chapter 5.4, while the UCP1-independent thermogenesis in eWAT induced by cold exposure is discussed in detail in chapter 5.5.

To sum up, mild calorie restriction augments the ability of ω-3 PUFA to counteract WAT inflammation. This is related to substantial induction of lipolysis and β-oxidation accompanied by rise in lipogenesis (*de novo* FA synthesis and FA re-esterification) particularly in eWAT of cHF+F+CR group. The simultaneous stimulation of catabolic and anabolic processes can provide a way to dissipate excessive energy and prevent diet-induced obesity and obesity-associated insulin resistance.

5.4 Model of B6 and AJ mice exposed to cold: UCP1 induction in brown and subcutaneous white adipose tissue

In the experiments employing cold exposure, we compared two murine strains (AJ and B6) differing in their propensity to obesity. This may allow us to link the observed metabolic changes to the phenotype of selected strain of animals. As was already mentioned, AJ mice are thought to represent animals with high capacity to induce UCP1. In comparison to B6,

they gain less weight on high fat diet, while administration of β3-agonist helps to further prevent development of obesity in these mice (Collins, et al. 1997). Further studies investigated phenomenon of high-fat feeding-driven induction of UCP1 and other uncoupling proteins in many different fat depots (Surwit, et al. 1998; Watson, et al. 2000). However, UCP1 gene expression was studied only at the level of mRNA in these studies. According to our results, there is the same UCP1 gene expression in both strains (or, in some cases, slightly higher in AJ mice), while the striking induction of UCP1 in B6 (but not in AJ) mouse is visible only on the protein level. It can be hypothesized that low UCP1 protein synthesis in AJ mice leads to compensatory higher adrenergic stimulation and higher amount of mRNA without affecting UCP1 protein content. Nevertheless, the situation is likely to be more complex.

Another important factor is the depot, where UCP1 content is investigated. Our immunohistochemical data shows certain areas of scWAT, where (unlike in the rest of depot) the UCP1-positive cells are really more abundant in AJ than in B6 animals. The existence of fat depots with higher UCP1 inducibility in AJ mice is therefore possible. Studies comparing AJ and B6 animals often focus on retroperitoneal WAT (Guerra, et al. 1998), where some researchers indeed evaluated UCP1 protein (Xue, et al. 2005). Therefore, various strain-specific differences in UCP1 content in WAT depots are very likely to occur.

On the other hand, the results we obtained in BAT are more difficult to interpret. It was shown, that retriperitoneal fat of AJ mice contains higher amount of UCP1 protein in comparison to B6 animals at least during first 60 days of the postnatal development, but its levels in BAT were the same (Xue, et al. 2007). Our results showing much higher UCP1 content in interscapular BAT of B6 mice thus remain controversial. Currently, we plan to confirm these results at the functional level, e.g. by using norepinephrine test (i.e., the assessment of energy expenditure in anesthetized state in response to dose of norepinephrine, which should maximally stimulate UCP1-driven energy expenditure in BAT). Similar test on AJ and B6 animals was already performed in our laboratory (Kus, et al. 2008). The mice were not exposed to cold, but to high-fat (cHF) feeding: only AJ mice fed by cHF diet had increased metabolic rate after injection of norepinephrine. On the other hand, young AJ mice on low-fat diet (i.e. 2 weeks younger mice than those in the current experiment) were not able to survive when exposed to cold while none of other experimental groups faced the same problem (Kus, et al. 2008).

If our results concerning low inducibility of UCP1 protein in our AJ mice are correct, the obesity resistence of these mice cannot be explained by increased UCP1-dependent energy

dissipation. Instead, alternative mechanism, such as NST in muscle (Kus, et al. 2008), must be involved.

Anyway, our experiments describes well the kinetics of cold adaptation regardless the strain. It should be stressed that all our cold-exposure studies last too short period (7 days maximally) to reach maximal NST. Actually, shivering prevails as a main source of heat production during most of the experiment and just slowly fades back to the background while newly recruited BAT takes the main role (Cannon and Nedergaard 2004). It seems that the first phase of cold exposure (at least till the 2nd day) is characterized by massive mobilization of lipid stores, while increased energy intake is insufficient for maintaining the stable body weight owing to hugely increased energy demands. All fat depots hence loose weight at first, but only BAT is able to elevate glucose and lipid uptake to regain its original mass later again.

Adrenergic activity stimulates lipolysis in all fat depots, and in parallel activates network of transcriptional factors involved in regulation of UCP1 expression. If the synthesis of UCP1 protein is not blocked (which may be the case in our AJ animals), brown and brite adipocytes increase their capacity for energy dissipation. Liberated FA further activate function of UCP1.

It was suggested that process of WAT browning includes lipolysis in big lipid droplets and esterification of the part of FA into numerous newly established smaller droplets (Barneda, et al. 2013). Glycerol kinase, which otherwise is not expressed in white adipocytes, is reported to be involved in this action as well. Thus, lipolysis, e.g. in scWAT, provides NEFA for energy demanding processes in other organs (such as shivering in skeletal muscle) and part of its adipocytes simultaneously exploit the elevated NEFA levels for synthesis of TAG incorporated to new lipid droplets. Thus, NEFA/TAG cycling represents integral part of browning process in scWAT. The differentiated brite precursors can still represent independent cell line distinct from classical white cells (see chapter 1.1). The biggest loss of scWAT weight is observed immediately after cold exposure, while later on, the weight is stabilized. It is probable that scWAT increases its lipid uptake and energy expenditure in later phases of cold stress similarly to BAT.

In short, we observed massive recruitment of UCP1 in both BAT and scWAT in response to cold. Surprisingly, AJ mice in our experiments exhibited significantly lower UCP1 protein content, but not UCP1 mRNA, in both BAT and scWAT. These results are in conflict with part of existing literature. Therefore, the high UCP1 inducibility in AJ mice should be re-examined.

BAT is likely to play major physiological role in whole body NST, although the muscle shivering prevails at first. Heat production requires increased lipolysis in all fat depots reflecting close functional links between adipocytes in WAT and BAT.

5.5 Inducibility of futile cycling in epididymal white adipose tissue

Previous chapter was dedicated to cold-induced changes in adipose tissues expressing significant amount of UCP1. TAG/NEFA cycling may represent an essential part of WAT browning. Nevertheless, as was already suggested in chapter 5.3, it can be upregulated in eWAT even in UCP1-independent manner under certain conditions. Here we are showing that also the prolonged cold exposure induces this pathway in eWAT. During first 2 days, eWAT loses substantial part of its weight, which suggests high lipolytic rate. Nevertheless, induction of anabolic processes such as FA and TAG synthesis is slightly delayed and manifests only after 7 days of the treatment. Therefore, TAG/NEFA cycling is not an automatic consequence of lipid catabolism, but rather flexible process, which can be activated on demand.

It is interesting that higher FA synthesis and esterification rate was detected in AJ than in B6 mice exposed to cold. The fact, that such result was not confirmed if the $^{2}H_2O$ exposure started already on 3rd day of cold exposure (instead of 5th day), suggests again that key activation of NEFA/TAG cycling in eWAT occurs in time period close to 7 days of cold exposure. Strain-dependent induction of futile cycling raises the question if this process can contribute to obesity-resistence of AJ animals.

Clearly, we showed the inducibility of FA and TAG synthesis by both cold exposure and combination treatment with ω-3 PUFA and calorie restriction (although we have only indirect evidence in the latter case as we have not measured ^{2}H incorporation into TAG in calorie restricted mice yet). This result is in accordance with older finding that FA re-esterification in WAT is probably essential for hypolipidaemic action of antidiabetic drug from the group of thiazolidinediones (Guan, et al. 2002; Tordjman, et al. 2003a). Similarly to the treatment in our experiment, TZD induced expression of Pepck (Tordjman, et al. 2003b) and surprisingly also glycerol kinase (Guan, et al. 2002) in WAT which resulted in greater TAG synthesis and consequent reduction of systemic NEFA levels.

Despite the fact that the oxidative capacity of classical WAT is usually neglected, we demonstrate the inducibility of catabolic pathways in WAT. Similar results were observed

also by others. E.g., an analysis of changes in mitochondrial proteome of 3T3-L1 adipocytes in response to lipolytic stimulus revealed induction of enzymes involved in β-oxidation which was attributed to the necessity to cover increased need of energy for NEFA re-esterification (Cho, et al. 2009). Nevertheless, it is important to address also the question of the contribution of TAG/NEFA cycling in eWAT to whole body energy expenditure. This contribution can be approximated based on the data drom ^{2}H enrichment of TAG in cold exposure experiments.

According to our results, more than 20% of total TAG in eWAT is newly synthesized during period of 2 days at the end of the cold exposure. It represents almost 50 mg lipids (more than 0.05 mmol TAG). This approximation probably underestimates the real situation, because part of the newly synthesized TAG is definitely lipolyzed again before the measurement. Nevertheless, 8 mol ATP (602.5 kJ) is required to cover costs of lipolysis and reesterification of 1 mol TAG including the regeneration of glycerol in liver (Baldwin 1970). It gives 30 J consumed during 2 days by TAG/NEFA futile cycling. Despite the fact that FA synthesis rate is much smaller in comparison to TAG synthesis, this process has higher energy demands and thus requires slightly higher portion of energy. Even after counting both FA and TAG synthesis together, the energy cost represents less than 200 J per 2 days while total metabolic rate under cold conditions (approximated on the base of energy intake) is 3-fold of magnitude higher. Thus, TAG/NEFA cycling in WAT contributes relatively little to whole body thermogenesis and energy expenditure. During prolonged cold exposure, the role of upregulated reesterification is rather in prevention of absolute depletion of eWAT lipid stores and deceleration of eWAT decline. On the other hand, the involvement of futile cycling in local regulation of adiposity may be possible.

Importantly, flexible regulation of FA re-esterification in WAT probably allows for efficient buffering of plasma NEFA levels. Moreover, the process of FA esterification requires also G3P, which can be derived from plasma glucose. Hence, the activation of TAG/NEFA cycling in WAT may also increased the consumption of glucose and contribute partially to lowering of glycaemia. Therefore, while obesity resistence of AJ mice can hardly be related to TAG/NEFA cycling, prevention of atherosclerosis and glucose intolerance may be at least partially caused by higher flexibility of re-estirification rate in AJ animals.

It is important to note that in cold exposure experiment, NEFA levels are transiently decreased after 2 days of cold exposure and elevated after 7 days. This fact does not seem to support the idea that re-esterification can buffer lipidaemia in 7^{th} day; however, the condition of prolonged cold is probably too extreme, and the role of FA re-esterification is thus covered

up by other effects. Other experimental model is needed to test assumption made on base of the results from cold-exposure experiments. Combination of calorie restriction and ω-3 PUFA seems to be promising in this respect; therefore, we plan to apply the NMR technique also on the future calorie restriction experiments.

Induction of TAG synthesis in eWAT can be also related to the recent finding that even short cold exposure induces adipogenesis de novo in eWAT (Wang, et al. 2013). This effect does not involve precursor proliferation, but rather differenciation of progenitor cells, which necessarily requires new TAG synthesis. The resultant cells are UCP1-negative, but provide additional stores for excessive lipids. The physiological role of these new adipocytes in cold stress is uncertain. Though, the presence of small adipocytes is undoubtedly beneficial considering the deterioration of insulin resistence and development of metabolic syndrome. Not only TAG/NEFA cycling was above suggested as an essential process in browning of scWAT, but it may plays also similar role in cold-induced adipogenesis in eWAT. To analyze among others the rate of adipogenesis in various adipose depots, the new experiment will be done using 5-bromouridine to immunocytochemically label newly synthesized RNA.

On the model of cold exposed mice of two strains differing in their propensity to obesity, we demonstrated the existence of TAG/NEFA cycling activity in eWAT, which can be flexibly regulated. This process probably plays an important role also in preservation of lean phenotype during high-fat feeding in animals on combination treatment of ω-3 PUFA and calorie restriction. Both the mice on the above mentioned combination treatment and the mice exposed to cold exhibit simultaneous activation of lipolysis, and FA and TAG synthesis. Contribution of this process to whole body energy balance is relatively small, but in a long-run, it could be important for control of body fat mass and metabolic flexibility.

6. Conclusion

Following conclusions could be made, corresponding to the specific aims of the thesis:

1) Bile acid CDCA exerts protective effects against development of obesity and metabolic syndrome. However, direct induction of BAT thermogenesis is involved only partially. The main effect depends on the transient decrease in food intake. The increase in BAT thermogenesis is probably involved in the maintenance of lean phenotype.

2) Food intake-independent effect of CDCA on UCP1 recruitment was observed also in scWAT. However the number of brite cells induced in scWAT was small in comparison to the content of brown adipocytes in BAT. Thus, the effect of the brite cells induced in scWAT on whole body energy balance is probably small.

3) Combination treatment using calorie restriction and ω-3 PUFA exhibits high potential to counteract deleterious consequences of high-fat feeding. The treatment leads to induction of lipid catabolism and mitochondrial oxidative phosphorylation specifically in eWAT. The resulted ATP may be consumed due to consequent stimulation of anabolic processes such as TAG synthesis. Complex network of transcription factors and PUFA-derived lipid mediators is likely to be involved in regulation of these processes.

4) Cold exposure stimulates mobilization of lipid stores in all adipose depots. Consequently, UCP1 gene expression is triggered in BAT, and to smaller extent also in scWAT. Surprisingly, this induction is reflected at the UCP1 protein levels only in B6 mice, while both depots of AJ mice exhibit only limited increase of UCP1. This result is in conflict with traditional view of AJ mice as animals extremely prone to adrenergic stimulation of UCP1-mediated thermogenesis. This discrepancy may be partially explained by the fact that previous studies focused largely on the UCP1 gene expression at the mRNA level, evaluated UCP1 gene expression in different adipose depots, or maybe even used different substrain(s) of the mice.

5) The inducibility of TAG/NEFA futile cycling was demonstrated both in animals on combination treatment of ω-3 PUFA and calorie restriction, and on mice exposed to cold. After 7 days (but not 2 days) of cold exposure, FA and TAG synthesis is induced in eWAT of both B6 and AJ animals, while this effect is more pronounced in AJ mice. This process may be related to new white cell formation and/or requirements for buffering plasma NEFA in association with differential propensity to obesity and associated metabolic disorder in B6 and AJ mice.

List of figures

List of tables

Reference list

Abdelkarim, M., et al.
2010 The farnesoid X receptor regulates adipocyte differentiation and function by promoting peroxisome proliferator-activated receptor-gamma and interfering with the Wnt/beta-catenin pathways. J Biol Chem 285(47):36759-67.

Ahmadian, M., et al.
2011 Desnutrin/ATGL is regulated by AMPK and is required for a brown adipose phenotype. Cell Metab 13(6):739-748.

Alberti, K. G., and P. Z. Zimmet
1998 Definition, diagnosis and classification of diabetes mellitus and its complications. Part 1: diagnosis and classification of diabetes mellitus provisional report of a WHO consultation. Diabet Med 15(7):539-53.

Andersson, U., J. Houstek, and B. Cannon
1997 ATP synthase subunit c expression: physiological regulation of the P1 and P2 genes. Biochemical Journal 323:379-385.

Baik, I., et al.
2000 Adiposity and mortality in men. Am J Epidemiol 152(3):264-71.

Baldwin, R. L.
1970 Metabolic functions affecting the contribution of adipose tissue to total energy expenditure. Fed Proc 29(3):1277-83.

Barbera, M. J., et al.
2001 Peroxisome proliferator-activated receptor alpha activates transcription of the brown fat uncoupling protein-1 gene. A link between regulation of the thermogenic and lipid oxidation pathways in the brown fat cell. Journal of Biological Chemistry 276(2):1486-1493.

Barneda, D., et al.
2013 Dynamic changes in lipid droplet-associated proteins in the "browning" of white adipose tissues. Biochim Biophys Acta 1831(5):924-33.

Bartolomucci, A., et al.
2006 TLQP-21, a VGF-derived peptide, increases energy expenditure and prevents the early phase of diet-induced obesity. Proc Natl Acad Sci U S A 103(39):14584-9.

Baur, J. A., et al.
2006 Resveratrol improves health and survival of mice on a high-calorie diet. Nature 444(7117):337-42.

Berry, M. N., and D. S. Friend
1969 High-yield preparation of isolated rat liver parenchymal cells: a biochemical and fine structural study. J Cell Biol 43(3):506-20.

Bezaire, V., et al.
2009 Contribution of adipose triglyceride lipase and hormone-sensitive lipase to lipolysis in hMADS adipocytes. J Biol.Chem. 284(27):18282-18291.

Blaxter, K.
1989 Energy Metabolism in Animal and Man. Cambridge, UK: Cambridge University Press.

Bonet, M. L., P. Oliver, and A. Palou
2013 Pharmacological and nutritional agents promoting browning of white adipose tissue. Biochim Biophys Acta 1831(5):969-85.

Bookelman, H., et al.

1978 Measurement of cytochromes in human skeletal muscle mitochondria, isolated from fresh and frozen stored muscle specimens. Biochem Med 19(3):366-73.

Boon, M. R., et al.

2013 BMP7 activates brown adipose tissue and reduces diet-induced obesity only at subthermoneutrality. PLoS One 8(9):e74083.

Bordicchia, M., et al.

2012 Cardiac natriuretic peptides act via p38 MAPK to induce the brown fat thermogenic program in mouse and human adipocytes. J Clin.Invest 122(3):1022-1036.

Bostrom, P., et al.

2012 A PGC1-alpha-dependent myokine that drives brown-fat-like development of white fat and thermogenesis. Nature 481(7382):463-8.

Bottcher, H., and P. Furst

1997 Decreased white fat cell thermogenesis in obese individuals. International Journal of Obesity 21(6):439-444.

Bronner-Fraser, M.

1994 Neural crest cell formation and migration in the developing embryo. FASEB J 8(10):699-706.

Bukowiecki, L. J., et al.

1983 Effects of sucrose, caffeine, and cola beverages on obesity, cold resistance, and adipose tissue cellularity. Am J Physiol 244(4):R500-7.

Butler, A. A., and L. P. Kozak

2010 A recurring problem with the analysis of energy expenditure in genetic models expressing lean and obese phenotypes. Diabetes 59(2):323-9.

Cabrero, A., et al.

1999 Uncoupling protein-3 mRNA levels are increased in white adipose tissue and skeletal muscle of bezafibrate-treated rats. Biochem Biophys Res Commun 260(2):547-56.

Cannon, B., and J. Nedergaard

2004 Brown adipose tissue: function and physiological significance. Physiol Rev 84(1):277-359.

—

2009 Thermogenesis challenges the adipostat hypothesis for body-weight control. Proc Nutr Soc 68(4):401-7.

—

2011 Nonshivering thermogenesis and its adequate measurement in metabolic studies. J Exp Biol 214(Pt 2):242-53.

—

2012 Cell biology: Neither brown nor white. Nature 488(7411):286-7.

Cao, L., et al.

2011 White to brown fat phenotypic switch induced by genetic and environmental activation of a hypothalamic-adipocyte axis. Cell Metab 14(3):324-38.

Cao, W., et al.

2004 p38 mitogen-activated protein kinase is the central regulator of cyclic AMP-dependent transcription of the brown fat uncoupling protein 1 gene. Mol Cell Biol 24(7):3057-67.

Carey, V. J., et al.

1997 Body fat distribution and risk of non-insulin-dependent diabetes mellitus in women. The Nurses' Health Study. Am J Epidemiol 145(7):614-9.

Cariou, B., et al.

2006 The farnesoid X receptor modulates adiposity and peripheral insulin sensitivity in mice. J Biol Chem 281(16):11039-49.

Carling, D., V. A. Zammit, and D. G. Hardie

1987 A common bicyclic protein kinase cascade inactivates the regulatory enzymes of fatty acid and cholesterol biosynthesis. FEBS Lett 223(2):217-22.

Carneheim, C., J. Nedergaard, and B. Cannon

1984 Beta-adrenergic stimulation of lipoprotein lipase in rat brown adipose tissue during acclimation to cold. American Journal of Physiology 246(4 Pt 1):E327-E333.

Celi, F. S., et al.

2010 Minimal changes in environmental temperature result in a significant increase in energy expenditure and changes in the hormonal homeostasis in healthy adults. Eur J Endocrinol 163(6):863-72.

Cinti, S.

2005 The adipose organ. Prostaglandins Leukot Essent Fatty Acids 73(1):9-15.

—

2009 Transdifferentiation properties of adipocytes in the adipose organ. Am J Physiol Endocrinol Metab 297(5):E977-86.

—

2011 Between brown and white: novel aspects of adipocyte differentiation. Ann Med 43(2):104-15.

—

2012 The adipose organ at a glance. Dis Model Mech 5(5):588-94.

Claessens-van Ooijen, A. M., et al.

2006 Heat production and body temperature during cooling and rewarming in overweight and lean men. Obesity (Silver Spring) 14(11):1914-20.

Collins, S., et al.

1997 Strain-specific response to beta 3-adrenergic receptor agonist treatment of diet-induced obesity in mice. Endocrinology 138(1):405-13.

Collins, S., et al.

1996 Role of leptin in fat regulation. Nature 380(6576):677.

Commins, S. P., et al.

2000 Central leptin regulates the UCP1 and ob genes in brown and white adipose tissue via different beta-adrenoceptor subtypes. J Biol Chem 275(42):33059-67.

Daval, M., et al.

2005 Anti-lipolytic action of AMP-activated protein kinase in rodent adipocytes. J Biol.Chem. 280(26):25250-25257.

Davis, T. A., et al.

2006 In vivo and in vitro lipid peroxidation of arachidonate esters: the effect of fish oil omega-3 lipids on product distribution. J Am Chem Soc. 128(46):14897-14904.

Davis, T. R.

1961 Chamber cold acclimatization in man. J Appl Physiol 16:1011-5.

Djouder, N., et al.

2010 PKA phosphorylates and inactivates AMPKalpha to promote efficient lipolysis. EMBO Journal 29(2):469-481.

Duran-Sandoval, D., et al.

2005 The farnesoid X receptor modulates hepatic carbohydrate metabolism during the fasting-refeeding transition. J Biol Chem 280(33):29971-9.

Elsen, M., S. Raschke, and J. Eckel

2014 Browning of white fat: does irisin play a role in humans? J Endocrinol 222(1):R25-38.

Enerback, S., et al.
1997 Mice lacking mitochondrial uncoupling protein are cold-sensitive but not obese. Nature 387(6628):90-4.
Esser, V., et al.
1996 Expression of a cDNA isolated from rat brown adipose tissue and heart identifies the product as the muscle isoform of carnitine palmitoyltransferase I (M-CPT I). M-CPT I is the predominant CPT I isoform expressed in both white (epididymal) and brown adipocytes. J Biol Chem 271(12):6972-7.
Feldmann, H. M., et al.
2009 UCP1 ablation induces obesity and abolishes diet-induced thermogenesis in mice exempt from thermal stress by living at thermoneutrality. Cell Metab 9(2):203-9.
Festuccia, W. T. L., et al.
2003 Expression of glycerokinase in brown adipose tissue is stimulated by the sympathetic nervous system. American Journal of Physiology-Regulatory Integrative and Comparative Physiology 284(6):R1536-R1541.
Fisher, F. M., et al.
2012 FGF21 regulates PGC-1alpha and browning of white adipose tissues in adaptive thermogenesis. Genes Dev 26(3):271-81.
Fitzgibbons, T. P., et al.
2011 Similarity of mouse perivascular and brown adipose tissues and their resistance to diet-induced inflammation. Am J Physiol Heart Circ Physiol 301(4):H1425-37.
Flachs, P., et al.
2005 Polyunsaturated fatty acids of marine origin upregulate mitochondrial biogenesis and induce beta-oxidation in white fat. Diabetologia 48(11):2365-75.
Flachs, P., et al.
2002 Impaired noradrenaline-induced lipolysis in white fat of aP2-Ucp1 transgenic mice is associated with changes in G-protein levels. Biochemical Journal 364(Pt 2):369-376.
Flachs, P., M. Rossmeisl, and J. Kopecky
2014 The effect of n-3 fatty acids on glucose homeostasis and insulin sensitivity. Physiol Res 63 Suppl 1:S93-118.
Flachs, P., et al.
2013 Stimulation of mitochondrial oxidative capacity in white fat independent of UCP1: A key to lean phenotype. Biochim.Biophys.Acta 1831(5):986-1003.
Foretz, M., et al.
1999 Sterol regulatory element binding protein-1c is a major mediator of insulin action on the hepatic expression of glucokinase and lipogenesis-related genes. Proc Natl Acad Sci U S A 96(22):12737-42.
Forman, B. M., et al.
1995 15-Deoxy-delta12,14-prostaglandin J2 is a ligand for the adipocyte determination factor PPARgama. Cell 83:803-812.
Foster, D. O., and M. L. Frydman
1978 Nonshivering thermogenesis in the rat. II. Measurements of blood flow with microspheres point to brown adipose tissue as the dominant site of the calorigenesis induced by noradrenaline. Can J Physiol Pharmacol 56(1):110-22.
Fromme, T., and M. Klingenspor
2011 Uncoupling protein 1 expression and high-fat diets. Am J Physiol Regul Integr Comp Physiol 300(1):R1-8.
Frontini, A., and S. Cinti

2010 Distribution and development of brown adipocytes in the murine and human adipose organ. Cell Metab 11(4):253-6.

Fujisaka, S., et al.
2009 Regulatory mechanisms for adipose tissue M1 and M2 macrophages in diet-induced obese mice. Diabetes 58(11):2574-2582.

Gaidhu, M. P., et al.
2009 Prolonged AICAR-induced AMP-kinase activation promotes energy dissipation in white adipocytes: novel mechanisms integrating HSL and ATGL. Journal of Lipid Research 50(4):704-715.

Galgani, J. E., C. Moro, and E. Ravussin
2008 Metabolic flexibility and insulin resistance. Am.J.Physiol Endocrinol.Metab 295(5):E1009-E1017.

Giordano, A., et al.
2014 White, brown and pink adipocytes: the extraordinary plasticity of the adipose organ. Eur J Endocrinol 170(5):R159-71.

Golozoubova, V., B. Cannon, and J. Nedergaard
2006 UCP1 is essential for adaptive adrenergic nonshivering thermogenesis. Am J Physiol Endocrinol Metab 291(2):E350-7.

Gong, D. W., et al.
2000 Lack of obesity and normal response to fasting and thyroid hormone in mice lacking uncoupling protein-3. J Biol Chem 275(21):16251-7.

Gonzalez-Periz, A., et al.
2009 Obesity-induced insulin resistance and hepatic steatosis are alleviated by omega-3 fatty acids: a role for resolvins and protectins. FASEB Journal 23(6):1946-1957.

Gonzalez-Periz, A., et al.
2006 Docosahexaenoic acid (DHA) blunts liver injury by conversion to protective lipid mediators: protectin D1 and 17S-hydroxy-DHA. FASEB Journal 20(14):2537-2539.

Gravholt, C. H., et al.
2001 Physiological levels of glucagon do not influence lipolysis in abdominal adipose tissue as assessed by microdialysis. J Clin Endocrinol Metab 86(5):2085-9.

Guan, H. P., et al.
2002 A futile metabolic cycle activated in adipocytes by antidiabetic agents. Nat.Med. 8(10):1122-1128.

Guerra, C., et al.
1998 Emergence of brown adipocytes in white fat in mice is under genetic control. Effects on body weight and adiposity. Journal of Clinical Investigation 102(2):412-420.

Haemmerle, G., et al.
2006 Defective lipolysis and altered energy metabolism in mice lacking adipose triglyceride lipase. Science 312(5774):734-737.

Hajri, T., and N. A. Abumrad
2002 Fatty acid transport across membranes: relevance to nutrition and metabolic pathology. Annu Rev Nutr 22:383-415.

Haus, J. M., et al.
2009 Plasma ceramides are elevated in obese subjects with type 2 diabetes and correlate with the severity of insulin resistance. Diabetes 58(2):337-43.

Himms-Hagen, J.

1979 Obesity may be due to a malfunctioning of brown fat. Can Med Assoc J 121(10):1361-4.

Himms-Hagen, J., and M. Desautels

1978 A mitochondrial defect in brown adipose tissue of the obese (ob/ob) mouse: reduced binding of purine nucleotides and a failure to respond to cold by an increase in binding. Biochem Biophys Res Commun 83(2):628-34.

Holland, W. L., et al.

2011 Receptor-mediated activation of ceramidase activity initiates the pleiotropic actions of adiponectin. Nat.Med. 17(1):55-63.

Hondares, E., et al.

2006 Thiazolidinediones and rexinoids induce PGC-1{alpha} gene transcription. An auto-regulatory loop controls PGC-1{alpha} expression in adipocytes via PPAR{gamma} co-activation. Endocrinology.

Hondares, E., et al.

2011 Peroxisome proliferator-activated receptor alpha (PPARalpha) induces PPARgamma coactivator 1alpha (PGC-1alpha) gene expression and contributes to thermogenic activation of brown fat: involvement of PRDM16. J Biol.Chem. 286(50):43112-43122.

Hossain, M. S., et al.

2012 Prostaglandin J2 series induces the gene expression of monocyte chemoattractant protein-1 during the maturation phase of cultured adipocytes. Gene 502(2):138-141.

Houstek, J., et al.

1995 The expression of subnit c correlates with and thus may limit the boisynthesis of the mitochondrial F0 F1-ATPase in brown adipose tissue. Journal of Biological Chemistry 270:7689-7694.

Chascione, C., et al.

1987 Effect of carbohydrate intake on de novo lipogenesis in human adipose tissue. American Journal of Physiology 253(6 Pt 1):E664-E669.

Cho, S. Y., et al.

2009 Proteomic analysis of mitochondrial proteins of basal and lipolytically (isoproterenol and TNF-alpha)-stimulated adipocytes. J Cell Biochem 106(2):257-66.

Chowdhury, S. K., et al.

2000 Activities of mitochondrial oxidative phosphorylation enzymes in cultured amniocytes192. Clin.Chim.Acta 298(1-2):157-173.

Ibrahimi, A., and N. A. Abumrad

2002 Role of CD36 in membrane transport of long-chain fatty acids. Curr Opin Clin Nutr Metab Care 5(2):139-45.

Iizuka, K.

2013 Recent progress on the role of ChREBP in glucose and lipid metabolism. Endocr J 60(5):543-55.

Ikeda, Y., K. Okamura-Ikeda, and K. Tanaka

1985 Purification and characterization of short-chain, medium-chain, and long-chain acyl-CoA dehydrogenases from rat liver mitochondria. Isolation of the holo- and apoenzymes and conversion of the apoenzyme to the holoenzyme. J Biol Chem 260(2):1311-25.

Ishibashi, J., and P. Seale

2010 Medicine. Beige can be slimming. Science 328(5982):1113-4.

Izai, K., et al.

1992 Novel fatty acid beta-oxidation enzymes in rat liver mitochondria. I. Purification and properties of very-long-chain acyl-coenzyme A dehydrogenase. J Biol Chem 267(2):1027-33.

Jelenik, T., et al.

2010 AMP-activated protein kinase {alpha}2 subunit is required for the preservation of hepatic insulin sensitivity by n-3 polyunsaturated fatty acids. Diabetes 59(11):2737-2746.

Jimenez, M., et al.

2003 Beta 3-adrenoceptor knockout in C57BL/6J mice depresses the occurrence of brown adipocytes in white fat. Eur J Biochem 270(4):699-705.

Jones, J. G., M. Merritt, and C. Malloy

2001 Quantifying tracer levels of (2)H(2)O enrichment from microliter amounts of plasma and urine by (2)H NMR. Magn Reson Med 45(1):156-8.

Kajimura, S., P. Seale, and B. M. Spiegelman

2010 Transcriptional control of brown fat development. Cell Metab 11(4):257-62.

Kakuma, T., et al.

2000 Role of leptin in peroxisome proliferator-activated receptor gamma coactivator-1 expression. Endocrinology 141(12):4576-82.

Kalant, D., and K. Cianflone

2004 Regulation of fatty acid transport. Curr Opin Lipidol 15(3):309-14.

Kanda, H., et al.

2006 MCP-1 contributes to macrophage infiltration into adipose tissue, insulin resistance, and hepatic steatosis in obesity. J Clin.Invest 116(6):1494-1505.

Kast, H. R., et al.

2001 Farnesoid X-activated receptor induces apolipoprotein C-II transcription: a molecular mechanism linking plasma triglyceride levels to bile acids. Mol Endocrinol 15(10):1720-8.

Kawamata, Y., et al.

2003 A G protein-coupled receptor responsive to bile acids. J Biol Chem 278(11):9435-40.

Kissebah, A. H., and G. R. Krakower

1994 Regional Adiposity and morbidity. Physilogical Reviews 74(4):761-811.

Kleiber, M.

1947 Body size and metabolic rate. Physiol Rev 27(4):511-41.

Kliewer, Steven A., et al.

1995 A prostaglandin J2 metabolite binds peroxisome proliferator-activated receptor gamma and promotes adipocyte differentiation. Cell 83(5):813-819.

Kloting, N., et al.

2010 Insulin-sensitive obesity. Am J Physiol Endocrinol Metab 299(3):E506-15.

Kopecky, J., P. Flachs, and M. Rossmeisl

2007 Vliv v¡cenenasycenìch mastnìch kyselin ýady n-3 na citlivost k inzulinu. *In* Trendy soudob, diabetologie. L. Houdek, ed. Pp. 247 -275. Praha: Gal,n.

Kopecky, J., et al.

2009 n-3 PUFA: bioavailability and modulation of adipose tissue function Proc.Nutr.Soc. 68(4):361-369.

Kopecky, J., et al.

1996 Reduction of dietary obesity in the aP2- Ucp transgenic mice: mechanism and adipose tissue morphology. American Journal of Physiology 270(5 Pt 1):E776-E786.

Kosteli, A., et al.

2010 Weight loss and lipolysis promote a dynamic immune response in murine adipose tissue. J Clin.Invest 120(10):3466-3479.

Kozak, L. P.

2010 Brown fat and the myth of diet-induced thermogenesis. Cell Metab 11(4):263-7.

Kuda, O., et al.

2009 n-3 fatty acids and rosiglitazone improve insulin sensitivity through additive stimulatory effects on muscle glycogen synthesis in mice fed a high-fat diet. Diabetologia 52(5):941-51.

Kunesova, M., et al.

2006 The influence of n-3 polyunsaturated fatty acids and very low calorie diet during a short-term weight reducing regimen on weight loss and serum fatty acid composition in severely obese women. Physiol Res 55(1):63-72.

Kus, V., et al.

2008 Induction of muscle thermogenesis by high-fat diet in mice: association with obesity-resistance. Am J Physiol Endocrinol.Metab 295(2):E356-E367.

Lafontan, M.

2008 Advances in adipose tissue metabolism. Int.J.Obes.(Lond) 32 Suppl 7:S39-S51.

Lagouge, M., et al.

2006 Resveratrol improves mitochondrial function and protects against metabolic disease by activating SIRT1 and PGC-1alpha. Cell 127(6):1109-22.

Lam, Y. Y., C. M. Peterson, and E. Ravussin

2013 Resveratrol vs. calorie restriction: data from rodents to humans. Exp Gerontol 48(10):1018-24.

Lan, F., et al.

2008 SIRT1 modulation of the acetylation status, cytosolic localization, and activity of LKB1. Possible role in AMP-activated protein kinase activation. J Biol Chem 283(41):27628-35.

Lasa, A., et al.

2012 Resveratrol regulates lipolysis via adipose triglyceride lipase. J Nutr Biochem 23(4):379-84.

Lean, M. E., et al.

1988 Metabolic and thyroidal responses to mild cold are abnormal in obese diabetic women. Clin Endocrinol (Oxf) 28(6):665-73.

Lee, Y. H., et al.

2012 In vivo identification of bipotential adipocyte progenitors recruited by beta3-adrenoceptor activation and high-fat feeding. Cell Metab 15(4):480-91.

Lee, Y., et al.

2002 PPAR alpha is necessary for the lipopenic action of hyperleptinemia on white adipose and liver tissue. Proc Natl Acad Sci U S A 99(18):11848-53.

Li, T., and J. Y. Chiang

2012 Bile Acid signaling in liver metabolism and diseases. J Lipids 2012:754067.

Liaset, B., et al.

2011 Nutritional regulation of bile acid metabolism is associated with improved pathological characteristics of the metabolic syndrome. J Biol Chem 286(32):28382-95.

Lindgren, E. M., et al.

2004 Noradrenaline represses PPAR (peroxisome-proliferator-activated receptor) gamma2 gene expression in brown adipocytes: intracellular signalling and effects on PPARgamma2 and PPARgamma1 protein levels. Biochem J 382(Pt 2):597-606.

Llado, I., et al.
1991 Dietary-induced permanent changes in brown and white adipose tissue composition in rats. Int J Obes 15(6):415-9.
Long, E. K., et al.
2013 Fatty acids induce leukotriene C4 synthesis in macrophages in a fatty acid binding protein-dependent manner. Biochim Biophys Acta 1831(7):1199-207.
Lumeng, C. N., et al.
2008 Phenotypic switching of adipose tissue macrophages with obesity is generated by spatiotemporal differences in macrophage subtypes. Diabetes 57(12):3239-46.
Ma, S. W., and D. O. Foster
1986 Uptake of glucose and release of fatty acids and glycerol by rat brown adipose tissue in vivo. Can J Physiol Pharmacol 64(5):609-14.
Madsen, L., et al.
2010 UCP1 induction during recruitment of brown adipocytes in white adipose tissue is dependent on cyclooxygenase activity. PLoS One 5(6):e11391.
Maruyama, T., et al.
2002 Identification of membrane-type receptor for bile acids (M-BAR). Biochem Biophys Res Commun 298(5):714-9.
Masoodi, M., et al.
2014 Lipid signaling in adipose tissue: Connecting inflammation & metabolism. Biochim Biophys Acta.
Mater, M. K., et al.
1998 Arachidonic acid inhibits lipogenic gene expression in 3T3-L1 adipocytes through a prostanoid pathway. J Lipid Res 39(7):1327-34.
Matthias, A., et al.
2000 Thermogenic responses in brown fat cells are fully UCP1-dependent. UCP2 or UCP3 do not substitute for UCP1 in adrenergically or fatty scid-induced thermogenesis. J Biol Chem 275(33):25073-81.
Mazzucotelli, A., et al.
2007 The transcriptional coactivator peroxisome proliferator activated receptor (PPAR)gamma coactivator-1 alpha and the nuclear receptor PPAR alpha control the expression of glycerol kinase and metabolism genes independently of PPAR gamma activation in human white adipocytes. Diabetes 56(10):2467-2475.
Meisinger, C., et al.
2006 Body fat distribution and risk of type 2 diabetes in the general population: are there differences between men and women? The MONICA/KORA Augsburg cohort study. Am J Clin Nutr 84(3):483-9.
Mercader, J., A. Palou, and M. L. Bonet
2011 Resveratrol enhances fatty acid oxidation capacity and reduces resistin and Retinol-Binding Protein 4 expression in white adipocytes. J Nutr Biochem 22(9):828-34.
Mercer, S. W., and P. Trayhurn
1987 Effect of high fat diets on energy balance and thermogenesis in brown adipose tissue of lean and genetically obese ob/ob mice. J Nutr 117(12):2147-53.
Misra, A., et al.
1997 Relationship of anterior and posterior subcutaneous abdominal fat to insulin sensitivity in nondiabetic men. Obes Res 5(2):93-9.
Mitchell, J. R., et al.
1992 Regulation of expression of the lipoprotein lipase gene in brown adipose tissue. Am J Physiol 263(3 Pt 1):E500-6.

Mulligan, J. D., et al.
2007 Upregulation of AMPK during cold exposure occurs via distinct mechanisms in brown and white adipose tissue of the mouse. J Physiol 580(Pt. 2):677-84.
Murray, R. K., et al.
2005 Harperova Biochemie: Nakladatelstv¡ a vydavatelstv¡ H and H, 1998.
Nedergaard, J., T. Bengtsson, and B. Cannon
2007 Unexpected evidence for active brown adipose tissue in adult humans. Am J Physiol Endocrinol Metab 293(2):E444-52.
Nedergaard, J., and B. Cannon
2013 UCP1 mRNA does not produce heat. Biochim Biophys Acta 1831(5):943-9.
Nemoto, S., M. M. Fergusson, and T. Finkel
2005 SIRT1 functionally interacts with the metabolic regulator and transcriptional coactivator PGC-1{alpha}. J Biol Chem 280(16):16456-60.
Nguyen, K. D., et al.
2011 Alternatively activated macrophages produce catecholamines to sustain adaptive thermogenesis. Nature 480(7375):104-8.
Nicholls, D. G., V. S. Bernson, and G. M. Heaton
1978 The identification of the component in the inner membrane of brown adipose tissue mitochondria responsible for regulating energy dissipation. Experientia Suppl 32:89-93.
Nisoli, E., et al.
2005 Calorie restriction promotes mitochondrial biogenesis by inducing the expression of eNOS. Science 310(5746):314-317.
Nye, C., et al.
2008 Reassessing triglyceride synthesis in adipose tissue. Trends Endocrinol.Metab 19(10):356-361.
O'Neill, L. A., and D. G. Hardie
2013 Metabolism of inflammation limited by AMPK and pseudo-starvation. Nature 493(7432):346-55.
Oudart, H., et al.
1997 Brown fat thermogenesis in rats fed high-fat diets enriched with n-3 polyunsaturated fatty acids. Int J Obes Relat Metab Disord 21(11):955-62.
Pardo, R., et al.
2011 Rosiglitazone-Induced Mitochondrial Biogenesis in White Adipose Tissue Is Independent of Peroxisome Proliferator-Activated Receptor gamma Coactivator-1alpha. Plos One 6(11):e26989.
Patel, M. S., and R. W. Hanson
1970 Carboxylation of pyruvate by isolated rat adipose tissue mitochondria. Journal of Biological Chemistry 245(6):1302-1310.
Petrovic, N., et al.
2010 Chronic peroxisome proliferator-activated receptor gamma (PPARgamma) activation of epididymally derived white adipocyte cultures reveals a population of thermogenically competent, UCP1-containing adipocytes molecularly distinct from classic brown adipocytes. Journal of Biological Chemistry 285(10):7153-7164.
Pischon, T., et al.
2008 General and abdominal adiposity and risk of death in Europe. N Engl J Med 359(20):2105-20.
Puigserver, P., et al.
1998 A cold-inducible coactivator of nuclear receptors linked to adaptive thermogenesis. Cell 92(6):829-39.

Qiao, Q., and R. Nyamdorj
2010 Is the association of type II diabetes with waist circumference or waist-to-hip ratio stronger than that with body mass index? Eur J Clin Nutr 64(1):30-4.
Qiu, Y., et al.
2014 Eosinophils and type 2 cytokine signaling in macrophages orchestrate development of functional beige fat. Cell 157(6):1292-308.
Rakhshandehroo, M., et al.
2010 Peroxisome proliferator-activated receptor alpha target genes. PPAR Res 2010.
Rayalam, S., et al.
2008 Resveratrol induces apoptosis and inhibits adipogenesis in 3T3-L1 adipocytes. Phytother Res 22(10):1367-71.
Rodbell, M.
1964 Metabolism of Isolated Fat Cells. I. Effects of Hormones on Glucose Metabolism and Lipolysis. J Biol Chem 239:375-80.
Rodriguez, A. M., et al.
2001 Sex-dependent dietary obesity, induction of UCPs, and leptin expression in rat adipose tissues. Obes Res 9(9):579-88.
Rolfe, D. F., and G. C. Brown
1997 Cellular energy utilization and molecular origin of standard metabolic rate in mammals. Physiol Rev 77(3):731-58.
Rosenwald, M., et al.
2013 Bi-directional interconversion of brite and white adipocytes. Nat Cell Biol 15(6):659-67.
Rosenwald, M., and C. Wolfrum
2014 The origin and definition of brite versus white and classical brown adipocytes. Adipocyte 3(1):4-9.
Rossmeisl, M., et al.
2002 Expression of the uncoupling protein 1 from the aP2 gene promoter stimulates mitochondrial biogenesis in unilocular adipocytes in vivo. European Journal of Biochemistry 269(1):19-28.
Rossmeisl, M., et al.
2009 Prevention and reversal of obesity and glucose intolerance in mice by DHA derivatives. Obesity (Silver Spring) 17(5):1023-31.
Rossmeisl, M., et al.
2000 Decreased fatty acid synthesis due to mitochondrial uncoupling in adipose tissue. FASEB Journal 14(12):1793-1800.
Rothwell, N. J., and M. J. Stock
1979 A role for brown adipose tissue in diet-induced thermogenesis. Nature 281(5726):31-5.
Rouru, J., et al.
1999 Effects of intravenously infused leptin on insulin sensitivity and on the expression of uncoupling proteins in brown adipose tissue. Endocrinology 140(8):3688-92.
Ruderman, N. B., et al.
2003 AMPK as a metabolic switch in rat muscle, liver and adipose tissue after exercise. Acta Physiol Scand. 178(4):435-442.
Saito, M., et al.
2009 High incidence of metabolically active brown adipose tissue in healthy adult humans: effects of cold exposure and adiposity. Diabetes 58(7):1526-31.
Salmon, D. M., and J. P. Flatt

1985 Effect of dietary fat content on the incidence of obesity among ad libitum fed mice. Int J Obes 9(6):443-9.

Sanchez-Gurmaches, J., et al.

2012 PTEN loss in the Myf5 lineage redistributes body fat and reveals subsets of white adipocytes that arise from Myf5 precursors. Cell Metab 16(3):348-62.

Scarpulla, R. C.

2006 Nuclear control of respiratory gene expression in mammalian cells. J Cell Biochem 97(4):673-83.

Seale, P., et al.

2008 PRDM16 controls a brown fat/skeletal muscle switch. Nature 454(7207):961-7.

Seale, P., et al.

2011 Prdm16 determines the thermogenic program of subcutaneous white adipose tissue in mice. J Clin Invest 121(1):96-105.

Seale, P., et al.

2007 Transcriptional control of brown fat determination by PRDM16. Cell Metab 6(1):38-54.

Shibata, H., et al.

1989 Cold exposure reverses inhibitory effects of fasting on peripheral glucose uptake in rats. Am J Physiol 257(1 Pt 2):R96-101.

Schulz, T. J., et al.

2011 Identification of inducible brown adipocyte progenitors residing in skeletal muscle and white fat. Proc Natl Acad Sci U S A 108(1):143-8.

Sivitz, W. I., et al.

1997 Effects of leptin on insulin sensitivity in normal rats. Endocrinology 138(8):3395-401.

Snijder, M. B., et al.

2003 Associations of hip and thigh circumferences independent of waist circumference with the incidence of type 2 diabetes: the Hoorn Study. Am J Clin Nutr 77(5):1192-7.

Stanford, K. I., et al.

2013 Brown adipose tissue regulates glucose homeostasis and insulin sensitivity. J Clin Invest 123(1):215-23.

Stayrook, K. R., et al.

2005 Regulation of carbohydrate metabolism by the farnesoid X receptor. Endocrinology 146(3):984-91.

Su, H. Y., et al.

2014 A calorie-restriction diet supplemented with fish oil and high-protein powder is associated with reduced severity of metabolic syndrome in obese women. Eur J Clin Nutr.

Surwit, R. S., et al.

1998 Diet-induced changes in uncoupling proteins in obesity-prone and obesity-resistant strains of mice. Proc Natl Acad Sci U S A 95(7):4061-5.

Terada, S., et al.

2002 Effects of low-intensity prolonged exercise on PGC-1 mRNA expression in rat epitrochlearis muscle. Biochem Biophys Res Commun 296(2):350-4.

Thurlby, P. L., P. Trayhurn, and W. P. James

1978 An explanation for the elevated efficiency of the genetically obese (obob) mouse. Proc Nutr Soc 37(2):55A.

Timmons, J. A., et al.

2007 Myogenic gene expression signature establishes that brown and white adipocytes originate from distinct cell lineages. Proc Natl Acad Sci U S A 104(11):4401-6.

Tiraby, C., et al.

2003 Acquirement of brown fat cell features by human white adipocytes. J Biol Chem 278(35):33370-6.

Tordjman, J., et al.

2003a Thiazolidinediones block fatty acid release by inducing glyceroneogenesis in fat cells3. J Biol.Chem. 278:18785-18790.

Tordjman, J., et al.

2003b Regulation of glyceroneogenesis and phosphoenolpyruvate carboxykinase by fatty acids, retinoic acids and thiazolidinediones: potential relevance to type 2 diabetes. Biochimie 85(12):1213-8.

Towler, M. C., and D. G. Hardie

2007 AMP-activated protein kinase in metabolic control and insulin signaling. Circ.Res. 100(3):328-341.

Trayhurn, P., P. L. Thurlby, and W. P. James

1976 A defective response to cold in the obese (obob) mouse and the obese Zucker (fafa) rat [proceedings]. Proc Nutr Soc 35(3):133A.

—

1977 Thermogenic defect in pre-obese ob/ob mice. Nature 266(5597):60-2.

Tseng, Y. H., et al.

2008 New role of bone morphogenetic protein 7 in brown adipogenesis and energy expenditure. Nature 454(7207):1000-4.

van Marken Lichtenbelt, W. D., and P. Schrauwen

2011 Implications of nonshivering thermogenesis for energy balance regulation in humans. Am J Physiol Regul Integr Comp Physiol 301(2):R285-96.

van Marken Lichtenbelt, W. D., et al.

2009 Cold-activated brown adipose tissue in healthy men. N Engl J Med 360(15):1500-8.

van Ooijen, A. M., et al.

2004 Seasonal changes in metabolic and temperature responses to cold air in humans. Physiol Behav 82(2-3):545-53.

van Ooijen, A. M., W. D. van Marken Lichtenbelt, and K. R. Westerterp

2001 Individual differences in body temperature and the relation to energy expenditure: the influence of mild cold. J Therm Biol 26(4-5):455-459.

Vegiopoulos, A., et al.

2010 Cyclooxygenase-2 controls energy homeostasis in mice by de novo recruitment of brown adipocytes. Science 328(5982):1158-61.

Vila-Bedmar, R., M. Lorenzo, and S. Fernandez-Veledo

2010 Adenosine 5'-monophosphate-activated protein kinase-mammalian target of rapamycin cross talk regulates brown adipocyte differentiation. Endocrinology 151(3):980-92.

Villarroya, F., R. Iglesias, and M. Giralt

2007 PPARs in the Control of Uncoupling Proteins Gene Expression. PPAR Res 2007:74364.

Virtanen, K. A., et al.

2009 Functional brown adipose tissue in healthy adults. N Engl J Med 360(15):1518-25.

Virtue, S., and A. Vidal-Puig

2008 It's not how fat you are, it's what you do with it that counts. PLoS.Biol. 6(9):e237.
Voet, D., and J. G. Voetova
1994 Biochemie 2. Praha: Victoria Publishing.
Wahli, W., and L. Michalik
2012 PPARs at the crossroads of lipid signaling and inflammation. Trends Endocrinol Metab 23(7):351-363.
Walden, T. B., et al.
2012 Recruited vs. nonrecruited molecular signatures of brown, "brite," and white adipose tissues. Am J Physiol Endocrinol Metab 302(1):E19-31.
Wan, Z., et al.
2012 IL-6 Indirectly Modulates the Induction of Glyceroneogenic Enzymes in Adipose Tissue during Exercise. Plos One 7(7):e41719.
Wan, Z., et al.
2010 Epinephrine-mediated regulation of PDK4 mRNA in rat adipose tissue. Am J Physiol Cell Physiol 299(5):C1162-70.
Wang, M. Y., Y. Lee, and R. H. Unger
1999 Novel form of lipolysis induced by leptin. J Biol Chem 274(25):17541-4.
Wang, Q. A., et al.
2013 Tracking adipogenesis during white adipose tissue development, expansion and regeneration. Nat Med 19(10):1338-44.
Wang, Q., et al.
1997 Interactions between leptin and hypothalamic neuropeptide Y neurons in the control of food intake and energy homeostasis in the rat. Diabetes 46(3):335-41.
Wang, T., et al.
2003 Metabolic partitioning of endogenous fatty acid in adipocytes. Obes.Res. 11(7):880-887.
Wang, Y., et al.
2005 Comparison of abdominal adiposity and overall obesity in predicting risk of type 2 diabetes among men. Am J Clin Nutr 81(3):555-63.
Warwick, P. M., and R. Busby
1990 Influence of mild cold on 24 h energy expenditure in 'normally' clothed adults. Br J Nutr 63(3):481-8.
Watanabe, M., et al.
2011 Lowering bile acid pool size with a synthetic farnesoid X receptor (FXR) agonist induces obesity and diabetes through reduced energy expenditure. J Biol Chem 286(30):26913-20.
Watanabe, M., et al.
2006 Bile acids induce energy expenditure by promoting intracellular thyroid hormone activation. Nature 439(7075):484-9.
Watanabe, M., et al.
2004 Bile acids lower triglyceride levels via a pathway involving FXR, SHP, and SREBP-1c. J Clin Invest 113(10):1408-18.
Watanabe, M., et al.
2012 Bile acid binding resin improves metabolic control through the induction of energy expenditure. PLoS One 7(8):e38286.
Watson, P. M., et al.
2000 Differential regulation of leptin expression and function in A/J vs. C57BL/6J mice during diet-induced obesity. Am J Physiol Endocrinol Metab 279(2):E356-65.
Weisberg, S. P., et al.

2003 Obesity is associated with macrophage accumulation in adipose tissue. Journal of Clinical Investigation 112(12):1796-1808.

White, P. J., et al.
2010 Transgenic restoration of long-chain n-3 fatty acids in insulin target tissues improves resolution capacity and alleviates obesity-linked inflammation and insulin resistance in high fat-fed mice. Diabetes 59(12):3066-3073.

White, P. J., and A. Marette
2014 Potential role of omega-3-derived resolution mediators in metabolic inflammation. Immunol Cell Biol 92(4):324-30.

Wijers, S. L., W. H. Saris, and W. D. van Marken Lichtenbelt
2010 Cold-induced adaptive thermogenesis in lean and obese. Obesity (Silver Spring) 18(6):1092-9.

Wijers, S. L., et al.
2008 Human skeletal muscle mitochondrial uncoupling is associated with cold induced adaptive thermogenesis. PLoS One 3(3):e1777.

Wijers, S. L., et al.
2011 Beta-adrenergic receptor blockade does not inhibit cold-induced thermogenesis in humans: possible involvement of brown adipose tissue. J Clin Endocrinol Metab 96(4):E598-605.

Wijkander, J., et al.
1998 Insulin-induced phosphorylation and activation of phosphodiesterase 3B in rat adipocytes: possible role for protein kinase B but not mitogen-activated protein kinase or p70 S6 kinase. Endocrinology 139(1):219-27.

Wilson-Fritch, L., et al.
2004 Mitochondrial remodeling in adipose tissue associated with obesity and treatment with rosiglitazone. J.Clin.Invest 114(9):1281-1289.

Wu, D., et al.
2011 Eosinophils sustain adipose alternatively activated macrophages associated with glucose homeostasis. Science 332(6026):243-7.

Xu, H., et al.
2003 Chronic inflammation in fat plays a crucial role in the development of obesity-related insulin resistance1. J.Clin.Invest 112(12):1821-1830.

Xue, B., et al.
2005 Transcriptional synergy and the regulation of Ucp1 during brown adipocyte induction in white fat depots. Mol Cell Biol 25(18):8311-22.

Xue, B., et al.
2007 Genetic variability affects the development of brown adipocytes in white fat but not in interscapular brown fat. J Lipid Res 48(1):41-51.

Xue, Y., et al.
2009 Hypoxia-independent angiogenesis in adipose tissues during cold acclimation. Cell Metab 9(1):99-109.

Yan, H., et al.
2003 Role of cyclooxygenases COX-1 and COX-2 in modulating adipogenesis in 3T3-L1 cells. J Lipid Res. 44(2):424-429.

Yen, C. L., et al.
2008 Thematic review series: glycerolipids. DGAT enzymes and triacylglycerol biosynthesis. J Lipid Res 49(11):2283-301.

Yoshizaki, Takeshi, et al.
2009 SIRT1 exerts anti-inflammatory effects and improves insulin sensitivity in adipocytes. Molecular and Cellular Biology 29(5):1363-1374.

Young, P., J. R. Arch, and M. Ashwell
1984 Brown adipose tissue in the parametrial fat pad of the mouse. FEBS Lett 167(1):10-4.
Zhang, C., et al.
2008 Abdominal obesity and the risk of all-cause, cardiovascular, and cancer mortality: sixteen years of follow-up in US women. Circulation 117(13):1658-67.
Zhou, D., et al.
2012 CD36 level and trafficking are determinants of lipolysis in adipocytes. FASEB Journal 26(11):4733-4742.
Zingaretti, M. C., et al.
2009 The presence of UCP1 demonstrates that metabolically active adipose tissue in the neck of adult humans truly represents brown adipose tissue. FASEB Journal 23(9):3113-3120.

List of all publications

A. Teodoro JS*, **Zouhar P***, Flachs P, Bardova K, Janovska P, Gomes AP, Duarte FV, Varela AT, Rolo AP, Palmeira CM, Kopecký J. *Enhancement of brown fat thermogenesis using chenodeoxycholic acid in mice*. **International Journal of Obesity, 2012, Vol. 38, 2, p. 216-223.** IF = 5.386

* These authors contributed equally to this work.

My personal contribution to this publication includes supervision over the second animal experiment (including pair-fed group of mice), participation in the analysis of plasma markers, evaluation of UCP1 protein content in adipose tissue, statistical analysis, creation of figures, and writing a draft of manuscript.

B. Flachs P, Rühl R, Hensler M, Janovská P, **Zouhar P**, Kůs V, Macek Jílková Z, Papp E, Kuda O, Svobodová M, Rossmeisl M, Tsenov G, Mohamed-Ali V, Kopecký J. *Synergistic induction of lipid catabolism and anti-inflammatory lipids in white fat of dietary obese mice in response to calorie restriction and n-3 fatty acids*. **Diabetologia, 2011, Vol. 54, 10, p. 2626-2638**. IF = 6.814

My personal contribution to this publication includes supervision over the last confirmatory animal experiments and experiments requested by reviewers, evaluation of mitochondrial oxidative capacity in isolated adipocytes, evaluation of cytochrome b content in epididymal adipose tissue, preparation of hepatocyte primary culture, evaluation of palmitate oxidation rate in these cells, and participation on quantitative real time PCR analysis of gene expression.

C. Publication under preparation

The different propensity to obesity in two strains of mice is related to the cold-induced rate of fatty acid re-esterification in their epididymal adipose tissue.

My personal contribution to this prepared paper includes supervision over the animal experiments (in collaboration with P. Flachs and M. Svobodova), evaluation of UCP1 using Western blotting, and evaluation of re-esterification rate using NMR (under supervision of J. Jones).

Appendix

A. Supplementary Figures

B. Publications enclosed in full
(Publication A, Publication B)

Supplementary Figures

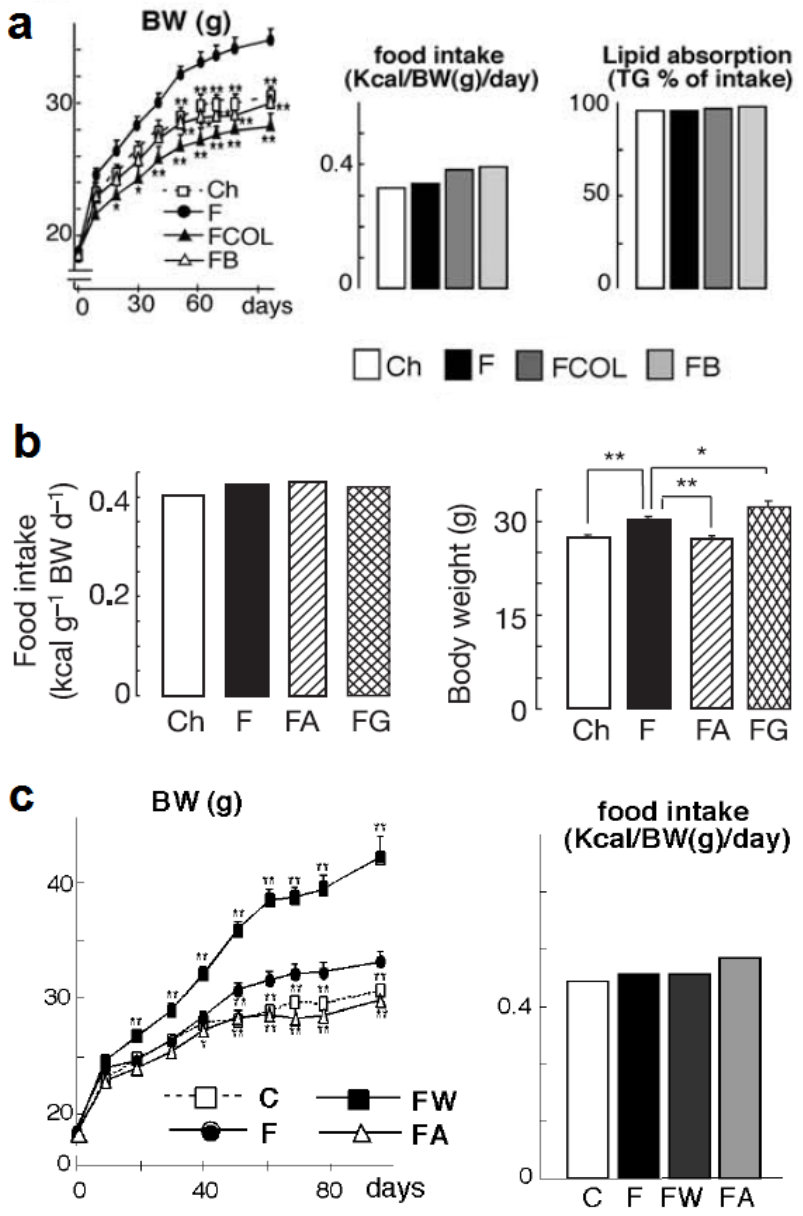

Fig. S-1 Body weight, food consumption adjusted to body weight, and lipid absorption in published articles of Watanabe.

a) Fig 1a in (Watanabe, et al. 2012);
b) Fig 1f in (Watanabe, et al. 2006);
c) Fig 1a in (Watanabe, et al. 2011);

C = Ch – control / chow diet, F – high fat diet, FCOL – high fat diet + colestimide, FB = FA – high fat diet + cholic acid, FG = FW – high fat diet + GW4064 (synthetic agonist of FXR-α).

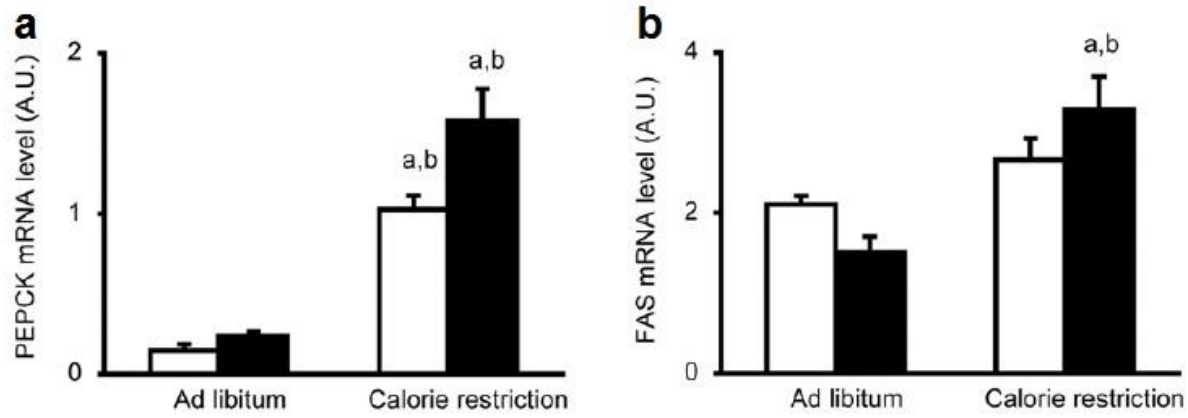

Fig. S-2 Induction of TAG/NEFA cycling in eWAT of animals after cHF+F+CR treatment.
Synergistic stimulation of PEPCK (a) and ATGL (b) gene expression – markers of glyceroneogenesis and lipolysis, respectively (Flachs, et al. 2013).

Publications enclosed in full

Publication A

International Journal of Obesity (2014) **38,** 1027–1034

www.nature.com/ijo

ORIGINAL ARTICLE

Enhancement of brown fat thermogenesis using chenodeoxycholic acid in mice

JS Teodoro[1,2,5], P Zouhar[3,5], P Flachs[3], K Bardova[3], P Janovska[3], AP Gomes[1,2], FV Duarte[1,2], AT Varela[1,2], AP Rolo[1,4], CM Palmeira[1,2] and J Kopecký[3]

OBJECTIVE: Besides their role in lipid absorption, bile acids (BAs) can act as signalling molecules. Cholic acid was shown to counteract obesity and associated metabolic disorders in high-fat-diet (cHF)-fed mice while enhancing energy expenditure through induction of mitochondrial uncoupling protein 1 (UCP1) and activation of non-shivering thermogenesis in brown adipose tissue (BAT). In this study, the effects of another natural BA, chenodeoxycholic acid (CDCA), on dietary obesity, UCP1 in both interscapular BAT and in white adipose tissue (brite cells in WAT), were characterized in dietary-obese mice.

RESEARCH DESIGN: To induce obesity and associated metabolic disorders, male 2-month-old C57BL/6J mice were fed cHF (35% lipid wt wt^{-1}, mainly corn oil) for 4 months. Mice were then fed either (i) for 8 weeks with cHF or with cHF with two different doses (0.5%, 1%; wt wt^{-1}) of CDCA (8-week reversion); or (ii) for 3 weeks with cHF or with cHF with 1% CDCA, or pair-fed (PF) to match calorie intake of the CDCA mice fed *ad libitum*; mice on standard chow diet were also used (3-week reversion).

RESULTS: In the 8-week reversion, the CDCA intervention resulted in a dose-dependent reduction of obesity, dyslipidaemia and glucose intolerance, which could be largely explained by a transient decrease in food intake. The 3-week reversion revealed mild CDCA-dependent and food intake-independent induction of UCP1-mediated thermogenesis in interscapular BAT, negligible increase of UCP1 in subcutaneous WAT and a shift from carbohydrate to lipid oxidation.

CONCLUSIONS: CDCA could reverse obesity in cHF-fed mice, mainly in response to the reduction in food intake, an effect probably occuring but neglected in previous studies using cholic acid. Nevertheless, CDCA-dependent and food intake-independent induction of UCP1 in BAT (but not in WAT) could contribute to the reduction in adiposity and to the stabilization of the lean phenotype.

International Journal of Obesity (2014) **38,** 1027–1034; doi:10.1038/ijo.2013.230

Keywords: white adipose tissue; uncoupling protein 1; energy expenditure; bile acids

INTRODUCTION

Bile acids (BAs) are essential for lipid absorption in the intestine. More recently, it was discovered that BAs administration could improve several parameters of lipid metabolism.[1] Thus, BAs could beneficially influence the health status of both patients and experimental models (reviewed in Teodoro *et al.*[2]). This finding made BAs a promising new tool for the treatment of metabolic syndrome—that is, the cluster of diseases associated with obesity.

BAs could act as signalling molecules through activation of the farnesoid X receptor (FXR).[3] FXR activation influences glucose and lipid metabolism; namely, it decreases plasma triglyceride (TG) levels by inhibiting lipogenesis and by increasing TG clearance.[3,4] Accordingly, FXR-null mice are obese and hypertriglyceridaemic.[5] FXR is also important for prevention of insulin resistance[6] and hypoglycaemia during fasting,[7] production of hepatic glycogen[8] and differentiation of adipocytes.[9] Moreover, the positive metabolic effect of BAs on glucose control and weight reduction could be mediated by G protein-coupled receptor 5 (TGR5).[10] However, some BAs are not competent activators of TGR5. The most potent natural activator of FXR, chenodeoxycholic acid (CDCA), used as a drug for the treatment of gallstones,[11] has been reported to be both a potent and a not very effective activator of TGR5.[10,12–14] Therefore, the mechanism by which BAs accomplish their beneficial metabolic functions is not yet fully understood.

A new insight into the mechanism of action of BAs was provided by the finding of Watanabe *et al.*[15] that BAs, namely, cholic acid, promote non-shivering thermogenesis in the interscapular brown adipose tissue (BAT) in mice and in skeletal muscle in humans. In BAT, energy expenditure (EE) is mediated by mitochondrial uncoupling protein 1 (UCP1)[16], and induction of the UCP1-based thermogenesis has been proposed as a possible therapeutic strategy against obesity and diabetes.[17,18] The BAs' binding to TGR5 in BAT leads to elevation of cAMP level and consequent activation of thyroid hormone-converting enzyme type 2 iodothyronine deiodinase.[15] BAs therefore facilitate thyroid hormone stimulatory influence on BAT thermogenesis. In fact, treatment with cholic acid was able to reverse diet-induced weight gain.[15] Also, other studies confirmed the ability of BAs to stimulate UCP1-mediated non-shivering thermogenesis in BAT.[10,19,20]

The interest in UCP1-mediated thermogenesis was boosted recently by the discovery of functional BAT in adult humans,[21] as well as by the finding of *Ucp1*-expressing adipocytes,[22–24] which

[1]Center for Neuroscience and Cell Biology, Faculty of Science and Technology, University of Coimbra, Coimbra, Portugal; [2]Department of Life Sciences, Faculty of Science and Technology, University of Coimbra, Coimbra, Portugal; [3]Department of Adipose Tissue Biology, Institute of Physiology Academy of Sciences of the Czech Republic v.v.i., Prague, Czech Republic and [4]Department of Biology, University of Aveiro, Aveiro, Portugal. Correspondence: Dr J Kopecký, Department of Adipose Tissue Biology, Institute of Physiology Academy of Sciences of the Czech Republic v.v.i., Videnska 1083, Prague 14220, Czech Republic.
E-mail: kopecky@biomed.cas.cz
[5]These authors contributed equally to this work.
Received 7 August 2013; revised 11 November 2013; accepted 24 November 2013; accepted article preview online 6 December 2013; advance online publication, 14 January 2014

could be induced in several white adipose tissue (WAT) depots in mice in response to various stimuli and represent a potential target for induction of fat burning (these cells are annotated 'brite' adipocytes in this article, as in Petrovic *et al.*;[25] reviewed in Wu *et al.*[17]). However, whether the brite cells reflect transdifferentiation of white adipocytes[26] or the existence of distinct brown and brite cell lineages (reviewed in Wu *et al.*[17]) is a subject of debate. Similarly, the origin of Ucp1-expressing adipocytes in humans (reviewed in Jespersen *et al.*[27]) and, importantly, the magnitude of energy dissipation in brite cells with respect to that in classical BAT, as well as the contribution of energy dissipation occurring in brite cells to total energy balance (compare Wu *et al.*,[17] and Nedergaard and Cannon[28]), remain all controversial.

We focused here on whether CDCA (similarly to cholic acid; see above) could influence energy balance and reverse the dietary obesity. Our results demonstrated a strong anti-obesity effect of CDCA, which could be explained in large by a transient decrease in food intake. The results suggest that induction of UCP1-mediated thermogenesis in adipocytes in BAT rather than in brite cells could contribute to stabilization of the lean phenotype under these conditions.

MATERIALS AND METHODS

Animals care and diet

C57BL/6J mice were obtained from the Jackson Laboratory (Bar Harbor, ME, USA) and bred at the Institute of Physiology for several generations. Single-caged male mice were maintained at 20 °C on a 12:12-hr light–dark cycle.

Two different experiments were conducted. In the first experiment (8-week reversion), 2-month-old mice were subjected to the high-fat-diet feeding (cHF, lipid content ~35.2% wt wt^{-1}, mainly corn oil, energy density 22.8 kJ g^{-1}; this diet was proven to be obesogenic in C57BL/6J mice, and it contained 15%, 59% and 26% energy as protein, fat and carbohydrate, respectively)[29] for another 4 months to induce obesity and associated metabolic disorders. After that, the animals were randomly divided into three experimental groups ($n = 10$–12 per group) and fed for 8 weeks either the cHF diet, the cHF diet supplemented with 0.5% CDCA (wt wt^{-1}) or the cHF diet supplemented with 1% CDCA (wt wt^{-1}, 95% pure; Sigma-Aldrich, St Louis, MO, USA). All the diets were fed *ad libitum*. Body weight (BW) and food intake were measured every week. During week 6 of the intervention, some of the animals (five mice randomly selected in each group) were subjected to an oral glucose tolerance test (see below). At the end of week 8, all the mice were killed in the morning in fed state by means of cervical dislocation. Plasma was collected (see below), and following tissues were also dissected: liver, gastrocnemius muscle, interscapular BAT, epididymal WAT and subcutaneous WAT (scWAT) from the dorsolumbar region. Moreover, faeces were also collected for further analysis.

In the second experiment (3-week reversion), adult mice already fed the cHF diet for 4 months (see above) were randomly assigned to one of the following: 1) a cHF diet, 2) a cHF diet containing 1% CDCA or 3) a cHF diet with food intake limited to that of animals on 1% CDCA (pair-fed group (PF); $n = 8$ per group). Animals fed standard laboratory chow (STD diet, lipid content ~3.4% wt wt^{-1}, energy density 13.0 kJ g^{-1}; contained 33, 9 and 58% energy as protein, fat and carbohydrate, respectively; extruded Ssniff R/M-H diet, Ssniff Spezialdieten GmbH, Soest, Germany) since weaning at 4 weeks of age were also included in the experiment ($n = 7$). The experiment continued for next 3 weeks. BW and food intake were measured four times each week (see Figures 1c and d). Between day 15 and day 17, indirect calorimetry was performed. At the end of the experiment, mice were killed as described above.

All experiments were performed in accordance with the guidelines for the use and care of laboratory animals of the Institute of Physiology, the directive of the European Communities Council (2010/63/EU) and the Principles of Laboratory Animal Care (NIH publication no. 85–23, revised 1985).

Evaluation of plasma parameters, glucose homeostasis and TG content in tissues and faeces

Blood was collected and analysed as described previously;[30] glycaemia, plasma levels of non-esterified fatty acids, TG, cholesterol, insulin and multimeric forms of adiponectin were evaluated. The remaining plasma was frozen at −80 °C for measurement of the activity of liver enzymes, as previously described.[31] Oral glucose tolerance test was conducted as described in Medrikova *et al.*[30] TG content in tissues and faeces was assessed.[32]

Light microscopy and immunohistology analysis

Adipose tissue samples were fixed in 10% neutral buffered formalin (Sigma-Aldrich) and embedded in paraffin. Sections (5 μm) were stained with haematoxylin–eosin for morphometry, or processed to detect UCP1-positive cells, using a rabbit anti-hamster UCP1 antibody.[33] Sections were deparaffinized and rehydrated, and 10 mM sodium citrate (pH 6.0) was used for antigen retrieval. Immunohistological detection of UCP1 was performed as follows: a) incubation with 3% hydrogen peroxide in methanol at room temperature for 10 min; b) incubation with the diluted goat serum 1:50 at room temperature for 30 min; c) incubation with the primary antibody diluted 1:4000 at 4 °C overnight; d) incubation with the secondary antibody anti-rabbit IgG biotinylated (Vector laboratories, Burlingame, CA, USA) 1:200 at room temperature for 1 h; e) incubation with ABC (Vectastain ABC kit, Vector laboratories) at room temperature for 1 h; f) visualization using diaminobenzidine. For each treatment, a negative control without the primary antibody was used. BAT was used as a positive control for UCP1 immunoreactivity. Digital images were captured using an Olympus AX70 light microscope and a DP 70 camera (Olympus, Tokyo, Japan). Morphometric analysis was performed using Imaging Software NIS-Elements AR3.0 (Laboratory Imaging, Prague, Czech Republic). The morphometry data are based on measurements of ~800 cells taken randomly from two to three different sections per animal (see Medrikova *et al.*[30]).

RNA isolation and real-time PCR

Total RNA was isolated from flash-frozen tissue (kit from Qiagen GmbH, Hilden, Germany). RNA yields were quantified using a Nanodrop instrument (Thermo Scientific, Waltham, MA, USA). Complementary DNA was produced using 1 μg of RNA with a Bio-Rad iScript cDNA synthesis kit (Bio-Rad, Hercules, CA, USA). Gene expression was evaluated using real-time PCR, LightCycler (Roche Diagnostics, Mannheim, Germany) and MiniOpticon (Bio-Rad) equipments. Primers used and their sequences are described in Supplementary Table S1.

Quantification of UCP1 using Western blots

Tissue membranous fraction was prepared using 70 mg interscapular BAT or 100 mg scWAT samples, by homogenization in a buffer containing 250 mM sucrose, 50 mM Tris, 5 mM Na-EDTA, 174 μg ml^{-1} phenylmethanesulphonylfluoride, 1 μg ml^{-1} aprotinin, leupeptin and pepstatin, followed by centrifugation at 100 000 *g*, for 45 min, at 4 °C. Membranous sample aliquots (2–5 μg protein) were then analysed using western blots and 10% polyacrylamide gels.[33] Immunodetection of UCP1 was performed similarly to the detection of adiponectin multimeric forms in plasma,[30] except that anti-UCP1 antibody (1:500)[33] and a secondary infrared dye-conjugated antibody (1:5000) were used. Mitochondria isolated from interscapular BAT of adult C57BL/6J mice reared at 4 °C were used to quantify the relative UCP1 content in each sample (the detection limit for UCP1 was about 0.5 μg of BAT mitochondrial protein and relative UCP1 content in whole interscapular BAT was also calculated. Protein was measured using bicinchoninic acid.[34]

Indirect calorimetry

To evaluate EE and fuel partitioning, indirect calorimetry was performed using INCA system from Somedic (Horby, Sweden).[35,36] Briefly, the measurements were performed in individually caged mice (Eurostandard type II mouse plastic cages; ~6000 ml; Techniplast, Milan, Italy), with the cages placed in a sealed measuring chamber equipped with thermostatically controlled heat exchangers at 22 °C. Oxygen consumption (VO_2) and carbon dioxide production (VCO_2) were recorded every 2 min under a constant airflow rate (1000 ml min^{-1}) for 24 h, starting at 0800 hours. EE was calculated using the following equation: $EE\ (cal) = 3.9 \times VO_2\ (ml) + 1.1 \times VCO_2\ (ml)$.[37,38] The level of substrate partitioning was estimated by calculating respiratory quotient (RQ; that is, VCO_2/VO_2 ratio). To compare subtle differences between groups, the percent relative cumulative frequency (PRCF) curves were constructed on the basis of RQ values pooled from all the animals within a given dietary group ($n = 7$–8) during the whole measurement

period, as described before.[35] Provided that the PRCF curves represent the normally distributed data, the values of 50th percentile of PRCF (EC_{50}) based on each individual animal correspond to RQ values.

Statistical analysis

All values are reported as means ± s.e.m. Statistical significance was analysed as indicated by one-way ANOVA with a Holm–Sidac correction in SigmaPlot 10 software (Systat Software, Point Richmond, CA, USA). The PRCF curves were analysed using nonlinear regression using SigmaPlot. Differences in EE were evaluated by ANCOVA using NCSS software. Differences were considered significant when $P<0.05$.

RESULTS

Reversal of dietary obesity and associated disorders in response to CDCA

First, the effects of CDCA admixed to the cHF diet (0.5% and 1% CDCA) were examined in the 8-week reversion of dietary obesity. Immediately following the switch to the CDCA-containing diets, food intake rapidly decreased reflecting the dose of CDCA, and it returned to the level observed in the control cHF-fed mice within 2–3 weeks of the intervention (Figure 1a). This transient drop due to habituation of mice to the new diets was not accompanied by any changes in plasma levels of liver transaminases (Table 1), arguing against hepatotoxic effects of CDCA. The transient decrease in food intake coincided with a CDCA dose-dependent decrease in BW (Figure 1b), with a maximum reduction reached by the end of week 2 of the intervention. Surprisingly, in spite of the normalization of food intake in the CDCA-intervention groups following week 2, the depression of BW lasted stable till the end of the experiment at week 8 (Figure 1b).

At week 8, plasma lipid levels (namely, TG and cholesterol) were decreased by the CDCA interventions, with a dose-dependent effect on TG levels, and maximum effect on cholesterol levels observed already at the lower CDCA dose (Table 1). Dose-dependent lowering of glycaemia, insulinaemia and glucose intolerance (manifested by changes of area under curve in glucose tolerance test) in response to CDCA documented improvement of glucose homeostasis by the interventions, which was in accordance with the increase in the ratio of high molecular weight adiponectin/total adiponectin plasma levels (Table 1). Lipid (TG and cholesterol) content in faeces was slightly decreased by CDCA treatment, independently of the dose.

Changes in BW could be explained by the changes in adiposity, as documented by weights of both epididymal WAT and scWAT (Table 1). Furthermore, the CDCA intervention prevented ectopic TG accumulation in liver and muscle (Table 1). Thus, the 8-week reversion experiment revealed strong normalization of BW and obesity-associated phenotypes in response to the CDCA intervention. However, it remained to be established what was the contribution of the transient decrease in food intake to the lasting effects of the intervention.

Reduction of adiposity in response to CDCA in a pair-feeding experiment

To dissect the role of the transient decrease in food intake and the CDCA-induced metabolic effects in the anti-obesity effect of the drug, the 3-week reversion experiment was conducted (Figures 1c and d), in which PF animals were also included. The duration of intervention was shortened to 3 weeks, in order to focus on the period when the decline in food intake occurred (see above). The transient decrease in food intake in the CDCA mice, normalized within 3 weeks (Figure 1c), was associated with a drop in BW, almost to the level of mice fed the STD diet since weaning (Figure 1d). This drop could be explained by the decrease in food intake, as it was also observed in the PF mice (Figure 1d). The animals maintained the decreased BW even after reaching the normal food consumption (Figures 1c and d).

Adipose tissue in the 3-week reversion experiment

Dietary obesity was associated with a strong increase in adiposity, as indicated by the differences in weights of all fat depots analysed in the STD mice and the cHF mice (Table 2). Weights of epididymal WAT and scWAT depots, as well as interscapular BAT, were significantly decreased in the PF mice (Table 2).

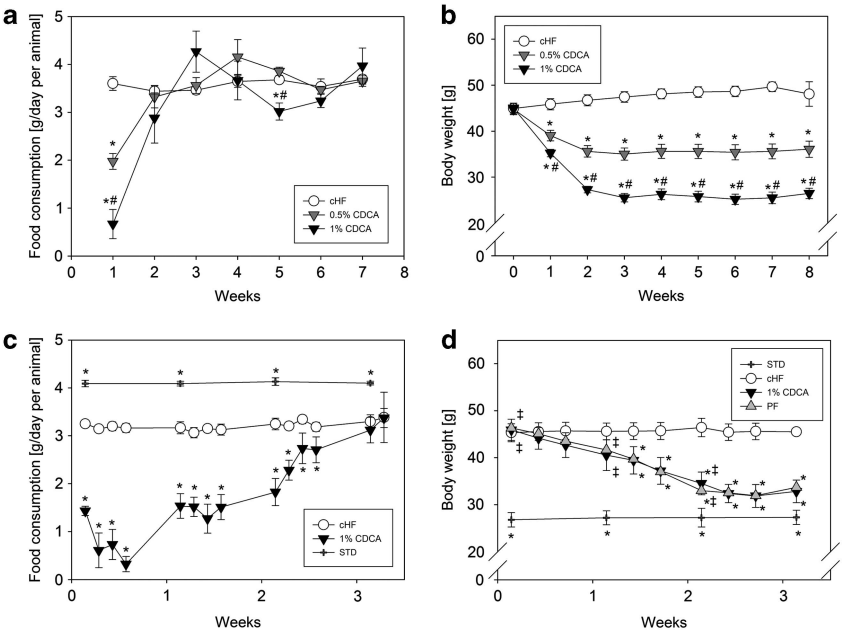

Figure 1. Growth curves and food intake. (**a**, **b**) Food intake (**a**) and growth curve (**b**) during the 8-week reversion experiment ($n=10$–12); (**c**, **d**) food intake (**c**) and growth curve (**d**) during the 3-week reversion experiment ($n=8$, except for STD, where $n=4$). Data are means ± s.e.m. *Significantly different in comparison to the cHF group; #significantly different in comparison to the 0.5% CDCA group (only in **a** and **b**); ‡significantly different in comparison to the STD group (only in **d**). cHF, high-fat diet; 0.5 and 1% CDCA, high-fat diet supplemented with 0.5% and 1% CDCA, respectively; PF, pair-fed group; STD, standard chow diet.

Table 1. Parameters measured in plasma, tissues and faeces at the end of the 8-week reversion experiment

	cHF	*0.5% CDCA*	*1% CDCA*
Plasma levels			
TG (mmol l^{-1})	1.56 ± 0.12	1.08 ± 0.12[a]	0.83 ± 0.10[a]
NEFA (mmol l^{-1})	0.86 ± 0.04	0.85 ± 0.04	0.65 ± 0.04[a,b]
Cholesterol (mmol l^{-1})	5.27 ± 0.26	3.15 ± 0.26[a]	2.70 ± 0.42[a]
Glucose (mg dl^{-1})	257 ± 10	191 ± 13[a]	143 ± 19[a]
Insulin (ng ml^{-1})	4.53 ± 0.43	0.71 ± 0.10[a]	0.19 ± 0.03[a]
Adiponectin HMW (AU)	0.43 ± 0.03	0.47 ± 0.04	0.62 ± 0.07[a]
Total (AU)	1.02 ± 0.06	0.98 ± 0.07	1.20 ± 0.10
HMW/totals	0.42 ± 0.02	0.48 ± 0.03	0.51 ± 0.03
Aspartate transaminase (uCAT l^{-1})	3.02 ± 0.32	3.01 ± 0.39	3.26 ± 0.30
Alanine transaminase (uCAT l^{-1})	1.12 ± 0.16	0.62 ± 0.03	0.88 ± 0.08
Oral glucose tolerance test			
Total AUC (mmol l^{-1} Glc 180 min)	3042 ± 189	2524 ± 158[a]	1654 ± 82[a,b]
Weight of tissues			
eWAT (mg)	2241 ± 105	1419 ± 147[a]	513 ± 66[a,b]
scWAT (mg)	1295 ± 60	612 ± 102[a]	191 ± 19[a,b]
Liver (mg)	2328 ± 132	1873 ± 95	2060 ± 204
Tissue TG content			
Liver TG (mg g^{-1} tissue)	377 ± 41	49 ± 6[a]	30 ± 1[a,b]
Muscle TG (mg g^{-1} tissue)	113 ± 11	50 ± 7[a]	35 ± 7[a]
Faeces lipid content			
TG (mg g^{-1})	62.8 ± 14	47.5 ± 4.7	49.2 ± 2.9
Cholesterol (mg g^{-1})	12.3 ± 0.8	10.4 ± 0.4[a]	10.5 ± 0.3[a]

Abbreviations: AUC, area under the curve; CDCA, chenodeoxycholic acid; cHF, high-fat diet; eWAT, epididymal WAT; HMW, high molecular weight; NEFA, non-esterified fatty acid; scWAT, subcutaneous WAT; TG, plasma triglyceride. Data are means ± s.e.m. ($n = 10$–12, except for oral glucose tolerance test, where $n = 5$; see Materials and Methods). [a]Significant differences in comparison to the cHF group. [b]Significant differences in comparison to the 0.5% CDCA group.

Table 2. Fat depots at the end of the 3-week reversion experiment

	STD	*cHF*	*1% CDCA*	*PF*
Weight of tissues				
eWAT (mg)	553 ± 94[a]	2490 ± 208	899 ± 147[a]	979 ± 154[a]
scWAT (mg)	183 ± 14[a]	1163 ± 168	417 ± 78[a]	498 ± 83[a]
Interscapular BAT (mg)	121 ± 19[a]	228 ± 20	92 ± 9[a]	125 ± 17[a]
Average adipocyte area				
scWAT (μm^2)	1040 ± 190[a]	3474 ± 240	1652 ± 193[a]	2191 ± 186[a,b]

Abbreviations: BAT, brown adipose tissue; CDCA, chenodeoxycholic acid; cHF, high-fat diet; eWAT, epididymal WAT; PF, pair-fed group; scWAT, subcutaneous WAT; STD, standard chow diet. Data are shown as means ± s.e.m. ($n = 8$, except for STD, where $n = 4$; see Materials and Methods). [a]Significant differences in comparison to the cHF group. [b]Significant differences in comparison to the STD group.

Morphometry of adipocytes in scWAT indicated that the differences in adiposity were reflected by the size of adipocytes (Table 2). A similar conclusion could be made by a simple inspection of histological sections from both interscapular BAT (Figure 2a) and scWAT (Figure 3a). Weights of all fat depots analysed, as well as the size of adipocytes in scWAT, tended to be smaller in the CDCA as compared with the PF mice, but the differences were not statistically significant (Table 2).

To learn whether the reduction in BW and adiposity in response to both PF and CDCA intervention could be explained by induction of UCP1-mediated thermogenesis, as previously observed in the case of cholic acid,[15] *Ucp1* gene transcript levels in the interscapular BAT were quantified. As compared with the cHF mice, *Ucp1* gene expression was highly induced in the CDCA mice (Figure 2b), which was also in accordance with the increased expression of the *Prdm16* gene (which is essential for *Ucp1* gene expression and for the activation of the UCP1-mediated thermogenesis[39]) as well as the induction of selected markers of mitochondrial biogenesis (such as *Ppargc1a*, *Slc25a4* and *Cox4i1*; Figure 2b). On the other hand, no induction of these genes could be observed in the PF mice (Figure 2b). Total thermogenic activity of interscapular BAT could be assessed by evaluation of UCP1 content per depot.[28] Therefore, UCP1 was quantified in the membranous fraction prepared from interscapular BAT using western blots (data not shown). Although total UCP1 content was similar in the STD, cHF and PF mice, it was significantly increased in response to the CDCA intervention, and it was ~1.5-fold higher in the CDCA as compared with the cHF mice (Figure 2c).

Also in scWAT of the CDCA and PF mice, *Ucp1* gene transcript was detected. No *Ucp1* gene transcript could be detected in the cHF mice, and the transcript levels were much higher in the CDCA as compared with the PF mice. However, even in the CDCA mice, *Ucp1* transcript levels in scWAT were at least three orders of magnitude lower as compared with those in interscapular BAT of these mice (compare *Y* axes in Figures 2b and 3b, where *Ucp1* transcript levels were estimated under identical conditions).

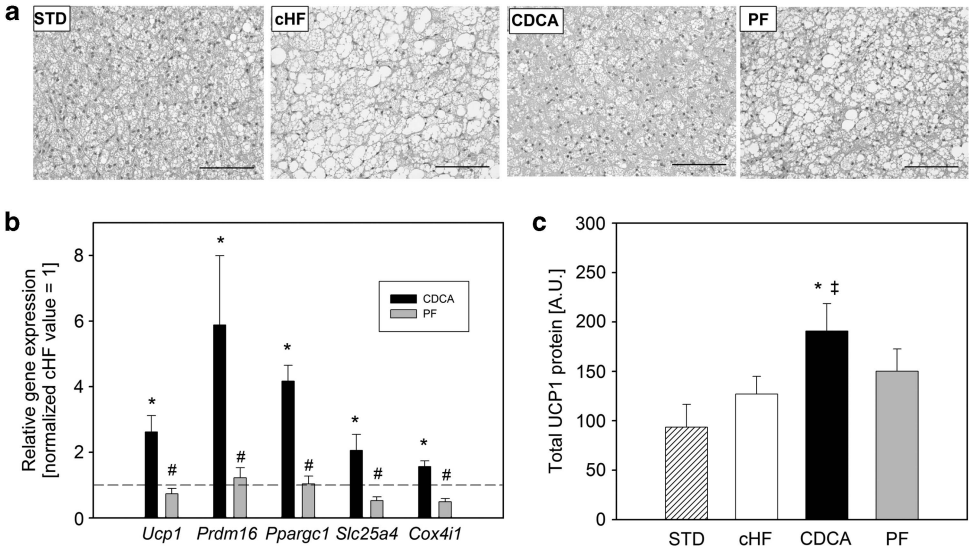

Figure 2. Interscapular BAT parameters in the 3-week reversion experiment. (**a**) Representative images of BAT. (**b**) Relative gene expression (cHF = 1, dashed line); data were normalized using 18S RNA as a housekeeping gene. (**c**) Content of UCP1 protein in whole interscapular BAT. *Significantly different in comparison to the cHF group; #significantly different in comparison to the CDCA group; ‡significantly different in comparison to the STD group. Data are means ± s.e.m. ($n = 8$, except for STD, where $n = 4$). (**a**) Bar = 0.1 mm. CDCA, high-fat diet supplemented with 1% CDCA; cHF, high-fat diet; PF, pair-fed group; STD, standard chow diet.

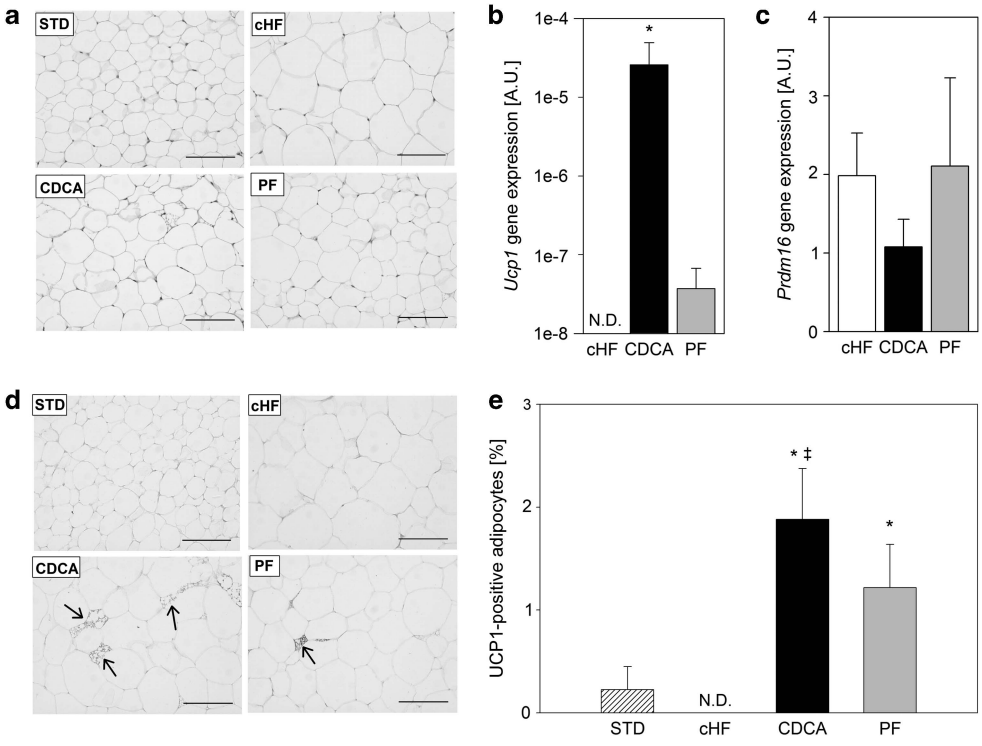

Figure 3. scWAT parameters in the 3-week reversion experiment. (**a**) Representative images of WAT. (**b** and **c**) *Ucp1* and *Prdm16* gene expression; data were normalized using 18S RNA as a housekeeping gene. (**d**) Representative images of immunostaining for UCP1; UCP1-positive cells are indicated by arrows. (**e**) Graphical representation of the percentage of UCP1-positive cells relative to all adipocytes visualized. *Significantly different in comparison to the cHF group; ‡significantly different in comparison to the STD group. Data are means ± s.e.m. ($n = 8$, except for STD, where $n = 4$). (**a** and **d**) Bar = 0.1 mm. CDCA, high-fat diet supplemented with 1% CDCA; cHF, high-fat diet; ND, not detected; PF, pair-fed group; STD, standard chow diet.

However, unlike in BAT, in scWAT, *Prdm16* gene expression did not reflect the activity of *Ucp1* gene, and expression of *Prdm16* gene in the cHF, CDCA and PF mice was similar (Figure 3c). In contrast to BAT, even in scWAT of the CDCA mice, we could not detect any UCP1 using western blots, indicating that in spite of the stimulation of *Ucp1* gene expression in WAT, UCP1 levels in this tissue were relatively low and that they were under the detection limit of the method (data not shown). Immunohistological analysis

revealed some UCP1-positive adipocytes (that is, 'brite' cells) in scWAT, especially in the CDCA mice (Figures 3d and e), but not in eWAT (data not shown).

Indirect calorimetry in the 3-week reversion experiment

To evaluate the effects of the CDCA intervention on EE and fuel partitioning, indirect calorimetry was performed during the third week of the 3-week reversion experiment. As expected, in all the groups, that is, the cHF, CDCA and PF mice, EE was relatively high during the dark phase of the day, when the mice are known to be active. However, except for a decline in EE during the dark phase in the PF mice, the expected effect of a limited food supply in the PF mice, no major differences in the time course of EE between the groups were observed (Figure 4a). Accordingly, analysis of mean EE over the whole day has not revealed any significant differences between the groups when the values are expressed per the whole animal even when evaluated by ANCOVA reflecting BW (Figure 4d). However, when EE was adjusted to BW, both the CDCA mice and the PF mice exhibited higher EE as compared with the control mice fed the cHF diet (Figure 4e). Whether this could suggest CDCA-induced increase in EE is a matter of debate (see Discussion). The evaluation of RQ, the marker of fuel partitioning, during the day revealed a decline in RQ during the dark phase in the PF mice (Figure 4b), suggesting a gradual shift from carbohydrate to lipid oxidation in response to the limited food supply (see above). Moreover, during the dark but not during the light phase of the day, the CDCA mice exhibited a lower RQ as compared with the cHF mice (Figure 4b). The robust PRCF analysis of the RQ data, which takes into account all the RQ values measured in each group (see Materials and methods), supported the shift from carbohydrate to lipid oxidation in response to pair-feeding, and, importantly, it also suggested a food consumption-independent shift to lipid oxidation in response to the CDCA intervention (Figure 4c). The PRCF data were evaluated for the whole day rather than separately for the light and the dark phase of day, to eliminate the influence of the shift in rhythmicity elicited in response to the pair-feeding. Also, the mean RQ during the whole day (Figure 4f) as well as the 50th percentile of the PRCF data (Figure 4g) tended to be the lowest in the CDCA mice, but these differences were not statistically significant. Taken together, these data suggest that CDCA increased lipid oxidation in expense of carbohydrate oxidation, especially during the dark phase of the day, independent of food intake.

DISCUSSION

In accordance with the previous studies using cholic acid in cHF-fed mice performed by the group of Auwerx,[10,15,20] we have demonstrated that supplementation of a cHF using BAs, namely CDCA, could reverse dietary obesity and associated metabolic disorders. Thus, in response to the 8-week intervention, a dose-dependent effect of CDCA was observed with respect to the reduction of obesity, amelioration of dyslipidaemia, normalization of glucose homeostasis and reduction of ectopic accumulation of lipids in the liver and skeletal muscle. No detrimental effects on hepatic markers were observed, and in accordance with the effect of cholic acid[15] used in several of the previous studies,[10,15,20] the CDCA intervention had no effect on lipid absorption.

Most of the above mentioned beneficial metabolic effects of CDCA could be related to a transient decrease in food consumption observed at the beginning of the intervention. This is not consistent with the outcomes of the previous studies in mice,[10,15,20] in which admixing of cholic acid to cHF was

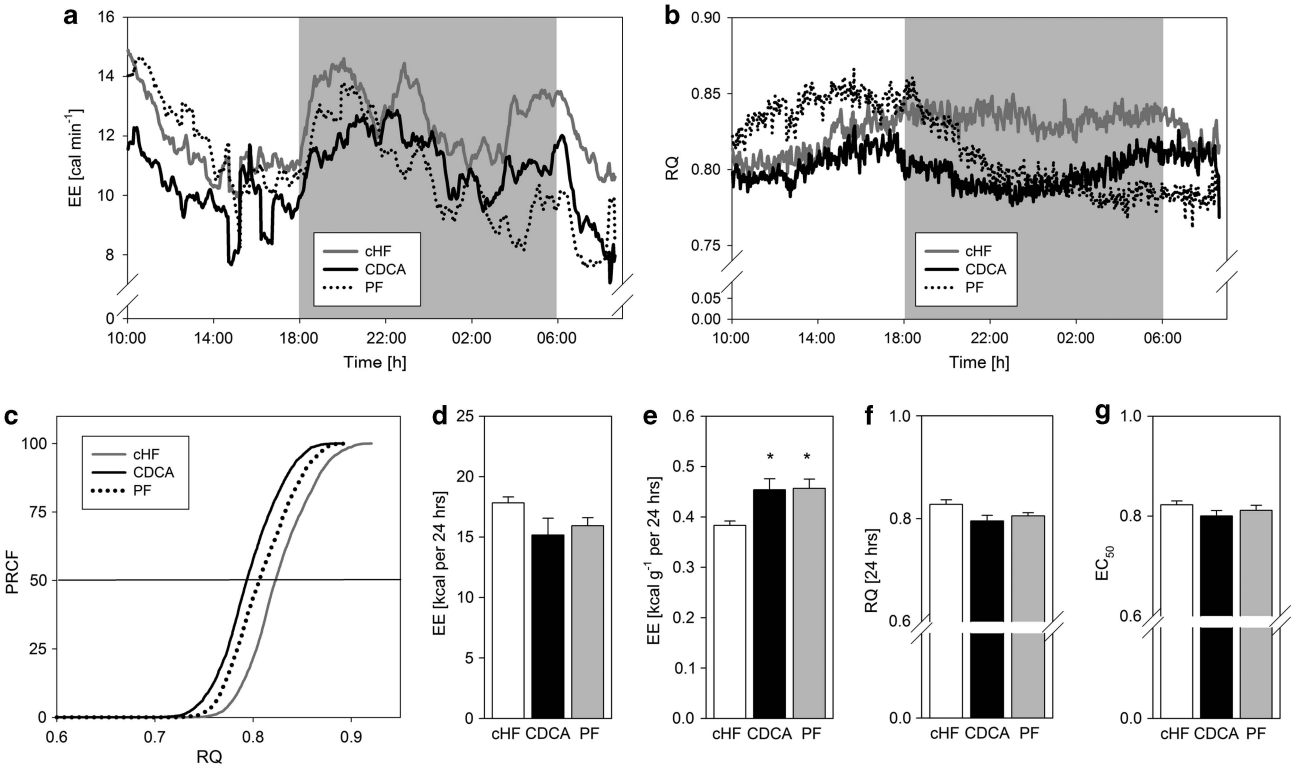

Figure 4. Indirect calorimetry performed between day 15 and day 17 of the 3-week reversion experiment. (**a**) Time course of the measurements of EE. (**b**) Time course of the RQ measurements; grey area in **a** and **b** represents the dark phase of the day. (**c**) Plot of PRCF of RQ values during the whole 24-h measurement period; each curve represents data pooled from all mice within a given group ($n = 7$–8; ~5 000 RQ measurements per curve). (**d**) Total EE per mouse (24 h). (**e**) Total EE per g BW (24 h). (**f**) Mean RQ (24 h). (**g**) 50th percentile value of PRCF (EC_{50}) derived from (**c**). *Significantly different in comparison to the cHF group. CDCA, high-fat diet supplemented with 1% CDCA; cHF, high-fat diet; PF, pair-fed group.

interpreted not to affect food consumption. However, in these previous studies, food intake was adjusted to BW of the animals (see Figure 1f in Watanabe *et al.*,[15] Figure 1a of Watanabe *et al.*,[20] Figure 1a of Watanabe *et al.*[10]), whereas in our study, food intake per mouse was considered. Therefore, in the previous studies, the decrease in absolute food intake could be masked when adjusted to BW, as BW was decreased in response to the cholic acid intervention. Owing to a relatively low specific metabolic rate of WAT, it is conceivable that non-adjusted (or lean body mass-adjusted) rather than total body mass-adjusted food intake should be considered when judging the impact of food intake on obesity.[40–42] However, neither lean body mass nor fat-free mass was evaluated in this study.

Therefore, in contrast with the previous studies, in which a potential effect of the decrease in food intake on obesity and associated disorders has been neglected,[10,15,20] we have attempted to dissect the roles of the decrease in food intake and the effect of CDCA *per se*, respectively, on obesity and energy metabolism by employing pair-feeding strategy. This approach revealed that the reduction of obesity could be mostly explained by the transient decrease in food intake during the initial phase of the intervention, whereas a relatively mild and food intake-independent reduction in adiposity (not detectable at the BW level) could also be observed.

The food intake-independent decrease in adiposity could result from the induction of UCP1-mediated thermogenesis, as suggested by upregulation of the *Ucp1* transcript and the increase in the total UCP1 protein in the interscapular BAT, as well as the upregulation of transcription of selected markers of mitochondrial biogenesis in BAT. This observation is in agreement with the previous study showing TGR5-mediated induction of the *Ucp1* transcript in response to cholic acid.[15] However, to our knowledge, our study demonstrates for the first time an elevation of UCP1 protein content in BAT in response to a BA. This is a critical observation, as UCP1 but not the UCP1 gene transcript is a relevant marker of the BAT thermogenic capacity.[28] The effect of the induction of UCP1-mediated thermogenesis of whole-body energy balance could be substantial for the stabilization of the lean phenotype in the long run, but it could not be detected using indirect calorimetry, reflecting the relatively low sensitivity of this technique and because lean BW data were not available in the present study (see above).

Concerning the inducible UCP1-mediated thermogenesis in brite cells located in WAT (see Introduction), our results document that brite cells could be induced in response to the CDCA intervention. However, in spite of a marked stimulation of the activity of the UCP1 gene at the transcript level observed in scWAT, the amount of UCP1 in the scWAT of the CDCA mice was very low as documented by both, undetectable UCP1 using western blots and a very small fraction of UCP1-positive adipocytes, as revealed using immunohistological analysis. Therefore, induction of UCP1 in interscapular BAT but not in brite cells interspersed in scWAT was probably involved in the induction of EE and lean phenotype in the CDCA mice. It remains to be established whether energy dissipation in other tissues, for example, TGR5-mediated thermogenesis in skeletal muscle,[15] could also be involved.

In spite of the induction of UCP1 in BAT as well the food intake-independent reduction in adiposity in the CDCA mice, indirect calorimetry could not reveal any difference in EE between the CDCA and PF mice, neither when EE per mice nor when EE adjusted to BW was considered. In accordance with the previous studies using cholic acid in cHF-fed mice,[15] also in our study, higher EE adjusted to BW was observed in the CDCA as compared with the cHF mice. However, this effect could be ascribed in full to the inappropriate normalization of EE to BW (see above, and Butler and Kozak[40]), as also documented by equal EE adjusted to BW in the CDCA and the PF mice. In accordance with the previous study using cholic acid,[15] a tendency to decrease RQ in response to the CDCA intervention was observed, which was independent on food intake, and suggested a shift from carbohydrate to lipid oxidation. Nevertheless, RQ changes during the day were affected by the shift in ingestion in the PF group.

Also, changes in gut microbiota can be possibly involved in the effects of CDCA on BAT, because some bacteria can convert CDCA to lithocholic acid, which is a more potent activator of TGR5 (reviewed in Greiner and Backhed [43]). However, this topic was out of the scope of this study.

In conclusion, our results document that CDCA could reduce obesity and associated metabolic disorders in the face of high lipid supply in mice and they suggest a major role of transient reduction in food intake in the anti-obesity effect. Moreover, our results indicate food intake-independent stimulation of UCP1-mediated thermogenesis in BAT in response to CDCA. Although the stimulation of EE in BAT was relatively low and could not be detected using indirect calorimetry, it could be important for the stabilization of the lean phenotype. In addition, the CDCA-induced increase in lipid catabolism could be beneficial with respect to reversal of obesity-associated metabolic disorders. Our results are consistent with the beneficial metabolic effects of BAs, which could be relevant in long-term treatments, but they also warn against overinterpretation of results of some of the previous studies using other BAs.

CONFLICT OF INTEREST

The authors declare no conflict of interest.

ACKNOWLEDGEMENTS

JST, FVD, APG and ATV were recipients of a Fundação para a Ciência e a Tecnologia PhD scholarship (SFRH/BD/38467/2007, SFRH/BD/38372/2007, SFRH/BD/44674/2008 and SFRH/BD/44796/2008, respectively). This project was supported by a FCT grant PTCD/SAU-OSM/72443/2006, PEst-C/SAU/LA0001/2011 and EU FP7 project DIABAT (HEALTH-F2—2011-278373) and by the Czech Science Foundation (13-00871S).

REFERENCES

1 Angelin B, Einarsson K, Hellstrom K, Leijd B. Effects of cholestyramine and chenodeoxycholic acid on the metabolism of endogenous triglyceride in hyperlipoproteinemia. *J Lipid Res* 1978; **19**: 1017–1024.
2 Teodoro JS, Rolo AP, Palmeira CM. Hepatic FXR: key regulator of whole-body energy metabolism. *Trends Endocrinol Metab* 2011; **22**: 458–466.
3 Watanabe M, Houten SM, Wang L, Moschetta A, Mangelsdorf DJ, Heyman RA *et al.* Bile acids lower triglyceride levels via a pathway involving FXR, SHP, and SREBP-1c. *J Clin Invest* 2004; **113**: 1408–1418.
4 Kast HR, Nguyen CM, Sinal CJ, Jones SA, Laffitte BA, Reue K *et al.* Farnesoid X-activated receptor induces apolipoprotein C-II transcription: a molecular mechanism linking plasma triglyceride levels to bile acids. *Mol Endocrinol* 2001; **15**: 1720–1728.
5 Sinal CJ, Tohkin M, Miyata M, Ward JM, Lambert G, Gonzalez FJ. Targeted disruption of the nuclear receptor FXR/BAR impairs bile acid and lipid homeostasis. *Cell* 2000; **102**: 731–744.
6 Stayrook KR, Bramlett KS, Savkur RS, Ficorilli J, Cook T, Christe ME *et al.* Regulation of carbohydrate metabolism by the farnesoid X receptor. *Endocrinology* 2005; **146**: 984–991.
7 Cariou B, van Harmelen K, Duran-Sandoval D, van Dijk TH, Grefhorst A, Abdelkarim M *et al.* The farnesoid X receptor modulates adiposity and peripheral insulin sensitivity in mice. *J Biol Chem* 2006; **281**: 11039–11049.
8 Duran-Sandoval D, Cariou B, Percevault F, Hennuyer N, Grefhorst A, van Dijk TH *et al.* The farnesoid X receptor modulates hepatic carbohydrate metabolism during the fasting-refeeding transition. *J Biol Chem* 2005; **280**: 29971–29979.
9 Abdelkarim M, Caron S, Duhem C, Prawitt J, Dumont J, Lucas A *et al.* The farnesoid X receptor regulates adipocyte differentiation and function by promoting peroxisome proliferator-activated receptor-gamma and interfering with the Wnt/beta-catenin pathways. *J Biol Chem* 2010; **285**: 36759–36767.
10 Watanabe M, Morimoto K, Houten SM, Kaneko-Iwasaki N, Sugizaki T, Horai Y *et al.* Bile acid binding resin improves metabolic control through the induction of energy expenditure. *PloS One* 2012; **7**: e38286.

11 Konikoff FM. Gallstones - approach to medical management. *MedGenMed* 2003; **5**: 8.
12 Prawitt J, Caron S, Staels B. Bile acid metabolism and the pathogenesis of type 2 diabetes. *Curr Diab Rep* 2011; **11**: 160–166.
13 Katona BW, Cummins CL, Ferguson AD, Li T, Schmidt DR, Mangelsdorf DJ *et al.* Synthesis, characterization, and receptor interaction profiles of enantiomeric bile acids. *J Med Chem* 2007; **50**: 6048–6058.
14 Neuschwander-Tetri BA. Farnesoid x receptor agonists: what they are and how they might be used in treating liver disease. *Curr Gastroenterol Rep* 2012; **14**: 55–62.
15 Watanabe M, Houten SM, Mataki C, Christoffolete MA, Kim BW, Sato H *et al.* Bile acids induce energy expenditure by promoting intracellular thyroid hormone activation. *Nature* 2006; **439**: 484–489.
16 Cannon B, Nedergaard J. Brown adipose tissue: function and physiological significance. *Physiol Rev* 2004; **84**: 277–359.
17 Wu J, Cohen P, Spiegelman BM. Adaptive thermogenesis in adipocytes: is beige the new brown? *Genes Dev* 2013; **27**: 234–250.
18 Rothwell NJ, Stock MJ. A role for brown adipose tissue in diet-induced thermogenesis. *Nature* 1979; **281**: 31–35.
19 da-Silva WS, Ribich S, Arrojo e Drigo R, Castillo M, Patti ME, Bianco AC. The chemical chaperones tauroursodeoxycholic and 4-phenylbutyric acid accelerate thyroid hormone activation and energy expenditure. *FEBS Lett* 2011; **585**: 539–544.
20 Watanabe M, Horai Y, Houten SM, Morimoto K, Sugizaki T, Arita E *et al.* Lowering bile acid pool size with a synthetic farnesoid X receptor (FXR) agonist induces obesity and diabetes through reduced energy expenditure. *J Biol Chem* 2011; **286**: 26913–26920.
21 Zingaretti MC, Crosta F, Vitali A, Guerrieri M, Frontini A, Cannon B *et al.* The presence of UCP1 demonstrates that metabolically active adipose tissue in the neck of adult humans truly represents brown adipose tissue. *FASEB J* 2009; **23**: 3113–3120.
22 Young P, Arch JR, Ashwell M. Brown adipose tissue in the parametrial fat pad of the mouse. *FEBS Lett* 1984; **167**: 10–14.
23 Loncar D. Convertible adipose tissue in mice. *Cell Tissue Res* 1991; **266**: 149–161.
24 Cousin B, Cinti S, Morroni M, Raimbault S, Ricquier D, Penicaud L *et al.* Occurrence of brown adipocytes in rat white adipose tissue: molecular and morphological characterization. *J Cell Sci* 1992; **103**: 931–942.
25 Petrovic N, Walden TB, Shabalina IG, Timmons JA, Cannon B, Nedergaard J. Chronic peroxisome proliferator-activated receptor gamma (PPARgamma) activation of epididymally derived white adipocyte cultures reveals a population of thermogenically competent, UCP1-containing adipocytes molecularly distinct from classic brown adipocytes. *J Biol Chem* 2010; **285**: 7153–7164.
26 Frontini A, Vitali A, Perugini J, Murano I, Romiti C, Ricquier D *et al.* White-to-brown transdifferentiation of omental adipocytes in patients affected by pheochromocytoma. *Biochim Biophys Acta* 2013; **1831**: 950–959.
27 Jespersen NZ, Larsen TJ, Peijs L, Daugaard S, Homoe P, Loft A *et al.* A classical brown adipose tissue mRNA signature partly overlaps with brite in the supraclavicular region of adult humans. *Cell Metab* 2013; **17**: 798–805.
28 Nedergaard J, Cannon B. UCP1 mRNA does not produce heat. *Biochim Biophys Acta* 2013; **1831**: 943–949.
29 Kuda O, Jelenik T, Jilkova Z, Flachs P, Rossmeisl M, Hensler M *et al.* n-3 fatty acids and rosiglitazone improve insulin sensitivity through additive stimulatory effects on muscle glycogen synthesis in mice fed a high-fat diet. *Diabetologia* 2009; **52**: 941–951.
30 Medrikova D, Jilkova ZM, Bardova K, Janovska P, Rossmeisl M, Kopecky J. Sex differences during the course of diet-induced obesity in mice: adipose tissue expandability and glycemic control. *Int J Obes* 2012; **36**: 262–272.
31 Rossmeisl M, Jelenik T, Jilkova Z, Slamova K, Kus V, Hensler M *et al.* Prevention and reversal of obesity and glucose intolerance in mice by DHA derivatives. *Obesity* 2009; **17**: 1023–1031.
32 Salmon DM, Flatt JP. Effect of dietary fat content on the incidence of obesity among ad libitum fed mice. *Int J Obes* 1985; **9**: 443–449.
33 Kopecky J, Rossmeisl M, Hodny Z, Syrovy I, Horakova M, Kolarova P. Reduction of dietary obesity in aP2-Ucp transgenic mice: mechanism and adipose tissue morphology. *Am J Physiol* 1996; **270**: E776–E786.
34 Smith PK, Krohn RI, Hermanson GT, Mallia AK, Gartner FH, Provenzano MD *et al.* Measurement of protein using bicinchoninic acid. *Anal Biochem* 1985; **150**: 76–85.
35 Kus V, Prazak T, Brauner P, Hensler M, Kuda O, Flachs P *et al.* Induction of muscle thermogenesis by high-fat diet in mice: association with obesity-resistance. *Am J Physiol Endocrinol Metab* 2008; **295**: E356–E367.
36 Flachs P, Ruhl R, Hensler M, Janovska P, Zouhar P, Kus V *et al.* Synergistic induction of lipid catabolism and anti-inflammatory lipids in white fat of dietary obese mice in response to calorie restriction and n-3 fatty acids. *Diabetologia* 2011; **54**: 2626–2638.
37 Weir JB. New methods for calculating metabolic rate with special reference to protein metabolism. *J Physiol* 1949; **109**: 1–9.
38 Even PC, Nadkarni NA. Indirect calorimetry in laboratory mice and rats: principles, practical considerations, interpretation and perspectives. *Am J Physiol Regul Integr Comp Physiol* 2012; **303**: R459–R476.
39 Seale P, Conroe HM, Estall J, Kajimura S, Frontini A, Ishibashi J *et al.* Prdm16 determines the thermogenic program of subcutaneous white adipose tissue in mice. *J Clin Invest* 2011; **121**: 96–105.
40 Butler AA, Kozak LP. A recurring problem with the analysis of energy expenditure in genetic models expressing lean and obese phenotypes. *Diabetes* 2010; **59**: 323–329.
41 Himms-Hagen J. On raising energy expenditure in ob/ob mice. *Science* 1997; **276**: 1132–1133.
42 Kaiyala KJ, Schwartz MW. Toward a more complete (and less controversial) understanding of energy expenditure and its role in obesity pathogenesis. *Diabetes* 2011; **60**: 17–23.
43 Greiner T, Backhed F. Effects of the gut microbiota on obesity and glucose homeostasis. *Trends Endocrinol Metab* 2011; **22**: 117–123.

Supplementary Information accompanies this paper on International Journal of Obesity website (http://www.nature.com/ijo)

Publication B

Diabetologia (2011) 54:2626–2638
DOI 10.1007/s00125-011-2233-2

ARTICLE

Synergistic induction of lipid catabolism and anti-inflammatory lipids in white fat of dietary obese mice in response to calorie restriction and *n*-3 fatty acids

P. Flachs · R. Rühl · M. Hensler · P. Janovska · P. Zouhar · V. Kus · Z. Macek Jilkova · E. Papp · O. Kuda · M. Svobodova · M. Rossmeisl · G. Tsenov · V. Mohamed-Ali · J. Kopecky

Received: 10 January 2011 / Accepted: 31 May 2011 / Published online: 21 July 2011

Abstract
Aims/hypothesis Calorie restriction is an essential component in the treatment of obesity and associated diseases. Long-chain *n*-3 polyunsaturated fatty acids (LC *n*-3 PUFA) act as natural hypolipidaemics, reduce the risk of cardiovascular disease and could prevent the development of obesity and insulin resistance. We aimed to characterise the effectiveness and underlying mechanisms of the combination treatment with LC *n*-3 PUFA and 10% calorie restriction in the prevention of obesity and associated disorders in mice.
Methods Male mice (C57BL/6J) were habituated to a corn-oil-based high-fat diet (cHF) for 2 weeks and then randomly assigned to various dietary treatments for 5 weeks or 15 weeks: (1) cHF, ad libitum; (2) cHF with LC *n*-3 PUFA concentrate replacing 15% (wt/wt) of dietary lipids (cHF+F), ad libitum; (3) cHF with calorie restriction (CR; cHF+CR); and (4) cHF+F+CR. Mice fed a chow diet were also studied.
Results We show that white adipose tissue plays an active role in the amelioration of obesity and the improvement of glucose homeostasis by combining LC *n*-3 PUFA intake and calorie restriction in cHF-fed mice. Specifically in the epididymal fat in the abdomen, but not in other fat depots, synergistic induction of mitochondrial oxidative capacity and lipid catabolism was observed, resulting in increased oxidation of metabolic fuels in the absence of mitochondrial uncoupling, while low-grade inflammation was suppressed, reflecting changes in tissue levels of anti-inflammatory lipid mediators, namely 15-deoxy-$\Delta^{12,15}$-prostaglandin J_2 and protectin D1.
Conclusions/interpretation White adipose tissue metabolism linked to its inflammatory status in obesity could be modulated by combination treatment using calorie restriction and dietary LC *n*-3 PUFA to improve therapeutic strategies for metabolic syndrome.

Keywords 15-Deoxy-$\Delta^{12,15}$-prostaglandin J_2 · DHA · EPA · Fish oil · Metabolic syndrome · White adipose tissue

Electronic supplementary material The online version of this article (doi:10.1007/s00125-011-2233-2) contains peer-reviewed but unedited supplementary material, which is available to authorised users.

P. Flachs · M. Hensler · P. Janovska · P. Zouhar · V. Kus · Z. Macek Jilkova · O. Kuda · M. Svobodova · M. Rossmeisl · J. Kopecky (✉)
Department of Adipose Tissue Biology, Institute of Physiology Academy of Sciences of the Czech Republic v.v.i.,
Videnska 1083,
14220 Prague, Czech Republic
e-mail: kopecky@biomed.cas.cz

R. Rühl · E. Papp
Department of Biochemistry and Molecular Biology,
Laboratory of Nutritional Bioactivation and Bioanalysis,
University of Debrecen,
Debrecen, Hungary

R. Rühl · E. Papp
Apoptosis and Genomics Research Group of the Hungarian Academy of Science,
Debrecen, Hungary

G. Tsenov
Department of Developmental Epileptology, Institute of Physiology, Academy of Sciences of the Czech Republic v.v.i.,
Prague, Czech Republic

V. Mohamed-Ali
Adipokines and Metabolism Research Group,
University College London,
London, UK

Abbreviations

15d-PGJ$_2$	15-Deoxy-$\Delta^{12,15}$-prostaglandin J$_2$
AA	Arachidonic acid
AMPK	AMP-activated protein kinase
cHF	Corn-oil-based high fat diet
cHF+F	cHF diet supplemented with LC *n*-3 PUFA concentrate (15% [wt/wt] of dietary lipids)
CLS	Crown-like structure
COX	Cyclooxygenase
CyOX	Cytochrome *c* oxidase
DHA	Docosahexaenoic acid
EPA	Eicosapentaenoic acid
FA	Fatty acid
FASTED	Fasted state, specifically defined
FCCP	Carbonyl cyanide-*p*-trifluoromethoxyphenylhydrazone
LC *n*-3	Long-chain *n*-3
LOX	Lipoxygenase
NF-κB	Nuclear factor κ light-chain enhancer of activated B cells
MAC-2	β-Galactoside-binding lectin
PD1	Protectin D1
PGC-1α	PPARγ coactivator 1α
PLS-DA	Partial least squares-discriminant analysis
PPARγ	Peroxisome proliferator-activated receptor γ
PUFA	Polyunsaturated fatty acids
RE-FED	Re-fed state, specifically defined
SIRT1	Sirtuin 1 (silent mating type information regulation 2, homologue) 1
TG	Triacylglycerol
UCP1	Uncoupling protein 1
WAT	White adipose tissue

Introduction

Intrinsic metabolic properties and secretory functions of white adipose tissue (WAT) have a major impact on the development of chronic morbidities associated with obesity, including type 2 diabetes, dyslipidaemia and hypertension. When (post)prandial plasma levels of NEFA and triacylglycerol (TG) exceed the storage capacity of WAT [1], other tissues including the liver and muscle become overloaded with lipids, which results in insulin resistance, the key event in the pathophysiology of metabolic syndrome [2]. The important role of WAT in energy homeostasis is underscored by the findings that WAT is one of the key organs affected by calorie restriction, the most effective strategy to prolong a healthy life in several species [3], and by the fact that accumulation of body fat can be reduced through upregulation of lipid catabolism in WAT [4–10]. The metabolism and secretory functions of WAT are also modulated by long-chain (LC) *n*-3 polyunsaturated fatty acids (PUFA), namely eicosapentaenoic acid (EPA; 20:5 *n*-3) and docosahexaenoic acid (DHA; 22:6 *n*-3), which exert numerous beneficial effects on health, including improvements in lipid metabolism and prevention of obesity and diabetes [11], while decreasing the rate of fatal coronary heart disease in diabetic patients who have had a myocardial infarction [12]. The metabolic changes induced by both calorie restriction and LC *n*-3 PUFA include induction of mitochondrial biogenesis and lipid catabolism in WAT [3, 13].

Importantly, LC *n*-3 PUFA also decrease inflammation [14], including obesity-associated low-grade inflammation of WAT [15, 16], characterised by altered secretion patterns of adipokines, which contributes to insulin resistance [1]. The anti-inflammatory effects of LC *n*-3 PUFA probably depend on the formation of their active metabolites. These lipid mediators originate from either targeted enzymatic synthesis, such as resolvins and protectins [17, 18], or from non-enzymatic oxidation reactions [19, 20]. They can act as ligands for surface receptors or can interact with signalling proteins including the transcription factors peroxisome proliferator-activated receptor γ (PPARγ) and nuclear factor κ light-chain enhancer of activated B cells (NF-κB) [19]. Notably, resolvins and protectins mediate the anti-inflammatory and protective actions of LC *n*-3 PUFA in obesity-induced insulin resistance and hepatic steatosis [17, 21]. As LC *n*-3 PUFA and LC *n*-6 PUFA compete for common enzymatic pathways, a relatively small increase in the LC *n*-3 PUFA intake usually slows down synthesis of pro-inflammatory metabolites derived from arachidonic acid (AA; 20:4 *n*-6) [17, 18]. Given the complexity of factors contributing to the development of metabolic syndrome, its prevention and treatment requires strategies combining several approaches. Clinical studies suggest [22–24] that combining calorie restriction and LC *n*-3 PUFA intake may be helpful. As both treatments could promote fatty acid (FA) oxidation in WAT (see above), we have endeavoured in this study to establish whether lipid catabolism in WAT could be augmented by calorie restriction combined with LC *n*-3 PUFA intake. Our results in dietary obese mice show additive effects of calorie restriction and LC *n*-3 PUFA in the induction of mitochondrial biogenesis and lipid catabolism, occurring with a surprising specificity in intra-abdominal WAT, which could contribute to the beneficial systemic effects of the combination treatment. The tissue-specificity could be explained by formation of anti-inflammatory lipid mediators derived from both LC *n*-3 and LC *n*-6 PUFA.

Methods

Animal treatment Male mice (C57BL/6J; Jackson Laboratory, ME, USA) were weaned onto standard laboratory chow (Chow; extruded R/M-H diet; Ssniff Spezialdiäten, Soest, Germany). Singly caged mice were habituated to a corn-oil-based high-fat diet (cHF; lipid content 35%, wt/wt; [16]) for 2 weeks starting at 2 months of age and then randomly assigned for 5 weeks (four independent experiments) or 15 weeks (one experiment) to various dietary treatments (see electronic supplementary material [ESM] Fig. 1): (1) cHF, ad libitum; (2) cHF supplemented with LC *n*-3 PUFA concentrate (46% wt/wt DHA, 14% wt/wt EPA; product EPAX 1050 TG; EPAX, Alesund, Norway) replacing 15% wt/wt of dietary lipids (cHF+F), ad libitum; (3) cHF with restriction of energy intake—the ration was reduced by 10% wt/wt compared with mice fed ad libitum with the same type of diet (CR; cHF+CR); and (4) cHF+F+CR. When indicated, plasma was collected by using tail bleeds during the FASTED to RE-FED transition (for the detailed definition of FASTED and RE-FED state, see ESM). An OGTT was performed in overnight-fasted mice as in Kuda et al. [16], except that glucose was administered by oral gavage. At the end of the treatment, mice were killed in a random fed state (between 08:00 hours and 10:00 hours).

Experiments were conducted according to the guidelines for the use and care of laboratory animals of the Institute of Physiology.

Tissue lipid content The tissue content of TG was estimated in ethanolic KOH tissue solubilisates [25].

Energy expenditure and metabolic flexibility Energy expenditure and fuel partitioning were evaluated using the indirect calorimetry system INCA (Somedic, Horby, Sweden) at 30°C [26]. Metabolic flexibility was assessed as a maximal induction in RQ ($\dot{V}CO_2/\dot{V}O_2$) values in response to a glucose load (0.45 ml of 50% [wt/vol.] D-glucose) administered by intragastric gavage to overnight (12 h) fasted animals. The induction was calculated from RQ values averaged over 60 min intervals before and after the gavage (ESM Fig. 2).

Physical activity Animal behaviour was recorded by video camera and analysed off-line (see ESM).

Plasma variables Levels of glucose, NEFA, TG, leptin, total adiponectin, IL-6, β-hydroxybutyrate and insulin were determined in plasma [16, 27].

Gene expression Transcript levels were evaluated using quantitative real-time RT-PCR (see ESM).

Ex vivo biochemical analysis FA oxidation was measured using [1-^{14}C]palmitate in fragments of epididymal fat or gastrocnemius muscle or whole soleus muscle [28], in isolated adipocytes [29], and in hepatocytes isolated from mice following the in vivo treatment [30]. The rate of FA synthesis in epididymal fat was measured by incorporation of ^3H_2O into saponifiable FAs [9]. Mitochondrial respiration was evaluated using high-resolution respirometry in digitonin-permeabilised adipocytes [29] using OROBOROS Oxygraph-2k (Oroboros Instruments, Innsbruck, Austria; see Fig. 4c,d legend).

Activity of cytochrome c oxidase and cytochrome b and protein content Crude membrane fraction was used to evaluate activity of cytochrome *c* oxidase (CyOX) spectrophotometrically [10] and to quantify cytochrome *b* using a pseudo-dual-wavelength spectrophotometry [29].

Immunohistochemical analysis Morphometry of adipocytes was performed (5 μm sections) using Lucia IMAGE software (Laboratory Imaging, Prague, Czech Republic). In the case of epididymal fat, sections were processed to detect β-galactoside-binding lectin (MAC-2) and perilipin [16].

Lipidomic analysis In total, 24 lipid molecular species were quantified in epididymal fat and liver extracts using HPLC MS-MS analysis [31] (see ESM).

Statistical analysis All values are presented as means±SEM. Comparisons were judged to be significant at $p \leq 0.05$ (see ESM).

Results

Combination treatment counteracts development of obesity and accumulation of ectopic fat Feeding mice a cHF diet increased their body weight (Fig. 1a). Either cHF+F or cHF+CR treatment partially prevented the cHF-induced obesity, while the combination treatment (cHF+F+CR) provided full protection, as shown by the treatments lasting either 5 weeks (Fig. 1a and Table 1) or 15 weeks (see legend to Fig. 1). As already described [13, 30], food consumption was not affected by dietary LC *n*-3 PUFA (Table 1). Physical activity, evaluated after 3 weeks of the treatment (ESM Fig. 1) as total distance travelled and total duration of moving per 4 h, was similar in the cHF, cHF+F and cHF+CR mice, while it was lower in the cHF+F+CR mice (Table 1). Prevention of dietary obesity by various treatments correlated with reduction of both adiposity and fat cell size in all fat depots analysed at

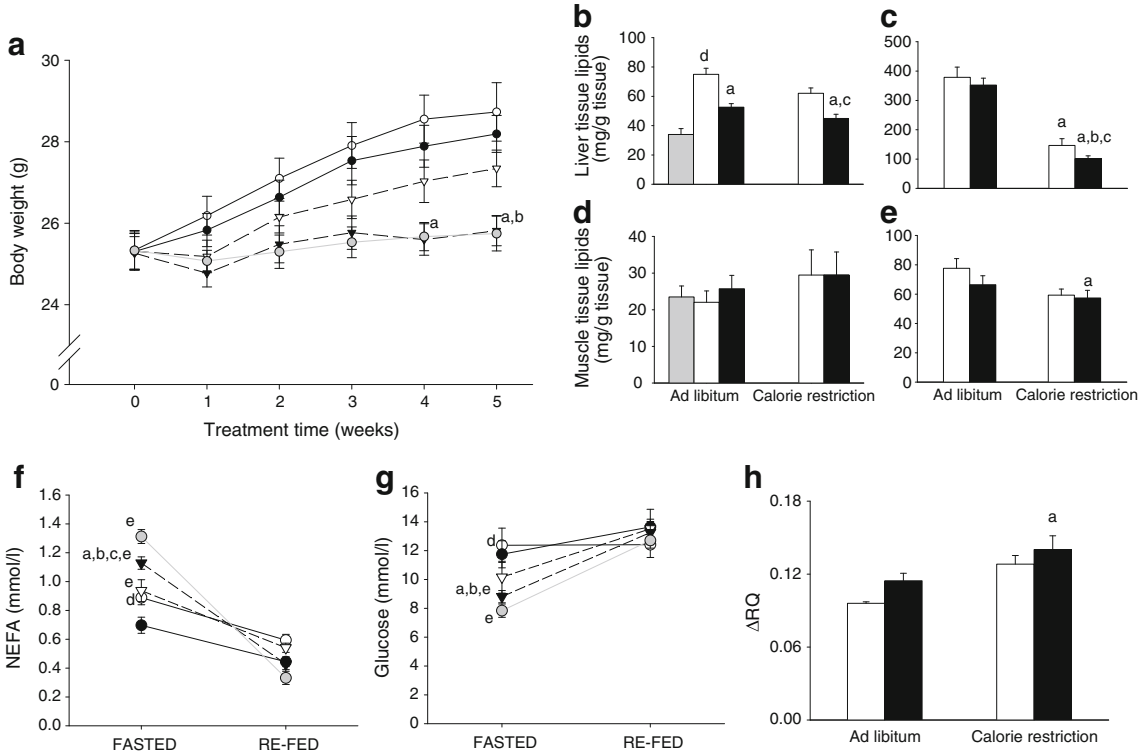

Fig. 1 Prevention of diet-induced obesity, hepatic steatosis, and metabolic inflexibility. **a** Body weight of mice; week 0, start of the differential dietary treatment. Results from a typical experiment (n=10; see also Table 1). White circles, cHF; black circles, cHF+F; white triangles, cHF+CR; black triangles, cHF+F+CR; grey circles, Chow. Five independent short-term (5 weeks) and one long-term (15 weeks) experiments were performed with similar results (not shown). After 15 weeks, body weights in mice fed different diets were as followed: cHF, 42.7±1.2 g; cHF+F, 36.8±1.9 g; cHF+CR, 34.7±2.5 g; cHF+F+CR, 33.1±0.8 g; $p<0.05$ vs cHF for all the treatments. **b–e** Ectopic lipid accumulation in liver (**b**, **c**) and gastrocnemius muscle (**d**, **e**) after 5 weeks (**b**, **d**) or 15 weeks (**c**, **e**) of the treatment; n=10. Data for the Chow-fed mice are shown only for week 5, but similar values at week 15 should be expected [16]. NEFA (**f**) and (**g**) glucose levels in plasma after 4 weeks of the treatment, measured in either the FASTED or RE-FED state (see ESM; n=10). White circles, cHF; black circles, cHF+F; white triangles, cHF+CR; black triangles, cHF+F+CR; grey circles, Chow. **h** During the fourth week of the treatment, metabolic flexibility was assessed as a maximal induction in RQ values in response to a glucose load administered by intragastric gavage to animals fasted overnight (12 h) (n=9–10). White bars, cHF or cHF+CR diet; black bars, cHF+F or cHF+F+CR. Data from an independent experiment using the Chow-fed mice showed ΔRQ=0.15±0.01 (n=9). For details, see ESM Fig. 2 and ESM Table 1. Data are means±SEM. [a,b,c]Significant difference (ANOVA) compared with cHF, cHF+F, and cHF+CR, respectively; [d]significant difference (t test) compared with Chow-fed mice [e]significant difference (repeated-measures ANOVA) between the FASTED and RE-FED states

5 weeks (Table 1). Significant differences in both variables were observed between the cHF mice and the cHF+F+CR mice, with the strongest effects elicited in the epididymal fat (Table 1). Feeding of the cHF diet induced accumulation of lipids in the liver and skeletal muscle. In the liver, all the treatments decreased TG accumulation and the effect of LC n-3 PUFA was stronger at 5 weeks (Fig. 1b) than at 15 weeks (Fig. 1c). In response to the longer treatment, the maximal reduction of TG accumulation in skeletal muscle was observed in the case of cHF+F+CR mice (Fig. 1e).

Combination treatment improves lipid and glucose homeostasis and preserves metabolic flexibility After 5 weeks of the treatment and in the ad libitum fed state, plasma TG levels were strongly reduced through either LC n-3 PUFA or calorie restriction alone, and even more with the combination treatment (Table 1). This hypolipidaemic effect was negatively correlated with the effect of the treatments on plasma β-hydroxybutyrate, the marker of lipid catabolism. Glucose levels in plasma were similar in all the groups; however, insulin levels were decreased by cHF+CR treatment and even more by the cHF+F+CR treatment (Table 1). In this respect, cHF+F exerted a smaller but still significant effect. In the fasted state (Fig. 1g), the plasma concentration of glucose was lowered in response to calorie restriction, independent of dietary LC n-3 PUFA, with a trend for the lowest value in the cHF+F+CR mice. Levels of adiponectin were increased by cHF+F to a similar extent in mice with free access to food and in the mice with restricted energy intake (Table 1), also in agreement with our previous findings [27]. As expected from the effects of treatments on adiposity, leptin levels tended to be reduced by cHF+F and were significantly lowered by calorie

Table 1 Body weight gain, food consumption, physical activity, organ weights, size of adipocytes and plasma variables in mice

Variable	cHF	cHF+F	cHF+CR	cHF+F+CR
Body weight gain (g)	3.7±0.5	2.9±0.6	2.1±0.3[a]	0.8±0.2[a,b,c]
Food consumption (kJ/day per animal)	74.6±0.6	73.7±1.8	67.1±0.5[a,b]	66.3±1.6[a,b]
Physical activity				
Total distance moved (m)	236±22	231±65	200±19	152±19[a]
Moving time (s)	3668±432	3424±775	2974±359	2204±362[a]
Epididymal fat				
Weight (mg)	624±74	566±90	408±58	262±26[a,b]
Adipocyte area (μm^2)	2395±147	1920±160	1851±300	1690±152[a]
Mesenteric fat				
Weight (mg)	298±31	277±19	268±22	205±16[a,b]
Adipocyte area (μm^2)	1217±84	1136±136	1315±153	997±108[a,c]
Subcutaneous fat				
Weight (mg)	284±26	269±21	233±20	208±10[a]
Adipocyte area (μm^2)	1356±60	1055±69[a]	1188±2	1069±124[a]
Interscapular brown fat				
Weight (mg)	173±10	121±5[a]	119±4.8[a]	76±5[a,b,c]
Liver				
Weight (mg)	1148±59	1233±18	1134±26	1009±36[b]
Plasma				
TG (mmol/l)	1.24±0.11	0.62±0.06[a]	0.65±0.06[a]	0.35±0.05[a,b,c]
β-Hydroxybutyrate (mmol/l)	0.09±0.01	0.13±0.02[a]	0.20±0.01[a,b]	0.28±0.02[a,b,c]
Glucose (mmol/l)	17.2±0.5	17.0±0.4	17.4±0.5	15.5±0.8
Insulin (pmol/l)	300±35	219±37[a]	57±5[a,b]	35±9[a,b,c]
Adiponectin (μg/ml)	8.9±0.3	12.1±0.5[a]	9.3±0.2[b]	11.1±0.5[a,c]
Leptin (ng/ml)	77.2±7.6	66.2±8.3[a]	15.5±1.7[a,b]	5.3±0.7[a,b,c]

All the variables were evaluated after 5 weeks of the treatment, except for physical activity, which was evaluated during week 4 and is represented by the total distance moved and moving time during both time intervals of the measurement (2 h during light phase and 2 h during dark phase, see Methods). In the case of WAT, subcutaneous dorsolumbar, epididymal and mesenteric depots were collected. Tissue dissection and plasma collection were performed in random-fed state (between 08:00 hours and 10:00 hours)

Data are means±SEM; n=10

[a,b,c] Significant differences (ANOVA) compared with cHF, cHF+F, and cHF+CR, respectively

restriction, with the cHF+F+CR mice showing the lowest leptin levels (Table 1).

To characterise whole-body metabolic flexibility, which is associated with insulin sensitivity [2, 32], the metabolic response to the FASTED/RE-FED transition was also analysed by assessing plasma levels of NEFA and glucose after 4 weeks of the treatment (Fig. 1f,g and ESM Fig. 1). Only in the FASTED, and not in the RE-FED state, did the metabolite levels differ between groups. Among the mice fed cHF-based diets, the cHF+F+CR mice showed the highest NEFA and the lowest glucose levels, while exhibiting the largest differences in plasma levels of both metabolites in response to the re-feeding. In fact, the cHF+F+CR treatment normalised the metabolic response when compared with the Chow-fed mice (Fig. 1f,g). In contrast, the cHF mice showed the lowest NEFA and the highest glucose levels in fasted state, with a minimum response to the FASTED/RE-FED transition observed with both metabolites (Fig. 1f,g). Indirect calorimetry was performed after 3 weeks of the treatment (ESM Figs 1 and 2) to characterise metabolic flexibility, as well as whole-body capacity to use carbohydrate and lipid fuels (Fig. 1h). When metabolic flexibility was expressed as maximal induction of RQ in response to the intragastric gavage of glucose, the combination treatment preserved metabolic flexibility better than any of the treatments applied separately. No effect of any of the treatments on energy expenditure, assessed as oxygen consumption ($\dot{V}O_2$)/animal, was observed either before or after the glucose gavage (ESM Fig. 2 and ESM Table 1).

To further characterise changes in glucose homeostasis, fasted plasma was analysed (Fig. 2a,b) and an OGTT was performed (Fig. 2c and ESM Fig. 3) after 3–4 weeks of treatment (ESM Fig. 1). Compared with cHF diet, only the combination treatment significantly decreased fasted insulinaemia and HOMA index (Fig. 2a,b). Specifically in mice subjected to calorie restriction, glucose levels were increased in response to overnight fasting, which preceded the glucose tolerance test (ESM Fig. 3). Feeding cHF diet resulted in glucose intolerance (Fig. 2c), while the deterioration of glucose homeostasis was prevented by the combination treatment with the other treatments tending to exert similar effects. In addition, insulin levels estimated in plasma during the test, 30 min after the glucose gavage, revealed the protective effect of the combination treatment (220±51, 296±37, and 253±41 pmol insulin/l in the Chow-fed, cHF and cHF+F+CR mice, respectively). Ex vivo analysis of insulin-stimulated de novo FA synthesis in

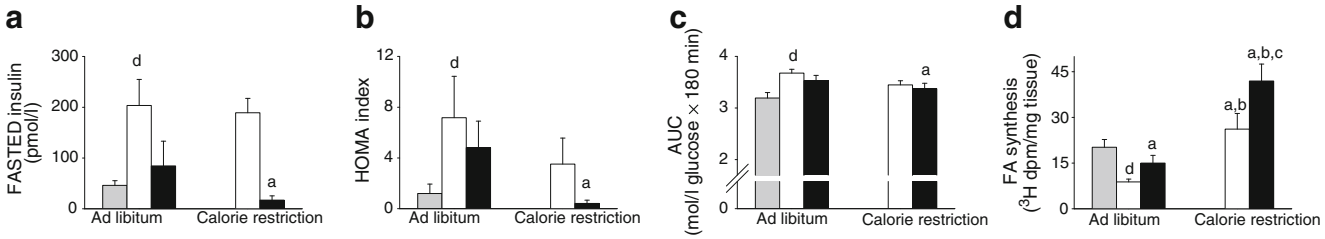

Fig. 2 Improvement of glucose homeostasis. **a** Insulin levels in plasma and **b** HOMA index of insulin resistance after 4 weeks of the treatment, calculated (see ESM) from the insulin levels (see **a**) and glycaemia measured in the fasted state (see Fig. 1g); **c** OGTT after 3 weeks of treatment (0.5 ml 30% [wt/vol.] D-glucose in water; see ESM Fig. 3). The results are expressed as AUC values; **d** ex vivo analysis of de novo FA synthesis in epididymal fat after 5 weeks of the treatment, measured in the presence of insulin (80 μU/ml) and expressed as dpm ^{3}H incorporated to saponifiable FAs/mg tissue. White bars, cHF or cHF+CR; black bars, cHF+F or cHF+F+CR; grey bars, Chow. Data are means±SEM. [a,b,c]Significant difference (ANOVA) compared with cHF, cHF+F, and cHF+CR, respectively; [d]significant difference (*t* test) compared with Chow-fed mice

epididymal fat after 5 weeks of treatment showed an increased rate of FA synthesis due to either LC *n*-3 PUFA or calorie restriction alone, and a synergistic induction in response to the combination treatment (Fig. 2d).

Synergistic induction of genes of mitochondrial biogenesis and lipid catabolism in epididymal fat Based on the previous results showing induction of mitochondria and lipid catabolism by LC *n*-3 PUFA [13] and calorie restriction [3], we investigated gene expression in WAT, interscapular brown fat, liver and muscle (Fig. 3a–e). In epididymal WAT (Fig. 3a), the analysis revealed a strong induction of PPARγ co-activator 1α (*Pgc-1α* [also known as *Ppargc1a*]), peroxisome proliferator-activated receptor α

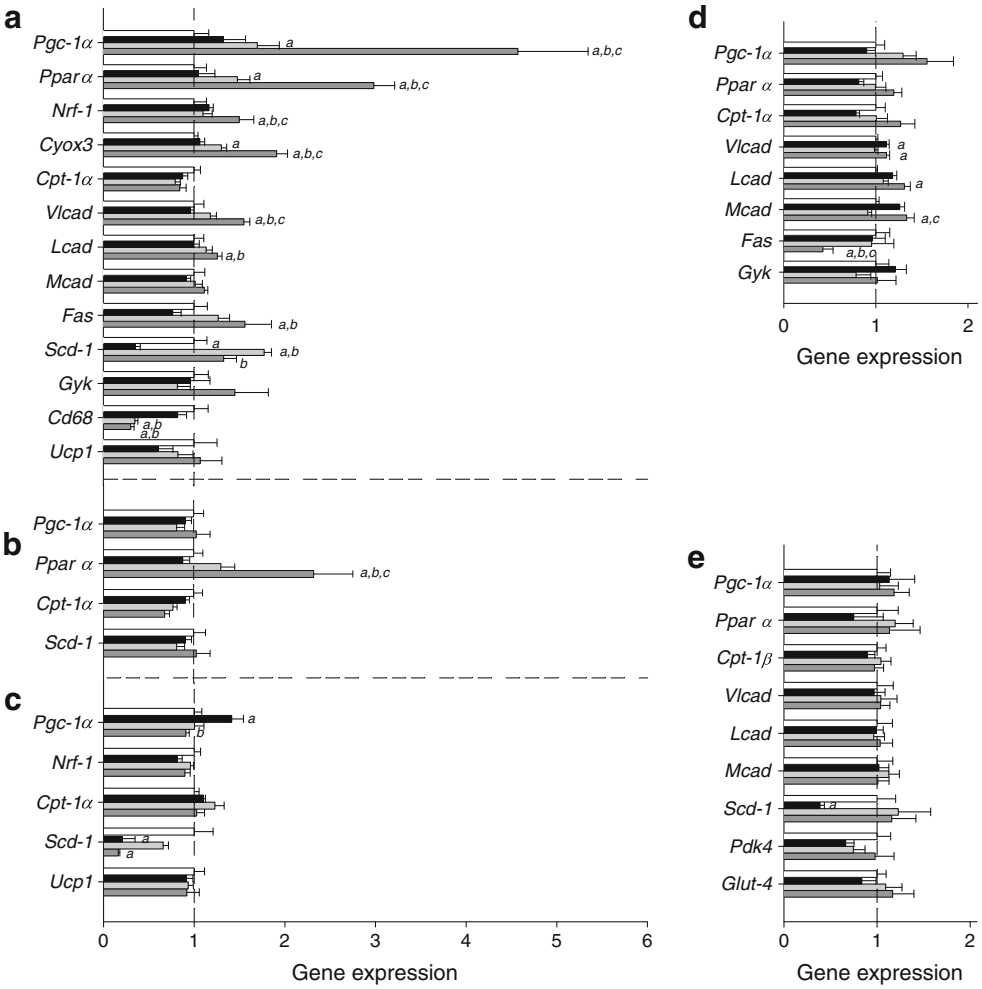

Fig. 3 Specific induction of mitochondrial genes in epididymal fat. Quantitative real-time RT-PCR data showing relative levels of gene expression (cHF=1) in epididymal (**a**) and subcutaneous (**b**) WAT, interscapular brown fat (**c**), liver (**d**), and gastrocnemius muscle (**e**) after 5 weeks of the treatment. Data are means±SEM; $n=10$; white bars, cHF; black bars, cHF+F; light grey bars, cHF+CR; dark grey bars, cHF+F+CR; [a,b,c]Significant difference (ANOVA) compared with cHF, cHF+F and cHF+CR, respectively. An independent experiment showed no difference in either *Pgc-1α* or *Pparα* expression in epididymal fat between the cHF and the Chow-fed mice (the cHF/Chow ratio of the *Pgc-1α* and *Pparα* transcript levels was 1.08±0.05 and 1.04±0.08, respectively; $n=6$). All analyses were performed after 5 weeks of treatment

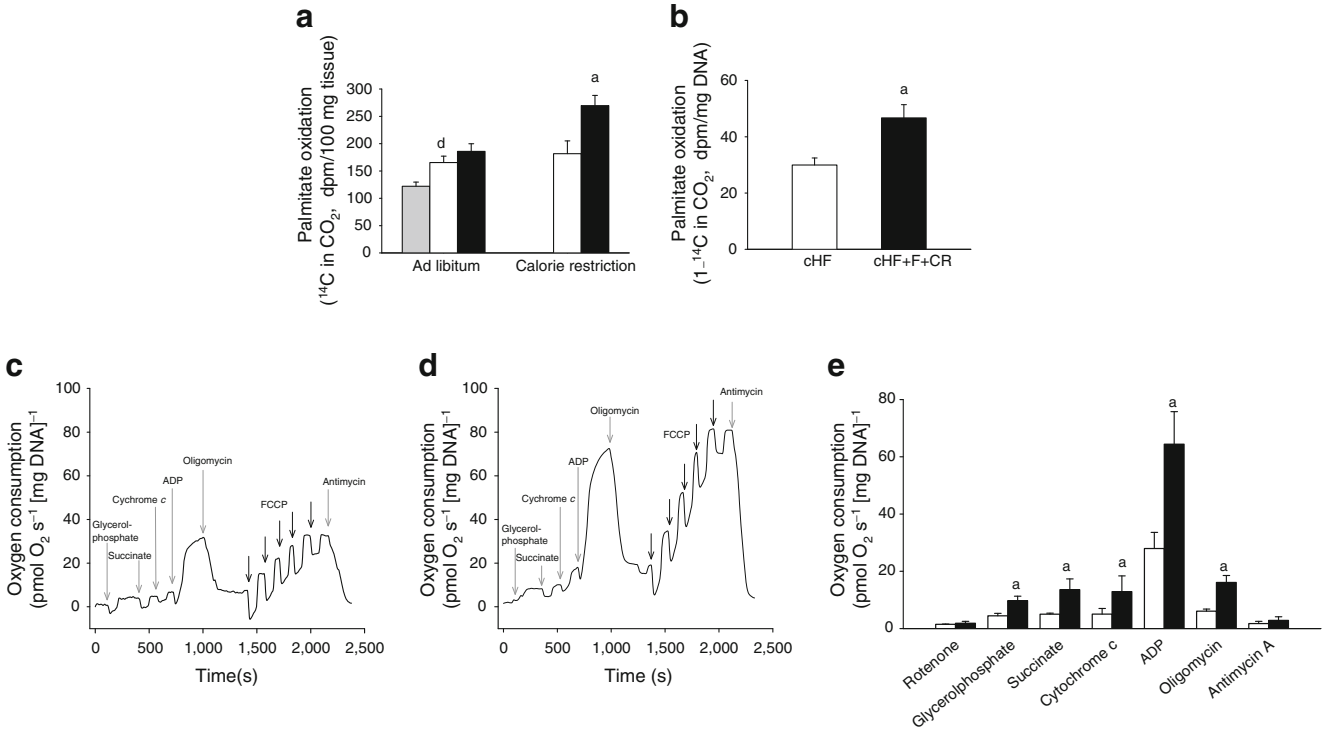

Fig. 4 Induction of fatty acid oxidation and mitochondrial oxidative capacity in epididymal fat. **a** Oxidation of [1- ^{14}C]palmitate into CO_2 by tissue fragments. Data are means±SEM; n= 10. White bars, cHF or cHF+CR; black bars, cHF+F or cHF+F+CR; grey bars, Chow. [a]Significant difference (ANOVA) compared with cHF; [d]significant difference (t test) compared with Chow-fed mice. **b** Oxidation of [1-^{14}C]palmitate into CO_2 by freshly isolated adipocytes. Data are means±SEM; n= 8. [a]Significant difference (t test). **c**, **d, e** Evaluation of mitochondrial respiratory capacity and oxidative phosphorylation in permeabilised adipocytes isolated from epididymal fat of the cHF and cHF+F+CR mice using multiple substrate-inhibitor titration respirometry. **c, d** Representative oxygen flux curves (**c** cHF; **d** cHF+F+CR). Adipocyte added in suspension (0.2 ml) to 2 ml incubation medium (10 mmol/l Tris-HCl, 80 mmol/l KCl, 3 mmol/l $MgCl_2$, 5 mmol/l KH_2PO_4, 1 mmol/l EDTA and 1% wt/wt fatty-acid-free BSA, pH 7.4) were permeabilised with the addition of 3 μl digitonin (10 mg/ml DMSO), mitochondrial complex I was inhibited by 2 μl of 1 mmol/l rotenone, and respiration was stimulated by successive additions of: (1) 20 μl 1 mol/l glycerol 3-phosphate; (2) 20 μl 1 mol/l succinate; and (3) 10 μl 0.3 mol/l ADP (before the ADP addition, mitochondrial integrity was tested by addition of 10 μl of 4 mmol/l reduced cytochrome c). Subsequently, ATP synthase was inhibited by 2 μl oligomycin (4 mg/ml), respiration was re-activated by additions of uncoupler of oxidative phosphorylation (carbonyl cyanide-p-trifluoromethoxyphenylhydrazone; FCCP; 0.5 μl of 1 mmol/l FCCP at each addition), and finally, respiration was inhibited by 2 μl of 5 mmol/l antimycin A (inhibitor of complex III). **e** Averaged values from respirometry (n=4; pooled samples from two animals). White bars, cHF; black bars, cHF+F+CR. Data are means± SEM. [a]Significant difference (paired t test) between the groups. All analyses were performed after 5 weeks of treatment

(*Pparα* [also known as *Ppara*]), nuclear respiratory factor 1 (*Nrf1*) and CyOX subunit 3 (*Cyox3* [also known as *Cox3*]) by the combination treatment, suggesting increased biogenesis and oxidative capacity of mitochondria, independent of the type of diet (see legend for Fig. 3). Only *Pparα* expression was upregulated in subcutaneous WAT by the combination treatment, while no significant changes in the expression of the above gene cluster was observed in interscapular brown fat (Fig. 3c), liver (Fig. 3d) or skeletal muscle (Fig. 3e). Concerning the genes of β-oxidation such as very long-chain, long-chain and medium-chain acyl-CoA dehydrogenases (*Vlcad* [also known as *Acadvl*], *Lcad* [also known as *Acadl*] and *Mcad* [also known as *Acadm*], respectively), additive induction of *Vlcad* and *Lcad* was noted in the epididymal WAT (Fig. 3a), and a slight increase in the expression of the β-oxidation genes observed in response to cHF+F or cHF+F+CR treatments in the liver (Fig. 3d) but not in the muscle (Fig. 3e). FA synthase (*Fas*) was upregulated in epididymal WAT of the cHF+F+CR mice (Fig. 3a), but significant downregulation of *Fas* was observed in the liver of these animals (Fig. 3d). No induction of uncoupling protein 1 (*Ucp1*) by any of the treatments either in epididymal fat or in interscapular brown fat was detected (Fig. 3a,c).

Combination treatment induced FA oxidation and mitochondrial oxidative capacity in epididymal fat To confirm the synergistic induction of mitochondrial FA oxidation by LC *n*-3 PUFA and calorie restriction in epididymal fat, biochemical assessment was performed ex vivo after 5 weeks of the dietary treatment. First, [1-^{14}C]palmitate oxidation was measured in fragments of epididymal fat. Feeding the cHF diet stimulated palmitate oxidation compared with Chow feeding, and this activity was further

significantly stimulated only by the combination treatment, documenting a synergism between LC *n*-3 PUFA and calorie restriction in the induction of FA oxidation (Fig. 4a). Accordingly, adipocytes isolated from epididymal fat of the cHF+F+CR mice also exerted a higher DNA-adjusted rate of palmitate oxidation compared with cHF mice (Fig. 4b). This analysis, as well as the analysis of mitochondrial function described below, was restricted to the comparison between the cHF mice and the cHF+F+CR mice, i.e. the two groups supposed to exhibit the largest differences in the metabolic variables.

Second, the activity of CyOX, the terminal component of the mitochondrial respiratory chain, and the content of cytochrome *b* were evaluated in epididymal fat. In the cHF+F+CR mice, the CyOX activity was higher compared with cHF mice (4.5±0.3 vs 3.5±0.4 μmol cytochrome *c* oxidised $min^{-1}mg\ protein^{-1}$, $p<0.05$), in accordance with the difference in the cytochrome *b* content (926±116 vs 590±34 pmol/mg protein, $p<0.05$).

Third, mitochondrial oxidative capacity was characterised in adipocytes using respirometry and adjusted to DNA content (Fig. 4c–e). Adipocytes from the cHF+F+CR mice exerted an approximately twofold higher rate of ADP-dependent oxygen consumption in the presence of respiratory substrates glycerol-3-phosphate and succinate (state 3 respiration) compared with the cHF mice. This indicates a much higher oxidative capacity of adipose tissue mitochondria in the cHF+F+CR mice. In addition, a similar degree of inhibition of state 4 respiration by oligomycin (Fig. 4c–e), similar respiratory control indexes (state 3/state 4; cHF+F+CR, 5.54±1.13 vs cHF, 5.57±1.15), and a reversal of the inhibitory effect of oligomycin by carbonyl cyanide-*p*-trifluoromethoxyphenylhydrazone (FCCP, see Fig. 4c,d) indicated tight coupling between respiration and phosphorylation in the epididymal fat mitochondria of both groups.

To assess changes in lipid catabolism in the other tissues, palmitate oxidation was measured in isolated hepatocytes and in skeletal muscles ex vivo, following the 5 week treatment (ESM Table 2). The combination treatment, but not the other treatments, increased the hepatic FA oxidation compared with the cHF mice, but it had no effect on FA oxidation in muscle.

Combination treatment ameliorates low-grade adipose tissue inflammation induced by high-fat diet As LC *n*-3 PUFA prevented obesity-associated low-grade inflammation of WAT in mice [15, 16], we analysed the anti-inflammatory action of LC *n*-3 PUFA in the context of mild restriction of energy intake. Immunohistochemical analysis of epididymal fat of various treatments revealed a reduced content of macrophages aggregated in crown-like structures (CLS) surrounding dead adipocytes [33] compared with the cHF mice. The macrophage infiltration was maximally reduced in mice subjected to the combination treatment (Fig. 5a–c) and mRNA levels for the macrophage marker CD68 were decreased in the epididymal fat of all treatment groups compared with the cHF controls (Fig. 3a). Moreover, plasma levels of IL-6, a marker of systemic inflammation, were significantly reduced only by the combination treatment (Fig. 5d).

Specific induction of anti-inflammatory lipid mediators in epididymal fat To investigate the possible involvement of bioactive lipids derived from PUFA and modulating inflammation (see Introduction and Fig. 6), lipidomic analysis was performed in epididymal fat and in the liver. In total, 24 lipid species were quantified (ESM Table 3). Partial least-squares-discriminant analysis (PLS-DA) revealed the major discriminating lipid species between the groups. In WAT, but not in the liver, the first two PLS-DA components separated mice into four distinct groups corresponding to dietary treatments (ESM Figs 4 and 5). Following contribution-score analysis, the most important lipids were identified for each of the intervention groups. As shown in Fig. 7a,c,e and in ESM Table 3, the levels of AA, EPA and DHA in the free FA fraction of WAT were significantly higher in all treated groups compared with the cHF mice (except for AA in the ad libitum mice treated by LC *n*-3 PUFA). The cHF+F+CR treatment exerted the most

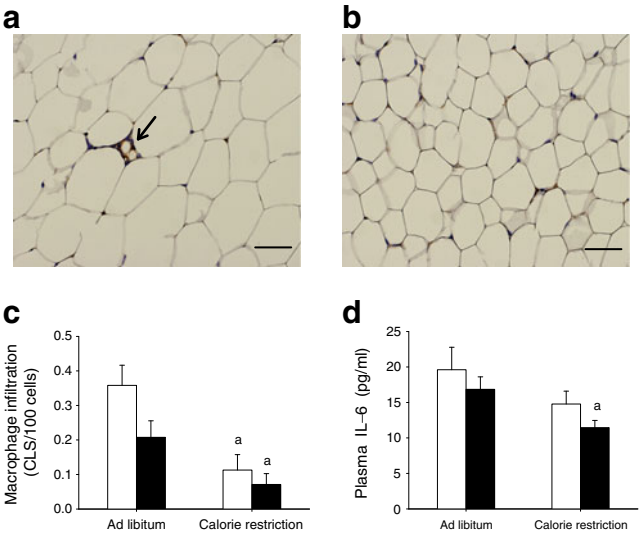

Fig. 5 Prevention of adipose tissue and systemic inflammation. Immunohistochemical analysis of epididymal fat of the cHF mice (**a**) and the cHF+F+CR mice (**b**) with visualised MAC-2 antigen (expressed on activated macrophages); arrow indicates aggregates of macrophages forming CLS, which surround dead adipocytes. **c** Relative count of CLS; $n=6$. **d** Plasma level of IL-6, marker of systemic inflammatory status. Data are means±SEM; $n=10$; white bars, cHF or cHF+CR; black bars, cHF+F or cHF+F+CR; [a]Significant difference (ANOVA) compared with the cHF mice. The morphometry data are based on more than 1,000 cells taken randomly from six different areas per animal. All analyses were performed after 5 weeks of the treatment

pronounced effect. In the liver, free EPA and DHA levels were significantly affected only by LC *n*-3 PUFA, independent of calorie restriction (Fig. 7d,f). In both tissues, the levels of primary monohydroxy metabolites derived from linoleic (HODE), AA (HETE), EPA (HEPE) and DHA (HDoHE) correlated with those of the corresponding FAs (Fig. 6). The lipoxygenase (LOX) products were the most abundant autacoids in both tissues of the cHF controls. Dietary supply of EPA and DHA triggered formation of LC *n*-3 PUFA-derived metabolites in both tissues. The WAT-specific liberation of FAs from membrane phospholipids in response to calorie restriction resulted in the formation of lipid mediators derived from both LC *n*-3 and LC *n*-6 PUFA (Fig. 6). Only in WAT, dietary LC *n*-3 PUFA combined with calorie restriction synergistically increased the levels of protectin D1 (PD1; Fig. 7g), a well described anti-inflammatory lipid mediator derived from DHA, or PD1 isomers such as PDX. In accordance with a previous finding [18], resolvin E1 (derived from EPA) was below the level of detection. Unexpectedly, 15-deoxy-$\Delta^{12,15}$-prostaglandin J_2 (15d-PGJ_2), an anti-inflammatory mediator and potent PPARγ agonist derived from AA [34], was also synergistically upregulated by the combination treatment specifically in WAT (Fig. 7i).

Discussion

We show here that the combination treatment of dietary LC *n*-3 PUFA and mild calorie restriction is more effective than each of the treatments applied separately in the protection against obesity in mice. Pronounced induction of mitochondrial lipid catabolism and synergistic induction of anti-inflammatory lipid mediators in WAT could contribute the systemic effects of the combination treatment (Fig. 8).

Our results demonstrate an improvement of metabolic flexibility by the combination treatment, based on both the

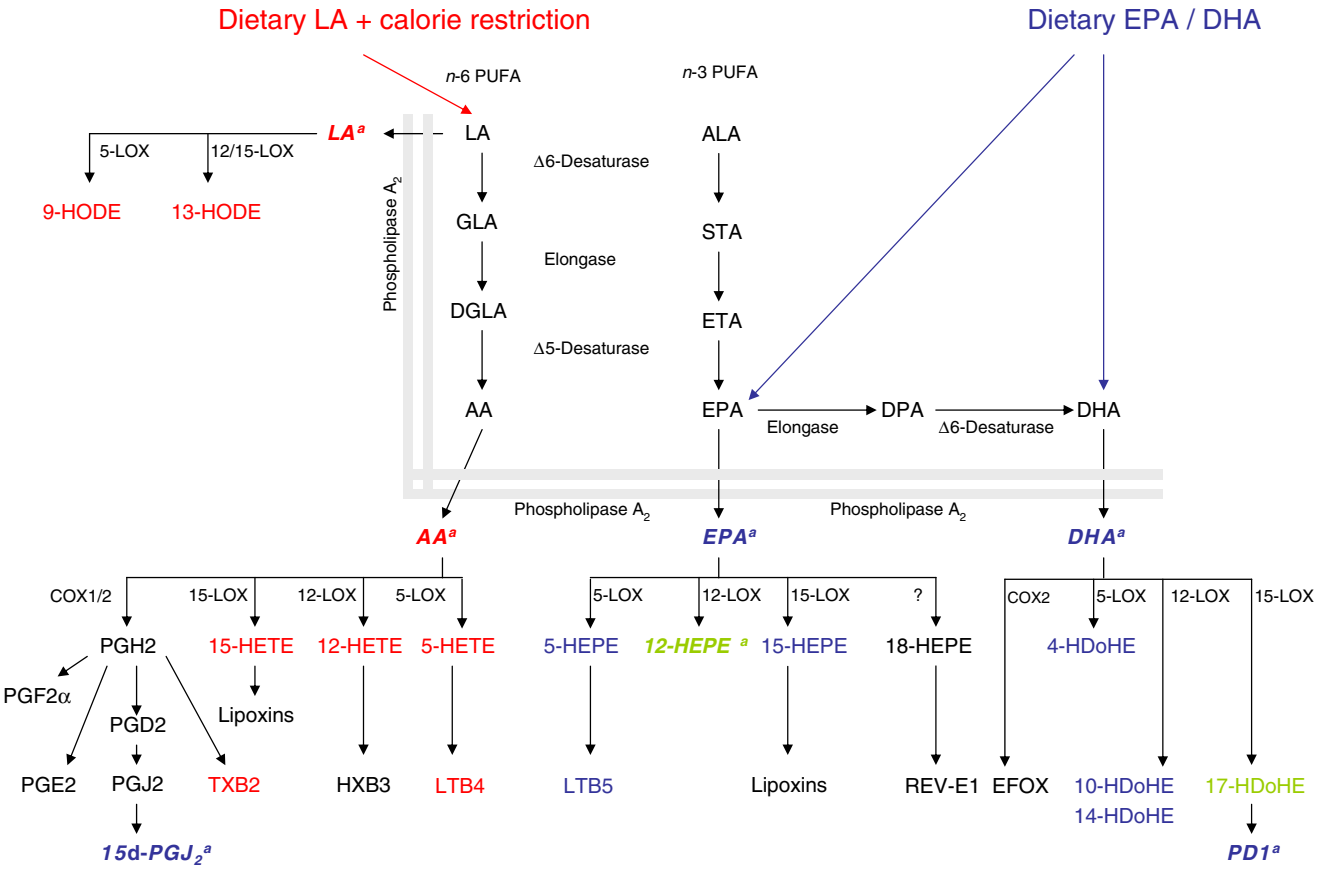

Fig. 6 Overview of the effects of calorie restriction, LC *n*-3 PUFA and the combination treatment on the levels of lipid mediators in epididymal fat. Scheme is based on the results of lipidomic analysis (see Fig. 7, ESM Table 3 and ESM Fig. 3). Significantly upregulated metabolites are marked by different colours; red colour, upregulated by calorie restriction; blue colour, upregulated by LC *n*-3 PUFA; green colour, upregulated by each of the treatments; [a]synergistic upregulation by the combination treatment. Some pathways mentioned in this figure are speculative and not conclusively described. The scheme is inspired by Larsson et al. [50]. ALA, α-linolenic acid (18:3 *n*-3); DGLA, dihomo-γ-linolenic acid (20:3 *n*-6); EFOX, electrophilic oxo-derivatives from DHA [19]; GLA, γ-linolenic acid (18:3 *n*-6); HXB3, hepoxilin B3; LA, linoleic acid (18:2 *n*-6); 5-,12-,15-LOX, 5,12,15-lipoxygenase; LTB4/B5, leukotriene B4/B5; PD1, protectin D1; PG, prostaglandin; PLA_2, phospholipase A_2; Rev-E1, resolvin E1; TXB2, thromboxane B2

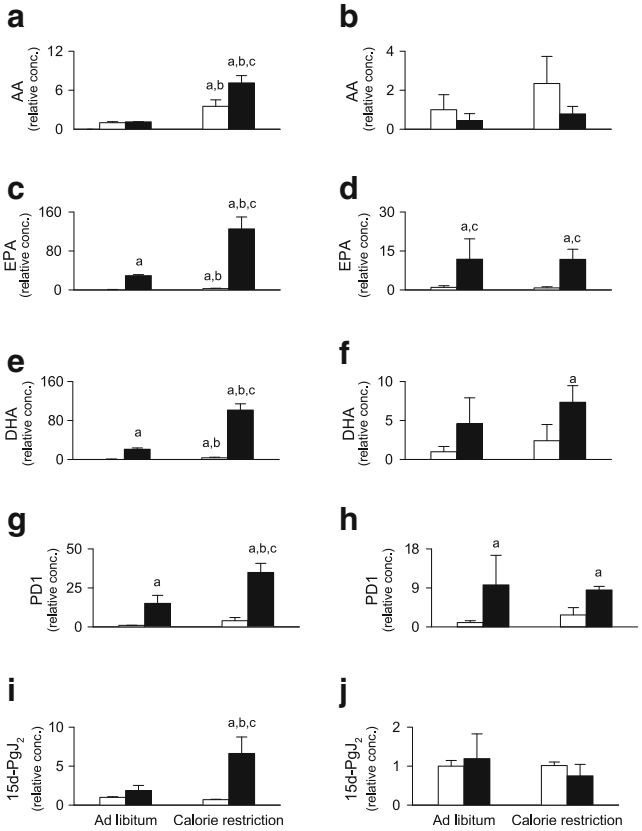

Fig. 7 Synergistic induction of anti-inflammatory lipid mediators in adipose tissue. **a**–**j** Selected results of lipidomic HPLC MS-MS analysis of epididymal fat (**a**, **c**, **e**, **g**, **i**) and liver (**b**, **d**, **f**, **h**, **j**) after 5 weeks of treatment. **a**, **b** AA; **c**, **d** EPA; **e**, **f** DHA; **g**, **h** PD1; **i**, **j** 15d-PgJ_2. Data are expressed as relative concentration of individual lipids adjusted to wet weight (cHF=1) and expressed as means±SEM; n=3. White bars, cHF or cHF+CR; black bars, cHF+F or cHF+F+CR. [a,b,c]Significant differences (ANOVA) compared with cHF, cHF+F, cHF+CR, respectively. For complete results, see ESM Table 3

response of plasma levels of NEFA and glucose to FASTED to RE-FED transition and the glucose-induced increase in RQ. This improvement of metabolic flexibility correlated with changes in body weight, adiposity and glycaemic control in accordance with the notion that metabolic flexibility is closely associated with insulin sensitivity [2, 32] and that impaired flexibility represents an early defect in the development of type 2 diabetes [35].

Metabolic syndrome is linked to inflammatory changes in both WAT and liver [1]. In this study, in accordance with the previous findings [17, 18, 21], dietary LC n-3 PUFA supplementation resulted in the inhibition of formation of various LC n-6 PUFA-derived pro-inflammatory eicosanoids in both tissues as well as in the induction of the anti-inflammatory molecules. In WAT, in contrast to the liver, the levels of EPA, DHA, AA and their active metabolites, including the anti-inflammatory molecules PD1 and prostaglandin 15d-PGJ_2, were increased in a synergistic manner by the combination treatment (Fig. 7). A key role of the enzyme involved in PD1/PDX formation, 12/15 LOX, in adipose tissue inflammation and insulin resistance has been described [36, 37]. The induction of prostaglandin 15d-PGJ_2 was an unexpected finding as 15d-PGJ_2 is derived from the metabolism of LC n-6 PUFA, and enzymatic formation of LC n-6 PUFA metabolites is, in general, inhibited upon LC n-3 PUFA supplementation. This suggests that dietary LC n-3 PUFA, especially in combination with calorie restriction, selectively activates formation of 15d-PGJ_2 from prostaglandin D2 (PGD2), the major product of cyclooxygenase (COX) in many tissues [34],

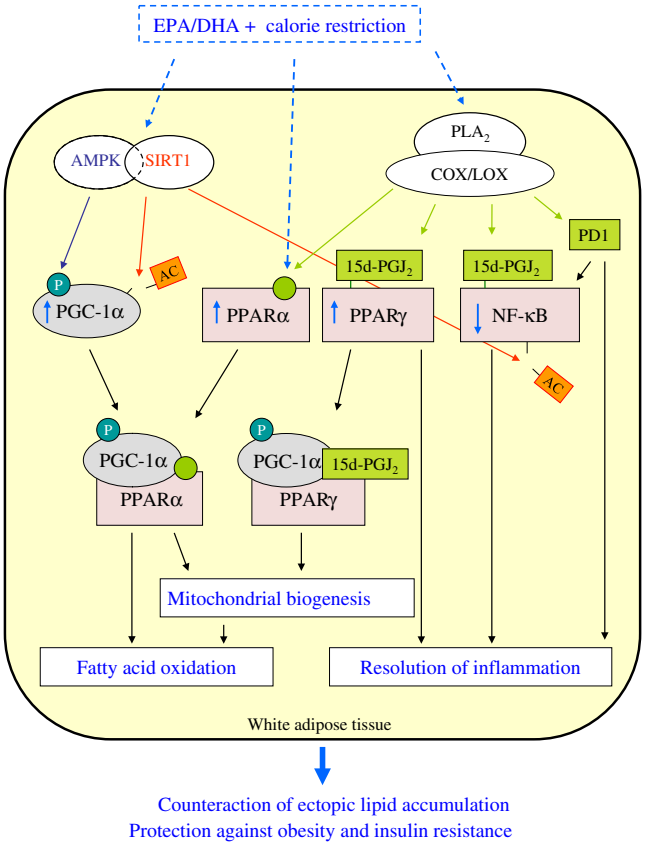

Fig. 8 Putative involvement of AMPK/SIRT1 signalling, 15d-PGJ_2 and PD1 in the additive metabolic and anti-inflammatory effects of the combination of LC n-3 PUFA and calorie restriction in adipose tissue. Dietary intake of LC n-3 PUFA combined with calorie restriction activates AMPK/SIRT1 signalling pathway and synergistically induces production of anti-inflammatory and pro-resolving lipid mediators by COX/LOX enzymatic systems. AMPK and SIRT1 can increase activity of transcriptional co-activator PGC-1α by phosphorylation and de-acetylation, respectively. PGC-1α can enhance transcriptional activity of PPAR nuclear receptors, resulting in higher mitochondrial oxidative capacity and induction of FA catabolism in situ in white fat. Simultaneously, unsaturated FAs (light green circle) as well as their active metabolites (lipid mediators) can also activate directly PPARα and PPARγ (e.g. 15d-PGJ_2). Lipid mediators are formed after the release of FAs from membrane phospholipids and can inhibit the NF-κB signalling pro-inflammatory pathway (15d-PGJ_2, PD1) or induce the resolution phase of inflammation (PD1). Of note, SIRT1 can also interfere with NF-κB signalling. AC, acetyl group; P, phosphate

reflecting possibly the ability of EPA- and DHA-derived peroxyl radicals to favour the formation of 'less pro-inflammatory' peroxidation products derived form AA [38].

Here we suggest for the first time that 15d-PGJ_2 represents an important mediator of LC *n*-3 PUFA effects. 15d-PGJ_2 can modulate the activity of various signalling molecules by covalent binding and their subcellular localisation [34], including various components of the NF-κB signalling pathway [19, 39]. Moreover, 15d-PGJ_2 is the most potent endogenous ligand for PPARγ [40, 41]. Interestingly, DHA is a precursor for anti-inflammatory electrophilic cyclopentenone neuroprostanes in macrophages [20] and electrophilic oxo-derivatives generated by COX-2 reactions [19], which can act similarly to 15d-PGJ_2. Thus, the activation of PPARγ via 15d-PGJ_2 binding could be responsible for the additive effects of the combination treatment on adipose tissue energy and lipid metabolism. This idea is supported by the fact that rosiglitazone, a PPARγ ligand, increases PPARγ coactivator 1α (PGC-1α) production, mitochondrial mass, palmitate oxidation and mitochondrial uncoupling protein 1 (UCP1) in the adipose tissue of genetically obese *ob*/*ob* mice [42].

It has been found that brown adipocyte-like cells originating from rosiglitazone-treated epididymal WAT cell precursors represent a new subtype of adipocytes, called 'brite' cells, which differ from classic white and brown adipocytes, but possess mitochondrial UCP1-mediated thermogenesis [43]. Recent studies [44, 45] demonstrated the involvement of COX-2 in the induction of these fat-burning cells and the importance of the COX-2-mediated mechanisms for the resistance to dietary obesity in mice. Our results convincingly demonstrate a marked induction of mitochondrial oxidative capacity in permeabilised adipocytes isolated from epididymal fat in response to mild calorie restriction combined with LC *n*-3 PUFA intake, using succinate as the optimum fuel [46]. Moreover, changes in palmitate oxidation in both intact isolated adipocytes and in fat fragments document induction of energy expenditure by the combination treatment. Importantly, these changes occurred even in the absence of UCP1, depending probably on the simultaneous activation of PPARα/PGC-1α and PPARγ signalling (Fig. 8). Induction of futile substrate cycling in adipocytes by this mechanism [7] might explain the increased lipid catabolism in the absence of mitochondrial uncoupling. This idea is consistent with our current findings that the combination treatment increases capacity for de novo lipogenesis in epididymal fat, both at the level of gene expression and biochemical activity. In adult mice reared at 20°C, total oxidative capacity in WAT represents ~30–50% of brown adipose oxidative capacity [10] indicating that energy expenditure in WAT may influence total energy balance (see Introduction). Even small but persistent changes in WAT energy expenditure, undetectable using indirect calorimetry, could influence body weight substantially. Fat-depot-specific differences affecting the inducibility of energy-dissipating adipocytes should be explored further. In addition to the stimulation of lipid catabolism in WAT, FA oxidation in liver—but not in skeletal muscle—could contribute to the whole-body effects of the combination treatment.

We have demonstrated previously that AMP-activated protein kinase (AMPK), a cellular energy sensor, is involved in the effects of LC *n*-3 PUFA on hepatic lipid and glucose metabolism [30] and that it is activated in WAT by LC *n*-3 PUFA [47]. AMPK activation in adipocytes results in increased mitochondrial biogenesis and lipid catabolism [4, 48]. Moreover, AMPK closely interacts with deacetylase sirtuin 1 (SIRT1), which controls metabolic processes in response to calorie restriction and exerts anti-inflammatory effects in WAT [49]. Therefore, AMPK/SIRT1 signalling is probably involved in the additive metabolic and anti-inflammatory effects of the combination treatments in epididymal WAT (Fig. 8).

In summary, dietary LC *n*-3 PUFA augment the anti-obesity effects of mild calorie restriction in mice while improving lipid metabolism and glucose homeostasis. These effects are probably reflected by the large synergistic induction of mitochondrial FA oxidation in WAT, linked to a suppression of low-grade inflammation of this tissue. The synergistic induction of specific anti-inflammatory lipid mediators, namely 15d-PGJ_2, the LC *n*-6 PUFA metabolite, and PD1, the LC *n*-3 PUFA metabolite, may underlie both the anti-inflammatory and metabolic effects of the combination treatment in WAT. Further exploration of the strategy to target WAT by combining two complementary and physiological approaches, i.e. dietary intake of LC *n*-3 PUFA and mild restriction of energy intake, may be valuable for the prevention and treatment of metabolic syndrome.

Acknowledgements This work was supported by the research project of the Ministry of Education, Youth and Sports (1M6837805002) and by the Czech Science Foundation (303/08/0664). Further support includes a grant from EPAX A.S. (Aalesund, Norway), COST action FA0602 and the research project AV0Z 50110509. We thank J. Bemova, S. Hornova and D. Salkova (Institute of Physiology AS CR, Prague) for technical assistance and U. Jahn (Institute of Organic Chemistry and Biochemistry AS CR, Prague, Czech Republic) for critical reading of the manuscript.

P.F. contributed to the conception and design of experiments, analysis and interpretation of data, and drafted the manuscript; R.R. and M.R. contributed to the conception and design of experiments, analysis and interpretation of data, and revising the manuscript; M.H., P.J., P.Z., V.K., Z.M.J., E.P., O.K., M.S., G.T. and V.M-A. contributed to the analysis and interpretation of data, and revising the manuscript; and J.K. coordinated the research, contributed to the conception and design of experiments, and drafted the manuscript. All authors approved the final version of the manuscript.

Duality of interest The authors declare that there is no duality of interest associated with this manuscript.

References

1. Virtue S, Vidal-Puig A (2008) It's not how fat you are, it's what you do with it that counts. PLoS Biol 6:e237
2. Galgani JE, Moro C, Ravussin E (2008) Metabolic flexibility and insulin resistance. Am J Physiol Endocrinol Metab 295:E1009–E1017
3. Nisoli E, Tonello C, Cardile A et al (2005) Calorie restriction promotes mitochondrial biogenesis by inducing the expression of eNOS. Science 310:314–317
4. Matejkova O, Mustard KJ, Sponarova J et al (2004) Possible involvement of AMP-activated protein kinase in obesity resistance induced by respiratory uncoupling in white fat. FEBS Lett 569:245–248
5. Orci L, Cook WS, Ravazzola M et al (2004) Rapid transformation of white adipocytes into fat-oxidizing machines. Proc Natl Acad Sci USA 101:2058–2063
6. Jaworski K, Ahmadian M, Duncan RE et al (2009) AdPLA ablation increases lipolysis and prevents obesity induced by high-fat feeding or leptin deficiency. Nat Med 15:159–168
7. Langin D (2010) Recruitment of brown fat and conversion of white into brown adipocytes: strategies to fight the metabolic complications of obesity? Biochim Biophys Acta 1801:372–376
8. Yehuda-Shnaidman E, Buehrer B, Pi J, Kumar N, Collins S (2010) Acute stimulation of white adipocyte respiration by PKA-induced lipolysis. Diabetes 59:2474–2483
9. Rossmeisl M, Syrovy I, Baumruk F, Flachs P, Janovska P, Kopecky J (2000) Decreased fatty acid synthesis due to mitochondrial uncoupling in adipose tissue. FASEB J 14:1793–1800
10. Kopecky J, Rossmeisl M, Hodny Z, Syrovy I, Horakova M, Kolarova P (1996) Reduction of dietary obesity in the aP2-*Ucp* transgenic mice: mechanism and adipose tissue morphology. Am J Physiol 270:E776–E786
11. Flachs P, Rossmeisl M, Bryhn M, Kopecky J (2009) Cellular and molecular effects of *n*-3 polyunsaturated fatty acids on adipose tissue biology and metabolism. Clin Sci 116:1–16
12. Kromhout D, Giltay EJ, Geleijnse JM (2010) *n*-3 fatty acids and cardiovascular events after myocardial infarction. N Engl J Med 363:2015–2026
13. Flachs P, Horakova O, Brauner P et al (2005) Polyunsaturated fatty acids of marine origin upregulate mitochondrial biogenesis and induce beta-oxidation in white fat. Diabetologia 48:2365–2375
14. Jolly CA, Muthukumar A, Avula CP, Troyer D, Fernandes G (2001) Life span is prolonged in food-restricted autoimmune-prone (NZB x NZW)F(1) mice fed a diet enriched with (n-3) fatty acids. J Nutr 131:2753–2760
15. Todoric J, Loffler M, Huber J et al (2006) Adipose tissue inflammation induced by high-fat diet in obese diabetic mice is prevented by *n*-3 polyunsaturated fatty acids. Diabetologia 49:2109–2119
16. Kuda O, Jelenik T, Jilkova Z et al (2009) *n*-3 Fatty acids and rosiglitazone improve insulin sensitivity through additive stimulatory effects on muscle glycogen synthesis in mice fed a high-fat diet. Diabetologia 52:941–951
17. Gonzalez-Periz A, Horrillo R, Ferre N et al (2009) Obesity-induced insulin resistance and hepatic steatosis are alleviated by omega-3 fatty acids: a role for resolvins and protectins. FASEB J 23:1946–1957
18. White PJ, Arita M, Taguchi R, Kang JX, Marette A (2010) Transgenic restoration of long-chain *n*-3 fatty acids in insulin target tissues improves resolution capacity and alleviates obesity-linked inflammation and insulin resistance in high-fat-fed mice. Diabetes 59:3066–3073
19. Groeger AL, Cipollina C, Cole MP et al (2010) Cyclooxygenase-2 generates anti-inflammatory mediators from omega-3 fatty acids. Nat Chem Biol 6:433–441
20. Musiek ES, Brooks JD, Joo M et al (2008) Electrophilic cyclopentenone neuroprostanes are anti-inflammatory mediators formed from the peroxidation of the omega-3 polyunsaturated fatty acid docosahexaenoic acid. J Biol Chem 283:19927–19935
21. Gonzalez-Periz A, Planaguma A, Gronert K et al (2006) Docosahexaenoic acid (DHA) blunts liver injury by conversion to protective lipid mediators: protectin D1 and 17S-hydroxy-DHA. FASEB J 20:2537–2539
22. Mori TA, Bao DQ, Burke V, Puddey IB, Watts GF, Beilin LJ (1999) Dietary fish as a major component of a weight-loss diet: effect on serum lipids, glucose, and insulin metabolism in overweight hypertensive subjects. Am J Clin Nutr 70:817–825
23. Ramel A, Martinez A, Kiely M, Morais G, Bandarra NM, Thorsdottir I (2008) Beneficial effects of long-chain *n*-3 fatty acids included in an energy-restricted diet on insulin resistance in overweight and obese European young adults. Diabetologia 51:1261–1268
24. Krebs JD, Browning LM, McLean NK et al (2006) Additive benefits of long-chain *n*-3 polyunsaturated fatty acids and weight-loss in the management of cardiovascular disease risk in overweight hyperinsulinaemic women. Int J Obes 30:1535–1544
25. Rossmeisl M, Jelenik T, Jilkova Z et al (2009) Prevention and reversal of obesity and glucose intolerance in mice by DHA derivatives. Obesity 17:1023–1031
26. Kus V, Prazak T, Brauner P et al (2008) Induction of muscle thermogenesis by high-fat diet in mice: association with obesity-resistance. Am J Physiol Endocrinol Metab 295:E356–E367
27. Flachs P, Mohamed-Ali V, Horakova O et al (2006) Polyunsaturated fatty acids of marine origin induce adiponectin in mice fed high-fat diet. Diabetologia 49:394–397
28. van Schothorst EM, Flachs P, Franssen-van Hal NL et al (2009) Induction of lipid oxidation by polyunsaturated fatty acids of marine origin in small intestine of mice fed a high-fat diet. BMC Genom 10:110
29. Baumruk F, Flachs P, Horakova M, Floryk D, Kopecky J (1999) Transgenic UCP1 in white adipocytes modulates mitochondrial membrane potential. FEBS Lett 444:206–210
30. Jelenik T, Rossmeisl M, Kuda O et al (2010) AMP-activated protein kinase $\alpha 2$ subunit is required for the preservation of hepatic insulin sensitivity by *n*-3 polyunsaturated fatty acids. Diabetes 59:2737–2746
31. Ruhl R (2006) Method to determine 4-oxo-retinoic acids, retinoic acids and retinol in serum and cell extracts by liquid chromatography/diode-array detection atmospheric pressure chemical ionisation tandem mass spectrometry. Rapid Commun Mass Spectrom 20:2497–2504
32. Storlien L, Oakes ND, Kelley De (2004) Metabolic flexibility. Proc Nutr Soc 63:363–368
33. Cinti S, Mitchell G, Barbatelli G et al (2005) Adipocyte death defines macrophage localization and function in adipose tissue of obese mice and humans. J Lipid Res 46:2347–2355
34. Scher JU, Pillinger MH (2005) 15d-PGJ2: the anti-inflammatory prostaglandin? Clin Immunol 114:100–109
35. Corpeleijn E, Mensink M, Kooi ME, Roekaerts PM, Saris WH, Blaak EE (2008) Impaired skeletal muscle substrate oxidation in glucose-intolerant men improves after weight loss. Obesity 16:1025–1032

36. Chakrabarti SK, Cole BK, Wen Y, Keller SR, Nadler JL (2009) 12/15-lipoxygenase products induce inflammation and impair insulin signaling in 3T3-L1 adipocytes. Obesity 17:1657–1663
37. Sears DD, Miles PD, Chapman J et al (2009) 12/15-lipoxygenase is required for the early onset of high fat diet-induced adipose tissue inflammation and insulin resistance in mice. PLoS One 4: e7250
38. Davis TA, Gao L, Yin H, Morrow JD, Porter NA (2006) In vivo and in vitro lipid peroxidation of arachidonate esters: the effect of fish oil omega-3 lipids on product distribution. J Am Chem Soc 128:14897–14904
39. Rossi A, Kapahi P, Natoli G et al (2000) Anti-inflammatory cyclopentenone prostaglandins are direct inhibitors of IkappaB kinase. Nature 403:103–118
40. Forman BM, Tontonoz P, Chen J, Brun RP, Spiegelman BM, Evans RM (1995) 15-Deoxy-delta 12, 14-prostaglandin J2 is a ligand for the adipocyte determination factor PPAR gamma. Cell 83:803–812
41. Kliewer SA, Lenhard JM, Willson TM, Patel I, Morris DC, Lehmann JM (1995) A prostaglandin J2 metabolite binds peroxisome proliferator-activated receptor gamma and promotes adipocyte differentiation. Cell 83:813–819
42. Wilson-Fritch L, Nicoloro S, Chouinard M et al (2004) Mitochondrial remodeling in adipose tissue associated with obesity and treatment with rosiglitazone. J Clin Invest 114:1281–1289
43. Nedergaard J, Cannon B (2010) The changed metabolic world with human brown adipose tissue: therapeutic visions. Cell Metab 11:268–272
44. Madsen L, Pedersen LM, Lillefosse HH et al (2010) UCP1 induction during recruitment of brown adipocytes in white adipose tissue is dependent on cyclooxygenase activity. PLoS One 5:e11391
45. Vegiopoulos A, Muller-Decker K, Strzoda D et al (2010) Cyclooxygenase-2 controls energy homeostasis in mice by de novo recruitment of brown adipocytes. Science 328:1158–1161
46. Wang T, Si Y, Shirihai OS et al (2010) Respiration in adipocytes is inhibited by reactive oxygen species. Obesity 18:1493–1502
47. Kopecky J, Rossmeisl M, Flachs P et al (2009) *n*-3 PUFA: bioavailability and modulation of adipose tissue function. Proc Nutr Soc 68:361–369
48. Gaidhu MP, Fediuc S, Anthony NM et al (2009) Prolonged AICAR-induced AMP-kinase activation promotes energy dissipation in white adipocytes: novel mechanisms integrating HSL and ATGL. J Lipid Res 50:704–715
49. Yoshizaki T, Milne JC, Imamura T et al (2009) SIRT1 exerts anti-inflammatory effects and improves insulin sensitivity in adipocytes. Mol Cell Biol 29:1363–1374
50. Larsson SC, Kumlin M, Ingelman-Sundberg M, Wolk A (2004) Dietary long-chain *n*-3 fatty acids for the prevention of cancer: a review of potential mechanisms. Am J Clin Nutr 79:935–945

Diabetologia
Clinical and Experimental Diabetes and Metabolism

10.1007/s00125-011-2233-2

Electronic Supplementary Material

Below is the link to the electronic supplementary material.
ESM Methods (PDF 168 kb)
ESM Table 1 Indirect calorimetry data evaluation (PDF 9 kb)
ESM Table 2 Palmitate oxidation rates in liver and skeletal muscle (PDF 12 kb)
ESM Table 3 HPLC MS/MS quantification of lipid-derived mediators in adipose tissue and liver (PDF 18 kb)
ESM Figure 1 Overview of experimental setup. Scheme of individual dietary experiments, which lasted for either 5 for 15 weeks (PDF 11 kb)
ESM Figure 2 Indirect calorimetry. Oxygen consumption (VO_2) and carbon dioxide production (VCO_2) were recorded in singly-caged mice every 2 min at 30°C. **a** Levels of substrate partitioning were estimated by calculating respiratory quotient (RQ; i.e. VCO_2/VO_2). Metabolic flexibility was assessed as a maximal induction in RQ values in response to a glucose load (0.45 ml of 50% D-glucose) administered by intragastric gavage to overnight (12 hours) fasted animals (Time 0). The induction was calculated from RQ values averaged over 60-min-intervals before and after gavage, respectively (indicated by horizontal bars). Black line-cHF; blue line- cHF+F; red line- cHF+CR; green line- cHF+F+CR. **b** *VO*2 before and after gavage. Data are means±SE. Mice were analyzed during the fourth week of the treatment, i.e. before any significant differences in body weights between the treatments appeared. For evaluation of calorimetric data see ESM Table 1 (PDF 47 kb)
ESM Figure 3 An oral glucose tolerance test was performed after overnight fasting (15–16 h). White circles- cHF; black circles- cHF+F; white inverted triangles- cHF+CR; black inverted triangles- cHF+F+CR; grey circles- Chow (PDF 9 kb)
ESM Figure 4 Partial least squares-discriminant analysis (PLS-DA) of lipidomic data in adipose tissue. In total, 24 lipid molecular species were quantified in epididymal fat using HPLC MS-MS after 5 weeks of the treatment (ESM Table 3). To identify the major lipid species discriminating between the groups, PLS-DA was performed using Umetrics SIMCA-P+12 statistical software. **a** 2D-scatter plots of the first (axis X) and the second (axis Y) PLS-DA component. Black circle- cHF; blue circle- cHF+F; red circle- cHF+CR; green circle- cHF+F+CR. **b** Contribution score analysis using the corresponding linear combination of the p vector as weights in the epididymal fat of mice fed respective diets. The dominating bars indicate which variables deviate the most from the average, and the sign of the bar (down and up means minus and plus, respectively) indicate in which direction the variables deviate (PDF 14 kb)
ESM Figure 5 PLS-DA of lipidomic data in liver. In total, 24 lipid species were quantified in liver after 5 weeks of the treatment (see ESM Table 3) and data were analyzed as in ESM Fig 3. Black circle- cHF; blue circle- cHF+F; red circle- cHF+CR; green circle- cHF+F+CR (PDF 15 kb)

ESM METHODS

HPLC MS-MS analysis of lipid-derived mediators in adipose tissue and liver

Sample pre-treatment/preparation – The whole analytical procedure is based on an established method used for retinoid quantification [1]. In summary, 100 mg of tissue was minced after addition of 0.2 ml of isopropanol using scissors to yield a homogenous suspension, while keeping the samples on ice. After shaking for 3 min, the precipitated protein was centrifuged at 13.000 rpm, 4°C, for 6 min. The supernatant was evaporated in Eppendorf reaction vials with an Eppendorf concentrator 5301 (Eppendorf, Germany) at 30 °C for ~45 min until the sample volume was ~10 µl. The Eppendorf concentrator was vented with argon to prevent eicosanoids/docosanoids degradation. The dried extract was resuspended with 25 µl of solvent A [64.3% water (water, Chromasolv plus from Sigma-Aldrich, Hungary); 35.5% acetonitrile (Merck KGaA, Germany); 0.2% formic acid (Fluka, Hungary)], vortexed (15 sec) and shaked (3 min) and transferred into micro injection inserts vials (Waters, Hungary). These glass vials with the 35 µl extract were transferred into brown screw top vials with PTFE / silicone septa sample (Waters, Hungary) and placed in the pre-cooled (15°C) autosampler of the Waters 2695XE separation module.

Chromatographic system - The HPLC system consisted of a Waters 2695XE separation module (Waters, Hungary) including a gradient pump, autosampler, degasser, heated column compartment. A MS-MS detector with an ESI ionizing option was used (Micromass Quattro Ultima PT from Waters, UK; a gift from Biosystems Int., France) as a detector. The system was controlled via the MassLynx software (Waters, Hungary).

HPLC conditions - The eluents were degassed in the Waters 2695XE separation module prior to mixing, then passed through an in-line filter (1-2 µm; Knauer, Germany) before reaching the analytical column (LiChroCART, 125 X 2 mm; Superspher 100, RP-18, endcapped) from Merck KgaA (Germany) embedded in the column compartment. A multilinear gradient was formed from solvent A (see above) and solvent B (methanol; Merck KGaA Germany). The gradient consisted of the following steps: 0.0 min 20% B, 3.0 min 20 % B, 5.0 min 60 % B, 15.0 min 100 % B, 15.9 min 100 % B and 16.0 min 5 % B. The flow rate was adjusted to 0.4 ml/min and the column was heated at 40°C. 10 µl for each HPLC analysis from the same biological extract was used. This step was performed two times using the same HPLC conditions and two different MS-MS analysis options for better resolution and quantification of the various analytes.

MS options - The Micromass Quattro Ultima PT was controlled via the MassLynx software. Argon with an inlet pressure of 0.8 bar was used. ESI (electro spray ionization source, Waters, Hungary) was vented by nitrogen continuously produced by nitrogen generator (Peak Scientific NM30 Nitrogen generator) including compressor (Waters, Hungary) with a setting of the inlet flow of 3.6 e^{-3} mbar.

Multiple reaction monitoring settings: ESI ionization (ESI - settings) was performed with the HPLC eluent following into the ion source temperature of 85°C. Desolvation gas flow was 780 l/hr, the desolvation temperature was 400°C,the cone gas flow of 10 l/hr, the capillary current was 3 μA, and the cone voltage was 50 V. Aperture voltage was set at 0 V and the RF lens voltage was set at 35 V (for 1) and 0.2 V (for 2). The analyzer setting were LM1 resolution 14.5; HM1 resolution 14.5; Ion energy 1 0.7; entrance –1; collision 0 (collision parameters are set for each substance at the MS – method parameters); exit 2; LM2 resolution 14.5; HM2 resolution 14.5; Ion energy2 5.0 and a multiplier energy of 650.

Multiple reaction monitoring settings for PUFA, eicosanoids/docosanoids semi-quantification were: Method A from 0.0 – 9.0 min for PGF2 349.0 -> 192.7, collision energy 22 eV; PD1 and PD1 isomers like PDX 359,0 -> 153.3, collision energy 17 eV; TXB2 369.0 -> 195.0, collision energy 13 eV, Rev-E1 375.1 -> 141.3, collision energy 13 eV; from 9.0 - 12.5 min for 13-HODE 294.7 -> 170.7, collision energy 16 eV; 9-HODE 294.7 -> 194.7, collision energy 16 eV; 5-HEPE 317.0 -> 115.0, collision energy 17 eV; 12-HEPE 317.0 -> 179.0, collision energy 17 eV; 15-HEPE 317.0 -> 219.0, collision energy 17 eV, LTC4 623.9 -> 272.0, collision energy 14 eV from 12.5 – 16.0 min for LA 279.3 -> 279.0, collision energy 10 eV; EPA 301.0 -> 203.2, collision energy 12 eV, 303.0 -> 259.3, collision energy 11 eV, DHA 327.1 -> 29.3, collision energy 14 eV. Method B from 0.0 – 9.8 min for PGE2, PGD2, 15dPGJ2, PGJ2 315.0 -> 271.3, collision energy 13 eV; LTB5 333.0 -> 195.0, collision energy 13 eV; LTB4 335.0 -> 195.0, collision energy 13 eV; from 9.8 - 12.5 min for 5-HETE 318.7 -> 115.0, collision energy 14 eV; 8-HETE 319.0 -> 155.0, collision energy 14 eV; 12-HETE 319.0 -> 179.0, collision energy 14 eV; 15-HETE 319.0 -> 218.9, collision energy 11 eV; 4-HDoHE 343.0 -> 101.0, collision energy 10 eV; 10-HDoHE 343.0 -> 181.0, collision energy 10 eV; 14-HDoHE 343.0 -> 205.0, collision energy 10 eV; 17-HDoHE 343.0 -> 245.0, collision energy 14 eV.

Standard solutions - Stock solutions of the 24 PUFAs and eicosanoids / docosanoids were prepared by dissolving the solutions obtained from Cayman-Chemicals (Estonia) with methanol to yield a final concentration of 10 μg/ml. All stock solutions were stored in darkness at -80°C. The reference PUFAs and eicosanoids/docosanoids were used for the assay validation.

Semi-quantification - Individual eicosanoids/docosanoids were semi-quantified based on the determination of the "area under the curve (AUC)" of these compounds and adjusted to tissue weight.

Collection of plasma samples during FASTED to RE-FED transition

When indicated EDTA-plasma was collected using tail bleeding and adapted procedure described by Viollet et al [2]. Before the bleeding, one half of mice within each experimental group was either (i) fasted for 14 hours (food was removed between 8:00 am and 10:00 pm, while mice were kept in a clean new cage), or (ii) fasted for 10 hours (between 8:00 am and 6:00 pm, similarly as above) and allowed free access to food for the following 3 hours. In each mouse, plasma glucose, NEFA, TG and insulin were assessed in both FASTED and RE-FED state, while altering the above protocols during two subsequent days. HOMA index was calculated by the following formula: FASTED plasma insulin (mU/l) x FASTED plasma glucose (mmol/l) / 22.5.

Quantitative Real Time RT-PCR

Total RNA isolated using TRI Reagent (Molecular Research Center, Inc, Cincinnati, OH, USA). Levels of various transcripts were evaluated using LightCycler 480 II instrument (Roche Diagnostic Ltd., Rotkreuz, Switzerland) and LightCycler 480 SYBR Green I Master kit (Roche Diagnostic Ltd., Mannheim, Germany). PCR condition were 95°C for 6 min and 45 cycles of 95°C for 10 s, 55-60°C for 10 s and 72°C for 20s. Specificity of the amplified PCR product was assessed by performing a melting curve analysis. Lasergene 7 software (DNASTAR, Inc. Madison, WI, USA) was used to design primers. To correct for intersample variation, levels of the transcript were normalized using geometrical mean of two reference genes – *Ef-1α* (Gene ID: 13627) and *Cyclophilin-β* (Gene ID: 19035). Similar results were obtained using *Rn18s* as reference. Primer sequence (forward/reverse) for detection of the specific transcripts were as follows: *Pparα* (Gene ID: 19013), TGCGCAGCTCGTACAGGTCATCAA/ CCCCCATTTCGGTAGCAGGTAGTCTTA; *Cd-68* (Gene ID: 12514), CACTTCGGGCCATGTTTCTCTTG/AGGGGCTGGTAGGTTGATTGTCGT; *Mcp-1* (Gene ID: 20296), GTTAACGCCCCACTCAC/GGTTCCGATCCAGGTTT; *Fas (*Gene ID: 14104) GGCTGCCTCCGTGGACCTTATC/ GTCTAGCCCTCCCGTACACTCACTCGT; *Gyk (*Gene ID: 14933), TCGTTCCAGCATTTTCAGGGTTAT/ TCAGGCATGGAGGGTTTCACTACT, *Mcad* (Gene ID: 11364) TCGCCCCGGAATATGACAAAA/ GCCAAGGCCACCGCAACT, *Lcad* (Gene ID: 11363) TGGCATCAACATCGCAGAGAAACA/ ACCGATACACTTGCCCGCCGTCAT and Vlcad (Gene ID: 11370)

CAGGGGTGGAGCGTGTGC/CATTGCCCAGCCCAGTGAGTTCC. Other primer sequences were already published before [3].

Physical activity

Animal behaviour was recorded on videocamera (resolution 320x240 pixels with sample frequency 25 frames/sec) and analyzed off-line with the EthoVision XT software (Noldus Information Technology, Wageningen, Netherlands). Central-point detection was used to track mouse position in the home cage. Total distance moved, total moving and unmoving time were evaluated for each animal at two time intervals, from 2 to 4 p.m. (light phase) and from 9 to 11 p.m. (dark phase of a 12 h light–dark cycle).

Statistical analysis

All values are presented as means±SEM. Logarithmic transformation was used to stabilize variance in cells when necessary. Data were analyzed by paired *t*-test or ANOVA (one-way or two-way) with Holm-Sidak posthoc tests using SigmaStat 3.5 statistical software. Comparisons were judged to be significant at $p<0.05$.Repeated measures ANOVA was used to analyze the response of plasma metabolites level to FASTED/RE-FED transition (Fig. 1c,d). Partial least squares-discriminant analysis (PLS-DA) using Umetrics SIMCA-P+12 statistical software was used for lipidomic data evaluation.

ESM References

1. Ruhl R (2006) Method to determine 4-oxo-retinoic acids, retinoic acids and retinol in serum and cell extracts by liquid chromatography/diode-array detection atmospheric pressure chemical ionisation tandem mass spectrometry. Rapid Commun Mass Spectrom 20: 2497-2504

2. Viollet B, Andreelli F, Jorgensen SB, et al (2003) The AMP-activated protein kinase alpha2 catalytic subunit controls whole-body insulin sensitivity. J Clin Invest 111: 91-98

3. Kuda O, Jelenik T, Jilkova Z, et al (2009) n-3 Fatty acids and rosiglitazone improve insulin sensitivity through additive stimulatory effects on muscle glycogen synthesis in mice fed a high-fat diet. Diabetologia 52: 941-951

ESM Table 1
Indirect calorimetry data evaluation

	cHF	cHF+F	cHF+CR	cHF+F+CR
Fasting				
RQ	0.78±0.02	0.79±0.02	0.78±0.01	0.78±0.01
VO_2 (ml/min)	0.86±0.07	0.83±0.03	0.93±0.11	0.78±0.05
Glucose gavage				
RQ	0.87±0.01	0.90±0.01	0.90±0.01	0.91±0.01[a]
VO_2 (ml/min)	0.94±0.09	0.95±0.04	1.04±0.07	1.01±0.07
Change				
RQ	0.09±0.01	0.12±0.01	0.13±0.01	0.14±0.01[a]
VO_2 (ml/min)	0.22±0.07	0.25±0.09	0.16±0.05	0.22±0.05

Table shows values of VO_2 and RQ in fasting state before glucose gavage, after the gavage, and the change in response to the gavage. Data are means±SEM, *a*- significant difference (ANOVA) compared to cHF. For details, see ESM Fig. 2.

ESM Table 2

Palmitate oxidation rates in liver and skeletal muscle

	Chow	cHF	cHF+F	cHF+CR	cHF+F+CR
Hepatocytes					
FA oxidation (dpm/μg DNA)	17±3	31±2*	36±4	27±2	42±4[a]
Gastrocnemius muscle					
FA oxidation (dpm/mg tissue)	N.E.	42±5	N.E.	N.E.	44±4
Soleus muscle					
FA oxidation (dpm/mg tissue)	N.E.	123±12	N.E.	N.E.	140±10

After 5 weeks of the treatment, oxidation of [1-^{14}C] palmitate was measured either in isolated hepatocytes, or in whole soleus muscle (oxidative type), or in a fragment of gastrocnemius muscle (mixed type). Data are expressed as means±SEM; *n*= 8-12; *a*- significant difference (ANOVA) compared to cHF. *- significant difference (*t*-test) compared to Chow. N.E. not estimated.

ESM Table 3
HPLC MS/MS quantification of lipid-derived mediators in adipose tissue and liver

Epididymal fat

	cHF	cHF+F	cHF+CR	cHF+F+CR
LA	1.0±0.2	1.8±0.2[a]	6.7±1.1[a,b]	15.0±1.9[a,b,c]
9-HODE	1.0±0.1	1.3±0.2	8.8±1.6[a,b]	2.7±0.3[c]
13-HODE	1.0±0.0	2.1±0.5	6.6±0.4[a,b]	4.7±1.5[a]
AA	1.0±0.2	1.1±0.0	3.5±1.0[a,b]	7.1±1.1[a,b,c]
PGE2	1.0±0.1	4.8±1.8	10.3±6.6	3.6±1.5
PGD2	1.0±0.1	1.4±0.2	9.1±5.2	2.4±0.9
d15-PGJ_2	1.0±0.1	1.9±0.7	0.7±0.1	6.6±2.1[a,b,c]
TXB2	1.0	7.5±2.5	24.0±10[b]	15.7±4.8
5-HETE	1.0±0.2	1.0±0.3	2.5±0.8[a,b]	2.0±0.6
8-HETE	1.0±0.3	0.7±0.1	3.8±1.3[a,b]	2.4±0.5
12-HETE	1.0±0.2	0.7±0.4	1.8±0.2[a,b]	7.9±0.4[a,b]
15-HETE	1.0±0.3	0.6±0.1	5.4±2.7[a,b]	0.8±0.0[c]
LTB4	1.0±0.0	1.4±0.5	7.4±8.1[a]	2.6±0.5
EPA	1.0±0.2	29.5±2.2[a]	2.9±0.8[a,b]	126±24[a,b,c]
5-HEPE	1.0±0.6	18.1±0.2[a]	2.3±2.0	32.8±0.2[a,c]
12-HEPE	1.0±0.1	47.1±0.2[a]	10.8±2.8[a,b]	211±73[a,b,c]
15-HEPE	1.0±0.6	16.7±4.5[a]	5.5±0.6[a,b]	55.2±20.9[a,c]
LTB5	1.0	29.3±8.1	15.5±7.5	14.3±8.8
DHA	1.0±0.2	21.2±0.1[a]	3.5±0.4[a,b]	101±13[a,b,c]
4-HDoHE	1.0±0.6	2.2±0.5[a]	0.7±0.2	1.8±0.6
10-HDoHE	1.0±0.8	3.8±1.6[a]	N.E.	16.1±4.2[a,b]
14-HDoHE	1.0±0.3	8.1±2.0[a]	3.6±1.9	22.0±9.3[a,c]
17-HDoHE	1.0±0.3	6.9±2.8[a]	6.9±1.7[a]	16.9±8.7[a,b,c]
PD1	1.0±0.1	15.1±5.1[a]	4.0±2.1	35.0±5.9[a,b,c]

ESM Table 3 (continued)

Liver

	cHF	cHF+F	cHF+CR	cHF+F+CR
LA	1.0±0.4	0.7±0.3	1.5±0.6	1.4±0.3
9-HODE	1.0±0.2	0.7±0.1	1.1±0.1	0.8±0.13
13-HODE	1.0±0.1	0.8±0.2	1.5±0.5	1.0±0.2
AA	1.0±0.4	0.4±0.2	3.3±1.6	0.8±0.2
PGE2	1.0±0.5	N.E.	2.6±1.3	N.E
PGD2	1.0±0.6	N.E.	4.4±2.9	0.3±0.1[c]
d15-PGJ_2	1.0±0.1	1.2±0.4	1.0±0.1	0.8±0.2
TXB2	1.0±0.4	0.1±0.0	1.7±0.9	0.3±0.1
5-HETE	1.0±0.5	0.5±0.3	0.6±0.1	0.6±0.3
8-HETE	1.0±0.4	0.2±0.0[a]	1.7±0.2	0.3±0.1
12-HETE	1.0±0.2	0.3±0.1	2.6±0.2[a,b]	0.7±0.1[c]
15-HETE	1.0±0.5	0.2±0.1	1.3±0.1[b]	0.3±0.0[c]
LTB4	1.0±0.2	0.2±0.1	1.0±0.4	0.46±0.2
EPA	1.0±0.4	11.9±4.5[a]	0.8±0.2[b]	11.8±2.2[a,c]
5-HEPE	1.0±0.3	18.7±4.6	0.6±0.30	7.3±3.4
12-HEPE	1.0±0.2	11.2±2.0[a]	0.7±0.1[b]	12.3±1.0[a,c]
15-HEPE	1.0±0.2	7.4±2.0[a]	0.4±0.1[b]	4.3±0.4[a,c]
LTB5	1.0±0.1	3.4±1.7	1.1±0.1	4.9±0.8[a,c]
DHA	1.0±0.4	4.6±1.9	3.4±1.2	7.3±1.2[a]
4-HDoHE	1.0	43±21	10.7±7.3	51.3±0.9[c]
10-HDoHE	1.0±0.5	5.6±2.2[a]	3.2±0.7	11.4±4.2[a]
14-HDoHE	1.0±0.4	4.4±1.7[a]	2.8±0.7	7. 3±1.0[a]
17-HDoHE	1.0±0.2	1.5±1.2	0.9±0.0	3.0±1.0
PD1	1.0±0.2	9.7±3.9[a]	2.8±1.0[b]	8.5±0.5[a]

The HPLC MS-MS data of epididymal fat and liver after 5 weeks of the treatment. Data are relative concentration adjusted to tissue weight and expressed as means±SEM (cHF=1); *n*=3; *a, b, c* - significant differences (ANOVA) compared to cHF, cHF+F, cHF+CR, respectively; N.E. not estimated.

ESM Figure 1 Experimental schedule and set-up

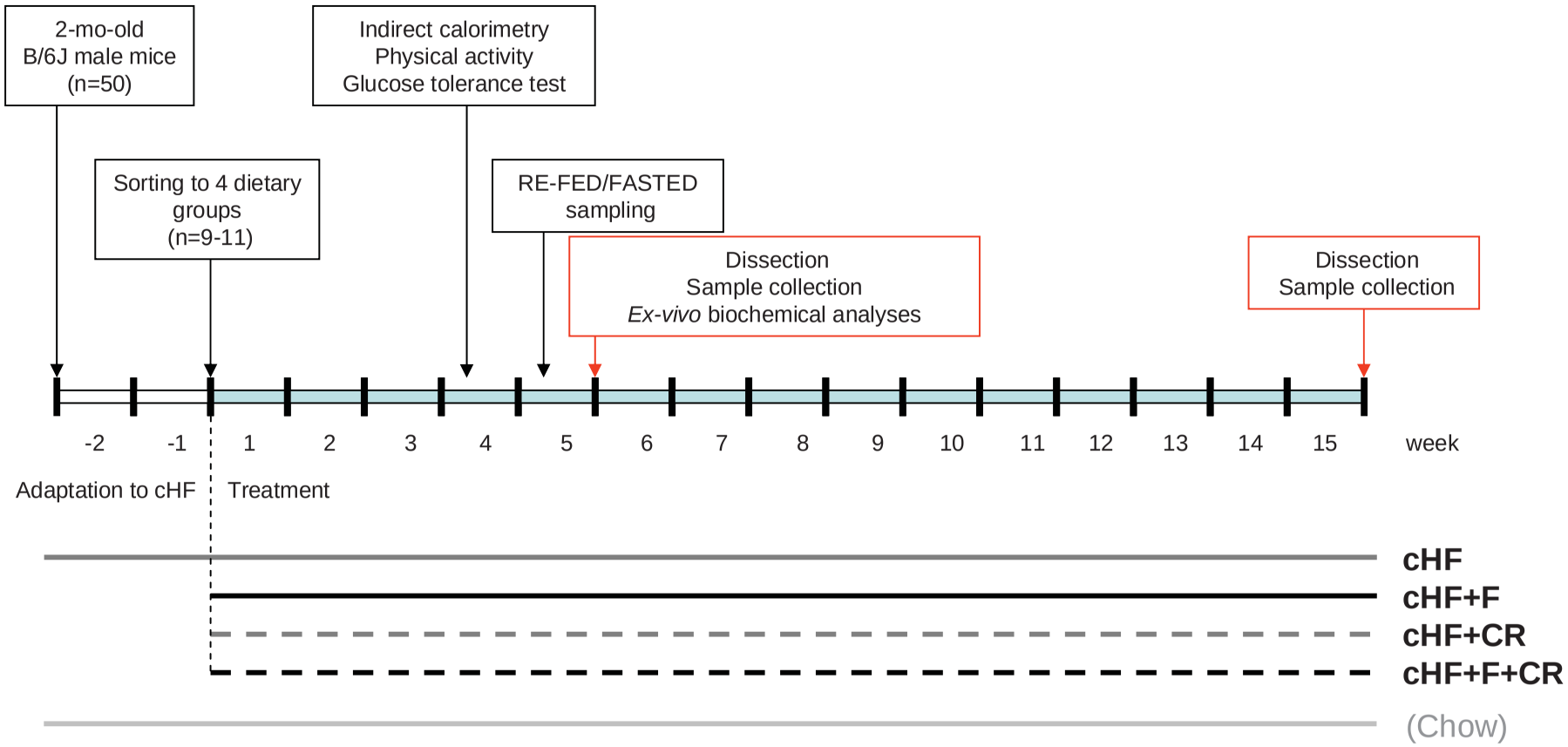

ESM Figure 2 Indirect calorimentry

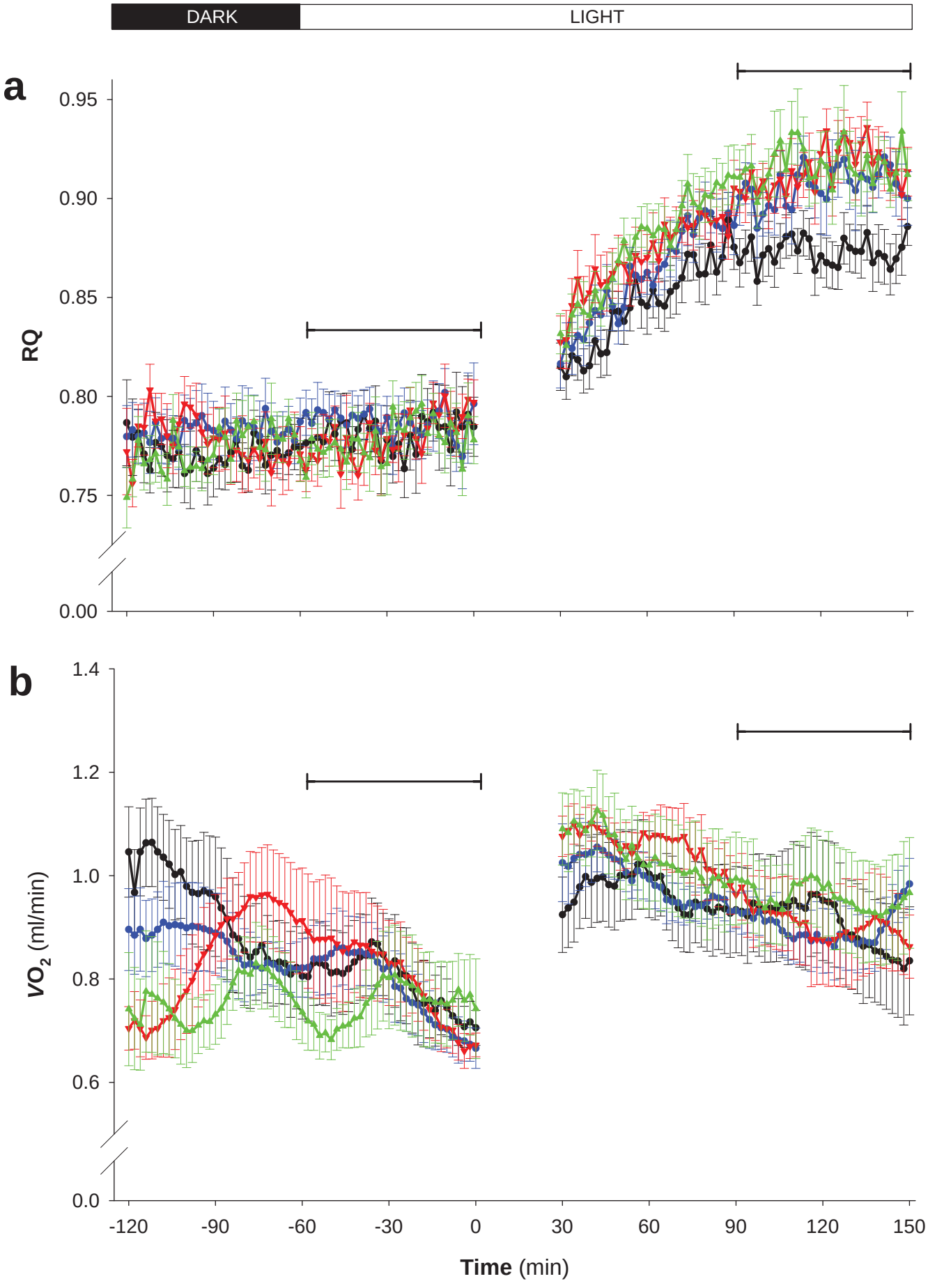

ESM Fig.3

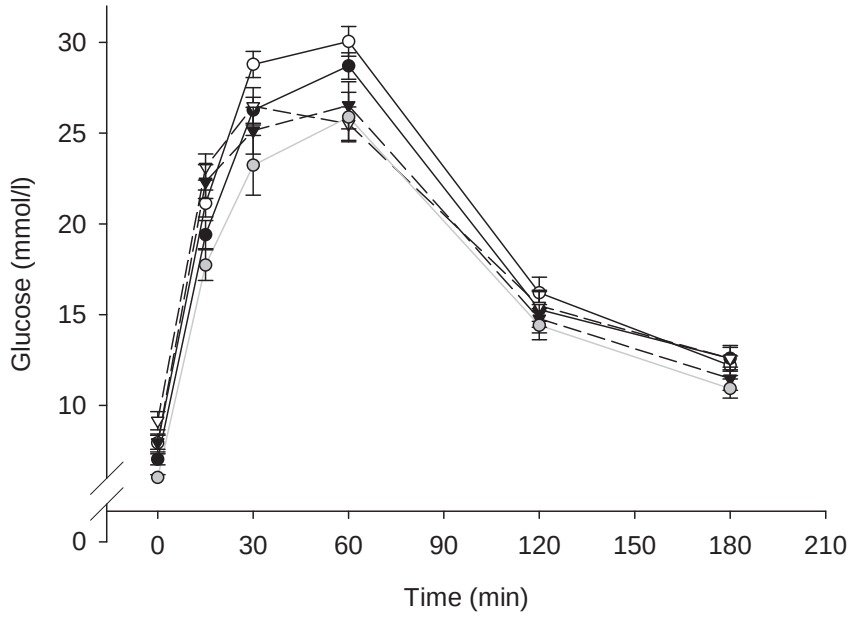

ESM Figure 4

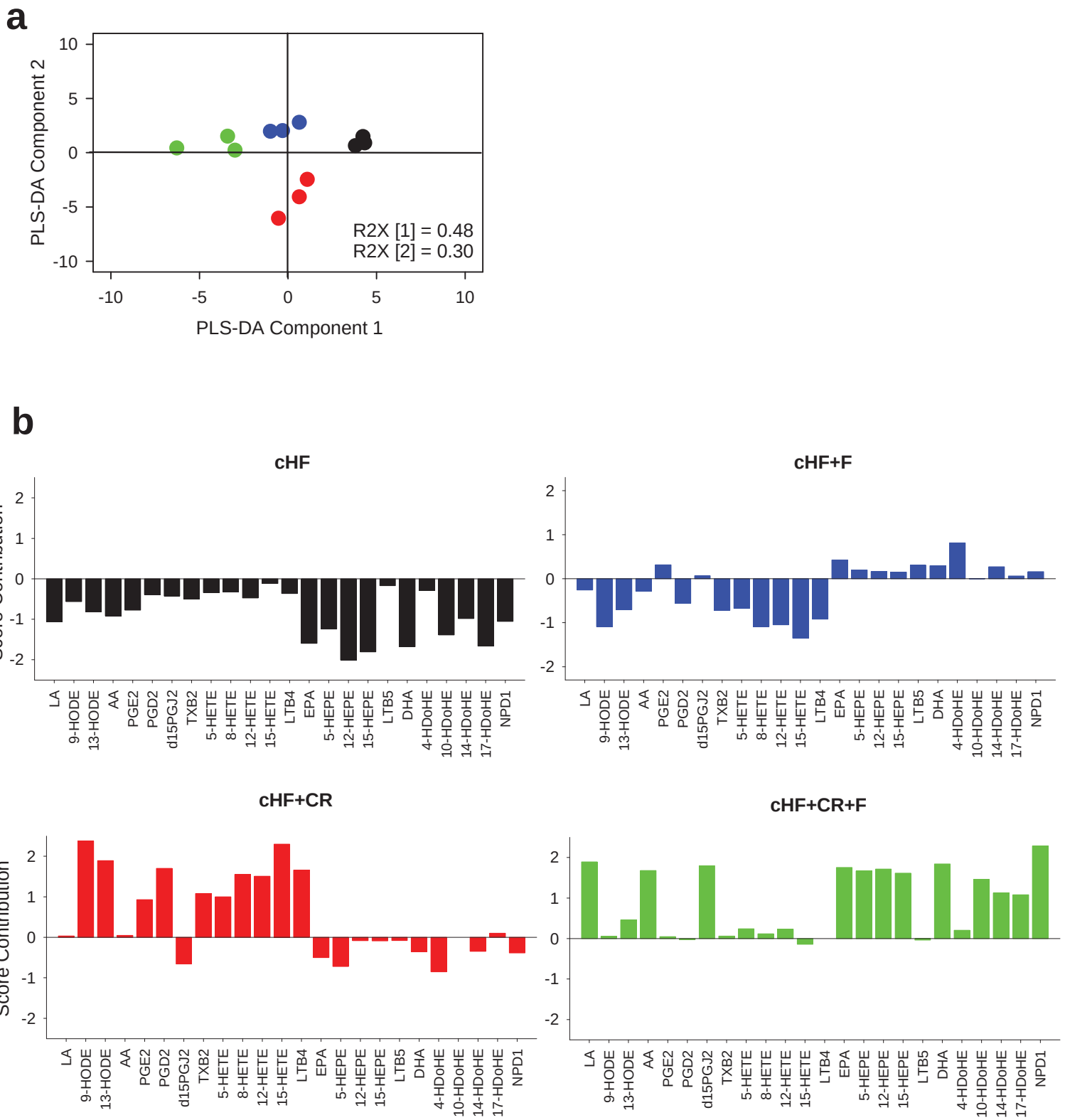
a
PLS-DA Component 2
PLS-DA Component 1
R2X [1] = 0.48
R2X [2] = 0.30
b
cHF
cHF+F
cHF+CR
cHF+CR+F
Score Contribution
LA
9-HODE
13-HODE
AA
PGE2
PGD2
d15PGJ2
TXB2
5-HETE
8-HETE
12-HETE
15-HETE
LTB4
EPA
5-HEPE
12-HEPE
15-HEPE
LTB5
DHA
4-HDoHE
10-HDoHE
14-HDoHE
17-HDoHE
NPD1

ESM Figure 5

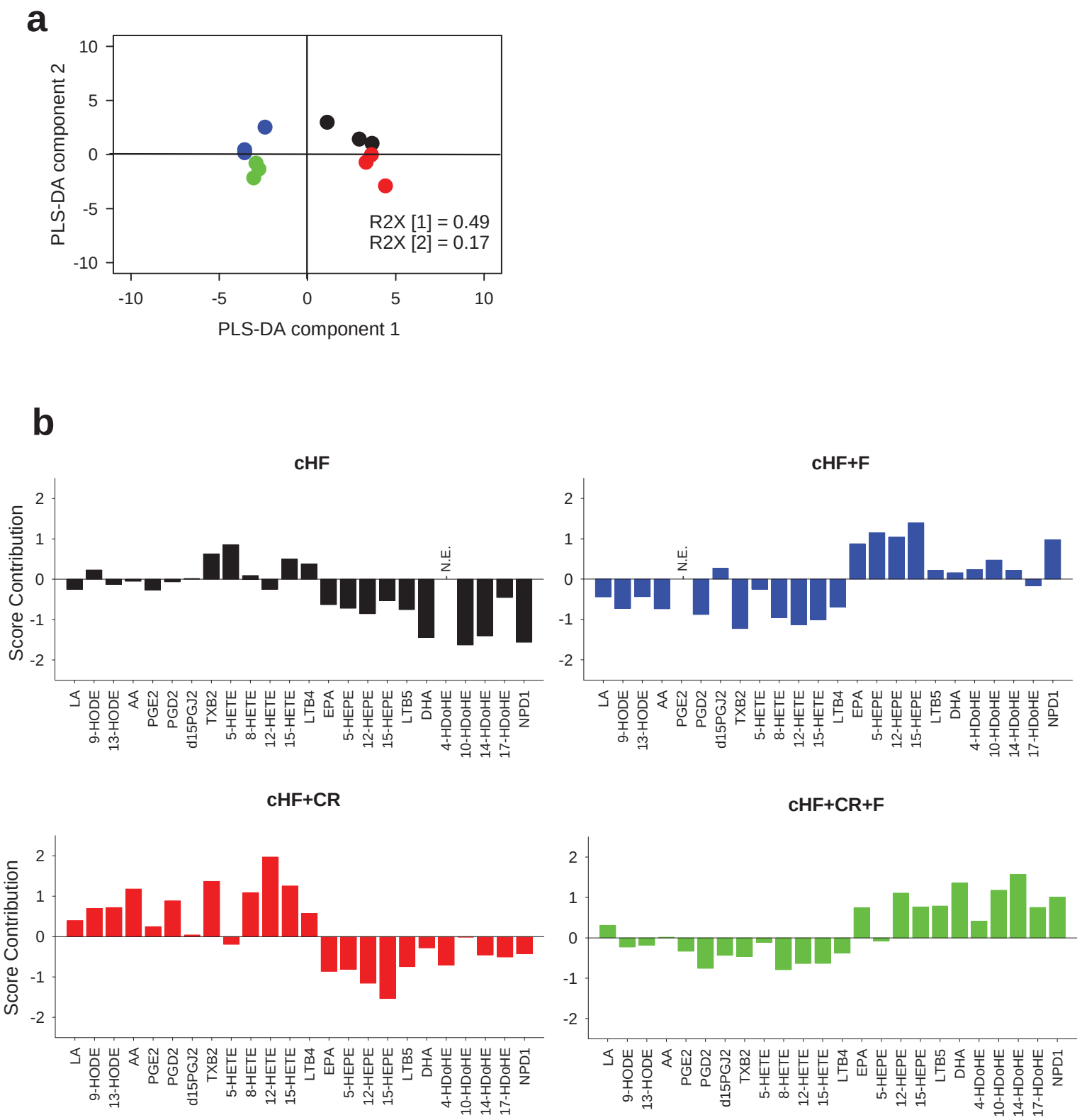
a
PLS-DA component 2
PLS-DA component 1
R2X [1] = 0.49
R2X [2] = 0.17
b
cHF
cHF+F
cHF+CR
cHF+CR+F
Score Contribution
N.E.
LA
9-HODE
13-HODE
AA
PGE2
PGD2
d15PGJ2
TXB2
5-HETE
8-HETE
12-HETE
15-HETE
LTB4
EPA
5-HEPE
12-HEPE
15-HEPE
LTB5
DHA
4-HDoHE
10-HDoHE
14-HDoHE
17-HDoHE
NPD1